Oxidative Medicine and Cellular Longevity

Oxidative Stress in Intervertebral Disc Degeneration and its Related Therapeutics 2022

Lead Guest Editor: Sidong Yang
Guest Editors: Wenyuan Ding, Guoyong Yin, Fengdong Zhao, and Xiaolong Chen

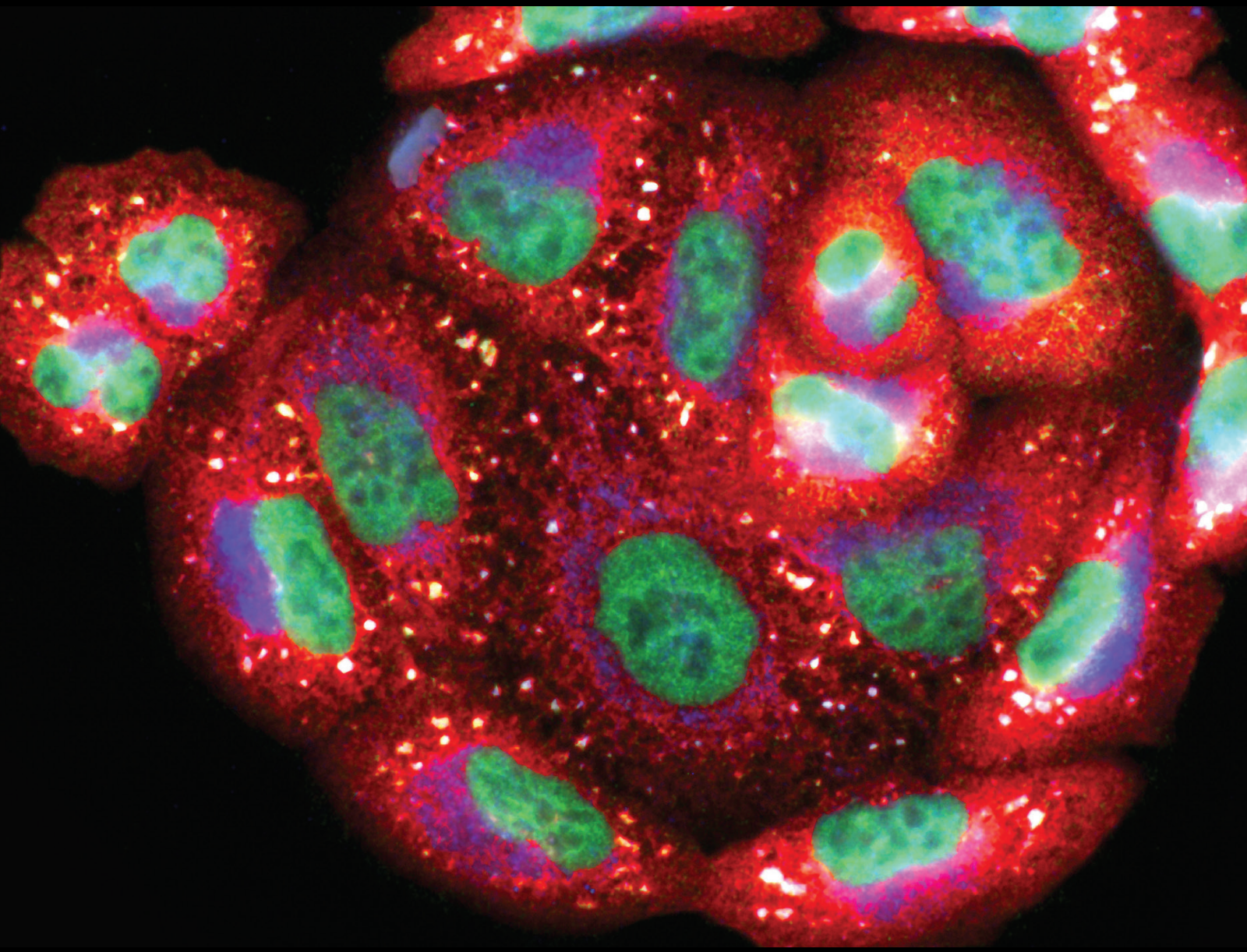

Oxidative Stress in Intervertebral Disc Degeneration and its Related Therapeutics 2022

Oxidative Medicine and Cellular Longevity

Oxidative Stress in Intervertebral Disc Degeneration and its Related Therapeutics 2022

Lead Guest Editor: Sidong Yang
Guest Editors: Wenyuan Ding, Guoyong Yin, Fengdong Zhao, and Xiaolong Chen

Contents

Hindawi
Oxidative Medicine and Cellular Longevity
Volume 2023, Article ID 9020236, 20 pages
https://doi.org/10.1155/2023/9020236

Research Article

Establishment of Ferroptosis-Related Key Gene Signature and Its Validation in Compression-Induced Intervertebral Disc Degeneration Rats

Jiangbo Guo,[1,2] **Yilin Yang**,[1,2] **Junjie Niu**,[1,2] **Zongping Luo**,[1,2] **Qin Shi**,[1,2] **and Huilin Yang**[1,2]

[1]*Department of Orthopaedics, The First Affiliated Hospital of Soochow University, Suzhou, Jiangsu 215000, China*
[2]*Orthopaedic Institute, Soochow University, Suzhou, Jiangsu 215000, China*

Correspondence should be addressed to Qin Shi; shiqin@suda.edu.cn and Huilin Yang; suzhouspine@163.com

Received 22 August 2022; Revised 3 December 2022; Accepted 25 January 2023; Published 10 February 2023

Academic Editor: Abdur Rauf

Cell death and functional loss of nucleus pulposus cell play essential roles in intervertebral disc degeneration (IDD). Ferroptosis is a newly identified cell death type, and its role in IDD is still under investigation. Identifying the key genes of ferroptosis in IDD helps to identify the therapeutic targets of IDD. In this study, we downloaded the human IDD mRNA microarray data from the Gene Expression Omnibus and ferroptosis genes from FerrDb, then performed a series of analyses using strict bioinformatics algorithms. In general, we obtained 40 ferroptosis-related differential expression genes (FerrDEGs) and identified six ferroptosis key gene signatures, namely, ATF3, EIF2S1, AR, NQO1, TXNIP, and AKR1C3. In addition, enrichment analysis of the FerrDEGs was conducted, the protein-protein interaction network was constructed, the correlations between ferroptosis key genes and immune infiltrating cells were analyzed, and the lncRNA-miRNA-mRNA ceRNA network was constructed. In particular, ATF3 and EIF2S1 showed the strongest correlation with immune cell function, which might lead to the development of IDD. Finally, the expressions of ferroptosis key genes were verified in the rat compression-induced IDD. In conclusion, this preliminary study analyzed and verified the mechanism of ferroptosis in IDD, laid a foundation for the follow-up study of the mechanism of ferroptosis in IDD, and provided new targets for preventing and delaying IDD.

1. Introduction

Low back pain was the most common reason for years lived with disability (YLDs) in 2016, based on the Global Burden of Disease Study [1]. Further, it was among the top 10 causes of YLDs in all 188 countries assessed [1]. Intervertebral disc degeneration (IDD) is an important cause, risk factor, and basic pathological process associated with low back pain, and IDD is a process involving many factors, including oxidative stress, abnormal stress load, aging, trauma, and genetics [2–5]. However, the specific mechanisms and triggering factors of IDD are still debatable. Currently, symptomatic treatment methods are used for managing IDD, such as oral anti-inflammatory analgesics and surgical fusion, rather than interfering with the progress of IDD [6]. However, these treatment methods are alone not adequate to treat IDD, such as recurrent low back pain and degeneration of adjacent spine segments [6]. On account of the heavy social and economic burden caused by low back pain, it is urgent to identify the underlying mechanisms for the onset and progression of IDD and develop new treatment strategies.

Nucleus pulposus is a gel-like structure located in the middle of the intervertebral disc, which synthesizes proteoglycan, absorbs water, provides osmotic pressure, and resists compressive stress [4]. Previous studies have found that apoptosis, autophagy, necroptosis, and pyroptosis are involved

in the death and functional loss of nucleus pulposus cells, leading to an imbalance in extracellular matrix metabolism and aggravating the progression of IDD [7–9]. Inhibition of apoptosis, necroptosis, and cell death could partially alleviate the progression of IDD. However, IDD may be a multifactorial pathological process involving multiple cell death modes. Therefore, clarifying other cell death modes would help to understand the mechanism of IDD and develop treatment targets.

Ferroptosis is a new mechanism of cell death, which is different from apoptosis [10]. It is a type of iron-dependent cell death due to the deposition of lipid peroxides on the cell membrane, characterized by lipid peroxidation and free iron-mediated Fenton reaction [10, 11]. The cells with ferroptosis lack the defense system required to eliminate lipid peroxide, accumulating lethal lipid peroxide levels [12]. Studies reported that oxidative stress and iron-dependent reactive oxygen species production primarily contribute to ferroptosis, suggesting that the initiation and effect of ferroptosis require a unique regulatory mechanism [11, 12]. Thus, studying the specific mechanisms of developing and inhibiting ferroptosis would help treat many diseases. Activation of excessive ferroptosis is related to degenerative diseases (e.g., Alzheimer's disease, Parkinson's disease, and acute kidney injury), and impaired ferroptosis often leads to tumor development [10]. Furthermore, some studies have shown that ferroptosis is involved in the IDD progression [13, 14]. Thus, inhibition of ferroptosis may help to treat IDD [15]. However, the research on the mechanism of ferroptosis in IDD is still at the initial stage and needs further exploration. Understanding the role of ferroptosis in IDD might provide therapeutic targets for delaying the IDD progression.

The intervertebral disc has been determined as an immune-privileged organ. The immune privilege is the basis of the intervertebral disc's homeostasis [16]. In addition, studies have shown that, after breaking the physical barrier, immune cell infiltration plays an essential role in the onset and development of IDD [16–18]. However, the relationship between ferroptosis and immune cell infiltration in IDD is still under investigation. Thus, clarifying the correlation between ferroptosis and immune cell infiltration would help understand the IDD progression and provide prevention and treatment targets.

In this study, we found that the gene expression in IDD was enriched in arachidonic acid metabolism according to the Gene Expression Omnibus database dataset and identified the ferroptosis-related differential expression genes (FerrDEGs) in IDD using the FerrDb database. Furthermore, we identified the functions of the genes involved in IDD and the characteristics of ferroptosis key genes and analyzed the correlations between ferroptosis key genes and immune infiltrating cells of IDD. Finally, the expression of ferroptosis key genes and IL-1β and TGF-β1 was verified in the compression-induced IDD rats. In conclusion, this study identified the key gene signature of ferroptosis in IDD and laid the foundation for future research targeting the prevention and treatment of IDD.

2. Material and Methods

Figure 1 shows the flow chart of the database, software, and research methods used in this study.

2.1. Dataset Acquisition and Preprocessing. The dataset GSE70362 was obtained from the Gene Expression Omnibus database. This dataset contained mRNA microarray data from 24 intervertebral disc nucleus pulposus samples, of which eight were Thompson grades I and II and were considered the normal control group, and 16 were Thompson grades III-V and were considered the IDD group [19]. The platform was GPL17810. We annotated the probes under the R environment, then got the maximum value of the repeated gene symbol, obtaining the expression matrix.

2.2. Gene Set Enrichment Analysis (GSEA). We downloaded the GSEA software from the official website (https://www.gsea-msigdb.org/gsea/index.jsp) and sorted out expression dataset files and phenotype label files according to the official instructions [20, 21]. We used the GSEA software to conduct the Kyoto Encyclopedia of Genes and Genomes (KEGG) pathway enrichment analysis on the expression profile of GSE70362. The number of permutations was 1000; permutation type was phenotype; the metric for ranking genes was signal2noise, and a pathway with the p value < 0.05 was considered a statistically significant enrichment pathway.

2.3. Screening of Differential Expression Genes (DEGs) and FerrDEGs. The "limma" package in the R environment was used to analyze the DEGs of the GSE70362 dataset. We selected the p value < 0.05 as the screening condition to obtain enough DEGs. We obtained ferroptosis-related genes from the FerrDb database (http://www.zhounan.org/ferrdb), including the ferroptosis marker genes, driver genes, and suppressor genes. The intersections of DEGs and ferroptosis-related genes were obtained using the Venn diagram and were considered FerrDEGs.

2.4. Enrichment Analysis of FerrDEGs. We used the "clusterProfiler" package under the R environment to perform Gene Ontology (GO) and KEGG enrichment analysis on FerrDEGs. The GO enrichment analysis included biological process (BP), cellular component (CC), and molecular function (MF), and the adjusted p value < 0.05 was considered statistically significant for the enrichment item. p value < 0.05 in the KEGG was considered statistically significant for the enrichment item. The top 10 enrichment projects of GO and KEGG were visualized in the histogram under the R environment, and the links between the top 5 enrichment entries of GOBP and FerrDEGs were visualized in the circle diagram.

2.5. Construction of FerrDEG Protein-Protein Interaction (PPI) Network and Screening of Ferroptosis Key Genes. We uploaded all FerrDEGs to the STRING version 11.5 website (https://cn.string-db.org/), then constructed a PPI network with confidence > 0.4, and hid the unconnected protein nodes [22]. We used Cytoscape 3.7.2 to visualize the PPI

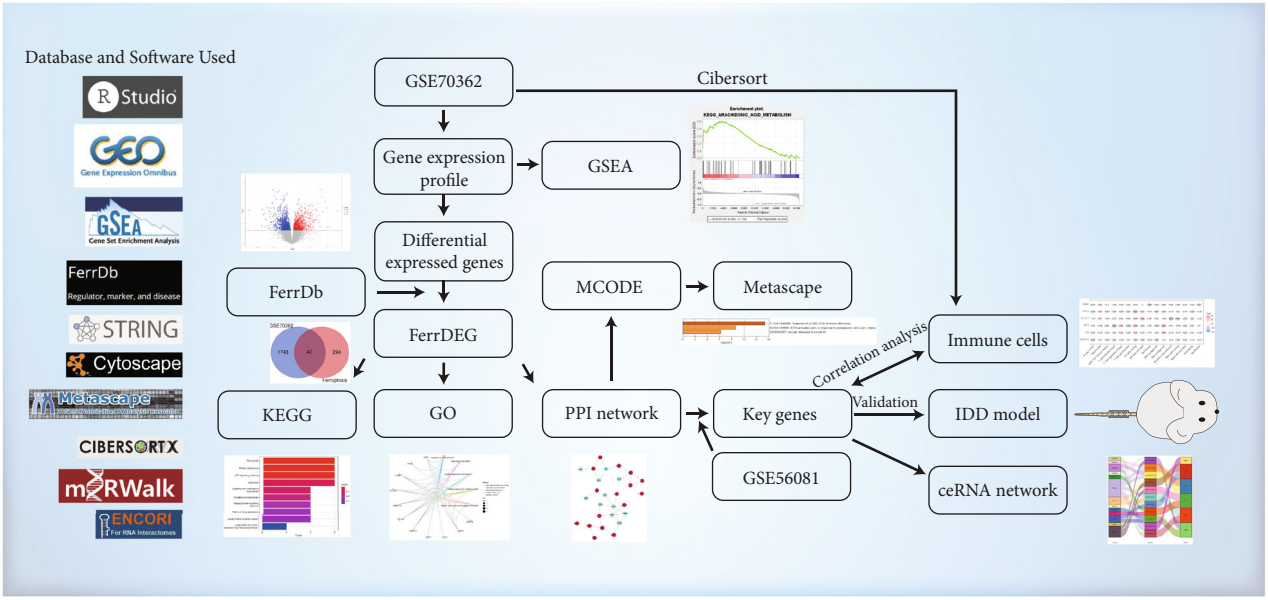

Figure 1: The flow chart of the study. A series of bioinformatics algorithms were conducted to analyze GSE70362. And the compression-induced IDD rat model was constructed to validate the expressions of ferroptosis key genes. The database and software used in this study were presented on the left side of the figure.

network [23], used the Mcode plug-in to screen the subnet, and used Metascape (http://www.metascape.org) to conduct enrichment analysis of the subnet. The MMC and betweenness algorithms in the plug-in cytoHubba were used to calculate the top 5 proteins, and the union was used to obtain the ferroptosis key candidate genes. The GSE56081 dataset was obtained from the Gene Expression Omnibus database, and the expression of the above candidate genes was extracted for verification under the R environment. Candidate genes with consistent expression trends in GSE70362 and GSE56081 were considered to be ferroptosis key genes.

2.6. Correlation Analysis between Immune Infiltration Cells and Ferroptosis Key Genes. The CIBERSORT algorithm under the R environment was used to analyze the immune cell infiltration of IDD. We removed the immune cell types, with an abundance of 0 in all samples. Each immune cell proportion in each sample and each immune cell type contents in all samples were visualized under the R environment. Spearman algorithm was used to analyze the correlations between 16 immune cell types and between 16 immune cells and six ferroptosis key genes. The "ggcorplot" package was used for visualization.

2.7. Construction of Potential lncRNA-miRNA-mRNA ceRNA Network of Ferroptosis Key Genes. The miRNA prediction of ferroptosis key genes was carried out using miRWalk 3.0 (http://mirwalk.umm.uni-heidelberg.de/) under the condition of score = 1, and the miRNA validated in miRDB was selected. The miRNA was sorted from large to small pairing numbers, and ENCORI was used (https://starbase.sysu.edu.cn/) to predict the upstream lncRNA of miRNA [24]. We selected the first two miRNAs with upstream lncRNA as candidate potential miRNA, and the lncRNA screening condition was clip data strict ≥ 5. We selected the top two largest of clipExpNum as candidate potential lncRNA. Finally, we used the Sankey map to visualize the lncRNA-miRNA-mRNA ceRNA network of ferroptosis key genes under the R environment.

2.8. Construction of a Compression-Induced IDD Rat Model. We constructed a rat compression-induced IDD model as previously described [25]. In brief, ten 12-week-old male Sprague-Dawley (SD) rats were randomly divided into the Sham and IDD groups ($n = 5$ in each group). As previously reported, Co8-Co9 intervertebral discs were compressed with a compression device in the IDD group to establish a long-term compression-induced IDD model in SD rats. However, only Kirschner wires were inserted in Co7-Co10 in the Sham group. The animal protocol was approved by the Institutional Animal Care Committee of the Laboratory Animal at the School of Medicine, Soochow University (Suzhou, China). Rats were raised under standardized conditions, with a light/dark circadian rhythm of 12/12 hours, an appropriate ambient temperature of about 23°C, and free access to food and water. After four weeks, magnetic resonance imaging (MRI) and X-ray imaging of the rat intervertebral disc were performed using a 1.5 T MRI scanner (GE-HDe, USA) and X-ray machine (SHIMADZU, Japan), respectively [26]. The relative quantification of T2 signal intensity was performed using Adobe Photoshop CS6 (California, USA). We calculated the disc height index (DHI) using radiography (X-ray) according to the previous report [27].

2.9. Validation of Ferroptosis Key Genes in Compression-Induced IDD Rats. Total RNA in nucleus pulposus was extracted using TRIzol reagent (Beyotime, China), and the RNA concentration was assessed with NanoDrop 2000 (ThermoFisher Scientific, USA). Then, mRNA was reverse transcribed into cDNA using 5× All-in-One RT Mastermix (abm, China), and real-time qPCR was carried out using iTaq Universal SYBR Green Supermix (Bio-Rad, USA) to detect the ferroptosis key genes and IL-1β and TGF-β1 expression on the CFX96 Real-Time System (Bio-Rad, USA). GAPDH was used as an internal control gene, and the relative expression of the genes was calculated using the comparative Ct method. The forward and reverse primer pairs used for all genes are shown in Supplementary Table 1.

2.10. Statistical Analysis. R software 4.2.0 and RStudio 2022.02 (Boston, USA) were used for data analysis and visualization. The comparison of gene expression between two groups was assessed by the two-tailed unpaired *t*-test using GraphPad Prism 8.0 (California, USA). The results were presented as means and standard deviations. Unless otherwise stated, the p value < 0.05 was considered statistically significant.

3. Results

3.1. GSEA. GSEA demonstrated that the degenerative nucleus pulposus of intervertebral disc was mainly enriched in arachidonic acid metabolism (NES = 1.675538, p value < 0.05), Toll-like receptor signaling pathway (NES = 1.6202703, p value < 0.05), and steroid hormone biosynthesis (NES = 1.5567781, p value < 0.05) (Figures 2(a), 2(c), and 2(e)). The expression of genes related to each pathway in the sample is shown in the heat map (Figures 2(b), 2(d), and 2(f)).

3.2. Screening of DEGs and FerrDEGs. There were 1783 DEGs in total, and the results of differential analyses were visualized using a heat map and volcano map (Figures 3(a) and 3(b)). There were 334 ferroptosis-related genes in total, and the intersection of the two gave 40 FerrDEGs (Figure 3(c)). Refer to Supplementary Table 2 for logFC, p value, and regulation of all FerrDEGs. Refer to Supplementary Table 3 for all categories related to FerrDEGs.

3.3. FerrDEG Enrichment Analysis. GOBP enrichment analysis demonstrated that FerrDEGs were primarily involved in the regulation of ferroptosis; GOCC showed that it was enriched in the intracellular ferritin complex. GOMF was primarily involved in ferric and ferrous iron binding; all had adjusted p value < 0.05 (Figure 4(a)). ATF3, PCK2, LAMP2, SLC2A1, AKR1C3, EIF2S1, MAP3K5, NQO1, AHCY, ASNS, and GDF15 participated in the first five entries of GOBP enrichment (Figure 4(b)). KEGG enrichment analysis demonstrated that FerrDEGs were primarily involved in ferroptosis, mineral absorption, and the p53 signaling pathway (p value < 0.05) (Figure 4(c)).

3.4. Construction of PPI Network and Screening of Ferroptosis Key Genes. PPI network was generated using STRING and visualized in Cytoscape 3.7.2. PPI network included 27 protein nodes, including 16 upregulated genes and 11 downregulated genes (Figure 5(a)). Mcode plug-in obtained three subnetworks of PPI (Supplementary Figure 1a, b, c). Metascape enrichment analysis showed that the three subnetworks were mainly involved in biological functions, including endoplasmic reticulum stress, negative regulation of cell cycle, and iron overload (Supplementary Figure 1d, e, f). MCC and betweenness calculated the PPI network to identify the top five proteins of their respective algorithms. After combining the results of each algorithm, we identified eight genes, ASNS, ATF3, EIF2S1, CEBPG, NQO1, AR, TXNIP, and AKR1C3 (Figures 5(b) and 5(c)). The expression of eight genes was extracted from the GSE56081 dataset. Unfortunately, the expression of ASNS and CEBPG was not verified. Therefore, the remaining six genes were considered ferroptosis key genes and used for follow-up research objects (Figures 5(d)–5(k)).

3.5. Correlation Analysis between Ferroptosis Key Genes and Immune Cell Infiltration in IDD. The CIBERSORT algorithm provided 22 types of immune cell infiltration analyses. In the GSE70362 dataset, we removed the cell types with an expression abundance of 0 in all samples, and 16 types of immune cell types remained. The expression of each immune cell type in each sample is shown in Figure 6(a). Among all immune cell types, CD4 memory resting T cells have the highest expression abundance in intervertebral disc tissue (Figure 6(b)). Spearman correlation analyses of 16 immune cell types (Figure 6(c)) showed that activated NK cells and resting mast cells showed the strongest positive correlation (correlation coefficient = 0.67, p value < 0.05), while activated NK cells and activated mast cells showed the strongest negative correlation (correlation coefficient = −0.78 , p value < 0.05). Spearman correlation analyses of 16 immune cells and six ferroptosis key genes (Figure 6(d)) showed that ATF3 had the strongest positive correlation with M2 macrophages (correlation coefficient = 0.524, p value < 0.05), and EIF2S1 showed the strongest negative correlation with activated dendritic cells (correlation coefficient = −0.552, p value < 0.05).

3.6. Construction of Potential ceRNA Network of Ferroptosis Key Genes. According to our screening conditions, 11 miRNAs and 13 lncRNA were obtained (Figure 7). The 11 potential miRNAs were hsa-miR-106b-5p, hsa-miR-135b-5p, hsa-miR-2115b-3p, hsa-miR-2467-3p, hsa-miR-302a-3p, hsa-miR-383-5p, hsa-miR-421, hsa-miR-4766-3p, hsa-miR-524-5p, hsa-miR-6763-5p, and hsa-miR-6884-5p. AKR1C3 has only one upstream miRNA, and the rest of the genes had two upstream miRNAs. The 13 potential lncRNA were AC005899.4, AC009032.1, AC016876.2, AC021078.1, LRRC75A-AS1, MALAT1, MIR17HG, MIR2HG, MIR29B2CHG, NEAT1, NORAD, SNHG1, and SNHG16. lncRNA MALAT1 showed the most degree of association, followed by lncRNA SNHG16.

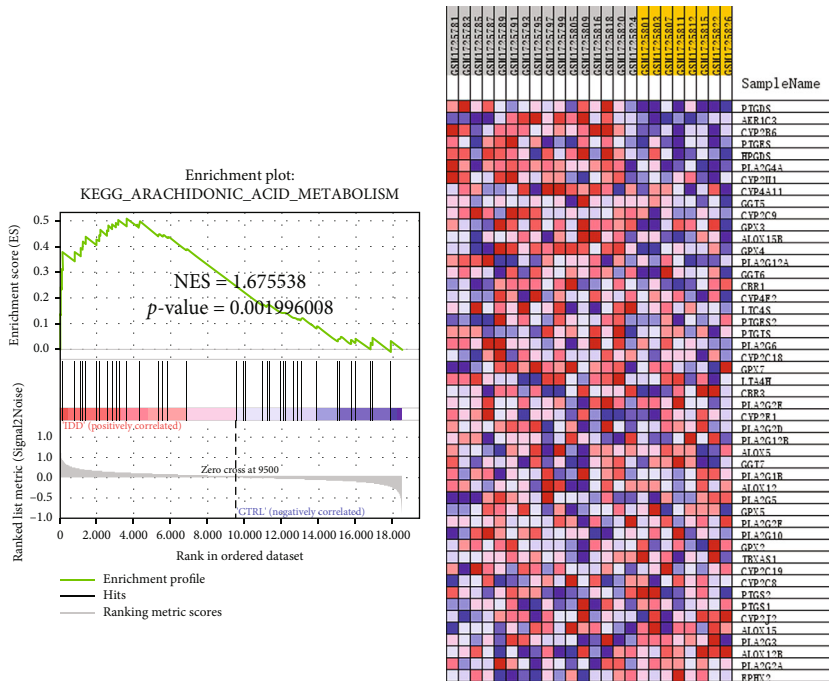

(a) (b)

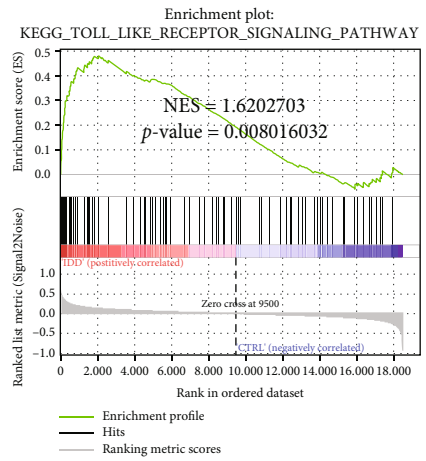

(c)

Figure 2: Continued.

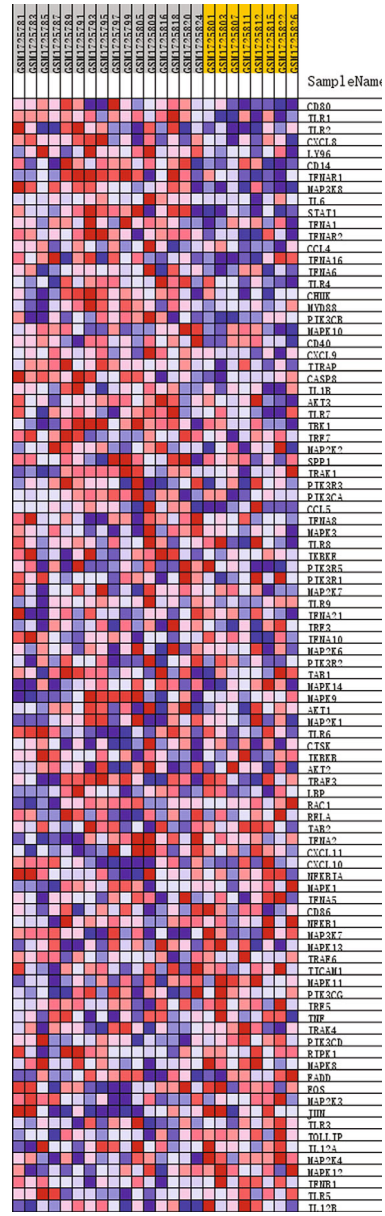

(d)

Figure 2: Continued.

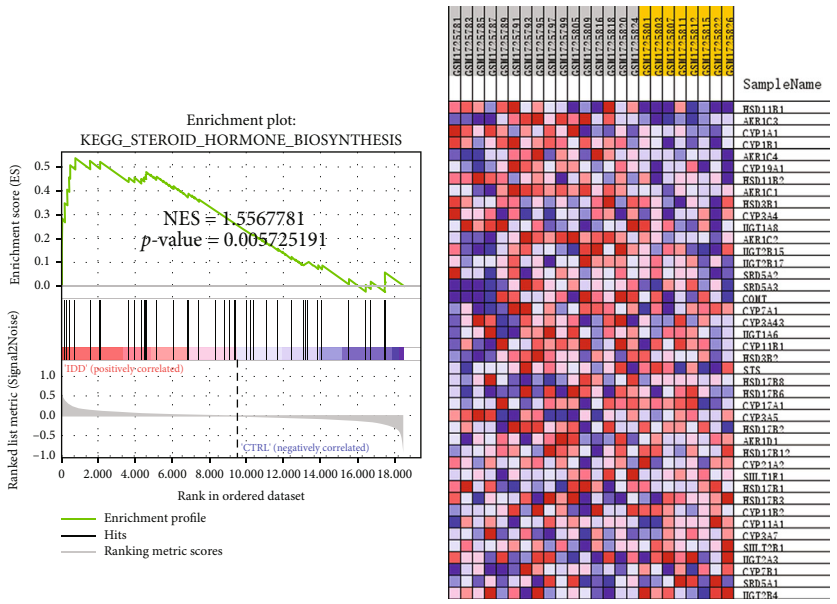

(e) (f)

Figure 2: GSEA of the KEGG pathway in IDD. (a, b) Arachidonic acid metabolism in IDD and its related gene expression in each nucleus pulposus sample. (c, d) Toll-like receptor signaling pathway in IDD and its related gene expression in each nucleus pulposus sample. (e, f) Steroid hormone biosynthesis in IDD and its related gene expression in each nucleus pulposus sample.

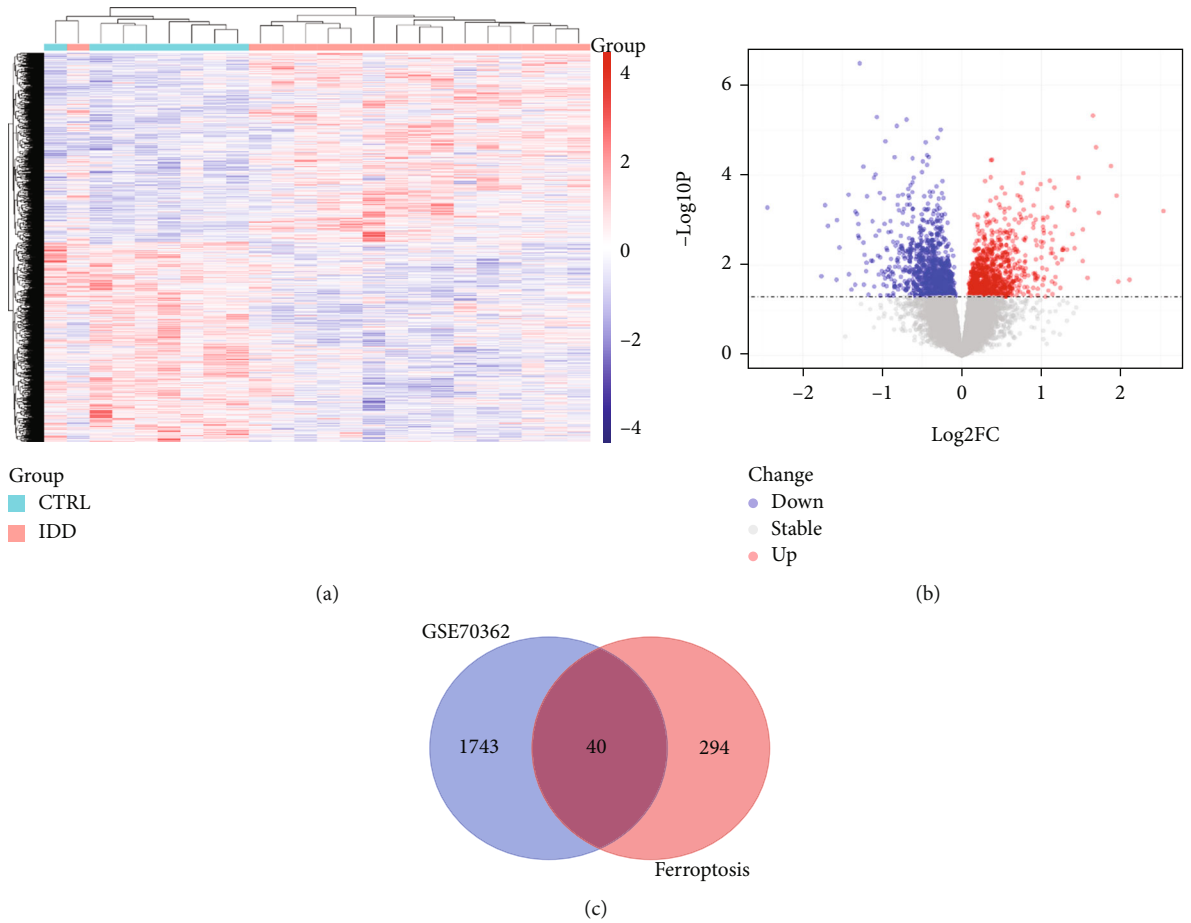

(a) (b)

(c)

Figure 3: Differential expression analysis and identification of FerrDEGs in IDD. (a) Heatmap of DEGs in IDD. (b) Volcano map of DEGs in IDD. (c) The intersection of DEGs and ferroptosis database genes.

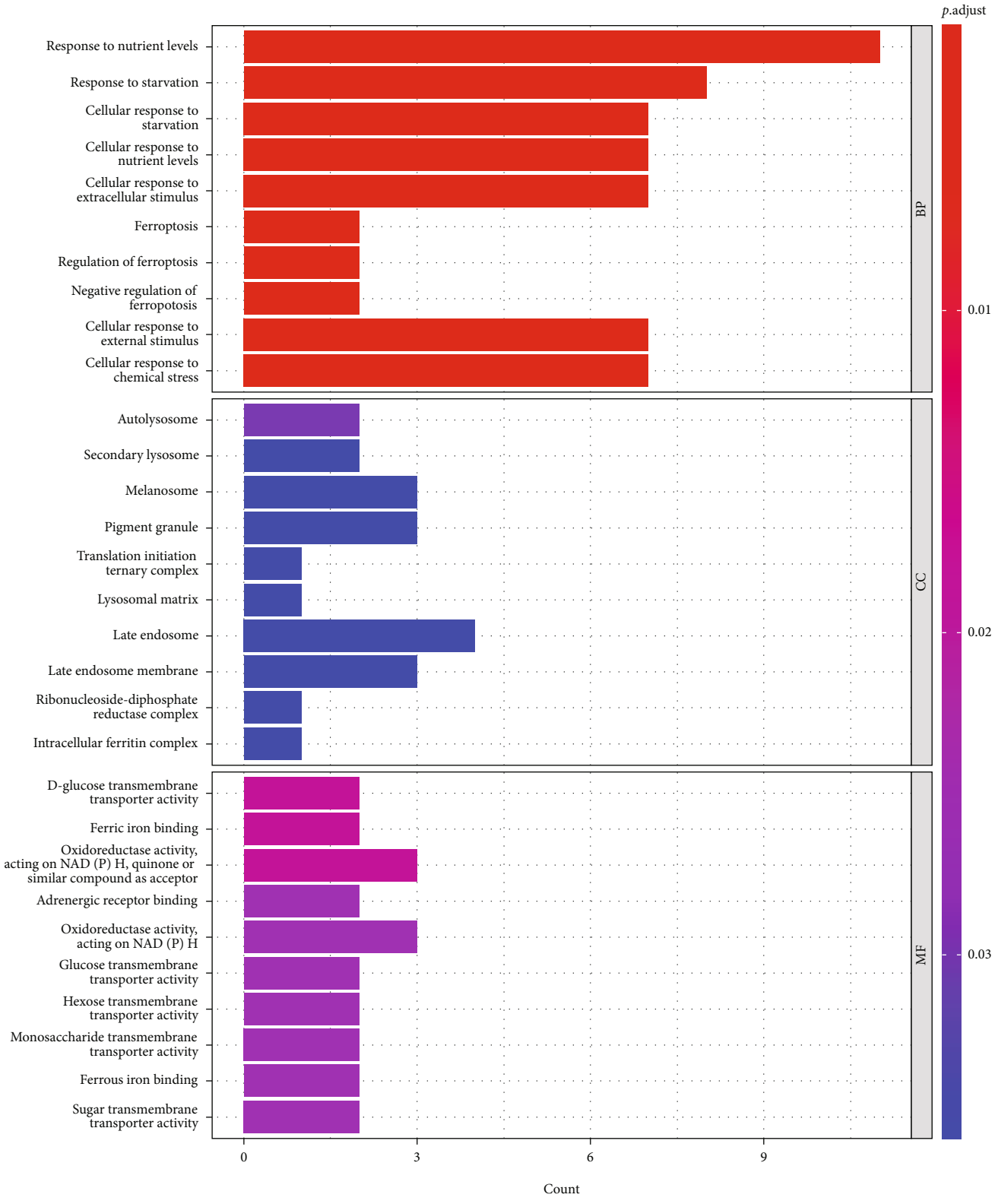

(a)

Figure 4: Continued.

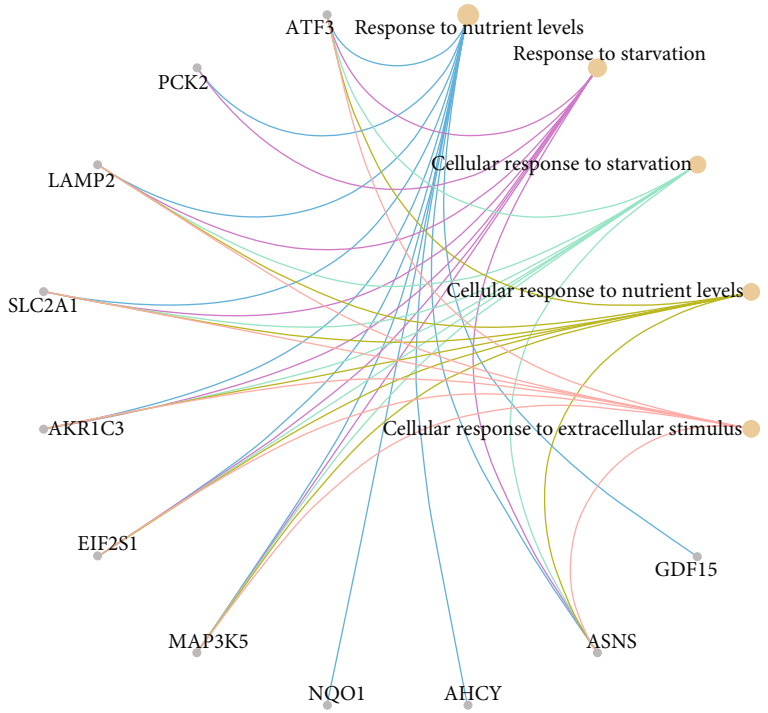

(b)

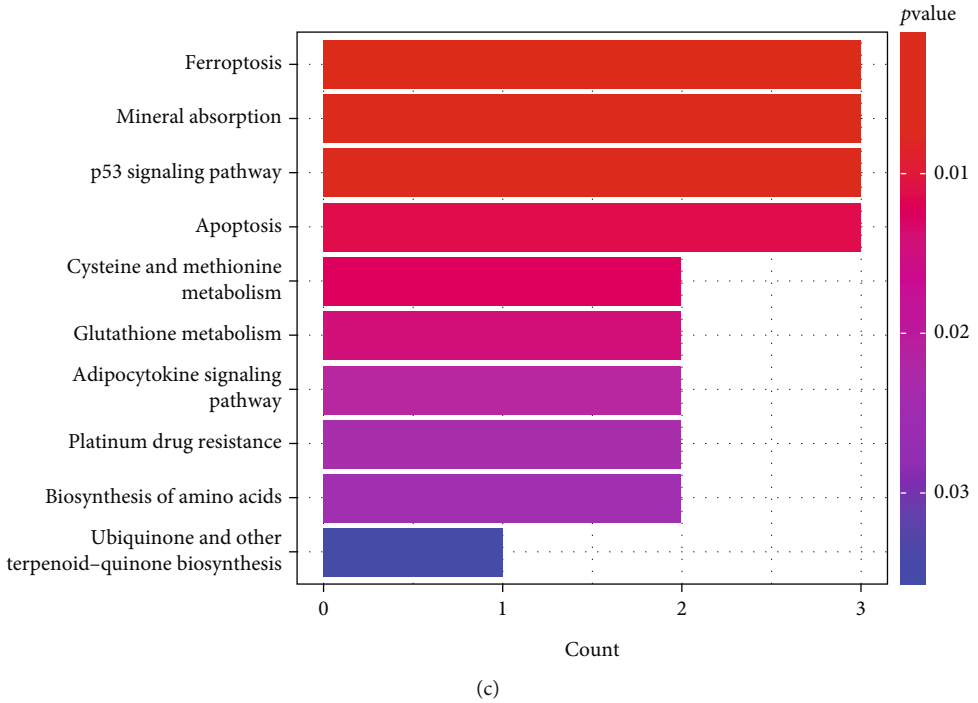

(c)

Figure 4: FerrDEG enrichment analysis. (a) GO analysis of FerrDEGs. (b) The top five entries of GOBP and relative genes. (c) KEGG analysis of FerrDEGs.

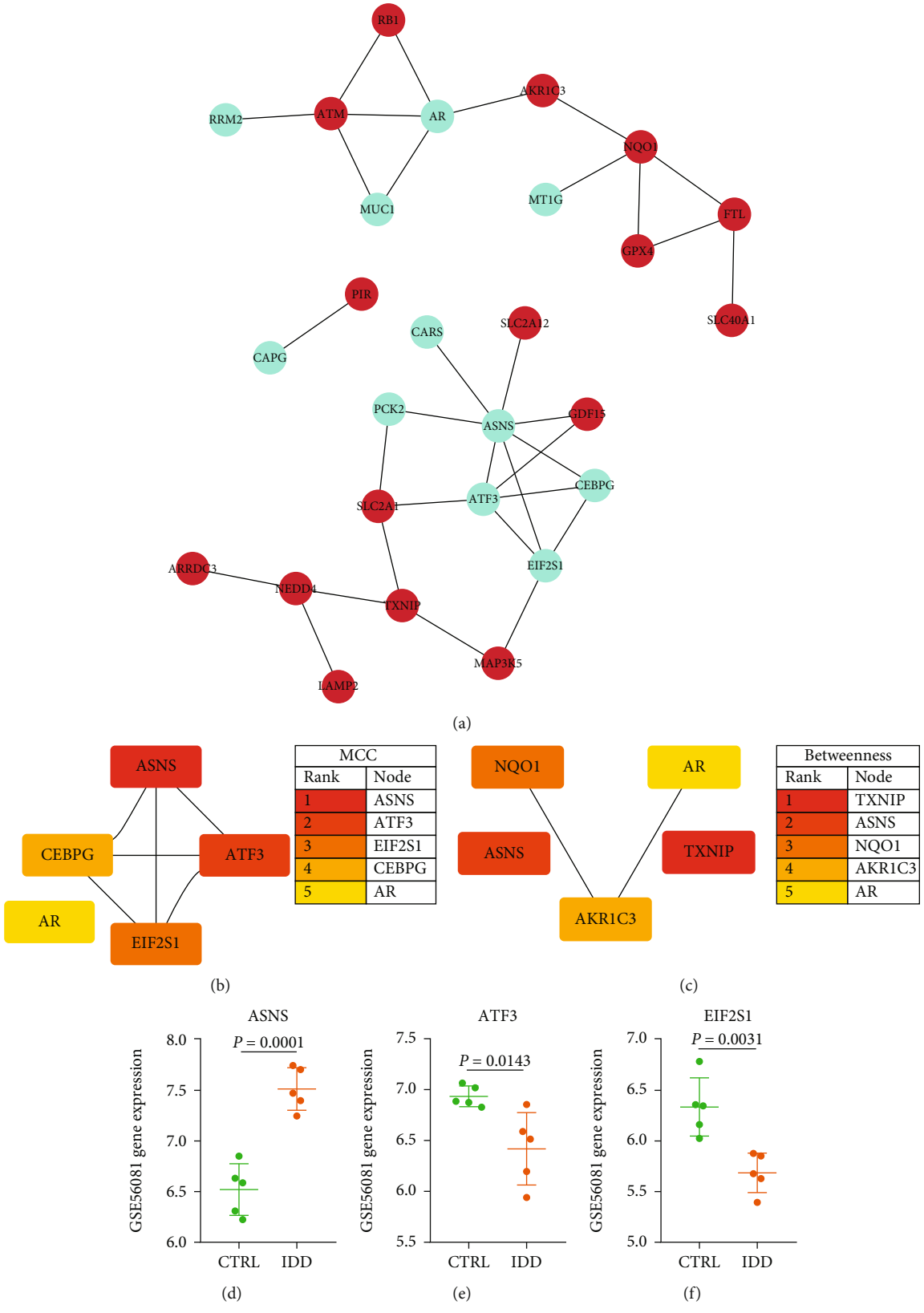

Figure 5: Continued.

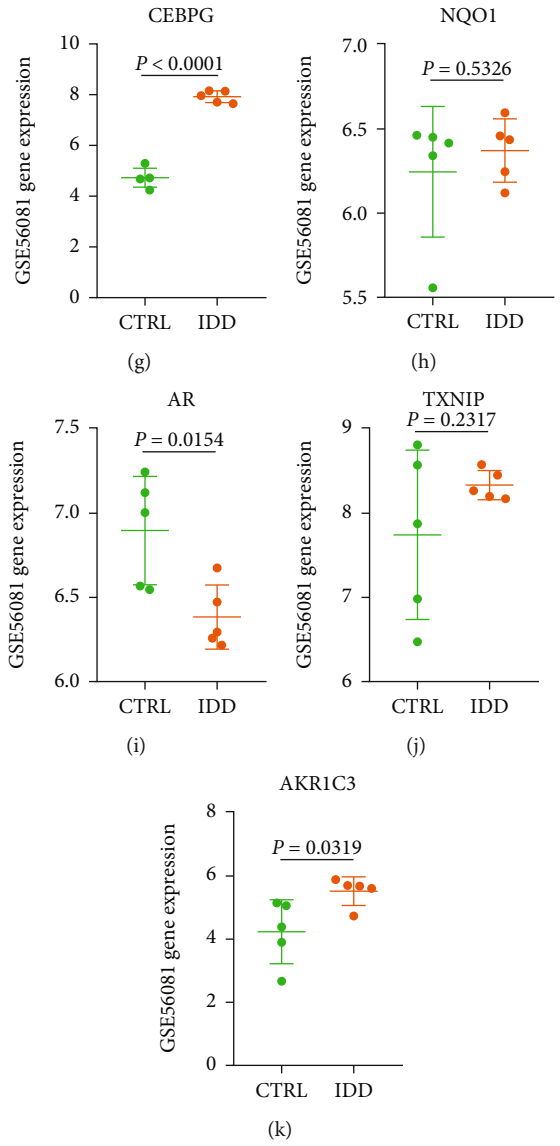

Figure 5: PPI network of FerrDEGs and identification of key genes in FerrDEGs. (a) PPI network of 27 FerrDEGs; red indicates upregulated genes, while green indicates downregulated genes. (b) The MCC algorithm was used to identify the top 5 genes in PPI. (c) The betweenness algorithm was used to identify the top 5 genes in PPI. (d–k) Eight candidate gene expressions in GES56081. Six genes with the same expression trend as GSE70362 were considered key genes of FerrDEGs.

3.7. Validation of Ferroptosis Key Genes in the Compression-Induced IDD Rats. The compression device was successfully fixed on the rat Co7-Co10, in which Co8-Co9 was compressed (Figure 8(a)). After four weeks of compression, MRI and X-ray showed that T2 intensity and DHI in the IDD group were significantly lower than those in the Sham group (p value < 0.01; Figures 8(b)–8(e)). The expressions of AR, ATF3, EIF2S1, and mRNA were significantly downregulated in the IDD group, and the expressions of AKR1C3, NQO1, and TXNIP mRNA were significantly upregulated in the IDD group (p value < 0.05; Figures 8(f)–8(k)) which were consistent with the results of database analyses. Besides, IL-1β mRNA was significantly upregulated in the IDD group compared to the Sham group, while TGF-β1 was significantly downregulated in the IDD group compared to the Sham group (p value < 0.05; Figures 8(l) and 8(m)).

4. Discussion

In this study, we identified six ferroptosis key genes associated with IDD and their biological functions through enrichment analysis, the potential ceRNA network, and the correlation with the immune function in IDD. Six key genes were verified in the rat IDD model, confirming that these genes were vital in the ferroptosis in IDD.

First, we used GSEA to explore the KEGG pathway of gene enrichment in IDD. Arachidonic acid metabolism, Toll-like receptor signaling pathway, and steroid hormone biosynthesis showed the highest enrichment in IDD. GSEA does not rely on differential gene screening conditions but conducts enrichment analysis of the entire gene expression profile [21]. Studies reported that arachidonic acid metabolism and Toll-like receptor signaling pathways were closely

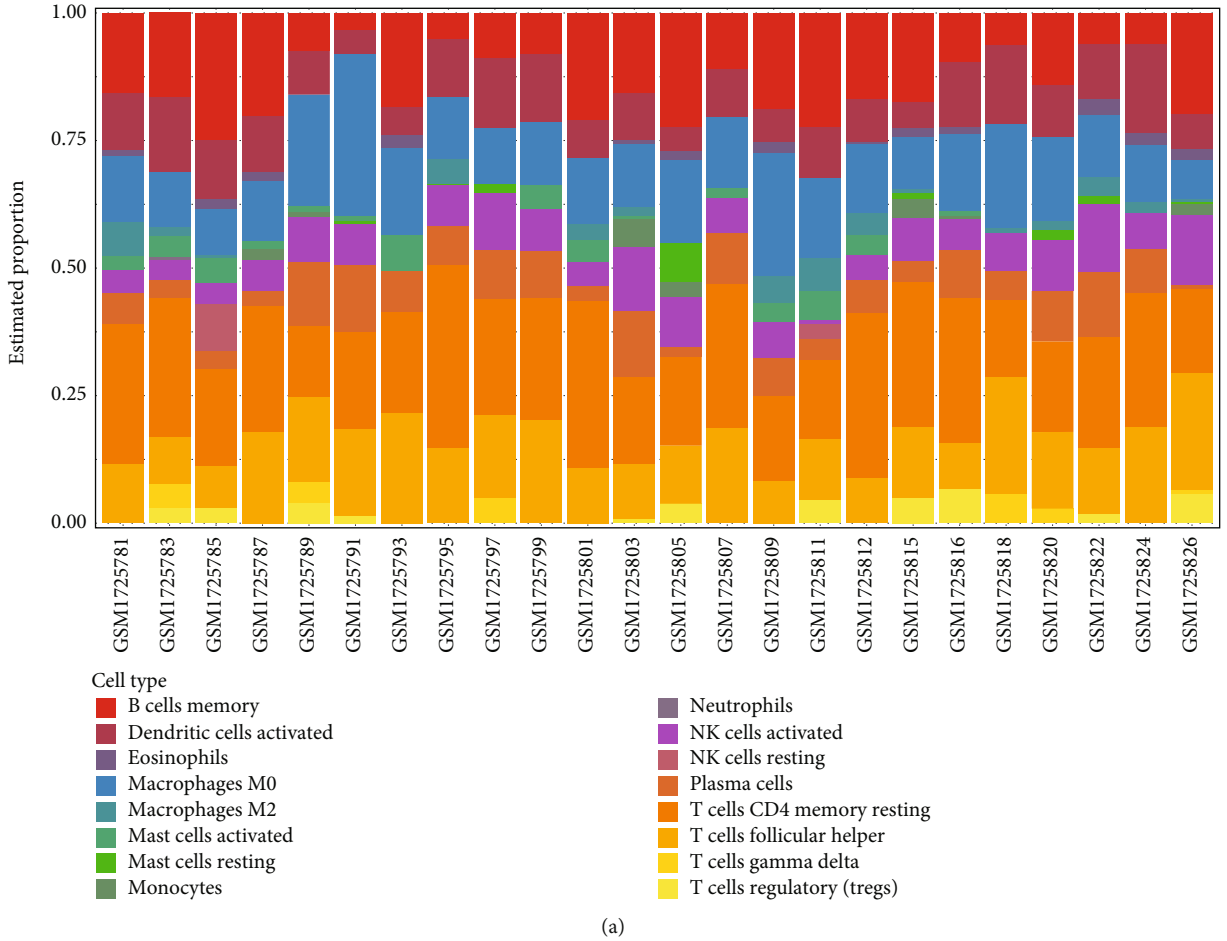

(a)

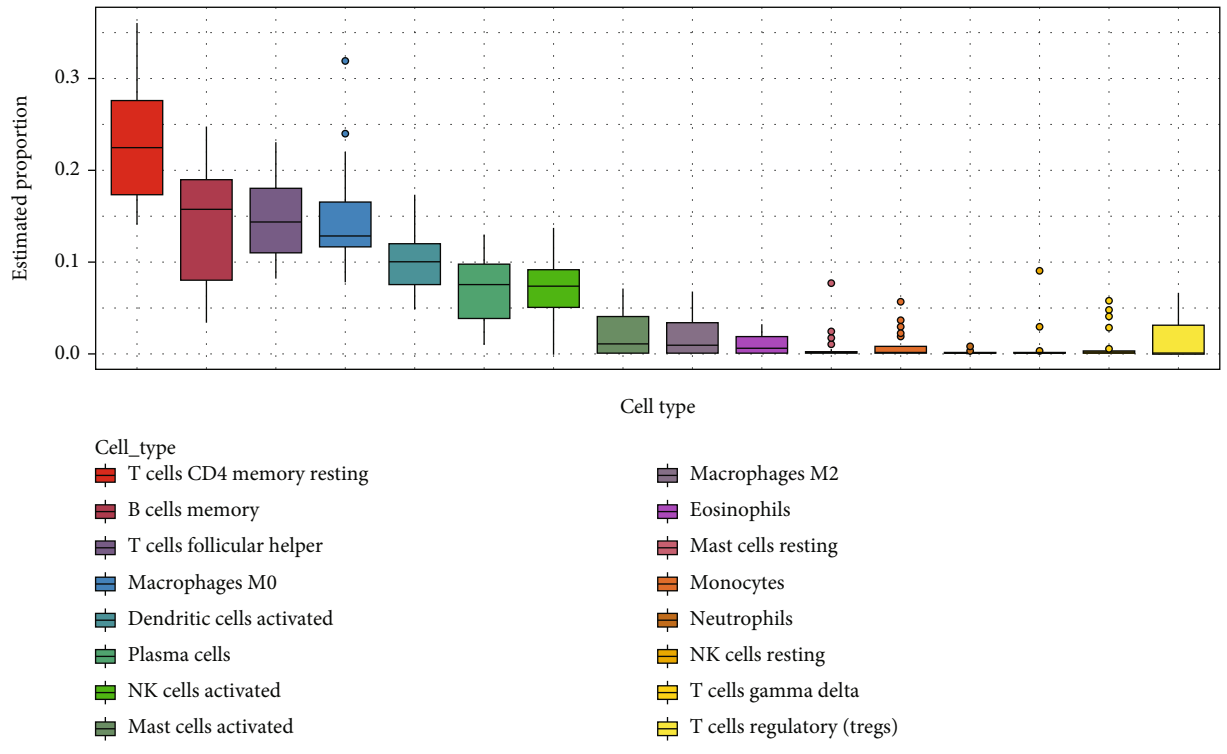

(b)

Figure 6: Continued.

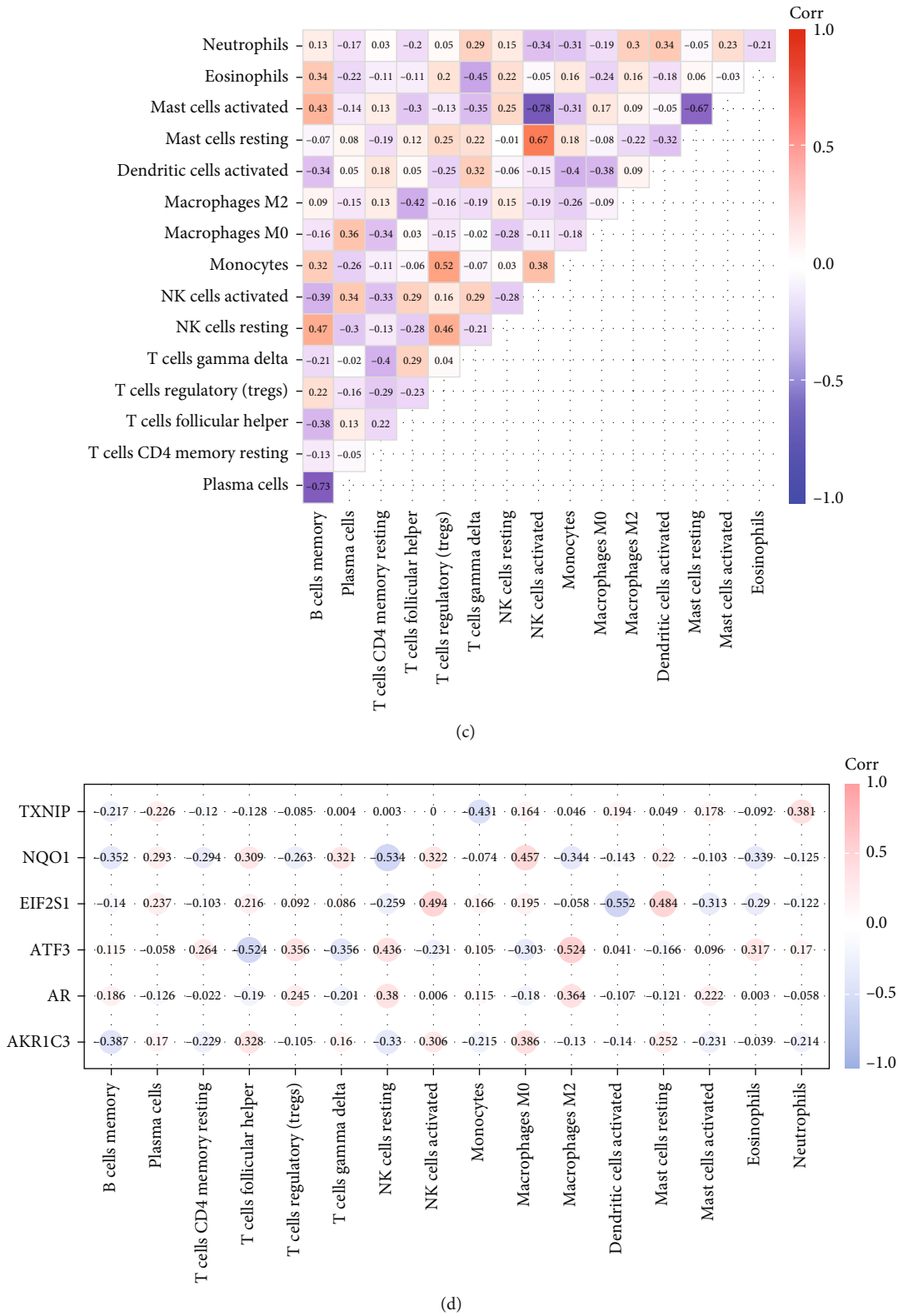

Figure 6: Correlation analyses between ferroptosis key genes and immune cell infiltration in IDD. (a) 16 immune cell type expression in each sample in GSE70362. (b) Each immune cell expression was estimated in all the samples in GSE70362. (c) Correlation analyses between immune cell types. (d) Correlation analyses between immune cell types and ferroptosis key genes.

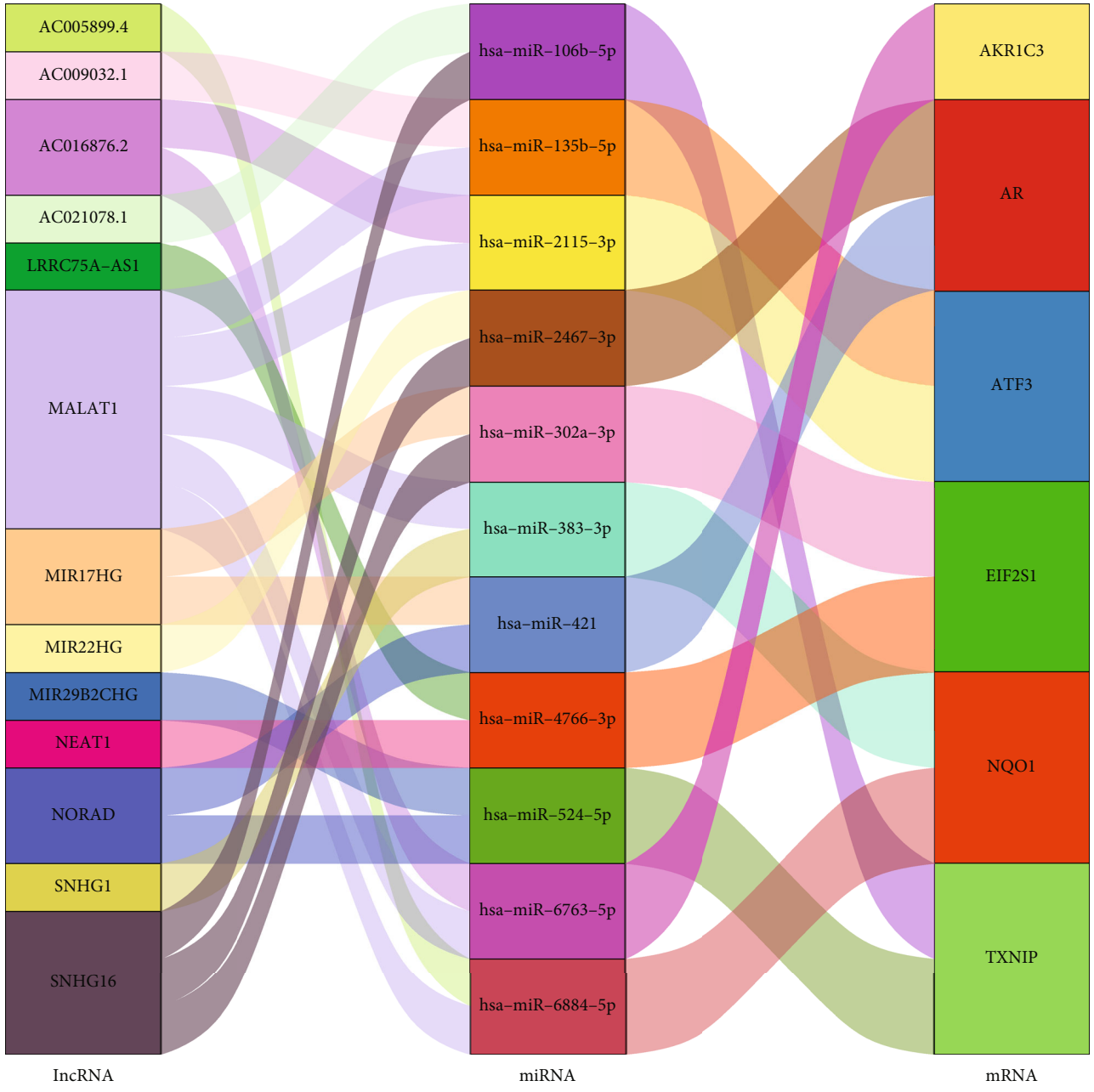

Figure 7: Potential lncRNA-miRNA-mRNA ceRNA network of ferroptosis key genes.

related to the onset of ferroptosis [28, 29]. Toll-like receptor-mediated signal promotes inflammatory response in IDD-related metabolic alterations and, thus, plays a role in IDD [30]. Next, we extracted FerrDb database genes and extracted FerrDEGs from the DEGs of GSE70362. These genes were enriched in biological processes and signal pathways related to ferroptosis through GO and KEGG analyses, proving that ferroptosis was involved in the IDD. Finally, we identified six key ferroptosis genes, ATF3, EIF2S1, NQO1, AR, TXNIP, and AKR1C3, through the PPI network and Cytoscape algorithm and the expression verification of GSE56081. And enrichment analysis of PPI subnetworks showed that subnetworks were mainly involved in endoplasmic reticulum stress, cell cycle, apoptotic signaling pathway, and iron overload, indicating these biological processes were important in IDD development.

ATF3, activating transcription factor 3, belongs to the ATF/cyclic AMP response element-binding (ATF/CREB) transcription factor family [31]. ATF3 has a close relationship with the Toll-like receptor signaling pathway, and ATF3 protein could inhibit the expression of many Toll-like receptor-driven proinflammatory genes [32]. Interestingly, as mentioned before, our GSEA showed that the degenerated nucleus pulposus was enriched with the Toll-like receptor signaling pathway. In the study of immune infiltration, we found that ATF3 was positively correlated with M2 macrophages, and as ATF3 level was downregulated in IDD, we speculated that the M2 functional state of

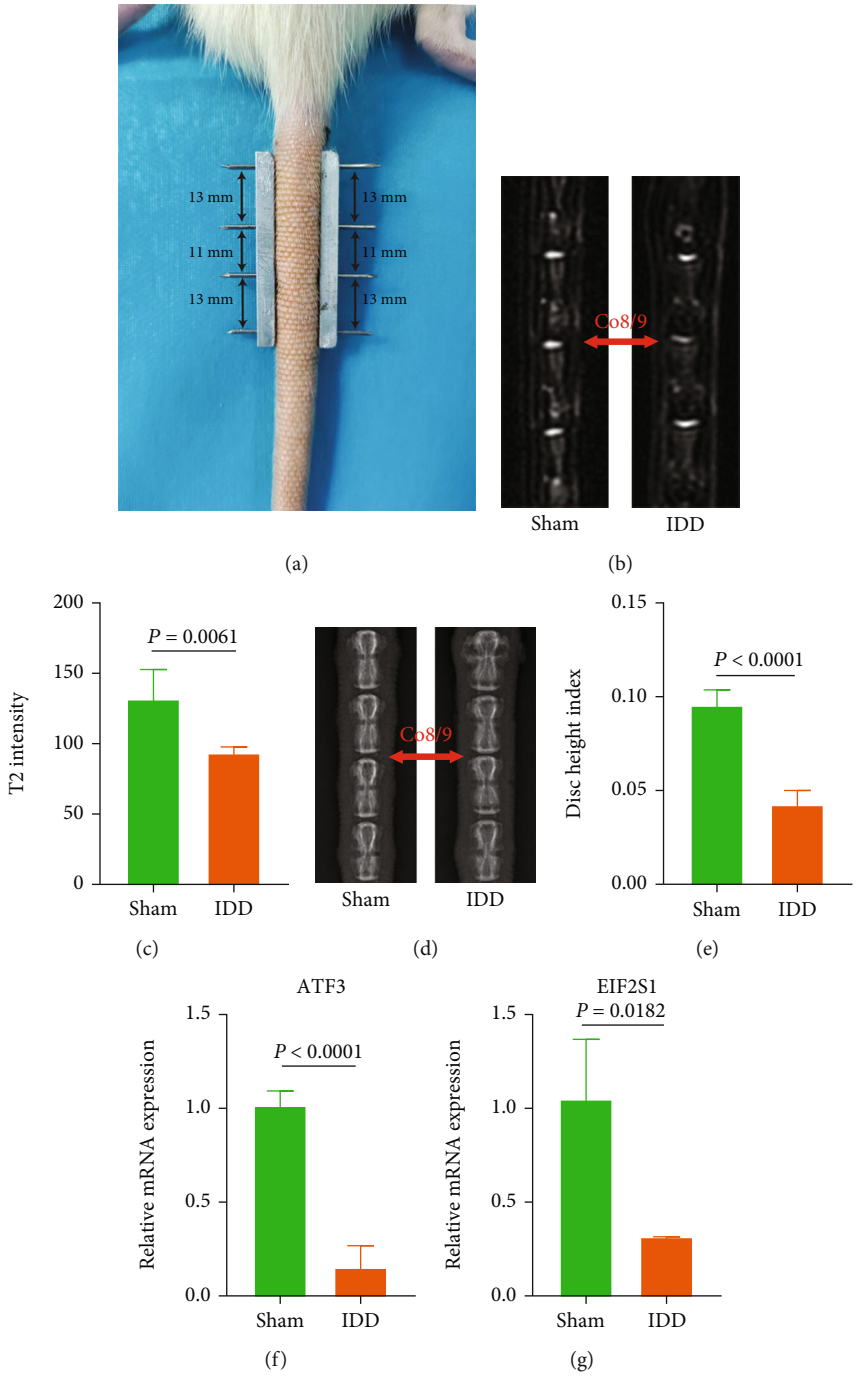

Figure 8: Continued.

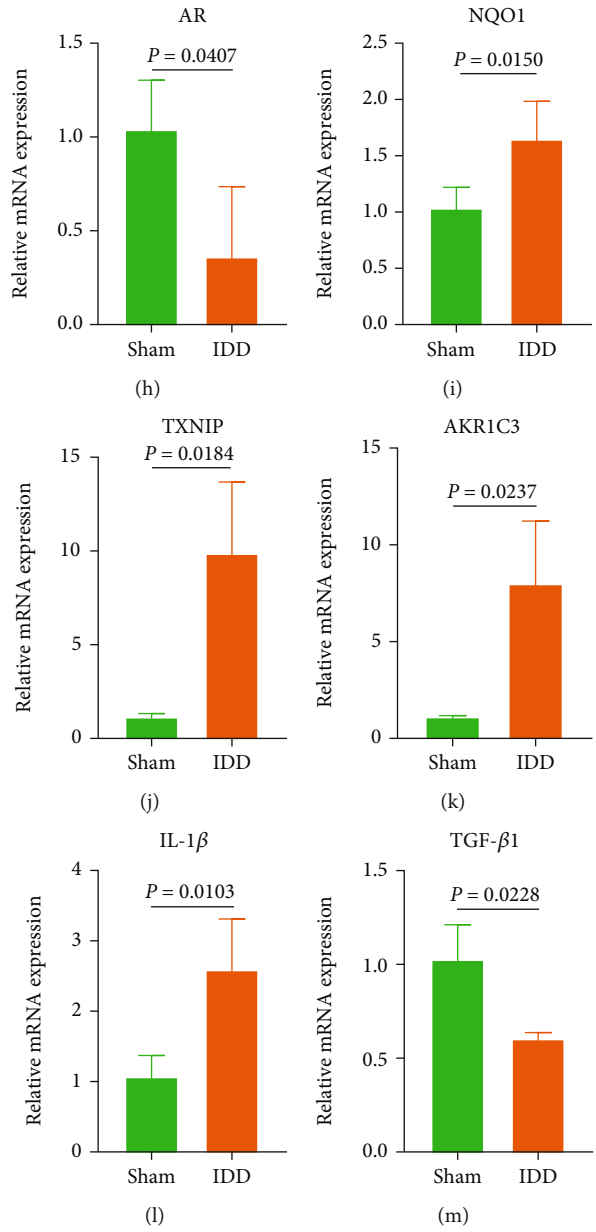

Figure 8: Validation of ferroptosis key genes in compression-induced IDD rats. (a) A compression device was fixed in the rat tail, and Co8-Co9 was compressed. (b) Representative MRI images of the Sham and IDD groups. (c) T2 intensity in the IDD group was significantly lower than that in the Sham group. (d) Representative X-ray images of the Sham and IDD groups. (e) DHI in the IDD group was significantly lower than that in the Sham group. (f–k) Ferroptosis key gene expression in compression-induced IDD rats. (l, m) IL-1β and TGF-β1 expression in compression-induced IDD rats.

intervertebral disc tissue decreased. These findings prove that ATF3, Toll-like receptor signaling pathway, M2 immune response, and ferroptosis play an essential role in IDD. Previous studies reported that ATF3, a wide range of stress sensors, could promote erastin-induced ferroptosis [33]. Meanwhile, several studies have shown that ATF3 knockdown could alleviate the progression of osteoarthritis [34], while some studies have shown that ATF3 is a highly conserved regenerative transcription factor in the vertebrate nervous system [35]. ATF3 protects retinal ganglion cells and promotes the functional preservation of optic nerve after crush [36]. However, only one study showed that ATF3 silencing could inhibit tert-Butyl Hydroperoxide- (TBHP-) induced IDD by inhibiting ferroptosis of nucleus pulposus cells [37]. Further, overexpression of ATF3 inhibits cardiomyocytes' ferroptosis induced by erastin and RSL3 [38]. In addition, ATF3 is a key transcriptional regulator and inhibits inflammatory response [39]. Furthermore, ATF3 can resist LPS-induced inflammatory response [40]. ATF3 could mediate prolonged expression of MMP13 and promote cell proliferation and collagen production in keloid fibroblast cells [41, 42]. Accordingly, the downregulating mechanism of ATF3 expression in IDD may be complex. In IDD, whether the downregulation of ATF3 expression

reduces the function of inhibiting inflammatory response, whether ATF3 promotes or inhibits ferroptosis, and the specific effect of ATF3 on extracellular matrix metabolism still need to be further explored.

EIF2S1, eukaryotic translation initiation factor 2 subunit-α, is a translation initiation factor [43], and phosphorylation of EIF2S1 is involved in neurodegenerative diseases [44]. EIF2S1 is an endoplasmic reticulum stress marker playing an essential role in maintaining lipid homeostasis [45]. Further, the EIF2S1-ATF4 pathway is closely related to autophagy [46]. EIF2S1 phosphorylation promotes ATF4 activation, increases glutathione synthesis, and improves antioxidant enzyme synthesis, thus, improving the ability of oxygen free radicals [47]. Due to this, the expression of EIF2S1 is downregulated in IDD, and we hypothesized that it might be unable to resist oxidative stress injury, aggravating the IDD progression.

NQO1, NAD (P) H: quinone oxidoreductase 1, plays a controlling role in redox modulation [48]. NQO1 is significantly induced during cell stress, which was verified by our dataset analysis and IDD model [49]. NQO1 has a protective effect on antioxidant stress. Thus, we speculated that the upregulation of NQO1 expression might play a role in inhibiting IDD. Moreover, acacetin alleviates reactive oxygen species produced by TBHP-stimulated nucleus pulposus cells by upregulating the antioxidant protein NQO1 [50]. However, there is little research on the effect of NQO1 in IDD currently, and the biological function of NQO1 still needs further investigation.

AR, androgen receptor, the member of the steroid hormone receptor superfamily, is a class of receptors that function by regulating the transcription of specific genes [51]. Interestingly, our GSEA also showed that IDD was enriched in steroid hormone biosynthesis. AR plays an essential role in many diseases, including complete androgen insensitivity syndrome, spinal bulbar muscular atrophy, prostate cancer, and breast cancer [52]. Several studies have shown that estrogen and its receptor could play a protective role in IDD [53, 54]. However, the relationship between AR and IDD has not been reported yet. An animal study investigating temporomandibular joint osteoarthritis reported that excessive mechanical stress stimulation was related to severe articular cartilage degeneration in the estrogen and androgen deficiency group [55]. Consistent with this work, AR was downregulated in our dataset analysis and compression-induced IDD model; we could speculate that androgen and AR might play a protective role in IDD, and the reduced expression of AR in IDD might lose its protective function and promote the progression of IDD.

AKR1C3, human Aldo-keto reductase family 1 member C3, is a hormone activity regulator [56]. On the one hand, AKR1C3 produces effective androgens in peripheral tissues and could activate AR [57]. Therefore, AKR1C3 might activate AR to protect the intervertebral disc from degeneration. And, the previous report has demonstrated that HOXB4 could serve as a transcriptional activator for AKR1C3 and suppress the ferroptosis of the H9C2 cells [58]. This suggests that the upregulation of AKR1C3 might inhibit ferroptosis in IDD somehow. On the other hand, AKR1C3 and β-catenin signaling may have a synergistic effect, and β-catenin signaling is often upregulated and contributes to IDD, suggesting AKR1C3 could promote IDD development through the β-catenin pathway [59, 60]. It seems that AKR1C3 cuts both ways in IDD. Therefore, we will design a thorough biological functional experiment to explore the mechanism of AKR1C3 in IDD.

TXNIP, thioredoxin interacting protein, is associated with neurodegenerative diseases [61]. TXNIP could promote nucleus pulposus cell pyroptosis, while TXNIP inhibitor Morin could alleviate nucleus pulposus cell pyroptosis [62]. TXNIP promotes oxidative stress by inhibiting the thioredoxin (TRX) system, and studies have shown that its expression is upregulated in brain diseases such as stroke [63]. In our study, TXNIP was upregulated in IDD in both databases and IDD models. Therefore, we could speculate that TXNIP may not only induce pyroptosis but also play an essential biological function in elevating ferroptosis through promoting oxidative stress in IDD.

Immune infiltration analysis is often used to analyze the distribution of immune cells in the microenvironment of tumors and other diseases [64]. We analyzed the immune infiltration of IDD and found that 16 types of immune cells were distributed in the intervertebral disc; not all immune cell types are expressed in the intervertebral disc, which might be determined by its own tissue characteristics. The intervertebral disc is a tissue with no blood supply and lymphatics [65]. The unique structures and molecular factors expressed in the intervertebral disc show inhibitory effects on immune cells and cytokine infiltration [16]. However, according to the correlation analysis of 16 immune cells, activated NK cells showed positive and negative correlations with resting and activated mast cells, respectively. Therefore, the function of NK cells is closely related to mast cells in intervertebral disc tissue. Furthermore, the correlation analysis between ferroptosis key genes and immune cells showed that ATF3 had the strongest positive correlation with M2 macrophages. EIF2S1 and activated dendritic cells showed the strongest negative correlation. Meanwhile, the expression of ATF3 and EIF2S1 was decreased in IDD, suggesting increased inflammation and reduced repair capability in IDD. Previous studies reported that ATF3 is a key transcriptional regulator that inhibits inflammatory response [39]. The ATF3 overexpression promotes macrophage migration and M2 phenotype, while the ATF3 knockdown leads to the opposite effect, which is consistent with our hypothesis [39]. Therefore, we investigated the IL-1β and TGF-β1 expression in the IDD model, and we found that IL-1β was significantly upregulated while TGF-β1 was significantly downregulated in IDD. We verified IL-1β and TGF-β1 expression in the IDD model and confirmed the above hypothesis.

ceRNA mechanism plays an essential role in treating many diseases, including IDD [66]. Using an online database, we could predict mRNA and its upstream miRNA and lncRNA. Among lncRNA, lncRNA MALAT1 showed the strongest association, followed by lncRNA SNHG16. Therefore, these genes might be involved in regulating ferroptosis genes in IDD. A previous study showed that

lncRNA MALT1 could suppress inflammation, inhibit nucleus pulposus cell apoptosis, promote cell proliferation, and attenuate aggrecan degradation [67]. Knockdown of lncRNA SNHG16 suppressed cell viability and induced apoptosis in chondrocytes [68]. Yet, there is no evidence about the biological function of lncRNA SNHG16 in IDD. However, this is a preliminary prediction and needs further experimental verification.

The limitation of the study was that we only verified the expression changes of ferroptosis key genes in IDD, and further experiments are needed to study their biological functions in IDD. In addition, the sample size of the dataset used in this study was small due to the lack of research on IDD in a public database. Meanwhile, obtaining normal human intervertebral disc tissue (control) is difficult and limits the progression of related research. Despite this, the animal model may cause inevitable bias as they have a different structure from the human sample. However, the compressive loading IDD model could lead to cell death and impaired matrix synthesis, and the IDD model has the advantage of controllability [69]. Therefore, we verified ferroptosis key genes in the compression-induced IDD rats. Besides, MRI and X-ray imaging confirmed that we successfully constructed the IDD model. In the follow-up study, complete biological function experiments are needed to investigate the role of these genes in IDD.

5. Conclusion

This study identified six ferroptosis key genes in IDD, their biological processes involved, and the correlation between immune infiltration cells, providing a reference for follow-up studies investigating the mechanism and treatment of IDD.

Data Availability

Data in this study are available from the corresponding authors upon reasonable request.

Conflicts of Interest

All authors declare that they have no conflicts of interest.

Authors' Contributions

Huilin Yang and Qin Shi conceived the research and revised the manuscript. Zongping Luo created the animal model. Jiangbo Guo conducted the bioinformatics analysis and experiment validation and drafted the manuscript. Yilin Yang and Junjie Niu contributed in the manuscript editing.

Acknowledgments

This work was supported by the National Natural Science Foundation of China (81972059, 82172485), the Social Development Project of Jiangsu Province (BK2019668), and the Priority Academic Program Development of Jiangsu Higher Education Institutions (PAPD).

Supplementary Materials

Supplementary Table 1: specific primers used for RT-qPCR. Supplementary Table 2: FerrDEGs of IDD. Supplementary Table 3: classification of FerrDEGs. Supplementary Figure 1: three subnetworks of PPI and Metascape enrichment analysis. (a, b, c) Three subnetworks of PPI. (d, e, f) Relevant Metascape enrichment analysis of each subnetwork. *(Supplementary Materials)*

References

[1] J. W. S. Vlaeyen, C. G. Maher, K. Wiech et al., "Low back pain," *Nature Reviews. Disease Primers*, vol. 4, no. 1, p. 52, 2018.

[2] J. Hartvigsen, M. J. Hancock, A. Kongsted et al., "What low back pain is and why we need to pay attention," *The Lancet*, vol. 391, no. 10137, pp. 2356–2367, 2018.

[3] N. N. Knezevic, K. D. Candido, J. W. S. Vlaeyen, J. Van Zundert, and S. P. Cohen, "Low back pain," *The Lancet*, vol. 398, no. 10294, pp. 78–92, 2021.

[4] S. Mohanty and C. L. Dahia, "Defects in intervertebral disc and spine during development, degeneration, and pain: new research directions for disc regeneration and therapy," *Wiley Interdisciplinary Reviews: Developmental Biology*, vol. 8, no. 4, article e343, 2019.

[5] P. H. Wu, H. S. Kim, and I. T. Jang, "Intervertebral disc diseases part 2: a review of the current diagnostic and treatment strategies for intervertebral disc disease," *International Journal of Molecular Sciences*, vol. 21, no. 6, p. 2135, 2020.

[6] P. Sampara, R. R. Banala, S. K. Vemuri, G. R. Av, and S. Gpv, "Understanding the molecular biology of intervertebral disc degeneration and potential gene therapy strategies for regeneration: a review," *Gene Therapy*, vol. 25, no. 2, pp. 67–82, 2018.

[7] S. Chen, X. Lv, B. Hu et al., "RIPK1/RIPK3/MLKL-mediated necroptosis contributes to compression-induced rat nucleus pulposus cells death," *Apoptosis*, vol. 22, no. 5, pp. 626–638, 2017.

[8] F. Zhang, X. Zhao, H. Shen, and C. Zhang, "Molecular mechanisms of cell death in intervertebral disc degeneration (review)," *International Journal of Molecular Medicine*, vol. 37, no. 6, pp. 1439–1448, 2016.

[9] K. Zhao, R. An, Q. Xiang et al., "Acid-sensing ion channels regulate nucleus pulposus cell inflammation and pyroptosis via the NLRP3 inflammasome in intervertebral disc degeneration," *Cell Proliferation*, vol. 54, no. 1, article e12941, 2021.

[10] B. Gan, "Mitochondrial regulation of ferroptosis," *The Journal of Cell Biology*, vol. 220, no. 9, article e202105043, 2021.

[11] M. Mazhar, A. U. Din, H. Ali et al., "Implication of ferroptosis in aging," *Cell Death Discovery*, vol. 7, no. 1, p. 149, 2021.

[12] X. Chen, J. Li, R. Kang, D. J. Klionsky, and D. Tang, "Ferroptosis: machinery and regulation," *Autophagy*, vol. 17, no. 9, pp. 2054–2081, 2021.

[13] R. Z. Yang, W. N. Xu, H. L. Zheng et al., "Involvement of oxidative stress-induced annulus fibrosus cell and nucleus pulposus cell ferroptosis in intervertebral disc degeneration pathogenesis," *Journal of Cellular Physiology*, vol. 236, no. 4, pp. 2725–2739, 2021.

[14] X. Zhang, Z. Huang, Z. Xie et al., "Homocysteine induces oxidative stress and ferroptosis of nucleus pulposus via enhancing methylation of GPX4," *Free Radical Biology & Medicine*, vol. 160, pp. 552–565, 2020.

[15] S. Lu, Y. Song, R. Luo et al., "Ferroportin-dependent iron homeostasis protects against oxidative stress-induced nucleus pulposus cell ferroptosis and ameliorates intervertebral disc degeneration in vivo," *Oxidative Medicine and Cellular Longevity*, vol. 2021, Article ID 6670497, 18 pages, 2021.

[16] Z. Sun, B. Liu, and Z. J. Luo, "The immune privilege of the intervertebral disc: implications for intervertebral disc degeneration treatment," *International Journal of Medical Sciences*, vol. 17, no. 5, pp. 685–692, 2020.

[17] L. Wang, T. He, J. Liu et al., "Revealing the immune infiltration landscape and identifying diagnostic biomarkers for lumbar disc herniation," *Frontiers in Immunology*, vol. 12, article 666355, 2021.

[18] F. Ye, F. J. Lyu, H. Wang, and Z. Zheng, "The involvement of immune system in intervertebral disc herniation and degeneration," *JOR Spine*, vol. 5, no. 1, article e1196, 2022.

[19] Z. Kazezian, R. Gawri, L. Haglund et al., "Gene expression profiling identifies interferon signalling molecules and IGFBP3 in human degenerative annulus fibrosus," *Scientific Reports*, vol. 5, no. 1, article 15662, 2015.

[20] V. K. Mootha, C. M. Lindgren, K. F. Eriksson et al., "PGC-1α-responsive genes involved in oxidative phosphorylation are coordinately downregulated in human diabetes," *Nature Genetics*, vol. 34, no. 3, pp. 267–273, 2003.

[21] A. Subramanian, P. Tamayo, V. K. Mootha et al., "Gene set enrichment analysis: a knowledge-based approach for interpreting genome-wide expression profiles," *Proceedings of the National Academy of Sciences of the United States of America*, vol. 102, no. 43, pp. 15545–15550, 2005.

[22] D. Szklarczyk, A. L. Gable, K. C. Nastou et al., "The STRING database in 2021: customizable protein-protein networks, and functional characterization of user-uploaded gene/measurement sets," *Nucleic Acids Research*, vol. 49, no. D1, pp. D605–D612, 2021.

[23] P. Shannon, A. Markiel, O. Ozier et al., "Cytoscape: a software environment for integrated models of biomolecular interaction networks," *Genome Research*, vol. 13, no. 11, pp. 2498–2504, 2003.

[24] J. H. Li, S. Liu, H. Zhou, L. H. Qu, and J. H. Yang, "starBase v2.0: decoding miRNA-ceRNA, miRNA-ncRNA and protein-RNA interaction networks from large-scale CLIP-Seq data," *Nucleic Acids Research*, vol. 42, no. D1, pp. D92–D97, 2014.

[25] Y. J. Che, J. B. Guo, T. Liang et al., "Assessment of changes in the micro-nano environment of intervertebral disc degeneration based on Pfirrmann grade," *The Spine Journal*, vol. 19, no. 7, pp. 1242–1253, 2019.

[26] Y. J. Che, J. B. Guo, T. Liang et al., "Controlled immobilization-traction based on intervertebral stability is conducive to the regeneration or repair of the degenerative disc: an in vivo study on the rat coccygeal model," *The Spine Journal*, vol. 19, no. 5, pp. 920–930, 2019.

[27] B. Han, K. Zhu, F. C. Li et al., "A simple disc degeneration model induced by percutaneous needle puncture in the rat tail," *Spine*, vol. 33, no. 18, pp. 1925–1934, 2008.

[28] S. R. A. El-Khalik, R. R. Ibrahim, M. T. A. Ghafar, D. Shatat, and O. S. El-Deeb, "Novel insights into the SLC7A11-mediated ferroptosis signaling pathways in preeclampsia patients: identifying pannexin 1 and toll-like receptor 4 as innovative prospective diagnostic biomarkers," *Journal of Assisted Reproduction and Genetics*, vol. 39, no. 5, pp. 1115–1124, 2022.

[29] P. Liao, W. Wang, W. Wang et al., "$CD8^+$ T cells and fatty acids orchestrate tumor ferroptosis and immunity via ACSL4," *Cancer Cell*, vol. 40, no. 4, pp. 365–378.e6, 2022.

[30] V. Francisco, J. Pino, M. A. Gonzalez-Gay et al., "A new immunometabolic perspective of intervertebral disc degeneration," *Nature Reviews Rheumatology*, vol. 18, no. 1, pp. 47–60, 2022.

[31] M. R. Thompson, D. Xu, and B. R. G. Williams, "ATF3 transcription factor and its emerging roles in immunity and cancer," *Journal of Molecular Medicine (Berlin, Germany)*, vol. 87, no. 11, pp. 1053–1060, 2009.

[32] N. D. Boespflug, S. Kumar, J. W. McAlees et al., "ATF3 is a novel regulator of mouse neutrophil migration," *Blood*, vol. 123, no. 13, pp. 2084–2093, 2014.

[33] L. Wang, Y. Liu, T. Du et al., "ATF3 promotes erastin-induced ferroptosis by suppressing system Xc^-," *Cell Death and Differentiation*, vol. 27, no. 2, pp. 662–675, 2020.

[34] T. Iezaki, K. Ozaki, K. Fukasawa et al., "ATF3 deficiency in chondrocytes alleviates osteoarthritis development," *The Journal of Pathology*, vol. 239, no. 4, pp. 426–437, 2016.

[35] H. R. Katz, A. A. Arcese, O. Bloom, and J. R. Morgan, "Activating transcription factor 3 (ATF3) is a highly conserved proregenerative transcription factor in the vertebrate nervous system," *Frontiers in Cell and Development Biology*, vol. 10, article 824036, 2022.

[36] C. Kole, B. Brommer, N. Nakaya et al., "Activating transcription factor 3 (ATF3) protects retinal ganglion cells and promotes functional preservation after optic nerve crush," *Investigative Ophthalmology & Visual Science*, vol. 61, no. 2, p. 31, 2020.

[37] Y. Li, D. Pan, X. Wang et al., "Silencing ATF3 might delay TBHP-induced intervertebral disc degeneration by repressing NPC ferroptosis, apoptosis, and ECM degradation," *Oxidative Medicine and Cellular Longevity*, vol. 2022, Article ID 4235126, 17 pages, 2022.

[38] H. Liu, H. Mo, C. Yang et al., "A novel function of ATF3 in suppression of ferroptosis in mouse heart suffered ischemia/reperfusion," *Free Radical Biology & Medicine*, vol. 189, pp. 122–135, 2022.

[39] H. Sha, D. Zhang, Y. Zhang, Y. Wen, and Y. Wang, "ATF3 promotes migration and M1/M2 polarization of macrophages by activating tenascin-C via Wnt/β-catenin pathway," *Molecular Medicine Reports*, vol. 16, no. 3, pp. 3641–3647, 2017.

[40] P. F. Lai, C. F. Cheng, H. Lin, T. L. Tseng, H. H. Chen, and S. H. Chen, "ATF3 protects against LPS-induced inflammation in mice via inhibiting HMGB1 expression," *Evidence-based Complementary and Alternative Medicine*, vol. 2013, Article ID 716481, 14 pages, 2013.

[41] C. M. Chan, C. D. Macdonald, G. J. Litherland et al., "Cytokine-induced *MMP13* expression in human chondrocytes is dependent on activating transcription factor 3 (ATF3) regulation," *The Journal of Biological Chemistry*, vol. 292, no. 5, pp. 1625–1636, 2017.

[42] X. M. Wang, X. M. Liu, Y. Wang, and Z. Y. Chen, "Activating transcription factor 3 (ATF3) regulates cell growth, apoptosis, invasion and collagen synthesis in keloid fibroblast through transforming growth factor beta (TGF-beta)/SMAD signaling pathway," *Bioengineered*, vol. 12, no. 1, pp. 117–126, 2021.

[43] J. Fucikova, O. Kepp, L. Kasikova et al., "Detection of immunogenic cell death and its relevance for cancer therapy," *Cell Death & Disease*, vol. 11, no. 11, p. 1013, 2020.

[44] S. Bond, C. Lopez-Lloreda, P. J. Gannon, C. Akay-Espinoza, and K. L. Jordan-Sciutto, "The integrated stress response and phosphorylated eukaryotic initiation factor 2α in neurodegeneration," *Journal of Neuropathology and Experimental Neurology*, vol. 79, no. 2, pp. 123–143, 2020.

[45] R. Anderson, A. Agarwal, A. Ghosh et al., "eIF2A-knockout mice reveal decreased life span and metabolic syndrome," *The FASEB Journal*, vol. 35, no. 11, article e21990, 2021.

[46] P. Sun, S. Zhang, X. Qin et al., "Foot-and-mouth disease virus capsid protein VP2 activates the cellular EIF2S1-ATF4 pathway and induces autophagy via HSPB1," *Autophagy*, vol. 14, no. 2, pp. 336–346, 2018.

[47] X. Bai, J. Ni, J. Beretov et al., "Activation of the eIF2α/ATF4 axis drives triple-negative breast cancer radioresistance by promoting glutathione biosynthesis," *Redox Biology*, vol. 43, article 101993, 2021.

[48] D. Ross and D. Siegel, "Functions of NQO1 in cellular protection and CoQ10 metabolism and its potential role as a redox sensitive molecular switch," *Frontiers in Physiology*, vol. 8, p. 595, 2017.

[49] D. Ross and D. Siegel, "The diverse functionality of NQO1 and its roles in redox control," *Redox Biology*, vol. 41, article 101950, 2021.

[50] H. Wang, Z. Jiang, Z. Pang, T. Zhou, and Y. Gu, "Acacetin alleviates inflammation and matrix degradation in nucleus pulposus cells and ameliorates intervertebral disc degeneration in vivo," *Drug Design, Development and Therapy*, vol. 14, pp. 4801–4813, 2020.

[51] C. Chang, A. Saltzman, S. Yeh et al., "Androgen receptor: an overview," *Critical Reviews in Eukaryotic Gene Expression*, vol. 5, no. 2, pp. 97–125, 1995.

[52] Y. Koryakina, H. Q. Ta, and D. Gioeli, "Androgen receptor phosphorylation: biological context and functional consequences," *Endocrine-Related Cancer*, vol. 21, no. 4, pp. T131–T145, 2014.

[53] Q. Liu, X. Wang, Y. Hua et al., "Estrogen deficiency exacerbates intervertebral disc degeneration induced by spinal instability in rats," *Spine*, vol. 44, no. 9, pp. E510–E519, 2019.

[54] M. X. Song, X. X. Ma, C. Wang et al., "Protective effect of estrogen receptors (ERα/β) against the intervertebral disc degeneration involves activating CCN5 via the promoter," *European Review for Medical and Pharmacological Sciences*, vol. 25, no. 4, pp. 1811–1820, 2021.

[55] T. Ootake, T. Ishii, K. Sueishi et al., "Effects of mechanical stress and deficiency of dihydrotestosterone or 17β-estradiol on temporomandibular joint osteoarthritis in mice," *Osteoarthritis and Cartilage*, vol. 29, no. 11, pp. 1575–1589, 2021.

[56] Y. Liu, S. He, Y. Chen et al., "Overview of AKR1C3: inhibitor achievements and disease insights," *Journal of Medicinal Chemistry*, vol. 63, no. 20, pp. 11305–11329, 2020.

[57] T. M. Penning, "AKR1C3 (type 5 17β-hydroxysteroid dehydrogenase/prostaglandin F synthase): roles in malignancy and endocrine disorders," *Molecular and Cellular Endocrinology*, vol. 489, pp. 82–91, 2019.

[58] J. Liang, Y. Cao, M. He et al., "AKR1C3 and its transcription factor HOXB4 are promising diagnostic biomarkers for acute myocardial infarction," *Frontiers in Cardiovascular Medicine*, vol. 8, article 694238, 2021.

[59] J. Chen, Z. Mei, B. Huang et al., "IL-6/YAP1/β-catenin signaling is involved in intervertebral disc degeneration," *Journal of Cellular Physiology*, vol. 234, no. 5, pp. 5964–5971, 2019.

[60] W. Xiong and X. H. W. Hu, "AKR1C3 and β-catenin expression in non-small cell lung cancer and relationship with radiation resistance," *Journal of BUON*, vol. 26, no. 3, pp. 802–811, 2021.

[61] H. Tsubaki, I. Tooyama, and D. G. Walker, "Thioredoxin-interacting protein (TXNIP) with focus on brain and neurodegenerative diseases," *International Journal of Molecular Sciences*, vol. 21, no. 24, p. 9357, 2020.

[62] Y. Zhou, Z. Chen, X. Yang et al., "Morin attenuates pyroptosis of nucleus pulposus cells and ameliorates intervertebral disc degeneration via inhibition of the TXNIP/NLRP3/Caspase-1/IL-1β signaling pathway," *Biochemical and Biophysical Research Communications*, vol. 559, pp. 106–112, 2021.

[63] S. Nasoohi, S. Ismael, and T. Ishrat, "Thioredoxin-interacting protein (TXNIP) in cerebrovascular and neurodegenerative diseases: regulation and implication," *Molecular Neurobiology*, vol. 55, no. 10, pp. 7900–7920, 2018.

[64] G. Sokratous, S. Polyzoidis, and K. Ashkan, "Immune infiltration of tumor microenvironment following immunotherapy for glioblastoma multiforme," *Human Vaccines & Immunotherapeutics*, vol. 13, no. 11, pp. 2575–2582, 2017.

[65] R. D. Bowles and L. A. Setton, "Biomaterials for intervertebral disc regeneration and repair," *Biomaterials*, vol. 129, pp. 54–67, 2017.

[66] J. Zhu, X. Zhang, W. Gao, H. Hu, X. Wang, and D. Hao, "lncRNA/circRNA-miRNA-mRNA ceRNA network in lumbar intervertebral disc degeneration," *Molecular Medicine Reports*, vol. 20, no. 4, pp. 3160–3174, 2019.

[67] H. Zhang, J. Li, D. Duan, W. She, L. Wang, and F. Zhang, "The role of lncRNA MALAT1 in intervertebral degenerative disc disease," *International Journal of Clinical and Experimental Pathology*, vol. 10, no. 10, pp. 10611–10617, 2017.

[68] W. Cheng, C. Y. Hao, S. Zhao, L. L. Zhang, and D. Liu, "SNHG16 promotes the progression of osteoarthritis through activating microRNA-93-5p/CCND1 axis," *European Review for Medical and Pharmacological Sciences*, vol. 23, no. 21, pp. 9222–9229, 2019.

[69] M. A. Adams and P. J. Roughley, "What is intervertebral disc degeneration, and what causes it?," *Spine*, vol. 31, no. 18, pp. 2151–2161, 2006.

Hindawi
Oxidative Medicine and Cellular Longevity
Volume 2022, Article ID 1372483, 35 pages
https://doi.org/10.1155/2022/1372483

Research Article

Integrative Bioinformatics Analysis Revealed Mitochondrial Dysfunction-Related Genes Underlying Intervertebral Disc Degeneration

Zhengya Zhu,[1] **Zhongyuan He**,[1,2] **Tao Tang**,[1,2] **Fuan Wang**,[1,2] **Hongkun Chen**,[1] **Baoliang Li**,[1,2] **Guoliang Chen**,[1,2] **Jianmin Wang**,[1] **Wei Tian**,[3] **Dafu Chen**,[3] **Xinbao Wu**,[3] **Xizhe Liu**,[2] **Zhiyu Zhou**,[1,2] **and Shaoyu Liu**[1,2]

[1]*Innovation Platform of Regeneration and Repair of Spinal Cord and Nerve Injury, Department of Orthopaedic Surgery, The Seventh Affiliated Hospital, Sun Yat-Sen University, Shenzhen 518107, China*
[2]*Guangdong Provincial Key Laboratory of Orthopedics and Traumatology, Orthopaedic Research Institute/Department of Spinal Surgery, The First Affiliated Hospital of sun Yat-Sen University, Guangzhou 510080, China*
[3]*Laboratory of Bone Tissue Engineering, Beijing Laboratory of Biomedical Materials, Beijing Research Institute of Orthopaedics and Traumatology, Beijing Jishuitan Hospital, Beijing 100035, China*

Correspondence should be addressed to Xizhe Liu; liuxizhe@mail.sysu.edu.cn and Zhiyu Zhou; zhouzhy23@mail.sysu.edu.cn

Received 6 July 2022; Accepted 15 August 2022; Published 11 October 2022

Academic Editor: Xiaolong Chen

Objective. Mitochondrial dysfunction plays an important role in intervertebral disc degeneration (IDD). We aim to explore the pathways and key genes that cause mitochondrial dysfunction during IDD and to further reveal the pathogenesis of IDD based on bioinformatic analyses. *Methods*. Datasets GSE70362 and GSE124272 were downloaded from the Gene Expression Omnibus. Differentially expressed genes (DEGs) of mitochondrial dysfunction between IDD patients and healthy controls were screened by package limma package. Critical genes were identified by adopting gene ontology (GO), Kyoto encyclopedia of genes and genomes (KEGG) pathways, and protein-protein interaction (PPI) networks. We collected both degenerated and normal disc tissues obtained surgically, and we performed western blot and qPCR to verify the key DEGs identified in intervertebral disc tissues. *Results*. In total, 40 cases of IDD and 24 healthy controls were included. We identified 152 DEGs, including 67 upregulated genes and 85 downregulated genes. Four genes related to mitochondrial dysfunction (SOX9, FLVCR1, NR5A1 and UCHL1) were screened out. Of them, SOX9, FLVCR1, and UCHL1 were down-regulated in peripheral blood and intervertebral disc tissues of IDD patients, while NR5A1 was up-regulated. The analysis of immune infiltration showed the concentrations of mast cells activated were significantly the highest in IDD patients. Compared with the control group, the level of T cells CD4 memory resting was the lowest in the patients. In addition, 24 cases of IDD tissues and 12 cases of normal disc tissues were obtained to verify the results of bioinformatics analysis. Both western blot and qPCR results were consistent with the results of bioinformatics analysis. *Conclusion*. We identified four genes (SOX9, FLVCR1, NR5A1 and UCHL1) associated with mitochondrial dysfunction that play an important role in the progress of disc degeneration. The identification of these differential genes may provide new insights for the diagnosis and treatment of IDD.

1. Introduction

Low back pain (LBP) is a common muscle bone disease that causes physical pains to patients and severe economic burden to the society [1, 2]. Intervertebral disc degeneration (IDD), as one major cause of LBP, is featured by structural destruction, apoptosis of nucleus pulposus cells, release of proinflammatory cytokines, and extracellular matrix degradation in the intervertebral disc [3, 4]. So far, the concrete pathology of IDD is unclear, and the clinical treatment strategies are mainly targeted at conservative treatment or surgical intervention for symptom relieving. Nevertheless, nearly

20% of IDD patients respond badly to non-surgical therapy [5]. Thus, further clarifying the molecular mechanism of IDD is a new route for precise intervention of LBP.

A normal intervertebral disc is anatomically composed of gelatinous nucleus pulposus (NP) in the center and annulus fibrosus tissues in the periphery, and is assisted by cartilaginous endplates (CEP) to enhance its mechanical strength. The intervertebral disc (especially nucleus pulposus tissues) is critical in maintaining the physiological functions of the spine, and can absorb and disperse the machinery loads of the spine that moves at all directions [6]. Intervertebral disc, the largest vessel-free organ in the human body, acquires energy mainly through anaerobic glycolysis [7], and mitochondria are critical in supply energy for the intervertebral disc to maintain normal physiological functions [5]. In addition to matter and energy metabolism, mitochondria are involved in regulation and control of second messenger functions, such as release of reactive oxygen species (ROS) and calcium ions, and further activate various signaling pathways to maintain the steady functions of nucleus pulposus cells. Reportedly, the mitochondria in the NP cells of IDD patients are structurally and functionally abnormal, and mitochondrial dysfunction may be one of the causes that accelerate the progression of IDD. As a by-product of aerobic respiration, ROS is mainly produced in the mitochondria by the electron transport chain and other mitochondrial located proteins. With the excessive accumulation of ROS, mitochondria are the main target of ROS attack in disc cells [8].

In this study, we screened out the differential expressions of mitochondrial genes, between normal people and IDD patients in both intervertebral disc tissues and peripheral blood, from the transcriptome sequencing gene data of Gene Expression Omnibus (GEO). The key pathways and proteins were identified from analysis of gene ontologies (GOs), Kyoto Encyclopedia of Genes and Genomes (KEGG) pathways, protein-protein interaction (PPI) networks, and some other bioinformatics analysis tools that offer a new clue to uncover the pathogenesis of IDD and theoretically underlies intervertebral disc repair and regeneration.

2. Materials and Methods

2.1. Data Downloading. Datasets GSE70362 [9] and GSE124272 [10, 11] were downloaded from GEO. GSE70362 containing 32 cases of IDD and 16 control cases was obtained from the GPL17810 sequencing platform. The GSE124272 containing 8 cases of IDD and 8 control cases was acquired from the GPL21185 sequencing platform. All cases were of human source. The above two datasets were integrated for downstream analysis. The batch effect between datasets was calibrated using package SVA of R language [12] and the data were normalized using log2. The expression distribution after the above processing was visualized in box plots, including 40 IDD cases and 24 control cases.

To analyze the expressions of mitochondrial dysfunction genes in all samples, we first identified 11 mitochondrial dysfunction genes from database GeneCards [13] by using keyword 'Mitochondrial dysfunction' (CGB5, KIT, FLVCR1, SP1, SOX9, UCHL1, CYP21A2, NR5A1, DAZ4, DHH, POMK). Then after intersection with the existing expression profiles, 9 genes were left (KIT, FLVCR1, SP1, SOX9, UCHL1, CYP21A2, NR5A1, DHH, POMK).

2.2. Panorama of Mitochondrial Dysfunction Genes. To further explore the correlations of mitochondrial dysfunction genes in all patients, we calculated the Pearson correlations between genes. The absolute value of correlation coefficient larger than 0.3 and $p < 0.05$ indicate the presence of correlation. The correlations between qualified genes were plotted on the R package ggplot2 [14].

To analyze the effects of expressions of mitochondrial functional genes on IDD, we analyzed the differentially expressed genes (DEGs) between the IDD group and the control group using the integrated dataset on the R package limma [15] and screened out the significant genes. The thresholds were absolute value of log2 (fold change) (log2FC) >1.5 and Padj<0.05. The genes with log2FC>1.5 and Padj<0.05 were upregulated, and the genes with log2FC< -1.5 and Padj<0.05 were downregulated. Especially, the volcano plots show the downregulated or upregulated DEGs. The heatmaps of all these DEGs in all samples were plotted on the R package pheatmap [16]. To analyze the expressions of mitochondrial dysfunction genes between the control and tested groups, we plotted the box plots of the two groups using the R package ggpubr [17]. The two groups were compared using Wilcoxon rank sum test. The significant level was $p < 0.05$.

Protein-protein interaction (PPI) networks are formed from the interactions of single proteins, and participate in all steps of the life process, including biosignal transfer, gene expression regulation, energy and substance metabolism, and cell cycle regulation. Systematic analysis of interactions among abundant proteins in biosystems is contributive to understanding the rationale of proteins in biosystems, clarifying the mechanisms of biosignals and energy/substance metabolism in special physiological states such as diseases, and for knowing the functional associations between proteins. STRING is a database for searching known PPIs and predicting PPIs [18]. We used STRING and chose the genes with combined score larger than 400 to build a network of interactions between DEG-related proteins. The PPI network was visualized on Cytoscape 3.7.2 [19].

2.3. Diagnostic Model Based on Mitochondrial Dysfunction Genes. Given the influence of mitochondrial dysfunction, the control samples and tested samples may contain different mitochondrial dysfunction genes that show different statuses. Hence, it is highly feasible to build a diagnostic model based on mitochondrial dysfunction genes.

Here, we first used ridge regression to screen all mitochondrial dysfunction genes on the R package glmnet [20], and found out the optimal λ. After the regression, the genes with coefficient not being 0 were remained. Then the genes were further screened through logistics regression. The genes chosen for modeling and their coefficients were displayed as forest map on the R package forestplot [21].

After that, to identify the multifactor influence of feature genes in the diagnostic model, we chose the genes with large absolute weights in the previous model on the R package rms [22] and built a new logistics multifactor regression model. To validate the predictive efficacy of the new diagnostic model, we plotted receiver's operating characteristic curve (ROC) and calculated the area under curve (AUC) on the R package pROC [23].

2.4. Gene Set Enrichment Analysis. To further uncover the biological differences between the tested samples and the control samples, we subjected the DEGs to gene set enrichment analysis (GSEA).

GSEA is a commonly-used method for large-scale function enrichment analysis at different dimensions and levels, and usually involves three aspects: bioprocesses, molecular functions, and cell components [24]. KEGG is a widely-used database that stores information of genome, biological pathways, diseases, and drugs [25]. All significant DEGs were subjected to GO function annotation and KEGG pathway enrichment analyses on the R package clusterprofiler [26, 27] to identify the significantly enriched bioprocesses. The results were visualized as bar charts and bubble plots. The significant threshold of enrichment analysis was set at adjusted $p < 0.05$.

Gene enrichment analysis determines whether a preset gene is significantly different between two biological states, and is often used to estimate the changes in pathways and bioprocesses in a dataset [28]. To study the differences in bioprocesses between two groups, we chose the gene profile dataset, and downloaded reference gene sets 'c5.go.v7.4.entrez.gmt' and 'c2.cp.kegg.v7.4. entrez.gmt' from database MSigDB [29]. The datasets were enriched and visualized using the GSEA from the R package clusterprofiler. The significant level was set at adjusted $p < 0.05$.

GSVA, the gene set variation analysis [30] and a nonparametric unsupervised method, converts the between-sample gene expression matrix into a between-sample gene set expression matrix, and thereby evaluates the gene set enrichment of chip nucleolus transcriptome. GSVA is used to evaluate whether a pathway is enriched between samples. Gene sets 'c5.go.v7.4.entrez.gmt' and 'c2.cp.kegg.v7.4. entrez.gmt' acquired from database MSigDB were sent to GSVA at the gene expression level, and thereby, the function enrichment differences were compared between two types of tissues.

2.5. WGCNA. Weighted gene correlation network analysis (WGCNA), a systematic biological method to describe gene association modes between samples, can identify the gene sets with highly collaborative changes, and identify the candidate biological marker genes or therapeutic targets according to the internality of gene sets and to the associations between gene sets and phenotypes [31]. The correlated key gene sets between the tested and control groups were identified using the R package WGCNA [31], which were used in subsequent analysis.

2.6. Protein-Protein Interaction (PPI) Network. The gene expressions are universally and mutually associated, and especially, the genes that regulate the same biological process are highly associated. Hence, to uncover the gene associations in the tested group or the control group through WGCNA, we built a PPI network.

Table 1: Primers used for RT-qPCR.

FLVCR1	F:5′- GGAACTTGAATCCAGCCAGAGAA -3′
	R:5′- GTCCGTTGTATCCATAAGGTAGCA -3′
NR5A1	F:5′- GACAGGGAGAAGTTGAGCAGGTAT -3′
	R:5′- TTGGGTGGGAGAGGGAATCAGT -3′
UCHL1	F:5′- GCTCAAGCCGATGGAGATCAAC -3′
	R:5′- ACTGCGTGAATAAGTCCGATTGTG -3′
SOX9	F:5′- GAGCAGCGAAATCAACGAGAAACT -3′
	R:5′- ACAAAGTCCAAACAGGCAGAGAGA -3′
GAPDH	F:5′- ACTTTGGTATCGTGGAAGGACTCA -3′
	R:5′- CCAGTAGAGGCAGGGATGATGTT -3′

The above genes from the database STRING [32] were inputted to build a PPI network at the default confidence level of 0.4. Then the PPI was outputted. Further analysis was done on Cytoscape [19]. The network attributes of nodes were calculated, and the hub nodes were identified with node degrees as the standard on the package Cytohubba [33]. The top 10 nodes ranked by the node degree were classified as the hub nodes. These nodes were highly associated with other nodes and thus may play critical roles in the regulation and control of all biological processes, which are worth of further research.

2.7. Identification and Correlation Analysis of Immune Infiltrating Cells. The immune microenvironment mainly consists of immune cells, inflammatory cells, fibroblasts, interstitium samples, and various cytokines and chemokines, and thus is a loaded comprehensive system. The infiltration analysis of immune cells is pivotal in disease research and prediction of therapeutic prognosis. CIBERSORT is an algorithm for deconvolution of expression matrix of immune cell subtypes according to the rationale of linear support vectors, and uses RNA-Seq data to estimate the abundance of immune cells in samples [34]. The CIBERSORT from R language [34] was used to calculate the abundance of 22 types of immune cells between the tested group and the control group, and the composition of immune cells was visualized as box plots. The differences in proportions of immune cells were calculated using Wilcoxon test, at the significant level of $P < 0.05$.

2.8. Unsupervised Clustering. Because of ubiquitous heterogeneity among patients, such heterogeneity can be interpreted using unsupervised clustering of samples according to hub genes, and the samples were reclassified. This classification can help us to comprehensively understand the mechanism of mitochondrial dysfunction in different modes of disc degeneration.

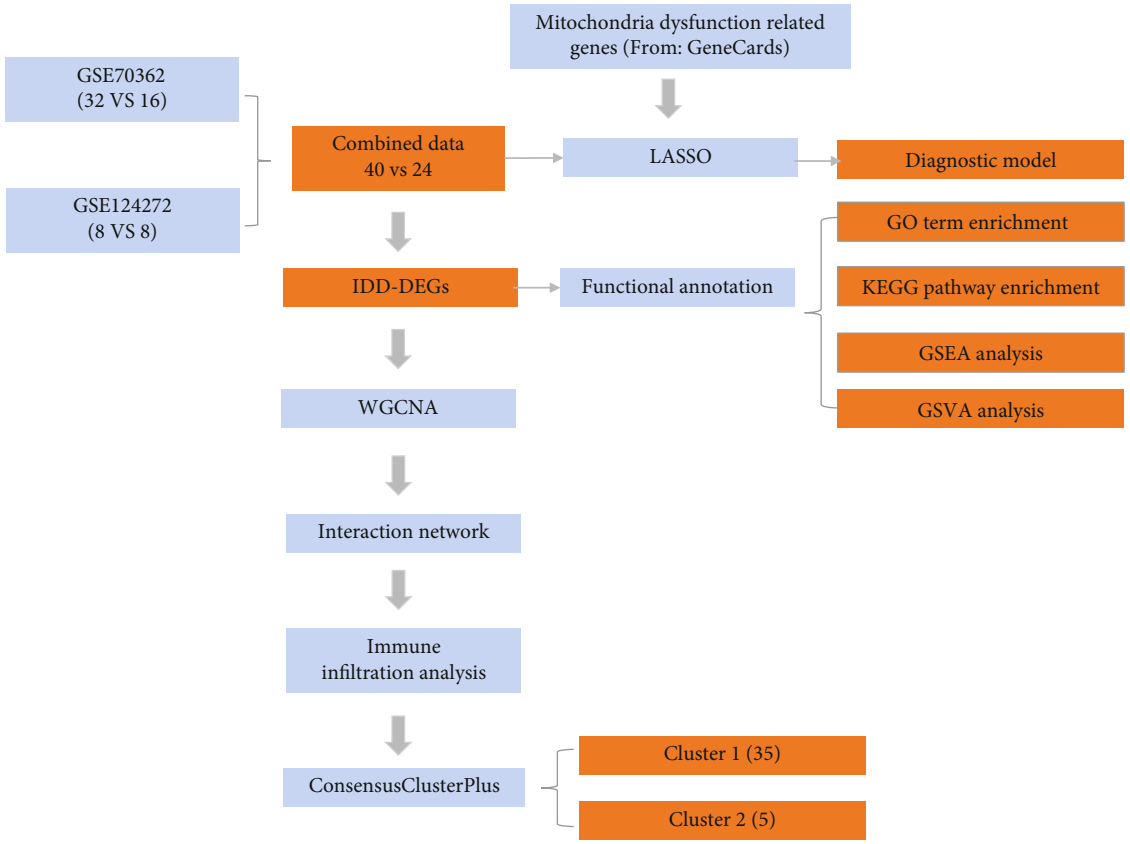

Figure 1: Flow diagram presenting the main plan and process of the study.

First, the optimal number of clusters was determined using the R package factoextra [35]. After that, all patients were clustered in an unsupervised way using k-mean clustering. The samples were classified into 2 clusters, and the final clustering effect was examined using factoextra. The expressions of the 10 hub genes between the two groups were displayed as heatmaps. Histograms of groups were plotted on R package ggpubr [17] with the sample clustering label. The two groups were compared using Wilcoxon rank sum test at the significant level $p < 0.05$.

2.9. RNA Extraction and Real-Time Quantitative Polymerase Chain Reaction (RT-qPCR). The ethics approvals were provided by the institutional review board of the Seventh Affiliated Hospital of Sun Yat-sen University (KY-2021-030-01). All enrolled patients provided written informed consent for the research protocol. The degree of IDD was determined by magnetic resonance imaging (MRI) following Pfirrmann classification [36]. Tissues of Pfirrmann I-II were used as controls. Human lumbar disc tissues were obtained from patients who underwent spinal canal decompression treatment. The nucleus pulposus and annulus fibrosus tissues were separated and RNA was extracted directly from tissues according to a previous protocol [37]. In brief, 150 mg of a sample was cut up and then digested with 2 mg/ml pronase at 37°C, flash-frozen, pulverized in liquid nitrogen, and homogenized with a tissue lyser. Total RNA was extracted using a TRI Reagent (Invitrogen, USA) and 400 ng of RNA was then converted to cDNA using a cDNA synthesis kit (Takara, Japan).

RT-qPCR was performed using Power Up SYBR Green Master Mix (Thermo Fisher Scientific, USA) on a real-time system (Bio-Rad, USA). As described in the protocol, each reaction mixture consisted of 5 μl of 2 × Power Up SYBR Green Master Mix, 2 μl of nuclease-free water, 0.5 μl of each of 10 μM forward and reverse primers and 2 μl of cDNA. The applied cycle conditions were: 50°C for 2 min and 95°C for 2 min followed by 44 cycles of 15 s at 95°C and 1 min at 60°C. The specific primers used here were designed using Primer 6.0 (Applied Biosystems, CA), and the sequences are provided in Table 1. Results were normalized to housekeeping gene glyceraldehyde 3-phosphate dehydrogenase (GAPDH) expression using the $2^{-\Delta\Delta Ct}$ algorithm.

2.10. Extraction and Culture of Primary Intervertebral Disc Cells. NP tissues and AF tissues were digested using 2 mg/ml type II collagenase (Gibco, USA) at 37°C. After washing with PBS, the digested tissues were transferred to DMEM/F12 (Gibco, USA) containing 10% fetal bovine serum (Gibco, USA) and 1% penicillin/streptomycin (Gibco, USA) in the incubator at 5% CO_2 and 37°C. The cells at the confluent stage were passaged after digestion with 0.25% Trypsin-EDTA (Gibco, USA). Cells after the second passage were used in the following experiments.

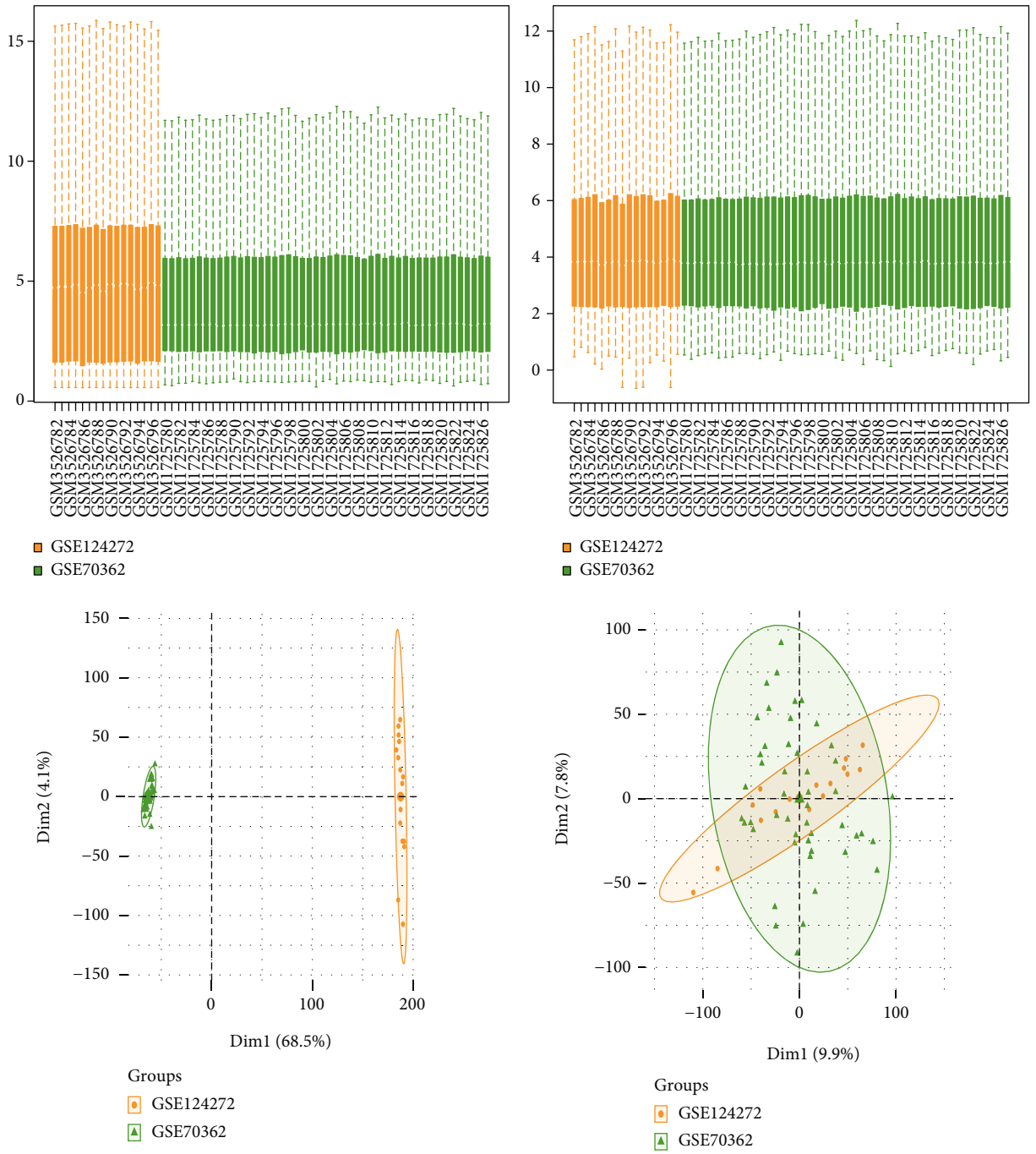

(a)

Figure 2: Continued.

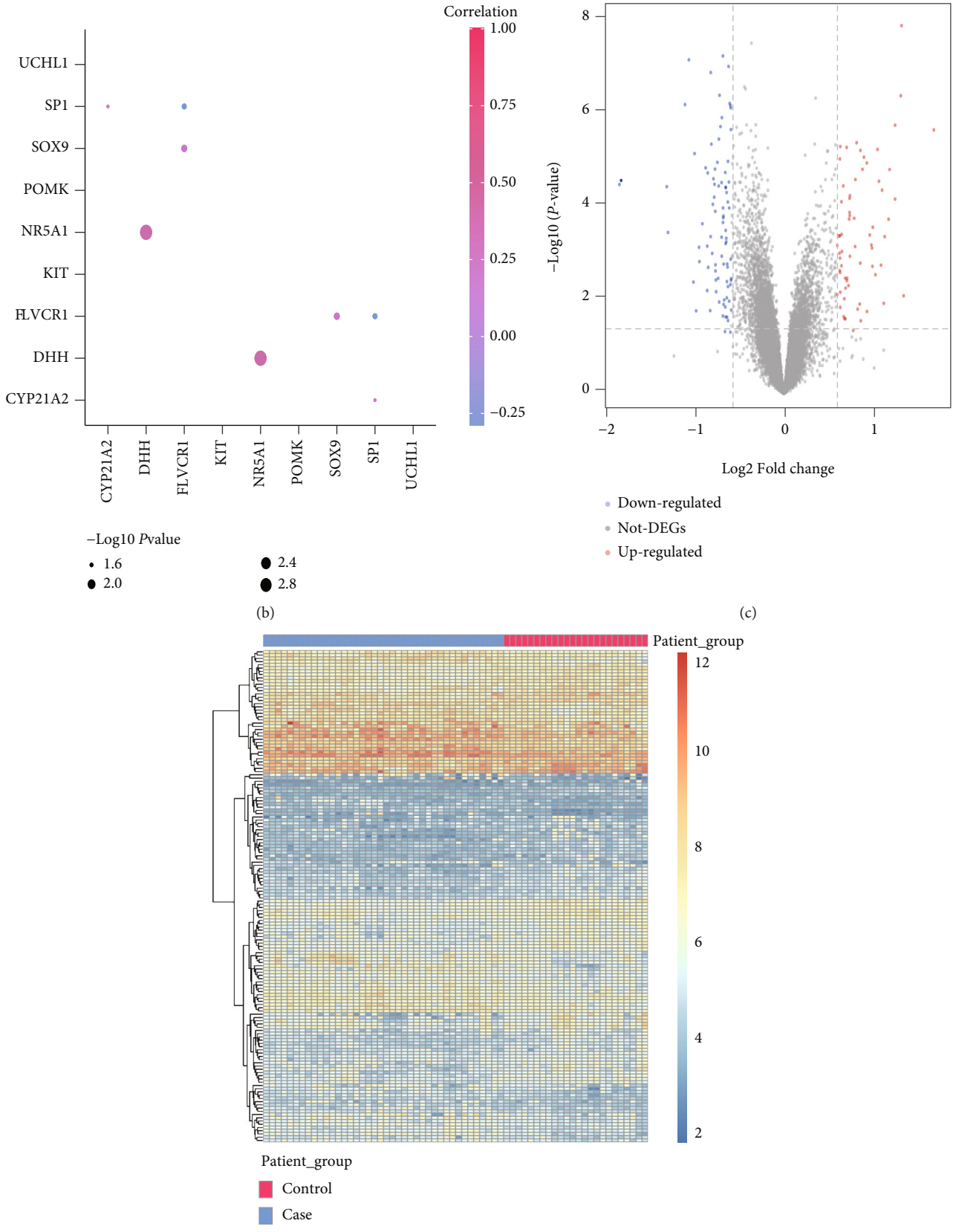

Figure 2: Continued.

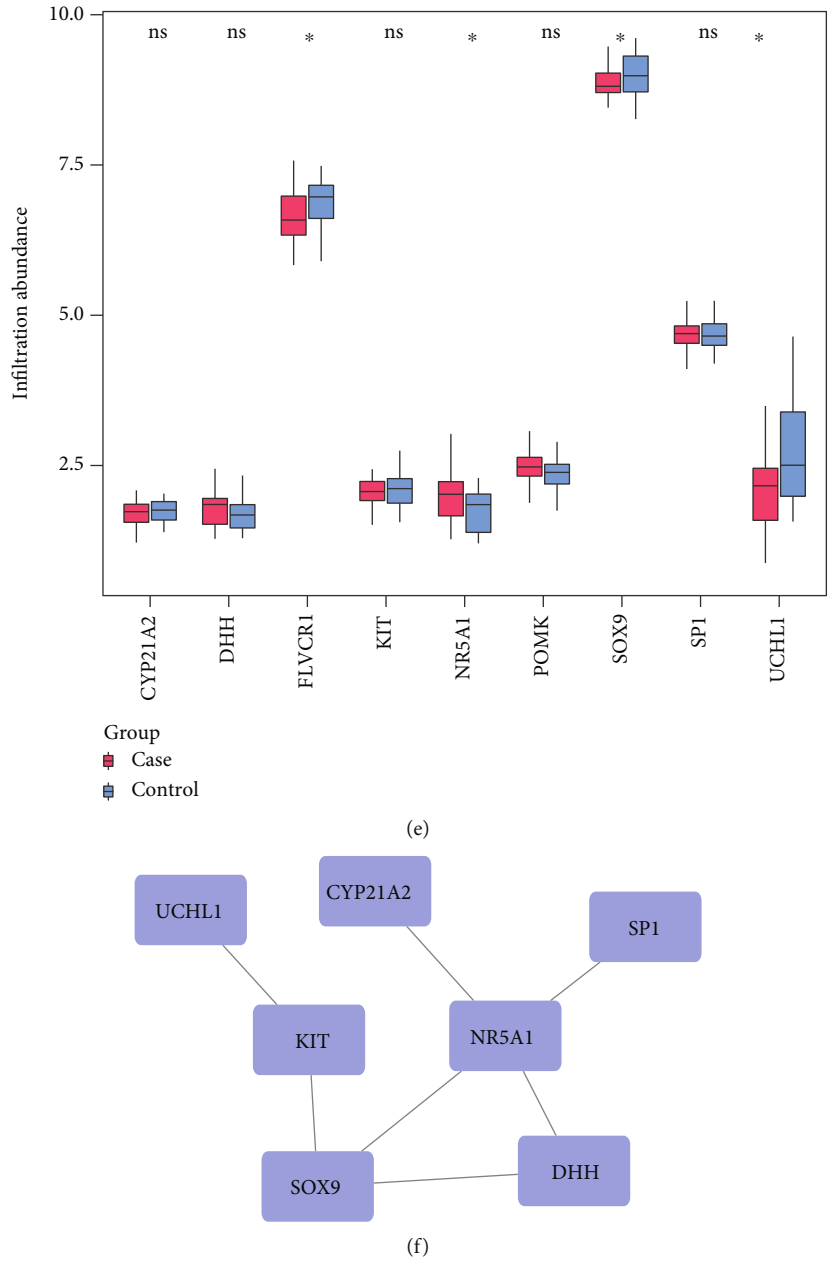

Figure 2: Genes related to mitochondrial dysfunction. (a): box plot and PCA of gene expressions before and after batch effect removal in the GEO data. (b): correlations among mitochondrial dysfunction genes. Colors indicate correlations. A pinker color means stronger correlation. Node size indicates -log10 (*P*-value), and a larger node means higher significance. (c): volcano plots of DEGs, *x*-axis: log2FoldChange, *y*-axis: -log10 (adjust P-value); red, gray and blue nodes indicate the differentially expressed genes are upregulated, insignificant, and downregulated, respectively. (d): heat maps of DEGs, blue: degeneration group, red: control group. (e): histograms of expressions of mitochondrial dysfunction genes in test group and control group; *x*-axis: mitochondrial dysfunction genes, *y*-axis: gene expression level; red: test group, blue: control group. P <0.05: significant level. (f): PPI network of mitochondrial dysfunction genes.

2.11. Total Protein Extraction and Western Blot. Total proteins were extracted with an RIPA buffer (Thermo Fisher Scientific, USA) and the concentrations were determined by a BCA kit (Boster, China). Proteins were electrophoresed in premade polyacrylamide gels containing SDS, and transferred to polyvinylidene fluoride(PVDF)membranes from the gels. After blocking with 5% non-fat milk (Solarbio, China) for 1 h, the PVDF membranes were incubated with primary antibody overnight at 4°C and then incubated with secondary antibody (coupled with horseradish peroxidase) for 1 h at room temperature. The protein signal was visualized by an ECL chemiluminescence kit (EpiZyme, China), and the grayscale of band was quantified using Image J.

2.12. Statistical Analysis. All data were analyzed and processed on R 4.1.1. Continuous variables in normal distribution were compared between groups using independent Student t test, and those in nonnormal distribution were

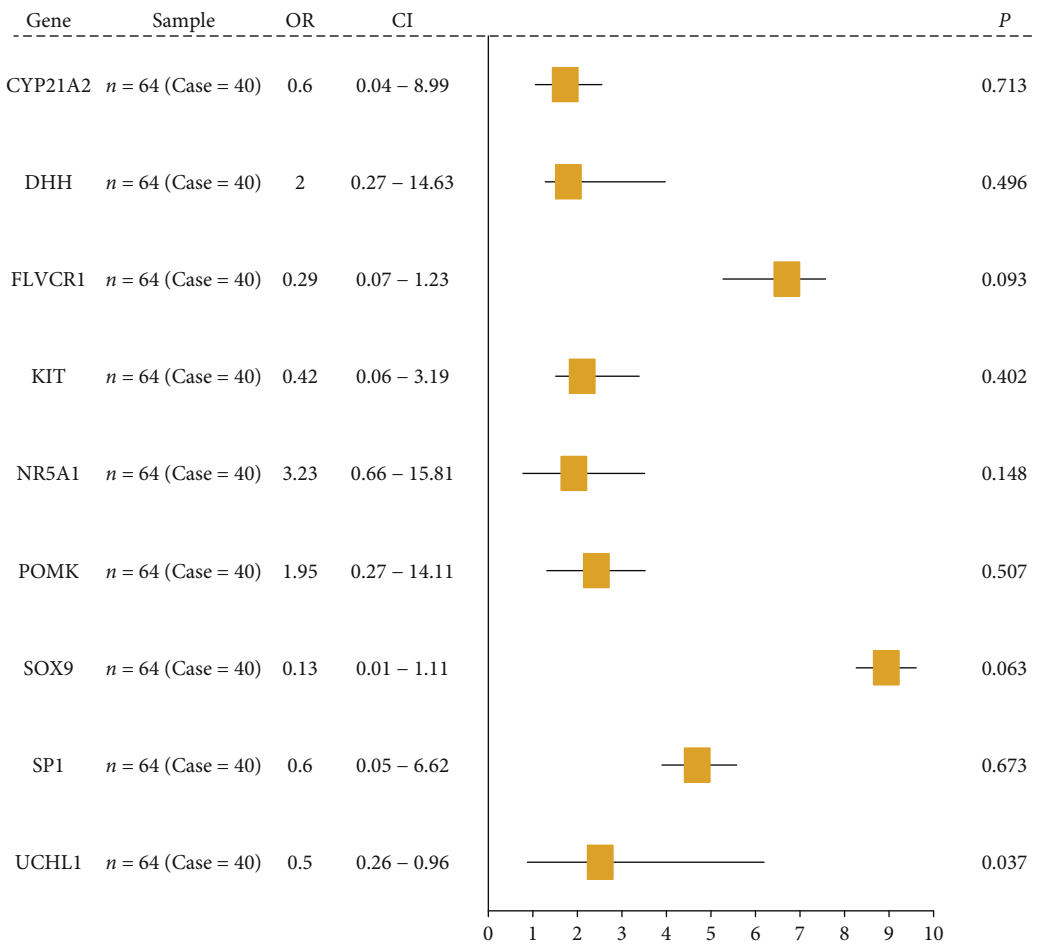

(a)

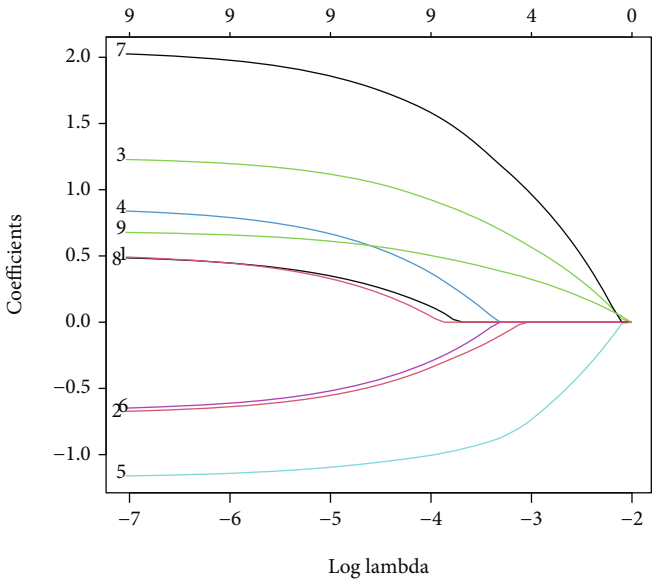

(b)

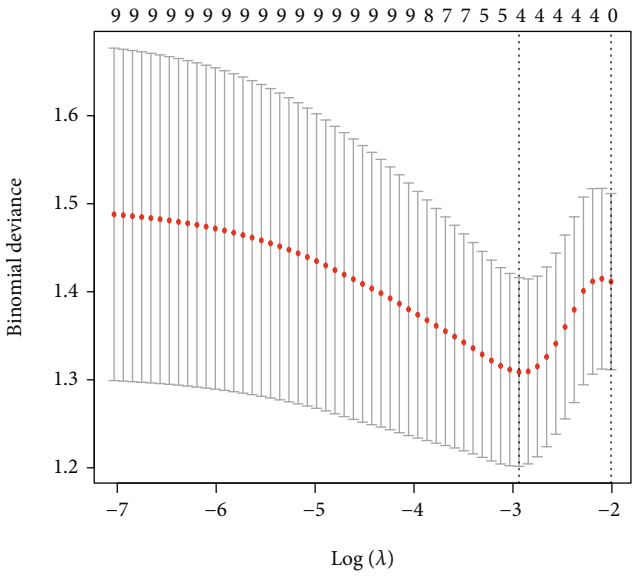

(c)

Figure 3: Continued.

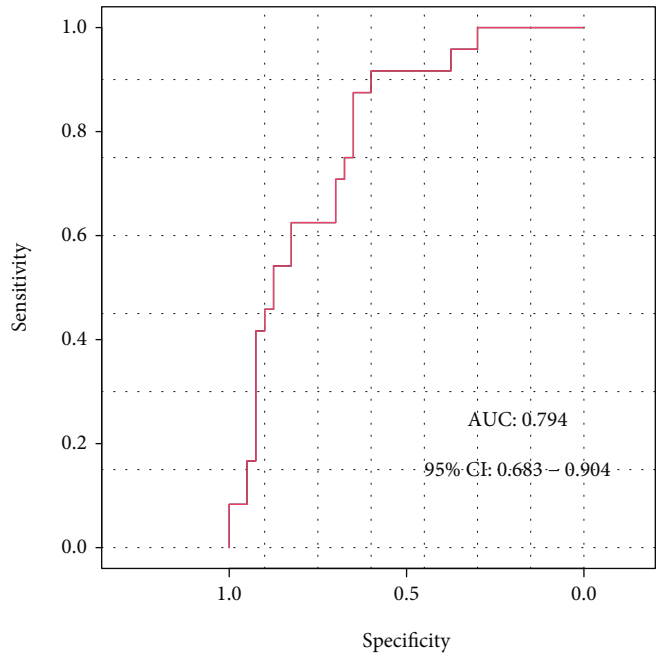

(d)

Figure 3: Construction of IDD model. (a): single-factor regression analysis. (b)–(c): mitochondrial dysfunction genes identified by LASSO regression. (d): ROC curve of IDD diagnostic model.

compared using Mann–Whitney *U* test (namely Wilcoxon rank sum test). Variables between groups were statistically analyzed using Chi-square test or Fisher's exact test. The correlation coefficients between genes were calculated via Pearson correlation analysis. All *P* values are two-sided. $P < 0.05$ indicates significance.

3. Results

3.1. Data Processing. This study procedure was conducted methodically based on the steps outlined in the flow diagram (Figure 1). To build a panorama of mitochondrial dysfunction genes in all samples, we first integrated the expression profiles from two data sets. Given the severe batch effect of data sets from different sources, we first corrected the batch effect of original data, and log-normalized the data. Results showed that the expression distributions of all samples after the above processing were distributed in consistent ways, which helped improve the accuracy and robustness of downstream analyses (Figure 2(a)). The integrated data set after the removal of batch effect contained 40 IDD samples and 24 control samples.

3.2. Panorama of Mitochondrial Dysfunction Genes. The expression levels of mitochondrial dysfunction genes were sent to correlation analysis. Results showed gene NR5A1 and gene DHH were very highly positively correlated, and gene SOX9 and gene FLVCR1, and gene CYP21A2 and gen SP1 were highly correlated (Figure 2(b)).

To analyze the differences between the control and test groups, we obtained 152 DEGs, including 67 upregulated genes and 85 downregulated genes (Figure 2(c)). A heat map of these DEGs was plotted, and the two groups of samples were well differentiated using gene clustering (Figure 2(d)). Histograms of mitochondrial dysfunction genes between the test group and the control group were plotted. Results showed FLVCR1, NR5A1, SOX9, and UCHL1 were significantly different (Figure 2(e)). A PPI network with 9 mitochondrial dysfunction genes from the gene expression profile was plotted, of which 7 genes were interactive (Figure 2(f)).

3.3. Construction of Risk Model. To analyze the effects of mitochondrial dysfunction genes on IDD patients, we conducted logistic single-factor regression analysis, and identified 9 mitochondrial dysfunction genes that largely affected IDD, including 4 significant genes (FLVCR1, NR5A1, SOX9, UCHL1) (Figure 3(a)). The coefficients of the 9 genes were calculated using LASSO (Figures 3(b)–3(c)). The gene expression level of each gene was multiplied by the corresponding coefficient, and then added together, forming a IDD predicted score. The final predicted score of each sample was calculated, and plotted on an ROC curve. Results showed the prediction curve call well predict IDD (Figure 3(d)).

3.4. Biological Differences between Groups. To explore the effects of between-group DEGs on the biological functions of patients, we first annotated the GO functions of DEGs (Table S1). Results showed these DEGs are mainly enriched in bioprocesses of extracellular matrix organization, epithelial cell migration, endodermal cell

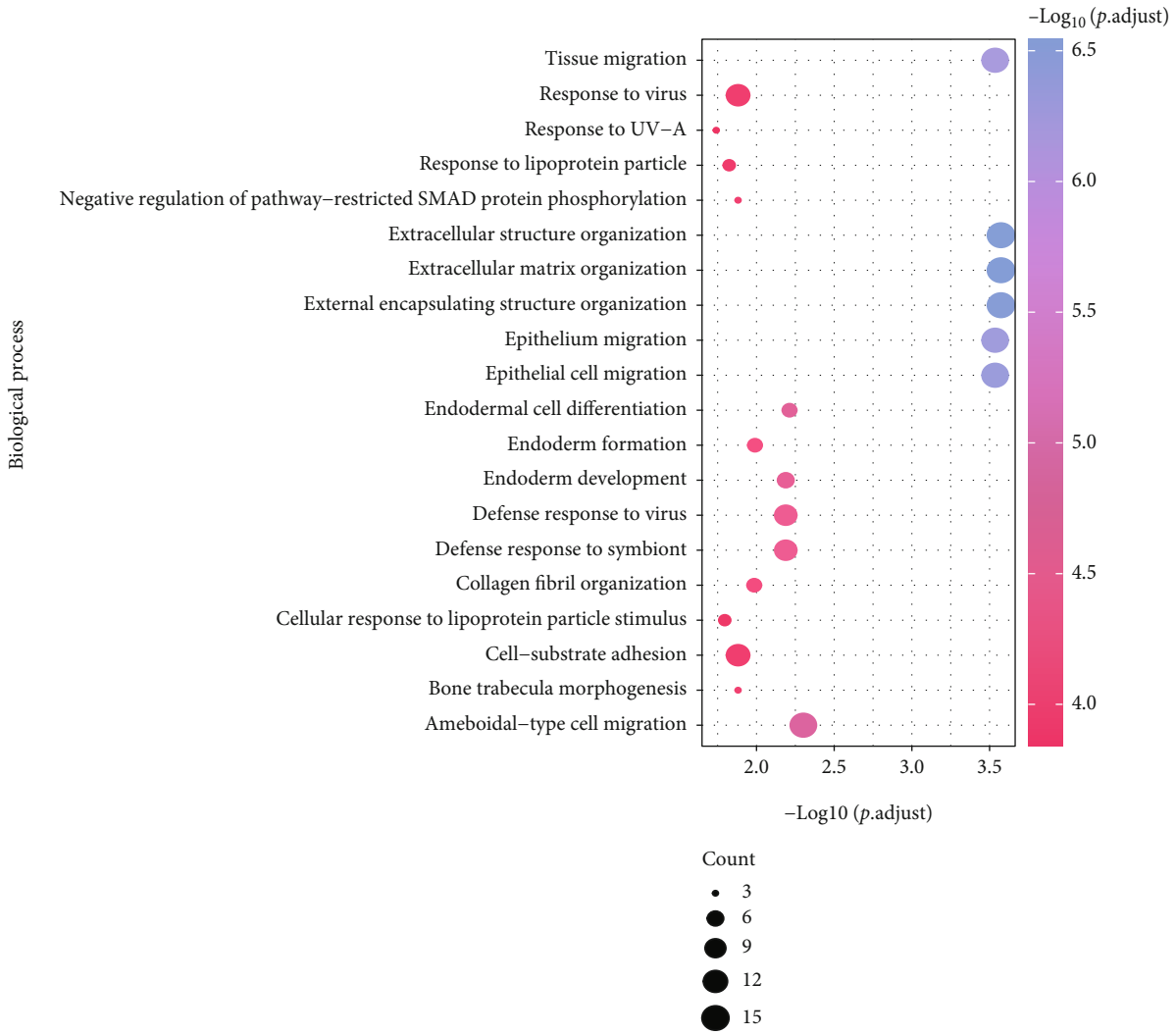

(a)

Figure 4: Continued.

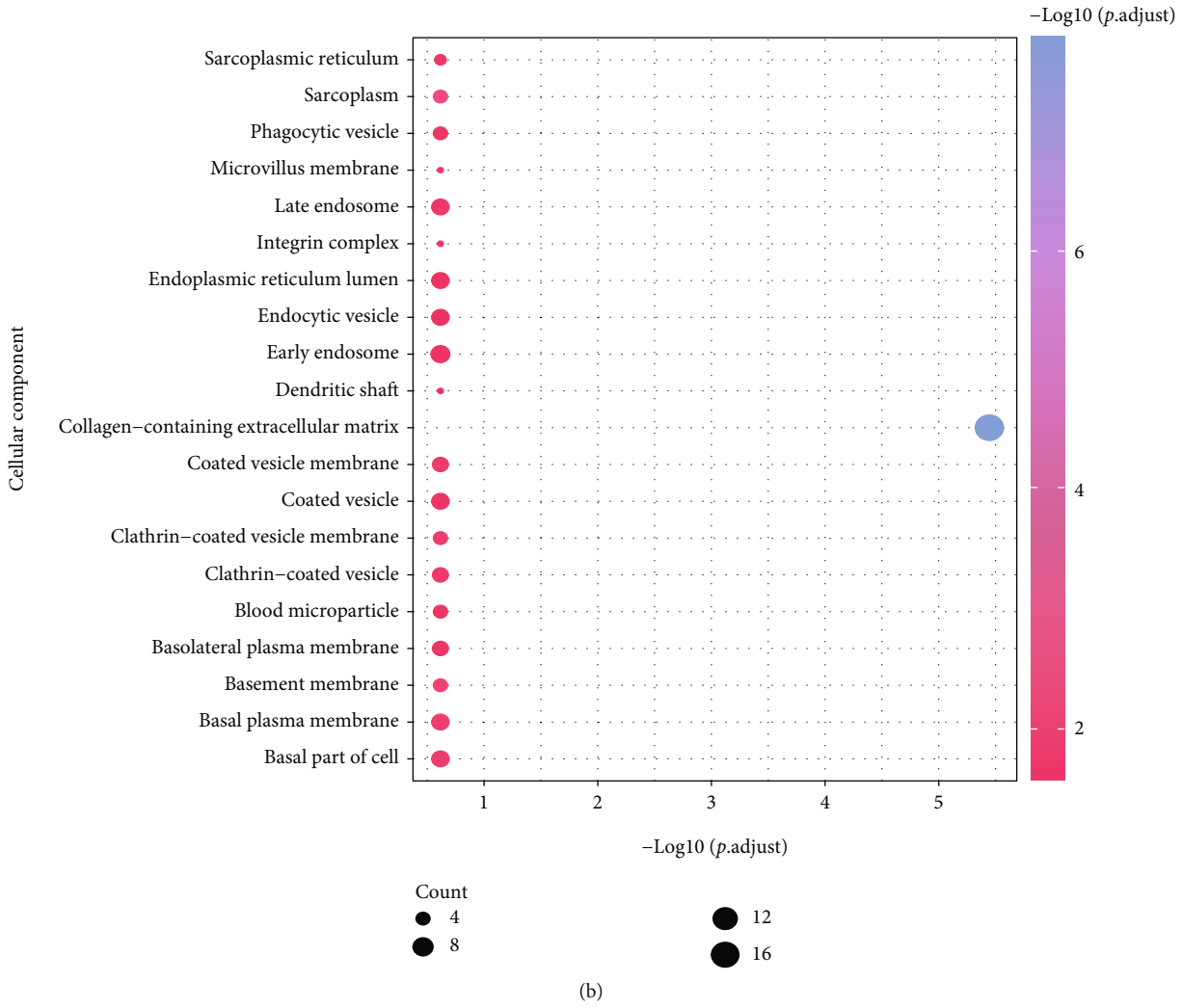

(b)

Figure 4: Continued.

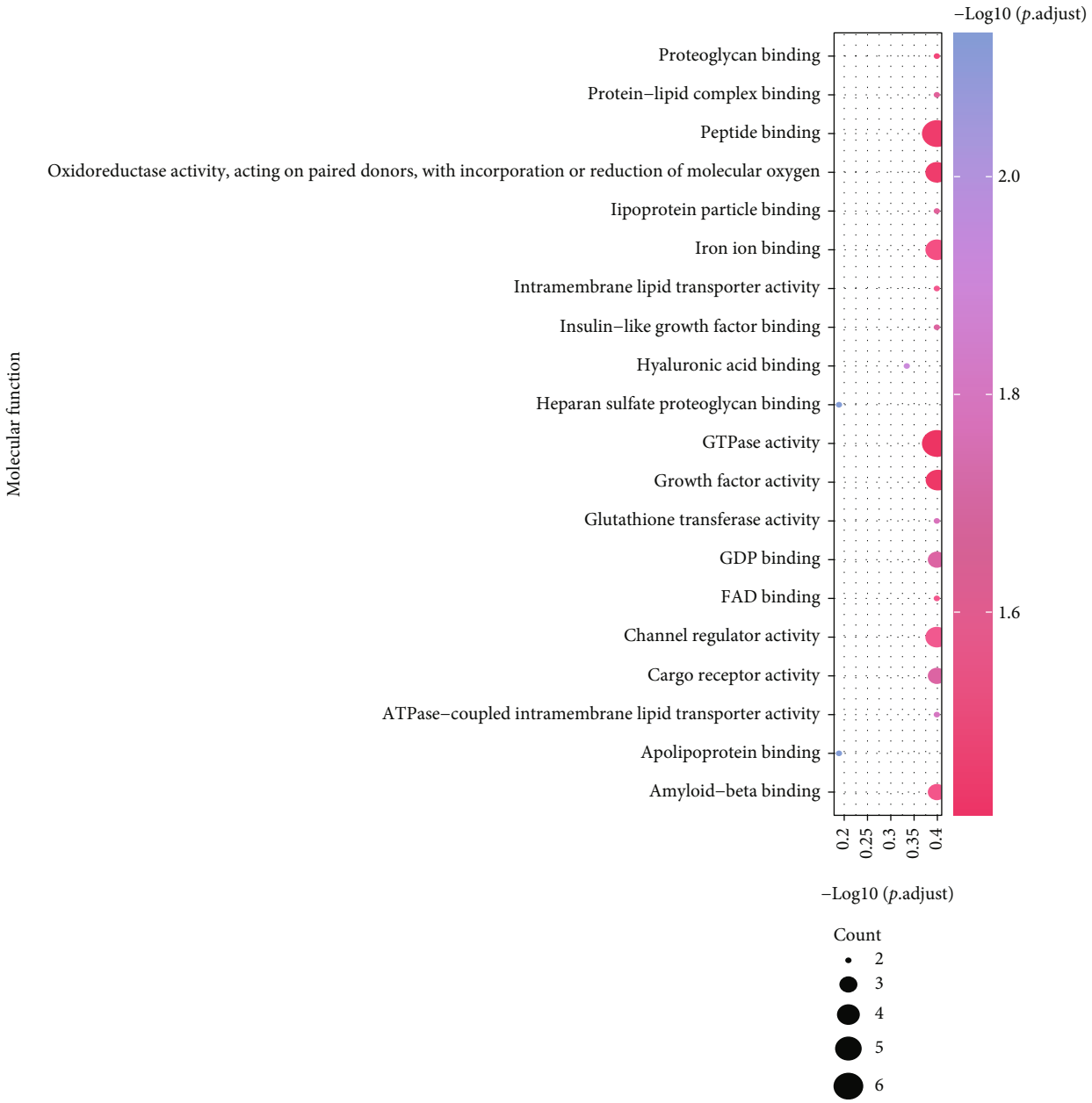

(c)

Figure 4: Continued.

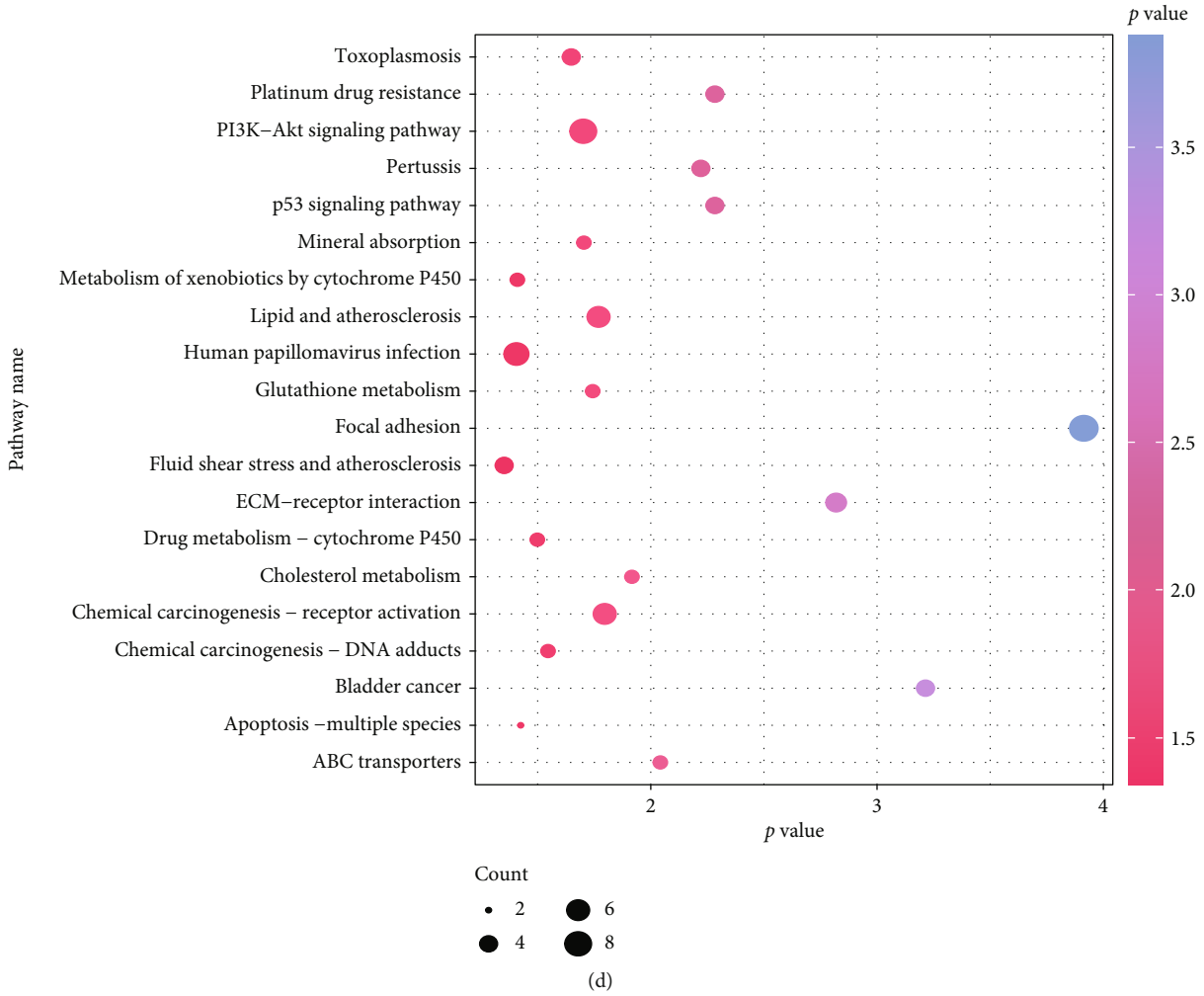

Figure 4: GO and KEGG enrichment analysis. (a): BP enrichment results, *x*-axis: -log10 (*p* value), *y*-axis: GO terms, node colors indicate -log10 (p value), node size indicates the number of genes contained the current GO Term. (b): CC enrichment results. (c): MF enrichment results. (d): KEGG enrichment results.

differentiation, defense response to symbiont (Figure 4(a)), cellular components of collagen-containing extracellular matrix (Figure 4(b)), and molecular functions of collagen binding, glycosaminoglycan binding, extracellular matrix structural constituent, heparin binding (Figure 4(c)). These DEGs were also enriched in KEGG pathways related to Focal adhesion, PI3K-Akt signaling pathway, Chemical carcinogenesis - receptor activation, and ECM-receptor interaction (Figure 4(d), Table S2).

Then all genes between groups were subjected to GSEA (Table S3). Results showed the following biological processes were significantly enriched between groups. In the IDD samples, bioprocesses including response to oxidative stress, response to virus, acute inflammatory response, wound healing, and positive regulation of protein kinase activity were activated, while bioprocesses including tRNA metabolic process, RNA modification, ribosome biogenesis, and ribonucleoprotein complex biogenesis were inhibited (Figures 5(a)–5(b)). Moreover, MAPK signaling pathway, toll like receptor signaling pathway, and nod like receptor signaling pathway were activated, but purine metabolism, DNA replication, and ECM receptor interaction pathways were inhibited (Figures 5(c)–5(d)).

The results of GSVA were basically consistent with the GSEA results. Especially, cellular response to hydroperoxide, copper ion import, positive regulation of platelet activation, and ipaf inflammasome complex were activated in the disease samples, while cysteine type exopeptidase activity, and oxidative DNA demethylation were inhibited (Figure 5(e)). In the meantime, olfactory transduction, nod like receptor signaling pathway, and gap junction were activated, but pyruvade metabolism, riboflavin metabolism, and DNA replication were inhibited (Figure 5(f)).

3.5. WGCNA and PPI Network. To probe into the associations between DEGs, we first subjected the DEGs to WGCNA (Figure 6(a)). One coexpression gene module was identified (Figure 6(b)), from which the gene set with the highest correlation was picked out and used in subsequent analysis (Figures 6(d)–6(d)), which returned 136 key genes.

From the PPI network involving the 136 key genes, we analyzed the effects of the genes on all steps of the life

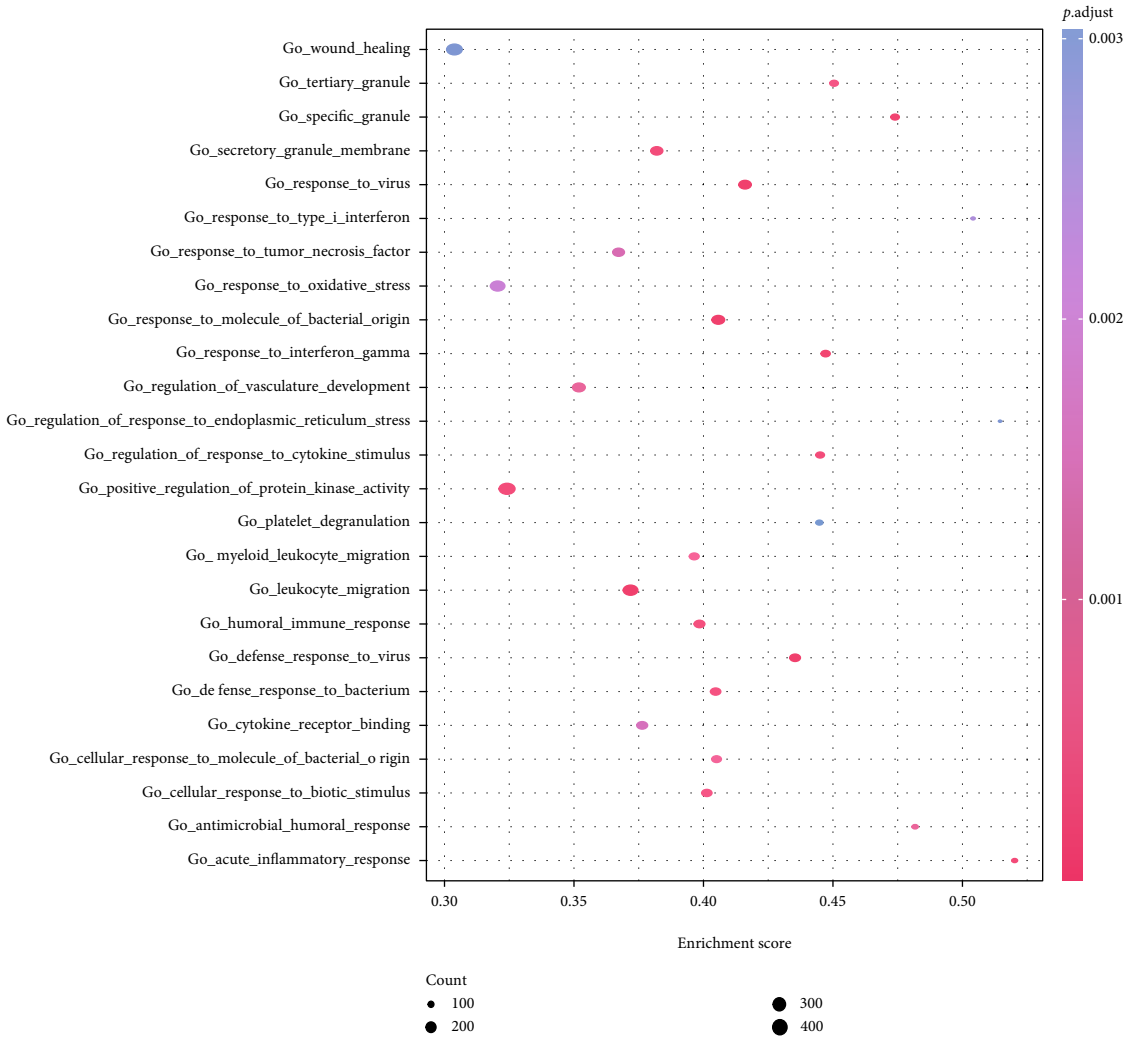

(a)

Figure 5: Continued.

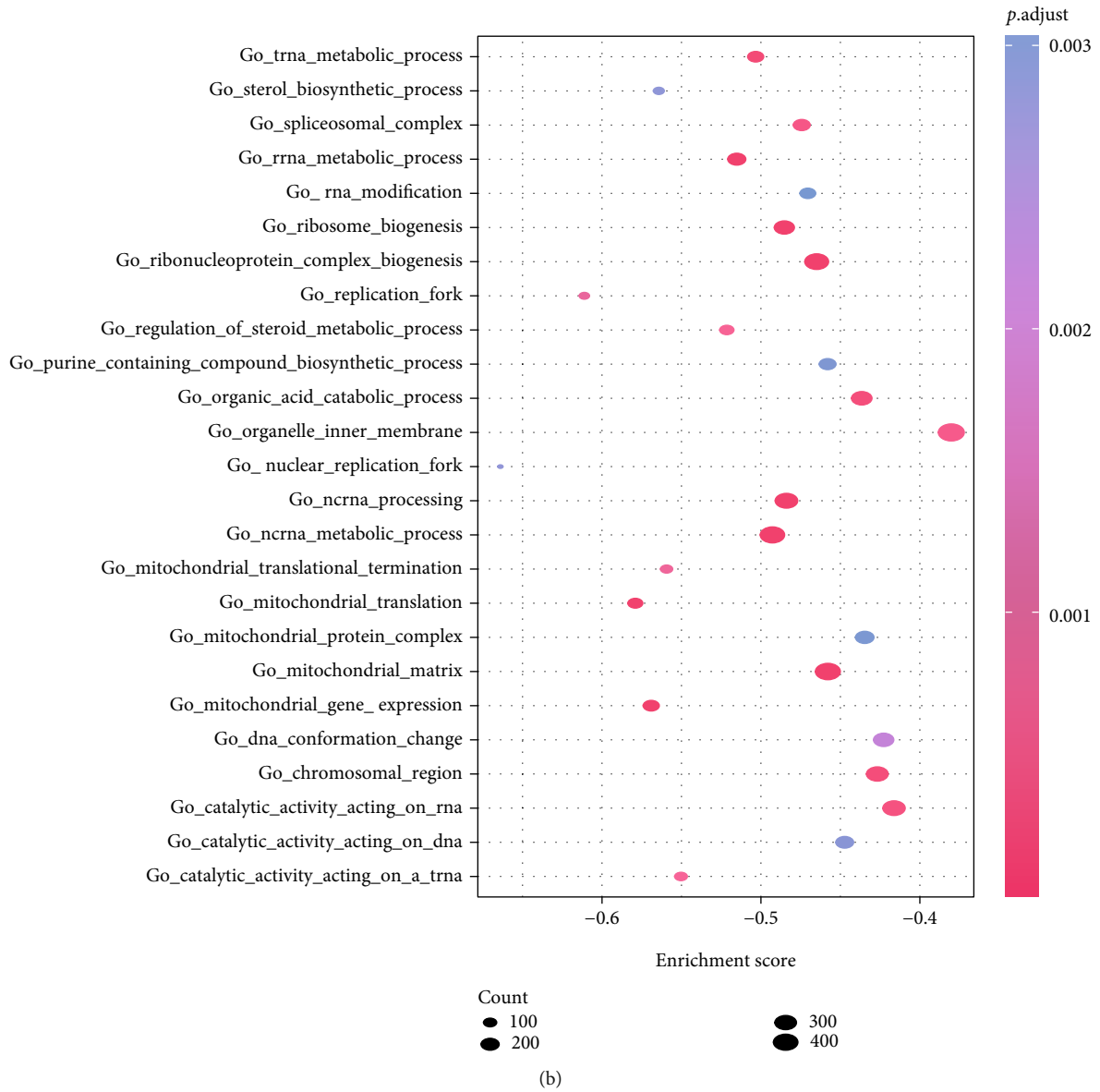

(b)

Figure 5: Continued.

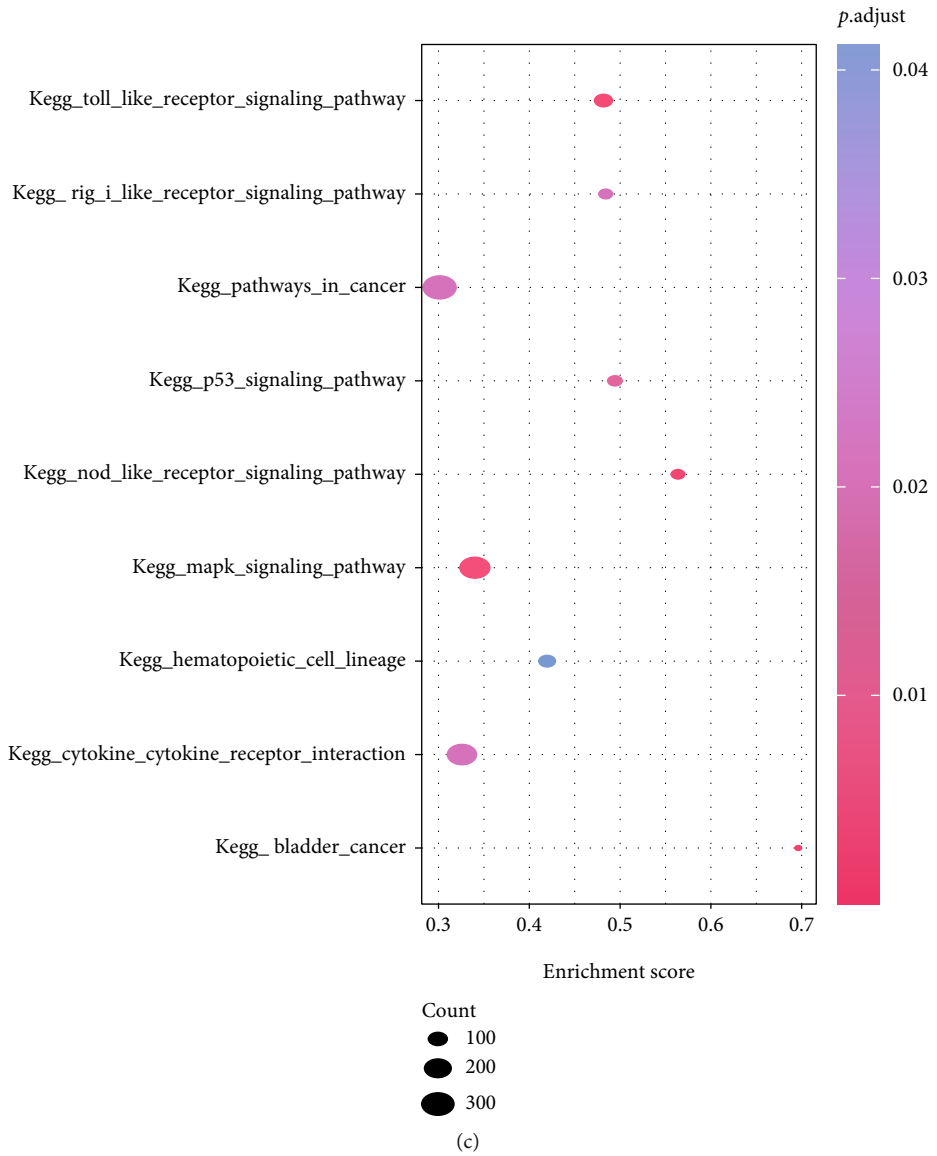

(c)

Figure 5: Continued.

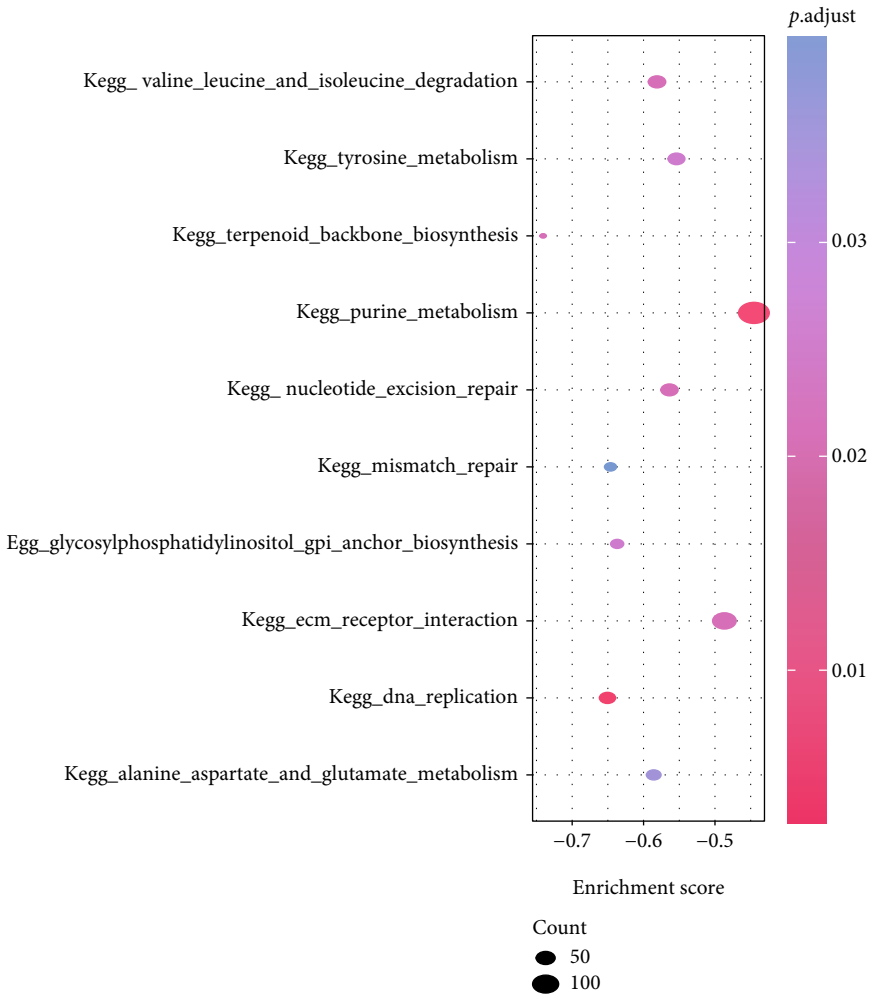

(d)

Figure 5: Continued.

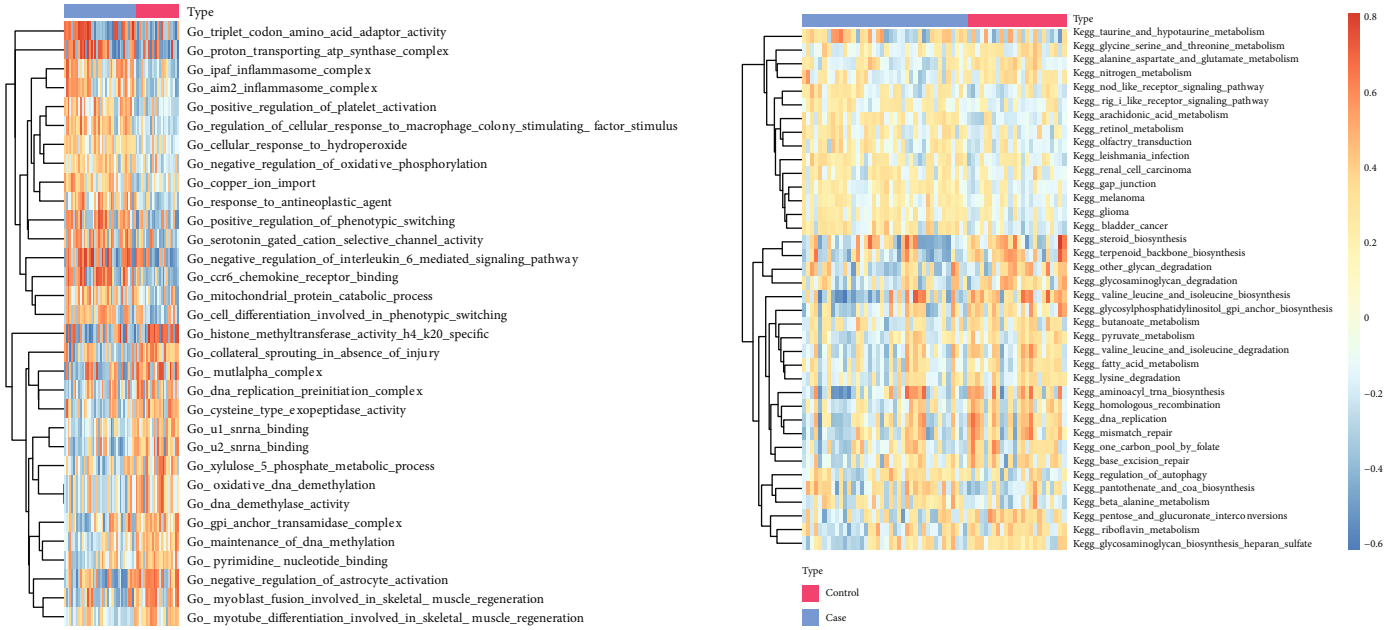

(e)

Figure 5: GSEA and GSVA. (a)–(b): GSEA-GO, *x*-axis: gene ratio, *y*-axis: GO terms, colors indicate -log10 (p value), node size indicate the number of genes enriched in GO terms. GO pathways activated (a) and inhibited (b) in the tested group. (c)–(d): GSEA-KEGG, *x*-axis: gene ratio, *y*-axis: KEGG pathway, node size indicates the number of genes enriched in the pathway, node colors indicate -log10 (p value). KEGG pathways activated (c) and inhibited (d) in the tested group. (e)–(f): heat map of functional scores in GSVA, *x*-axis: samples, *y*-axis: biological functions, node colors indicate the corresponding function is activated (red) or inhibited (blue). Red: control group, blue: test group.

process, including biosignal transfer, gene expression regulation, energy and substance metabolism, and cell cycle regulation. Through visualization on Cytoscape (Figure 7(a)), the network contains 120 interaction pairs and 87 genes. Specifically, CCND1 is closely connected with 11 DEGs, and CXCL8 is closely associated with 13 DEGs. The function interactive subnetworks were extracted on CytoHubba (Figure 7(b)), which included 10 genes. The functional similarities among the genes on the PPI network were analyzed (Figure 7(c)). Results showed the genes in PPI were highly associated in terms of functions. An ROC curve with the 10 hub genes was plotted, which showed these genes can well differentiate the two groups of samples (Figure 7(d)).

3.6. Analysis of Immune Infiltration. CIBESORT (Figure 8(a)) showed the concentrations of mast cells activated were significantly the highest in IDD patients. Compared with the control group, the level of T cells CD4 memory resting was the lowest in the patients (Figure 8(b)). Furthermore, the correlations of mitochondrial dysfunction genes or hub genes with immune cell contents were calculated. Results showed macrophages M0, and dendritic cells activated were both closely associated with the expressions of several mitochondrial dysfunction genes (Figure 8(c)). Macrophages M0, NK cells resting, and mast cells activated were positively correlated with multiple hug genes, and B cells memory, and T cells CD8 were negatively correlated with several hub genes (Figure 8(d)). Moreover, the correlations of immune cell contents between the control group and the tested group were computed. Results showed the Mast cells activated contents in the patients were significantly correlated with several types of immune cells (Figure 8(e)). In the control group, the content of T cells CD4 naive was significantly correlated with several other types of immune cells (Figure 8(f)).

3.7. Two Mitochondrial Dysfunction Modes Identified Using Mitochondrial Dysfunction Genes. With ConsensusClusterPlus from the R software and based on the 9 mitochondrial dysfunction genes, the mitochondrial dysfunction modes were identified using consistency clustering, and two modes were identified (cluster1, cluster2)(Figure 9(a)). Cluster1 contains 35 samples, and cluster2 involves 5 samples. PCA showed the two clusters were significantly different (Figure 9(b)).

The differences of hub genes and mitochondrial dysfunction genes between the two clusters were compared. Results showed CCND1 and CYP1B1 were significantly down-expressed in cluster1, and MMP1 was significantly up-expressed in cluster2 (Figures 10(a) and 10(c)). In the meantime, UCHL1 expression of cluster1 was significantly lower than that of cluster2, and FLVCR1 expression of cluster1 was higher than that of cluster2 (Figures 10(b) and 10(d)).

3.8. Validation of the Mitochondria Dysfunction Genes. To validate the identified mitochondria dysfunction genes, we collected 36 human intervertebral disc tissues RNA

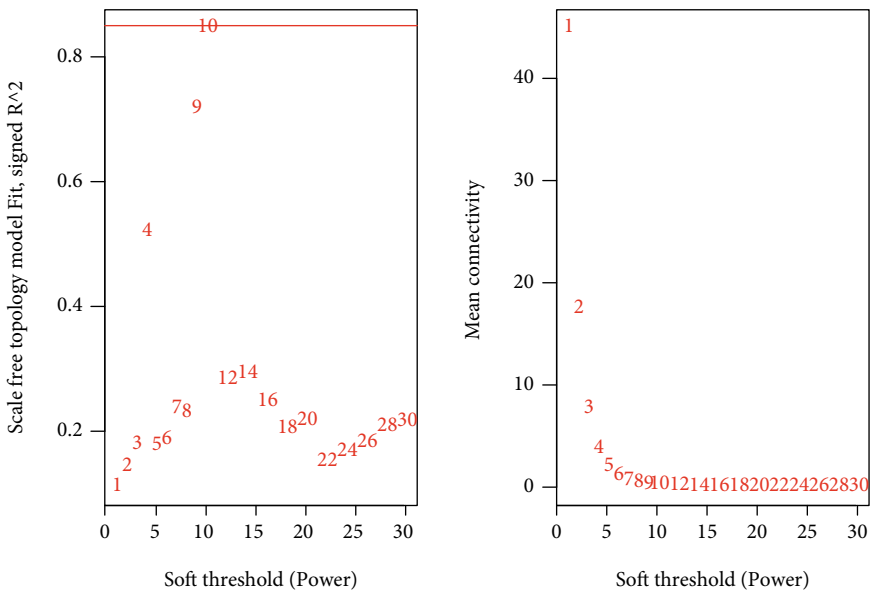

(a)

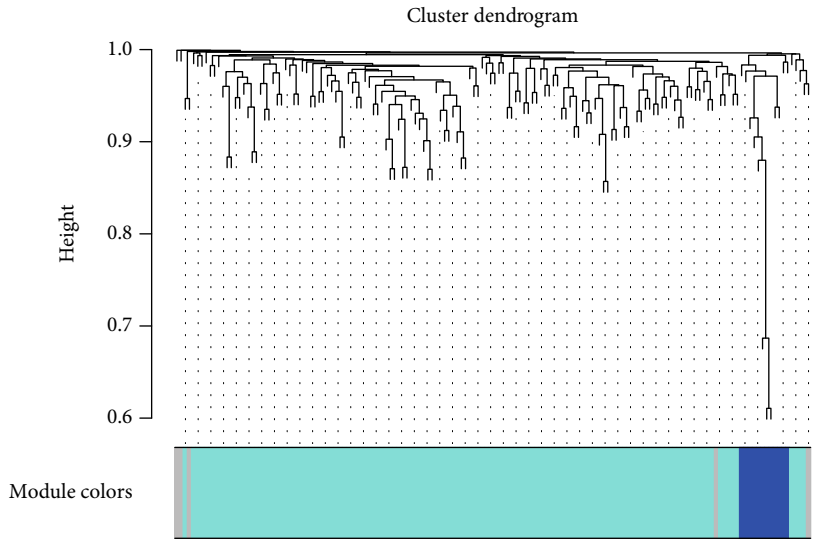

(b)

Figure 6: Continued.

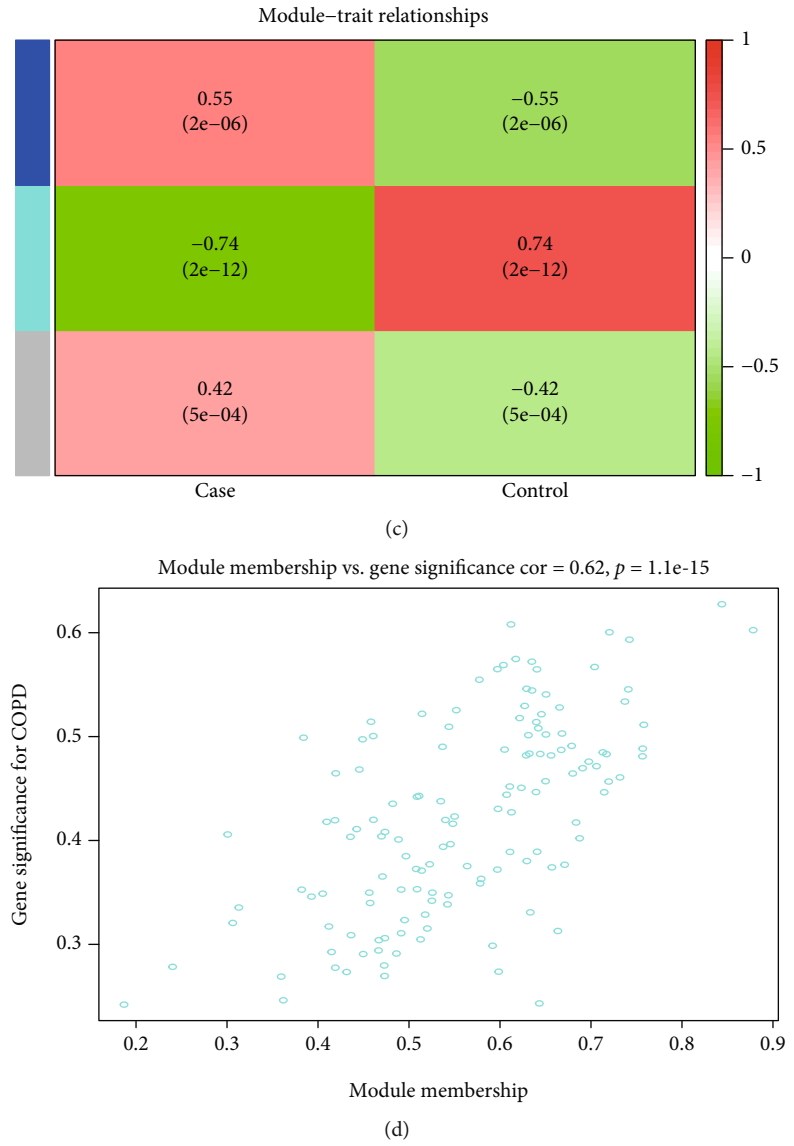

Figure 6: WGCNA. (a): WGCNA of threshold screening. (b): coexpression gene clustering. (c): correlations between gene clusters and diseased patients; (d): correlation analysis between most significant gene clusters and IDD.

including 12 from patients with degenerated discs of Pfirrmann level I or II and 24 from patients with degenerated discs of Pfirrmann level III to V. QPCR showed either in nucleus pulposus tissues or in anulus fibrous tissues, the mRNA levels of NR5A1 were upregulated in both degenerative NP tissues and AF tissues than in control groups. While the mRNA levels of FLVCR1, SOX9 and UCHL1 were downregulated. These results are shown in Figures 11(a)–11(b). Additionally, the protein level validation results were consistent with the gene level results. Western blot showed the relative expression levels of FLVCR1, SOX9 and UCHL1 proteins in both NP cells and AF cells of the degeneration group were significantly lower than that in the control group. But that of NR5A1 was higher than in the control group in fibrous anulus cells while there was no significant difference between these two groups in pulposus cells (Figures 11(c)–11(f)).

4. Discussion

Intervertebral disc (IVD) is a complex fibrocartilaginous tissue that connects adjacent vertebral bodies and maintains mechanical loading to enable spinal motion. In a healthy IVD, the balance between anabolic and catabolic processes maintains ECM homeostasis. However, aging and persistent mechanical stress can disrupt IVD metabolism, forcing an imbalance between the expressions of catabolic factors (e.g. pro-inflammatory cytokines and matrix metalloproteinases) and anabolic mediators (e.g. growth factors), leading to the loss of ECM homeostasis, destruction of macromolecules, and the subsequent development of IDD [38]. IDD plays an important role in spine-related diseases, and worsens with age. More than 80% of IDDs exhibit degeneration-related changes in people over 50 years [39].

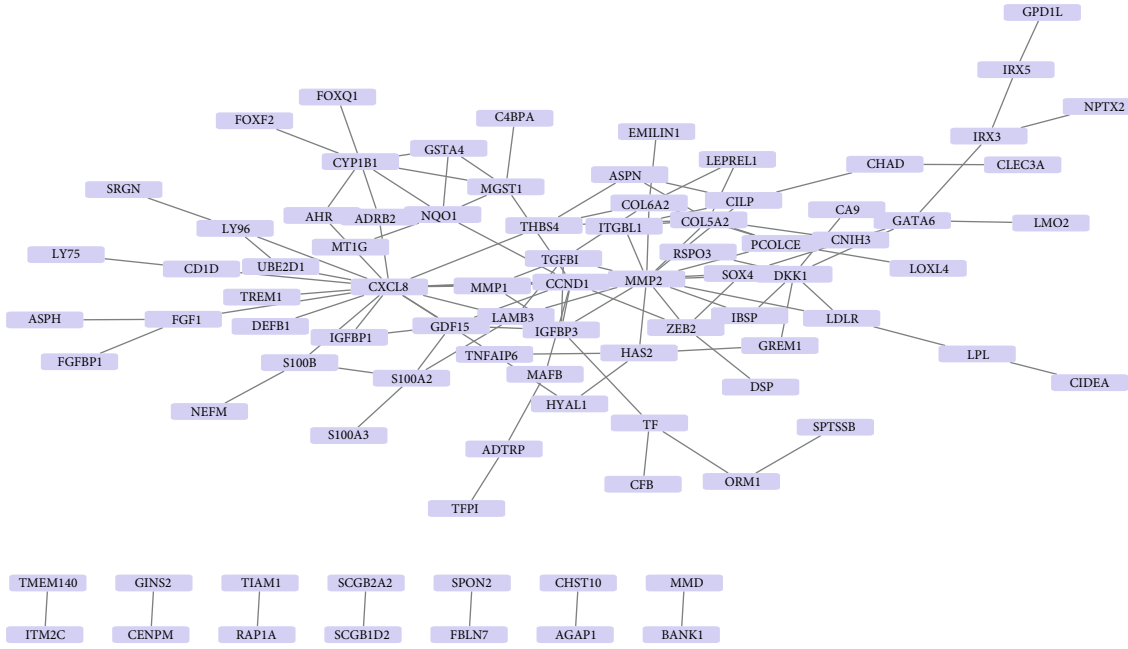

(a)

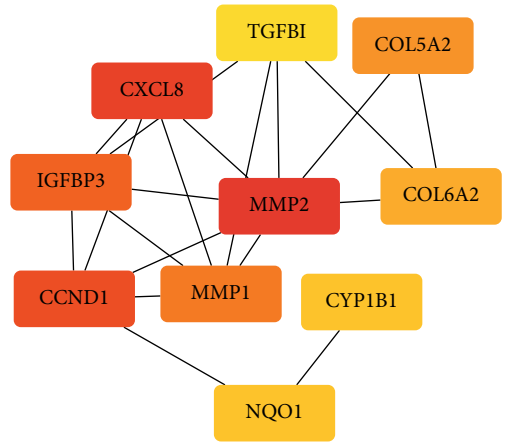

(b)

Figure 7: Continued.

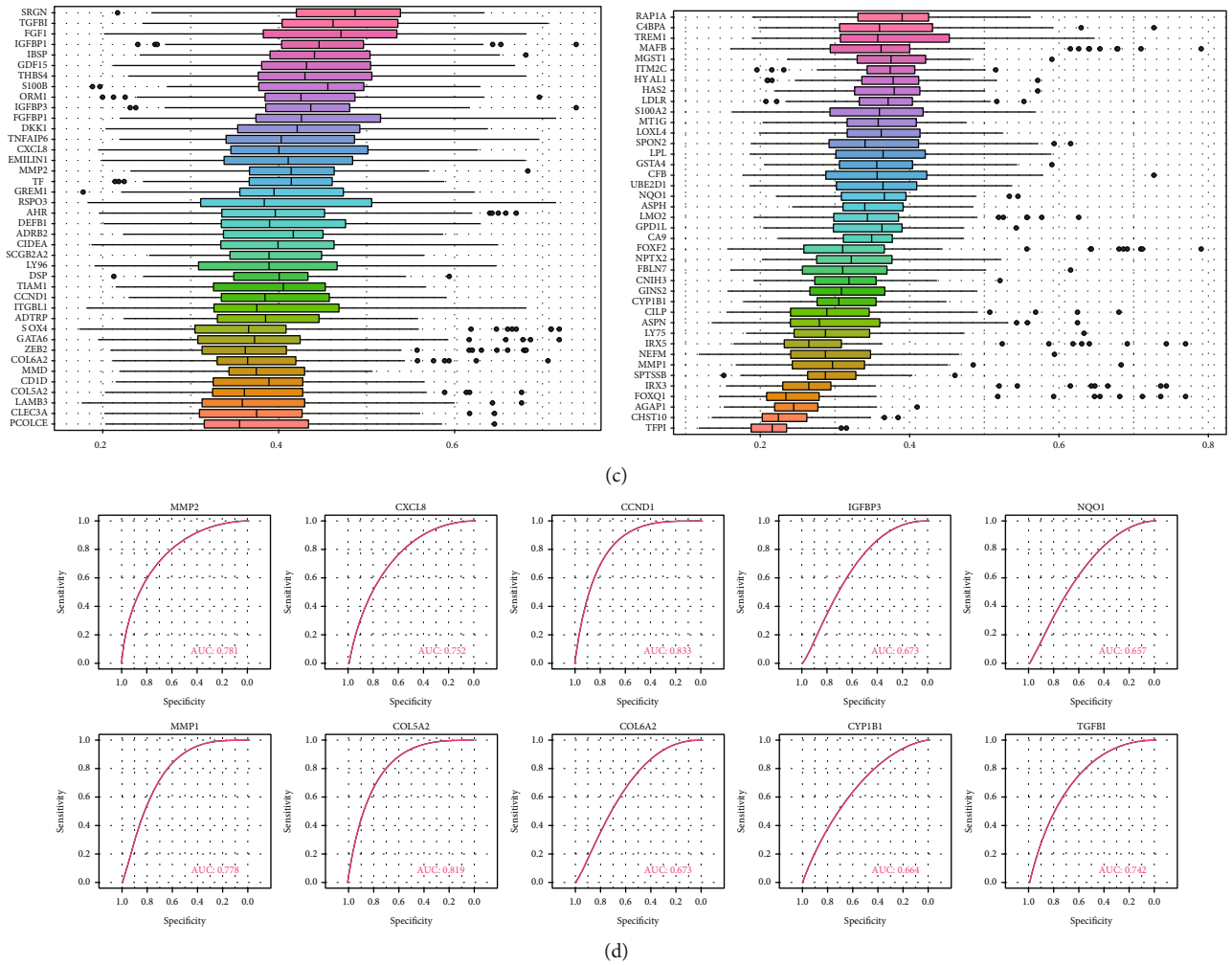

FIGURE 7: PPI network. (a): PPI network of key genes; (b): subnetwork of PPI network. (c): analysis of similarities of gene functions in subnetwork of PPI network; *x*-axis: magnitude of correlations; *y*-axis: gene name. (d): ROC curve of hub genes.

The widely-used treatment strategies for IDD include physiotherapy, drug therapy and surgery. However, these approaches have limited effects to reverse the IDD progression with current treatments. Therefore, it is necessary to fully understand the etiology of IDD. The important bioprocesses are related to immune response, innate immune response, cell division, mitochondrial homeostasis and cell proliferation. More studies have proved that mitochondrial dysfunction is pivotal in accelerating IDD. Mitochondria, a double-layer organelle in eukaryotic cells, is mainly involved in tricarboxylic acid cycle (TCA) and provides the body with adenosine-triphosphate enzyme (ATP). ATP is the most important energy source of cells, but mitochondria, while providing ATP, also produce ROS that cause oxidized stress response [40]. Along with cell aging, mitochondrial DNA injuries will induce mitochondrial dysfunction, destroying the redox balance, so ROS aggravate cell injuries, forming a vicious circle 'cell aging – mitochondrial dysfunction – ROS maladjustment accelerated cell aging'. In contrast, mitochondrial respiratory uncoupling reduces the production of H_2O_2, thereby delaying the replicative senescence of cells. Reportedly, the expression levels of mitochondrial function genes (including substrate dehydrogenase, cytochrome and substrate vectors) are significantly changed in aged intervertebral disc tissues.

The function of mitochondria depends on their morphological structure, and abnormal changes in the morphological structure can lead to mitochondrial dysfunction. The dynamic balance between mitochondrial fusion and division is one major link in maintaining cell homeostasis, and the destruction of this balance can cause a series of diseases [41, 42]. Mitochondrial homeostasis requires mitofusion and optic atrophy-associated protein 1 (OPA1) regulation [42, 43]. When mitochondria divide, the outer mitochondrial membrane molecule Fis1 recruits dynamin-related protein 1 (DRP1), a mitochondrial division regulator, translocating it to the outer mitochondrial membrane and enriching it at the site of division [43, 44]. OPA1 and mitochondrial fusion occur when disc tissue is subjected to excessive mechanical loading. Down-regulation of proteins leads to mitochondrial fusion disorders, resulting in NP cell damage [44]. When intervertebral disc cells are under hypoxia,

(a)

Figure 8: Continued.

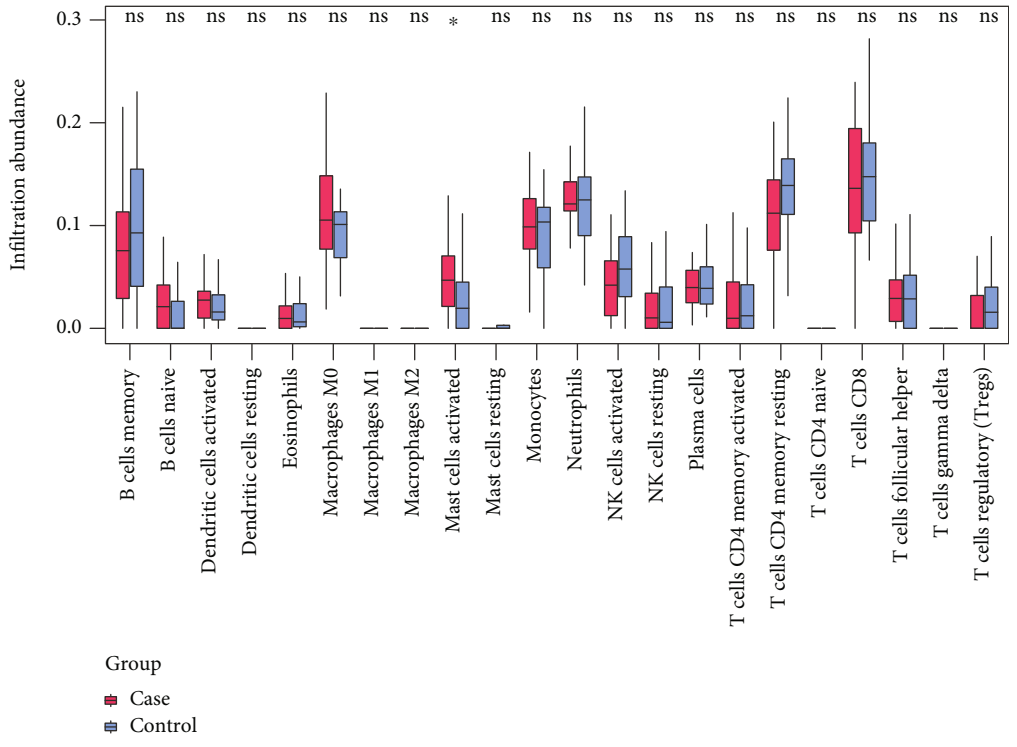

(b)

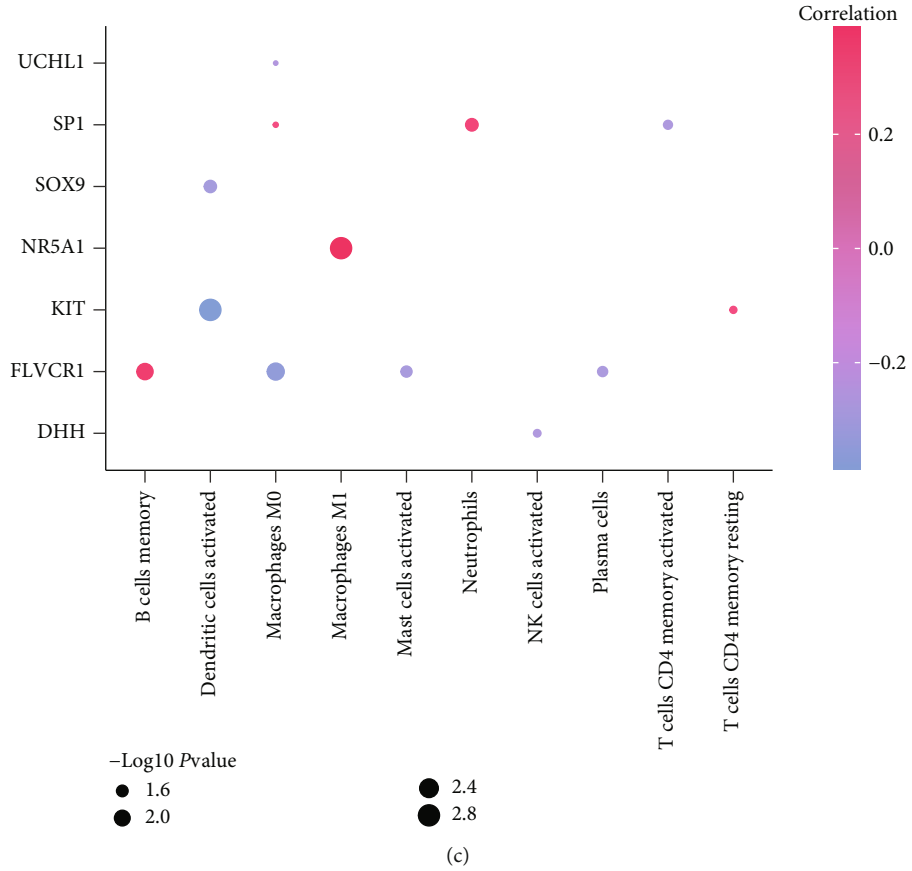

(c)

Figure 8: Continued.

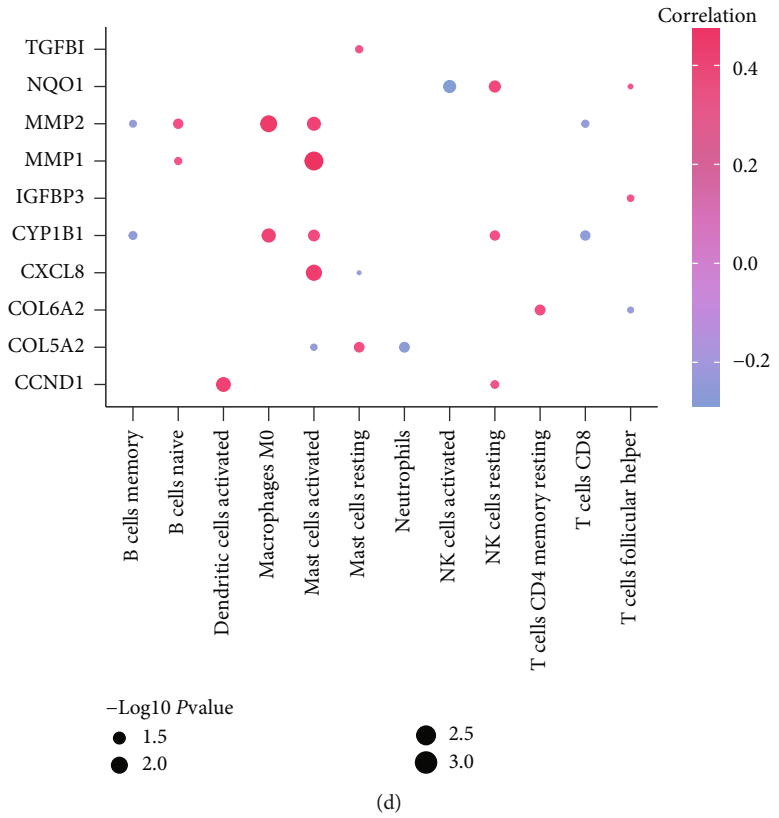

(d)

Figure 8: Continued.

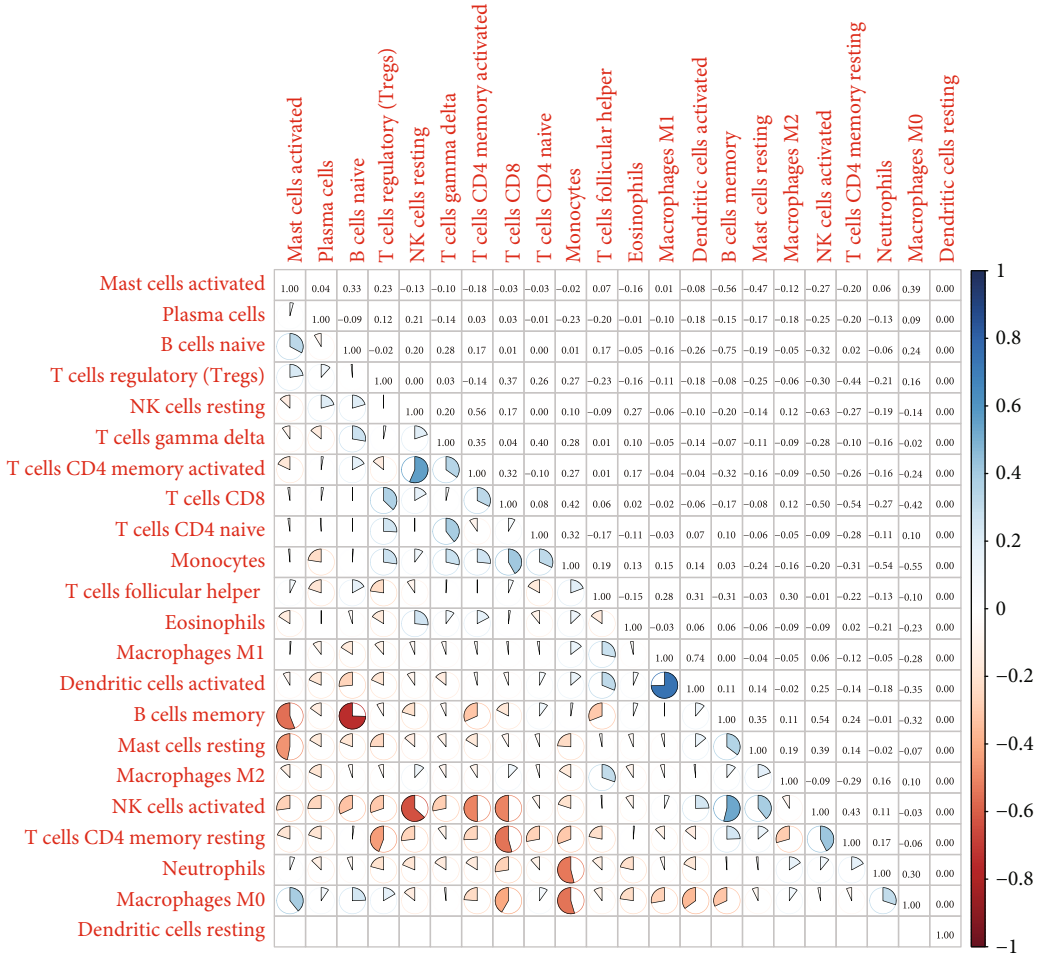

(e)

Figure 8: Continued.

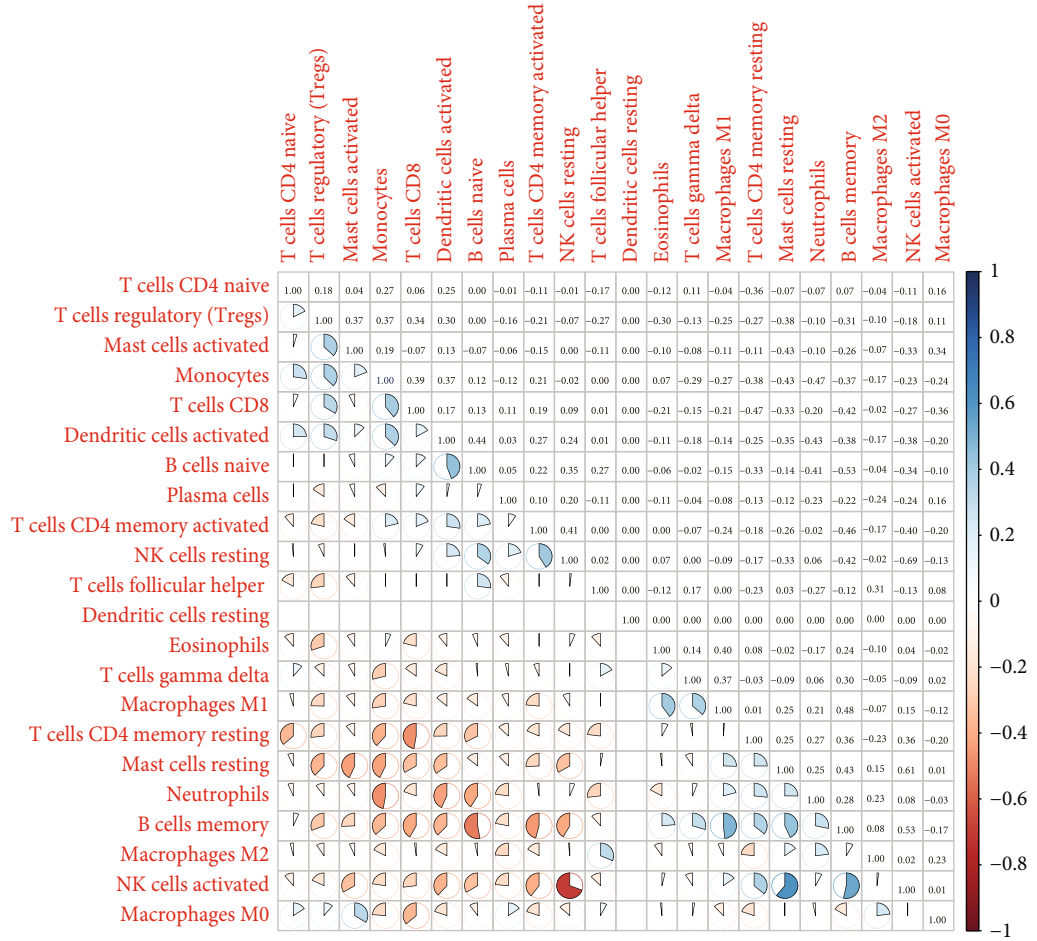

(f)

Figure 8: Immune infiltration analysis. (a): Accumulative immune cell concentrations in the test group and control group. Colors indicate immune cells. *x*-axis: id of patients. (b): histograms of immune cell concentrations; *x*-axis: immune cells; *y*-axis: cell concentration; red: IDD samples; blue: control samples. (c): correlations between mitochondrial dysfunction genes and immune cells; *x*-axis: immune cells, *y*-axis: mitochondrial dysfunction genes. Node colors indicate the magnitude of correlation, node sizes indicate the significance level. (d): correlations between hub genes and immune cells; *x*-axis: immune cells, *y*-axis: hub genes. Node colors indicate the magnitude of correlation, node sizes indicate the significance level. (e)–(f): correlations of immune cell concentrations in the test group (e) and control group (f); red: negative correlation, blue: positive correlation.

DRP1 migrates from the cytoplasm to mitochondria, aggravating mitochondrial dysfunction [8]. Therefore, an intervention targeting DRP1 is one of the feasible strategies to prevent IDD. Inhibition of DRP1 by siRNA or mitochondrial division inhibitor 1 (Mdivi-1) can prevent programmed necrosis in NP cells or AF cells exposed to excessive pressure [45, 46].

ROS are involved in signal transduction and metabolism of intervertebral disc cells to regulate death and senescence. Under physiological conditions, the production and clearance of intracellular ROS are under dynamic balance [47]. When the balance is broken, ROS levels in cells will exceed physiological thresholds, subjecting the cells to a state of oxidative stress dysfunction and excessive mitochondrial ROS level in intervertebral discs [48–53]. Mitochondrial DNA (mtDNA) and oxidative damage of respiratory enzymes lead to mitochondrial dysfunction, forming a vicious cycle [54]. In intervertebral disc tissues, ROS overproduction can lead to loss of proteoglycan collagen and accelerate IDD progression [55]. H_2O_2 significantly increases lysosomal membrane permeability in rat NP cells, leading to ROS overproduction and apoptosis [56]. Excessive increase in ROS in the intervertebral disk can cause oxidative damage to disk cells, leading to activation of NLRP3 inflammatory vesicles and increased interleukin (IL)1 release, exacerbating the inflammatory response. In the IL-1β inflammatory environment, ROS expression is elevated in NP cells, and ROS activates p53/P21 and P16/κb pathways to accelerate intervertebral disc cell senescence [57].

The emergence of bioinformatics methods has accelerated the research progress on the mechanisms of human diseases. In our study, comparative analyses of mitochondria dysfunction DEGs between normal individuals and IDD patients were performed. We integrated two databases

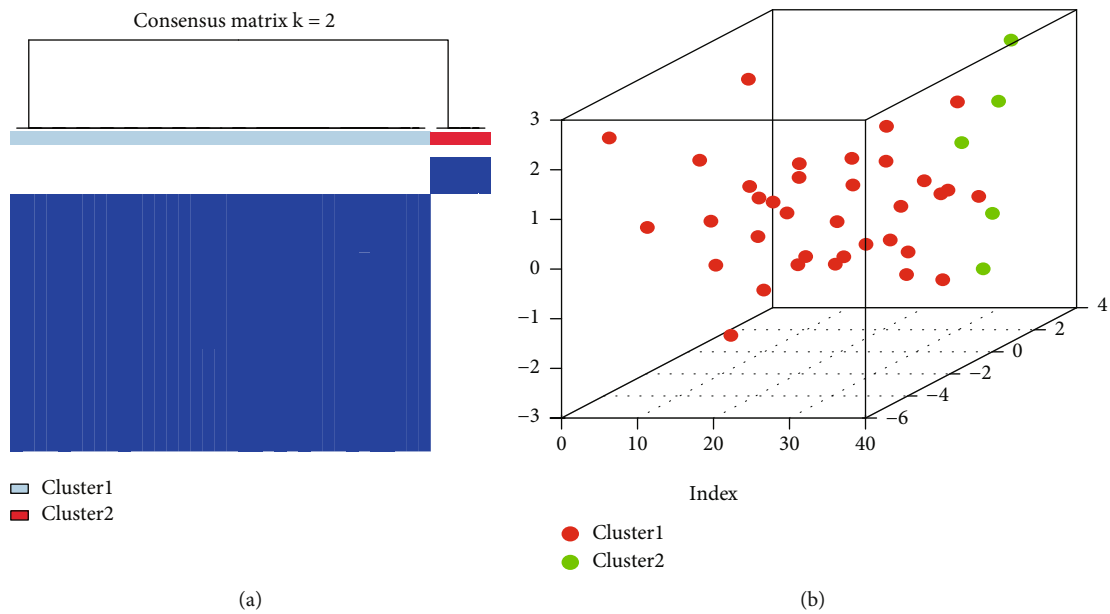

Figure 9: Consistency clustering of IDD patients according to mitochondrial dysfunction. (a): consistency clustering, blue: cluster1, red: cluster2. (b): PCA of cluster1 and cluster2, red: cluster1, blue: cluster2.

GSE7036 and GSE124272, which contained tissue and blood sequencing data. The analysis of immune infiltration showed that compared with the control group, the concentrations of mast cells activated were significantly the highest in IDD patients. Previous studies have shown that mast cells might play a key role in the repair of the injured anulus fibrosus and subsequent disc degeneration [58]. GSEA analysis indicated that the biological process of response to oxidative stress is activated in degeneration samples. In addition, GSVA analysis obtained a similar result: cellular response to hydroperoxide was overactivated in patient samples. These results further confirmed the role of oxidative stress response caused by mitochondrial dysfunction in the progression of IDD. Further analysis showed that 152 DEGs were obtained between degeneration group and control group, including 67 upregulated genes and 85 downregulated genes. Four mitochondrial dysfunction genes (FLVCR1, SOX9, UCHL1, NR5A1) were identified and validated at the gene and protein levels. After an extensive literature review of these 4 genes, we found no report about the associations of three genes with IDD (SOX9 was proved to be associated with IDD). Hence, our findings may be a new clue for the diagnosis and treatment of IDD.

Reportedly, mitochondrial injuries during cartilage degeneration will induce abnormal expressions in SOX9 and its downstream genes. We found in either IDD tissues or peripheral blood, the SOX9 gene expressions were significantly different between the degeneration group and the control group, and the SOX9 expression gradually decreased with the aggravation of degeneration. SOX9 was first noted in skeletogenic mesenchymal progenitors for its role in fate determination and differentiation within the chondrocyte lineage [59]. SOX9 efficiently binds to single or double HMG-box site(s) in DNA and thereby transactivates its target genes such as Col2a1 and aggrecan (Acan), which have stage-specific features for intervertebral disc cartilage development [60, 61].

Inactivation of Sox9 during early stages of chondrogenesis in Col2Cre-expressing chondrocytes showed that cells cannot express SOX9 targets, including Col2a1 and Acan [62]. Observations in the notochord during axial skeletogenesis complement the findings in chondrocytic cells. Sox9 deletion prevents matrix-rich notochordal sheath formation and results in notochordal cell death [63]. It is suggested that SOX9 regulates cell survival and differentiation in the inner AF during disc development [64]. These studies affirmed that SOX9 is critical in cartilage formation and vertebral column development [65]. Moreover, Sox9 deletion in Acan-expressing cells of adult mice results in proteoglycan loss, disc compression, and downregulation of various ECM-related genes [66]. A recent study from Maria demonstrated that SOX9 mutant mice experience early-onset, progressive disc degeneration characterized by increased cell death, alterations in ECM organization, and distinct transcriptomic changes in the NP and AF compartments.

Feline leukemia virus subgroup C receptor-1 (FLVCR1), a member of the SLC49 family of 4 paralogous genes, is a cell surface heme exporter essential for erythropoiesis and systemic iron homeostasis. It encodes two heme exporters: FLVCR1a [67], which localizes to the plasma membrane, and FLVCR1b, which localizes to mitochondria [68]. Upon the occurrence of mitochondrial dysfunction, FLVCR1b abnormality will lead to the accumulation of free heme, high levels of Hb and heme can be used to mark neovasculogenesis in herniated nucleus pulposus, which further promotes nucleus pulposus degeneration through heme iron-

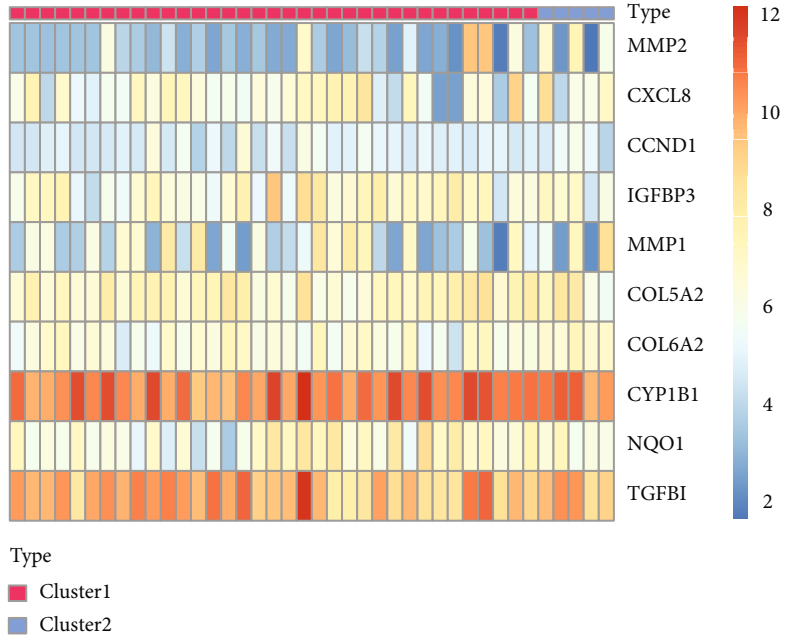

(a)

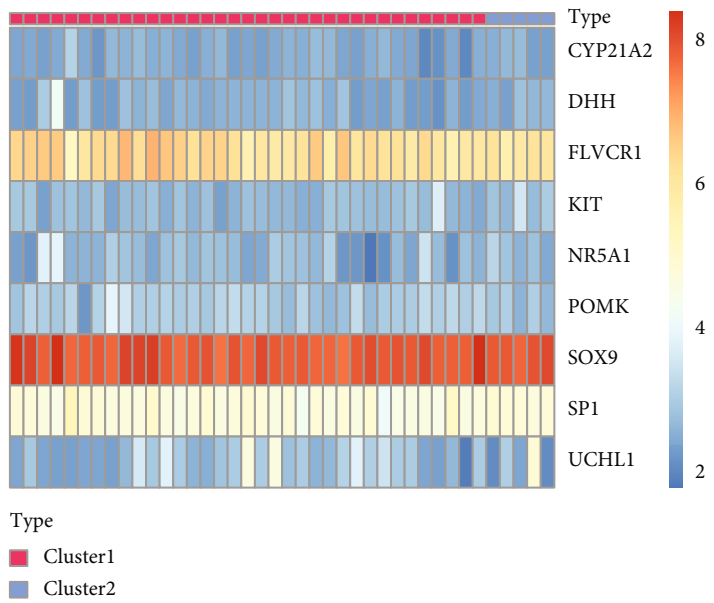

(b)

Figure 10: Continued.

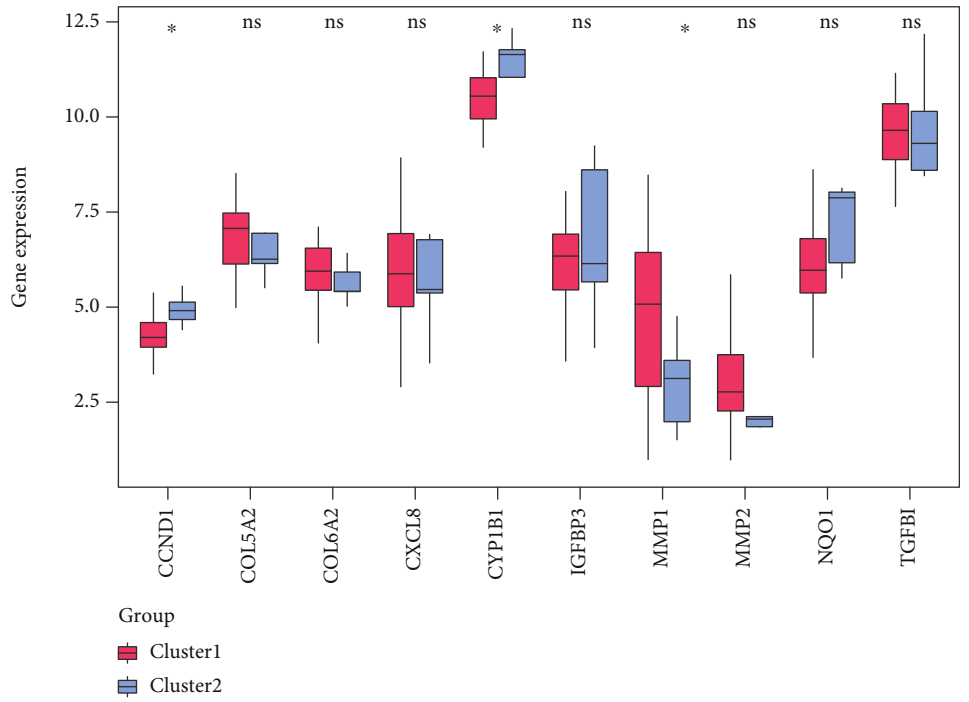

(c)

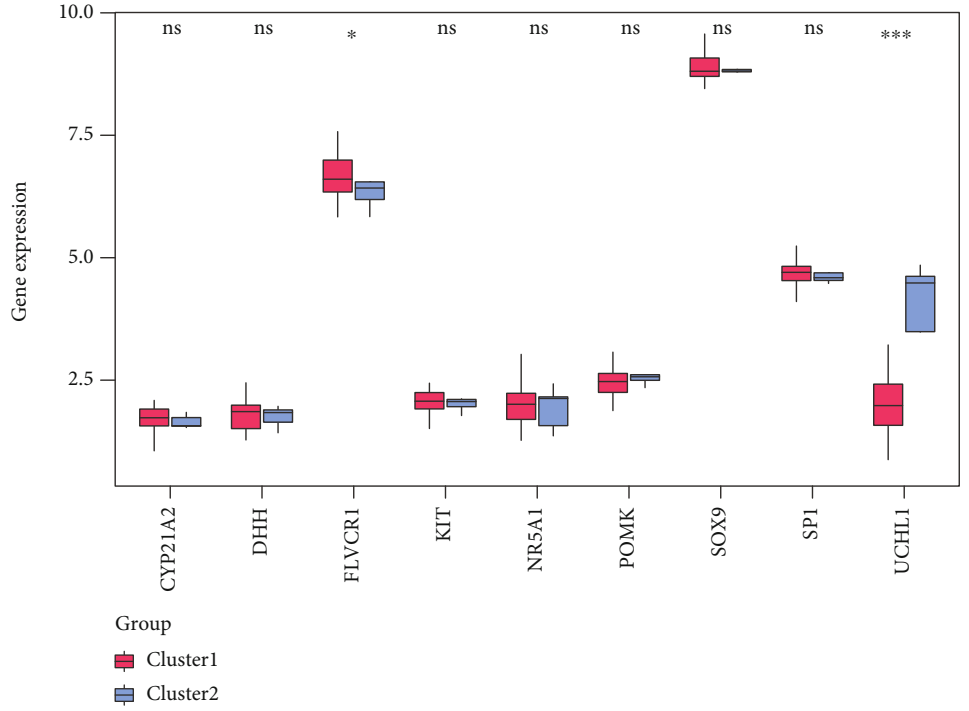

(d)

Figure 10: Differences of hub genes between two groups of IDD patients. (a)/(c): heatmaps and histograms of hub-related gene expressions in cluster1 and cluster2; (c): *x*-axis: hub genes; *y*-axis: gene expression level; red: cluster1, blue: cluster2. (b)/(d): heatmaps and histograms of mitochondrial dysfunction gene expressions in cluster1 and cluster2; (d): *x*-axis: mitochondria dysfunction genes; *y*-axis: gene expression level; red: cluster1, blue: cluster2. $P < 0.05$: significance.

dependent cell death. This finding is consistent with our validation results at the gene and protein levels. When IDD occurs, the FLVCR1 expression is low in both NP cells and AF cells.

NR5A1, also known as steroidogenic factor-1 (SF-1) or adrenal 4-binding protein (Ad4BP), was initially identified as a steroidogenic cell-specific transcription factor that regulates the transcription of steroidogenic genes. Recent

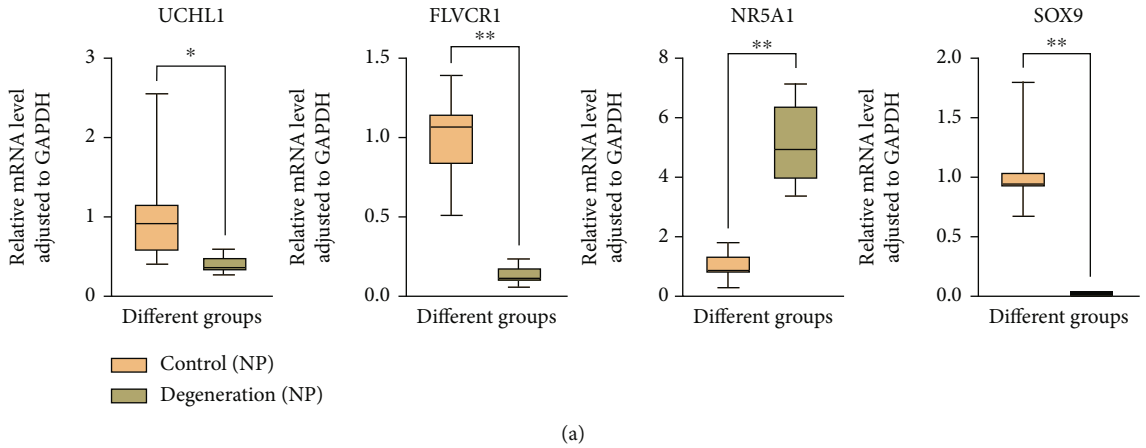

(a)

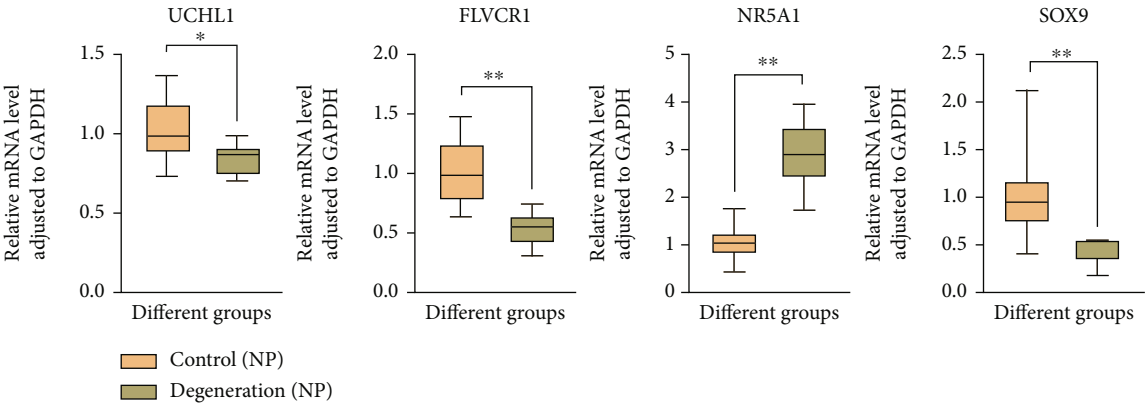

(b)

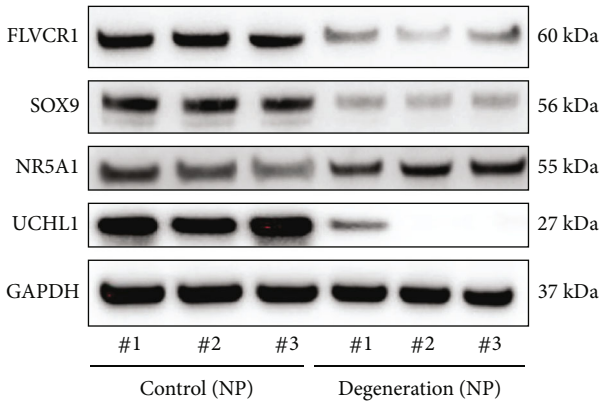

(c)

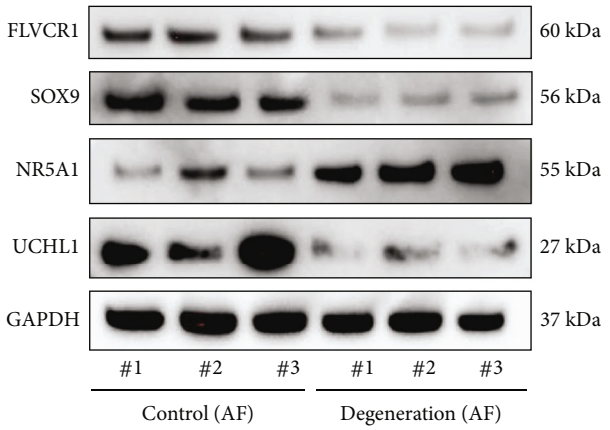

(d)

Figure 11: Continued.

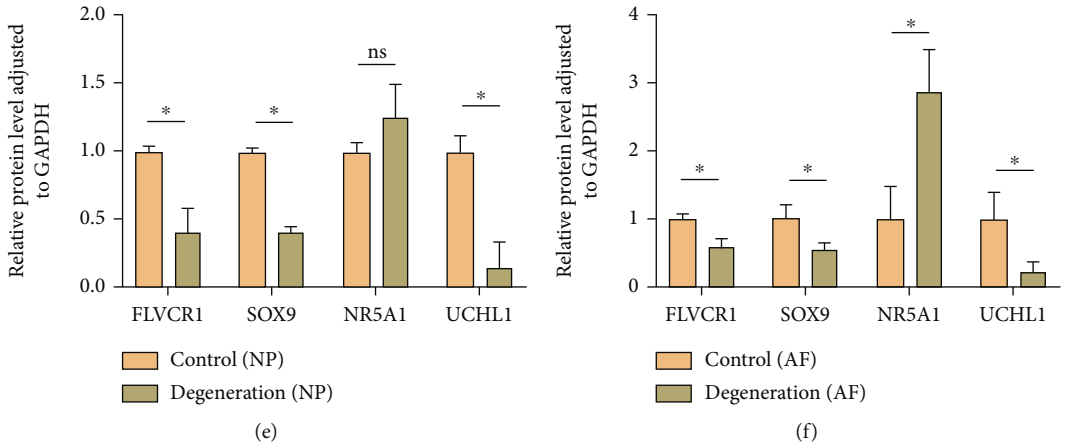

Figure 11: Validation of differential genes of mitochondrial dysfunction between normal intervertebral disc tissues and IDD tissues. (a)/(c): qPCR and WB results of normal intervertebral disc tissues and IDD nucleus pulposus tissues. (b)/(d): qPCR and WB results of normal intervertebral disc tissues and IDD anulus fibrous tissues. (e)–(f): quantitative analysis of protein expression (relative to GAPDH)∗ $p<0.05$; ∗∗$p<0.01$.

research proves NR5A1 can regulate nearly all glycolytic genes to adjust the nutrition metabolism of tissues. When normal IDD tissues are under a low oxygen condition, the physiologically hypoxic intervertebral disc rely on the hypoxia-inducible factor (HIF) family of transcription factors to mediate cellular responses to changes in oxygen tension. Mechanistically, HIF1 is the master regulator of glycolytic metabolism and cytosolic lactate levels. In addition, HIF1 regulates mitochondrial metabolism by promoting flux through the tricarboxylic acid cycle, inhibiting downsteam oxidative phosphorylation and controlling mitochondrial health through modulation of the mitophagic pathway [69]. The destruction to the low-oxygen condition of IDD will damage tricarboxylic acid cycle, so the energy metabolism is destroyed in cells. NR5A1, one of the important genes of glycolysis regulation and control, is significantly upregulated to correct energy metabolic disorders and maintain the normal energy metabolism in the intervertebral disc. Our bioinformatic analysis also validated this view that NR5A1 expression is significantly higher in IDD tissues.

Ubiquitin C-terminal hydrolase L1 (UCHL1) is a deubiquitinating enzyme that was originally found in neurons. UCHL1 was first studied in Alzheimer's disease (AD). UCHL1 protein expression decreased in the cerebral cortex of AD patients [70]. Our study confirmed that UCHL1 expression in IDD tissues decreases, which may be related to the regulating role of UCHL1 in mitochondria. Previous studies show that when UCHL1 is specifically knocked out, the key proteins involved in mitochondrial oxidative phosphorylation are significantly reduced, suggesting that UCHL1 may be involved in regulation of mitochondrial content and function [71]. When dUCH (a homolog of human UCHL1) was specifically knocked down in motor neurons, the motor neuron cells exhibited aberrant morphology and function of mitochondria, such as mtDNA depletion, an increase in mitochondrial size, and overexpression of antioxidant enzymes [72].

There were several limitations of our study. Firstly, only few RNA-sequencing datasets of IDD are available on the GEO database. Clinical data such as disease phenotype and radiological data are unavailable from published studies and public databases. Secondly, all of these analyses were obtained by data mining based on a series of bioinformatic algorithms, and we did not provide the original sequencing data with the clinical samples, so we cannot evaluate the quality of the sequencing samples, such as the actual degrees of IDD. Thirdly, the exact molecular mechanisms of candidate mitochondrial dysfunction related genes in IDD need to be further investigated using in-depth in vitro and in vivo scientific experiments. Finally, the nature of retrospective research limits the clinical value of this work, indicating multicentre or prospective studies are imperative to elucidate the relationship between mitochondrial dysfunction and IDD.

5. Conclusions

In this study, we used bioinformatics methods to compare tissue and peripheral blood RNA-seq data between IDD and control groups. We have successfully constructed a risk model which can call well predict IDD and have elaborated on the different groups of immune infiltrates and identified two modes of mitochondrial dysfunction. In addition, we identified four genes, verified the reliability by molecular biology experiment, associated with mitochondrial dysfunction. These findings may provide a new perspective for the diagnosis and treatment of IDD.

Data Availability

Publicly available datasets were analyzed in this study. This data can be found here: https://www.ncbi.nlm.nih.gov/geo/query/acc.cgi?acc=GSE70362;https://www.ncbi.nlm.nih.gov/geo/query/acc.cgi?acc=GSE124272.

Conflicts of Interest

The authors declare that they have no conflicts of interest.

Authors' Contributions

Zhengya Zhu, Zhongyuan He, and Tao Tang contributed equally to this work and should be regarded as co-first authors.

Acknowledgments

This work was supported by the National Natural Science Foundation of China (82102604, 31900583, 32071351, 81772400), the Natural Science Foundation of Guangzhou City (201807010031), foundation of Shenzhen Committee for Science and Technology Innovation (JCYJ20190809142211354, GJHZ20180929160004704), Sanming Project of Medicine in Shenzhen (SZSM201911002), the Beijing Municipal Health Commission (Grant No.BMHC-2021-6, BMHC-2019-9, BMHC-2018-4, PXM2020_026275_000002), AOCMF Translational approaches for bone constructs CPP, Sun Yat-sen University Clinical Research 5010 Program (2019009), Academic Affairs Office of Sun Yat-sen University(202211583, 202211589).

Supplementary Materials

Table S1 GO terms enrichment analysis. Table S2 KEGG pathway enrichment analysis. Table S3 GSEA. *(Supplementary Materials)*

References

[1] S. L. James, D. Abate, K. H. Abate et al., "Global, regional, and national incidence, prevalence, and years lived with disability for 354 diseases and injuries for 195 countries and territories, 1990-2017: A systematic analysis for the global burden of disease study 2017," *The Lancet*, vol. 392, no. 10159, pp. 1789–1858, 2018.

[2] R. A. Deyo, S. K. Mirza, and Clinical Practice, "Herniated lumbar intervertebral disk," *The New England Journal of Medicine*, vol. 374, no. 18, pp. 1763–1772, 2016.

[3] Y. Huo, D. Yang, L. Ma, H. Wang, W. Ding, and S. Yang, "Oblique lumbar interbody fusion with standalone cages for the treatment of degenerative lumbar spondylolisthesis: a retrospective study with 1-year follow-up," *Pain Research & Management*, vol. 2020, article 9016219, 6 pages, 2020.

[4] X. Guo, W. Ding, L. Liu, and S. D. Yang, "Intradiscal methylene blue injection for Discogenic low Back pain: a meta-analysis," *Pain Practice*, vol. 19, no. 1, pp. 118–129, 2019.

[5] B. L. Li, X. Liu, M. Gao et al., "Programmed NP cell death induced by mitochondrial ROS in a one-strike loading disc degeneration organ culture model," *Oxidative Medicine and Cellular Longevity*, vol. 2021, Article ID 5608133, 17 pages, 2021.

[6] P. J. Roughley, "Biology of intervertebral disc aging and Degeneration," *Spine*, vol. 29, no. 23, pp. 2691–2699, 2004.

[7] C. M. De Geer, "Intervertebral disk nutrients and transport mechanisms in relation to disk degeneration: a narrative literature review," *Journal of Chiropractic Medicine*, vol. 17, no. 2, pp. 97–105, 2018.

[8] L. Kang, S. Liu, J. Li, Y. Tian, Y. Xue, and X. Liu, "The mitochondria-targeted anti-oxidant MitoQ protects against intervertebral disc degeneration by ameliorating mitochondrial dysfunction and redox imbalance," *Cell Proliferation*, vol. 53, no. 3, article e12779, 2020.

[9] Z. Kazezian, R. Gawri, L. Haglund et al., "Gene expression profiling identifies interferon Signalling molecules and IGFBP3 in human degenerative annulus Fibrosus," *Scientific Reports*, vol. 5, no. 1, article 15662, 2015.

[10] Y. Wang, G. Dai, L. Jiang, S. Liao, and J. Xia, "Microarray analysis reveals an inflammatory transcriptomic signature in peripheral blood for sciatica," *BMC Neurology*, vol. 21, no. 1, p. 50, 2021.

[11] Y. Wang, G. Dai, L. Li et al., "Transcriptome signatures reveal candidate key genes in the whole blood of patients with lumbar disc prolapse," *Experimental and Therapeutic Medicine*, vol. 18, no. 6, pp. 4591–4602, 2019.

[12] J. T. Leek, W. E. Johnson, H. S. Parker, A. E. Jaffe, and J. D. Storey, "The sva package for removing batch effects and other unwanted variation in high-throughput experiments," *Bioinformatics*, vol. 28, no. 6, pp. 882-883, 2012.

[13] G. Stelzer, N. Rosen, I. Plaschkes et al., "The GeneCards suite: from gene data mining to disease genome sequence analyses," *Current protocols in bioinformatics*, vol. 54, no. 1, pp. 1–30, 2016.

[14] R. A. M. Villanueva and Z. J. Chen, "ggplot2: Elegant Graphics for Data Analysis," *Measurement: Interdisciplinary Research and Perspectives: Taylor & Francis*, vol. 17, no. 3, pp. 160–167, 2019.

[15] M. E. Ritchie, B. Phipson, D. I. Wu et al., "limma powers differential expression analyses for RNA-sequencing and microarray studies," *Nucleic Acids Research*, vol. 43, no. 7, article e47, 2015.

[16] R. Kolde and M. R. Kolde, "Package 'pheatmap'," *R Package*, vol. 1, no. 7, p. 790, 2015.

[17] A. Kassambara and M. A. Kassambara, "Package 'ggpubr'," *R Package*, vol. 6, 2020.

[18] D. Szklarczyk, A. L. Gable, D. Lyon et al., "STRING v11: protein-protein association networks with increased coverage, supporting functional discovery in genome-wide experimental datasets," *Nucleic Acids Research*, vol. 47, no. D1, pp. D607–D613, 2019.

[19] P. Shannon, A. Markiel, O. Ozier et al., "Cytoscape: a software environment for integrated models of biomolecular interaction networks," *Genome Research*, vol. 13, no. 11, pp. 2498–2504, 2003.

[20] J. Friedman, T. Hastie, N. Simon, R. Tibshirani, M. T. Hastie, and D. Matrix, "Package 'glmnet'," *Journal of Statistical Software*, vol. 33, no. 1, pp. 1–22, 2017.

[21] M. Gordon, T. Lumley, and M. M. Gordon, *Package 'forestplot'*, Advanced forest plot using 'grid'graphics. The Comprehensive R Archive Network, Vienna, Austria, 2019.

[22] F. E. J. B. Harrell, "Regression modeling strategies," *Bios*, vol. 330, no. 2018, p. 14, 2017.

[23] X. Robin, N. Turck, A. Hainard et al., "pROC: an open-source package for R and S+ to analyze and compare ROC curves," *BMC Bioinformatics*, vol. 12, no. 1, pp. 1–8, 2011.

[24] M. Ashburner, C. A. Ball, J. A. Blake et al., "Gene ontology: tool for the unification of biology," *Nature Genetics*, vol. 25, no. 1, pp. 25–29, 2000.

[25] M. Kanehisa and S. Goto, "KEGG: Kyoto encyclopedia of genes and genomes," *Nucleic Acids Research*, vol. 28, no. 1, pp. 27–30, 2000.

[26] G. Yu, L. G. Wang, Y. Han, and Q. Y. He, "clusterProfiler: an R package for comparing biological themes among gene clusters," *OMICS: A Journal of Integrative Biology*, vol. 16, no. 5, pp. 284–287, 2012.

[27] T. Wu, E. Hu, S. Xu et al., "ClusterProfiler 4.0: A universal enrichment tool for interpreting omics data," *The Innovation*, vol. 2, no. 3, article 100141, 2021.

[28] A. Subramanian, P. Tamayo, V. K. Mootha et al., "Gene set enrichment analysis: a knowledge-based approach for interpreting genome-wide expression profiles," *Proceedings of the National Academy of Sciences of the United States of America*, vol. 102, no. 43, pp. 15545–15550, 2005.

[29] A. Liberzon, C. Birger, H. Thorvaldsdóttir, M. Ghandi, J. . P. Mesirov, and P. Tamayo, "The Molecular Signatures Database Hallmark Gene Set Collection," *Cell Systems*, vol. 1, no. 6, pp. 417–425, 2015.

[30] S. Hanzelmann, R. Castelo, and J. Guinney, "GSVA: gene set variation analysis for microarray and RNA-seq data," *BMC Bioinformatics*, vol. 14, no. 1, p. 7, 2013.

[31] P. Langfelder and S. Horvath, "WGCNA: an R package for weighted correlation network analysis," *BMC Bioinformatics*, vol. 9, no. 1, p. 559, 2008.

[32] M. Cv, "STRING: a database of predicted functional associations between proteins," *Nucleic Acids Research*, vol. 31, no. 1, pp. 258–261, 2003.

[33] C.-H. Chin, S.-H. Chen, H.-H. Wu, C.-W. Ho, M.-T. Ko, and C.-Y. Lin, "cytoHubba: identifying hub objects and sub-networks from complex interactome," *BMC Systems Biology*, vol. 8, no. 4, pp. 1–7, 2014.

[34] A. M. Newman, C. B. Steen, C. L. Liu et al., "Determining cell type abundance and expression from bulk tissues with digital cytometry," *Nature Biotechnology*, vol. 37, no. 7, pp. 773–782, 2019.

[35] A. Kassambara and F. Mundt, "Package 'factoextra'," *Extract and visualize the results of multivariate data analyses*, vol. 76, 2017.

[36] C. W. Pfirrmann, A. Metzdorf, M. Zanetti, J. Hodler, and N. Boos, "Magnetic resonance classification of lumbar intervertebral disc degeneration," *Spine*, vol. 26, no. 17, pp. 1873–1878, 2001.

[37] S. Caprez, U. Menzel, Z. Li, S. Grad, M. Alini, and M. Peroglio, "Isolation of high-quality RNA from intervertebral disc tissue via pronase predigestion and tissue pulverization," *JOR Spine*, vol. 1, no. 2, article e1017, 2018.

[38] M. Saberi, X. Zhang, and A. Mobasheri, "Targeting mitochondrial dysfunction with small molecules in intervertebral disc aging and degeneration," *Geroscience*, vol. 43, no. 2, pp. 517–537, 2021.

[39] N. V. Vo, R. A. Hartman, P. R. Patil et al., "Molecular mechanisms of biological aging in intervertebral discs," *Journal of Orthopaedic Research*, vol. 34, no. 8, pp. 1289–1306, 2016.

[40] T. Matsuhashi, T. Sato, S. I. Kanno et al., "Mitochonic acid 5 (MA-5) facilitates ATP synthase oligomerization and cell survival in various mitochondrial diseases," *eBioMedicine*, vol. 20, pp. 27–38, 2017.

[41] E. Li, X. Li, J. Huang et al., "BMAL1 regulates mitochondrial fission and mitophagy through mitochondrial protein BNIP3 and is critical in the development of dilated cardiomyopathy," *Protein & Cell*, vol. 11, no. 9, pp. 661–679, 2020.

[42] T. Gao, X. Zhang, J. Zhao et al., "SIK2 promotes reprogramming of glucose metabolism through PI3K/AKT/HIF-1α pathway and Drp1-mediated mitochondrial fission in ovarian cancer," *Cancer Letters*, vol. 469, pp. 89–101, 2020.

[43] Y. Arribat, N. T. Broskey, C. Greggio et al., "Distinct patterns of skeletal muscle mitochondria fusion, fission and mitophagy upon duration of exercise training," *Acta Physiologica*, vol. 225, no. 2, article e13179, 2019.

[44] X. Xu, D. Wang, C. Zheng et al., "Progerin accumulation in nucleus pulposus cells impairs mitochondrial function and induces intervertebral disc degeneration and therapeutic effects of sulforaphane," *Theranostics*, vol. 9, no. 8, pp. 2252–2267, 2019.

[45] H. Lin, L. Zhao, X. Ma et al., "Drp1 mediates compression-induced programmed necrosis of rat nucleus pulposus cells by promoting mitochondrial translocation of p53 and nuclear translocation of AIF," *Biochemical and Biophysical Research Communications*, vol. 487, no. 1, pp. 181–188, 2017.

[46] W. Wu, D. Jing, X. Huang, W. Yang, and Z. Shao, "Drp1-mediated mitochondrial fission is involved in oxidized low-density lipoprotein-induced AF cella poptosis," *Journal of Orthopaedic Research*, vol. 39, no. 7, pp. 1496–1504, 2021.

[47] G. S. Shadel and T. L. Horvath, "Mitochondrial ROS signaling in organismal homeostasis," *Cell*, vol. 163, no. 3, pp. 560–569, 2015.

[48] S. Chen, L. Zhao, X. Deng et al., "Mesenchymal stem cells protect nucleus pulposus cells from compression-induced apoptosis by inhibiting the mitochondrial pathway," *Stem Cells International*, vol. 2017, Article ID 9843120, 10 pages, 2017.

[49] Z. Jiang, W. Lu, Q. Zeng, D. Li, L. Ding, and J. Wu, "High glucose-induced excessive reactive oxygen species promote apoptosis through mitochondrial damage in rat cartilage endplate cells," *Journal of Orthopaedic Research*, vol. 36, no. 9, pp. 2476–2483, 2018.

[50] J. Xu, H. Li, K. Yang et al., "Hyper-osmolarity environment-induced oxidative stress injury promotes nucleus pulposus cell senescence in vitro," *Bioscience Reports*, vol. 39, no. 9, 2019.

[51] R. Zhao, L. Yang, S. He, and T. Xia, "Nucleus pulposus cell senescence is regulated by substrate stiffness and is alleviated by LOX possibly through the integrin β1-p38 MAPK signaling pathway," *Experimental Cell Research*, vol. 417, no. 2, article 113230, 2022.

[52] H. Yin, K. Wang, A. Das et al., "The REDD1/TXNIP complex accelerates oxidative stress-induced apoptosis of nucleus pulposus cells through the mitochondrial pathway," *Oxidative Medicine and Cellular Longevity*, vol. 2021, Article ID 7397516, 22 pages, 2021.

[53] Z. L. Wu, Y. J. Chen, G. Z. Zhang et al., "SKI knockdown suppresses apoptosis and extracellular matrix degradation of nucleus pulposus cells via inhibition of the Wnt/β-catenin pathway and ameliorates disc degeneration," *Apoptosis*, vol. 27, no. 1-2, pp. 133–148, 2022.

[54] C. Feng, M. Yang, M. Lan et al., "ROS: crucial intermediators in the pathogenesis of intervertebral disc degeneration," *Oxidative Medicine and Cellular Longevity*, vol. 2017, Article ID 5601593, 12 pages, 2017.

[55] S. Rajasekaran, C. Tangavel, S. V. A. KS et al., "Inflammaging determines health and disease in lumbar discs–evidence from differing proteomic signatures of healthy, aging, and degenerating discs," *The Spine Journal*, vol. 20, no. 1, pp. 48–59, 2020.

[56] L. Yang, Z. Rong, M. Zeng et al., "Pyrroloquinoline quinone protects nucleus pulposus cells from hydrogen peroxide-induced apoptosis by inhibiting the mitochondria-mediated pathway," *European Spine Journal*, vol. 24, no. 8, pp. 1702–1710, 2015.

[57] Z. B. Chen, Y. B. Yu, Q. B. Wa, J. W. Zhou, M. He, and Y. Cen, "The role of quinazoline in ameliorating intervertebral disc degeneration by inhibiting oxidative stress and anti-inflammation via NF-κB/MAPKs signaling pathway," *European Review for Medical and Pharmacological Sciences*, vol. 24, no. 4, pp. 2077–2086, 2020.

[58] B. Peng, J. Hao, S. Hou et al., "Possible pathogenesis of painful intervertebral disc degeneration," *Spine*, vol. 31, no. 5, pp. 560–566, 2006.

[59] V. Lefebvre and M. Dvir-Ginzberg, "SOX9 and the many facets of its regulation in the chondrocyte lineage," *Connective Tissue Research*, vol. 58, no. 1, pp. 2–14, 2017.

[60] A. Symon and V. Harley, "SOX9: a genomic view of tissue specific expression and action," *The International Journal of Biochemistry & Cell Biology*, vol. 87, pp. 18–22, 2017.

[61] C. F. Liu, W. E. Samsa, G. Zhou, and V. Lefebvre, "Transcriptional control of chondrocyte specification and differentiation," *Seminars in Cell & Developmental Biology*, vol. 62, pp. 34–49, 2017.

[62] C. D. Oh, Y. Lu, S. Liang et al., "SOX9 regulates multiple genes in chondrocytes, including genes encoding ECM proteins, ECM modification enzymes, receptors, and transporters," *PLoS One*, vol. 9, no. 9, article e107577, 2014.

[63] F. Barrionuevo, M. M. Taketo, G. Scherer, and A. Kispert, "_Sox9_ is required for notochord maintenance in mice," *Developmental Biology*, vol. 295, no. 1, pp. 128–140, 2006.

[64] Y. Sugimoto, A. Takimoto, H. Akiyama et al., "Scx+/Sox9+ progenitors contribute to the establishment of the junction between cartilage and tendon/ligament," *Development*, vol. 140, no. 11, pp. 2280–2288, 2013.

[65] P. Smits and V. Lefebvre, "Sox5 and Sox6 are required for notochord extracellular matrix sheath formation, notochord cell survival and development of the nucleus pulposus of intervertebral discs," *Development*, vol. 130, no. 6, pp. 1135–1148, 2003.

[66] S. P. Henry, S. Liang, K. C. Akdemir, and B. de Crombrugghe, "The postnatal role of Sox9 in cartilage," *Journal of Bone and Mineral Research*, vol. 27, no. 12, pp. 2511–2525, 2012.

[67] J. G. Quigley, C. C. Burns, M. M. Anderson et al., "Cloning of the cellular receptor for feline leukemia virus subgroup C (FeLV-C), a retrovirus that induces red cell aplasia," *Blood*, vol. 95, no. 3, pp. 1093–1099, 2000.

[68] D. Chiabrando, S. Marro, S. Mercurio et al., "The mitochondrial heme exporter FLVCR1b mediates erythroid differentiation," *The Journal of Clinical Investigation*, vol. 122, no. 12, pp. 4569–4579, 2012.

[69] E. S. Silagi, E. Schipani, I. M. Shapiro, and M. V. Risbud, "The role of HIF proteins in maintaining the metabolic health of the intervertebral disc," *Nature Reviews Rheumatology*, vol. 17, no. 7, pp. 426–439, 2021.

[70] M. Guglielmotto, D. Monteleone, M. Boido et al., "Aβ1-42-mediated down-regulation of Uch-L1 is dependent on NF-κB activation and impaired BACE1 lysosomal degradation," *Aging Cell*, vol. 11, no. 5, pp. 834–844, 2012.

[71] H. Gao, R. Antony, R. Srinivasan, P. Wu, X. Wang, and Y. Li, "UCHL1 regulates oxidative activity in skeletal muscle," *PLoS One*, vol. 15, no. 11, article e0241716, 2020.

[72] T. K. T. Huynh, T. T. T. Mai, M. A. Huynh, H. Yoshida, M. Yamaguchi, and T. T. P. Dang, "Crucial roles of ubiquitin Carboxy-terminal hydrolase L1 in motor neuronal health byDrosophilaModel," *Antioxidants & Redox Signaling*, vol. 37, no. 4-6, pp. 257–273, 2022.

Hindawi
Oxidative Medicine and Cellular Longevity
Volume 2022, Article ID 3511967, 13 pages
https://doi.org/10.1155/2022/3511967

Research Article

miR-328-5p Induces Human Intervertebral Disc Degeneration by Targeting WWP2

Jing Yan,[1] Lun-Gang Wu,[1] Ming Zhang,[2] Tao Fang,[3] Wei Pan,[1] Jia-Li Zhao,[1] and Quan Zhou[1]

[1]*Department of Orthopaedics, The Affiliated Huai'an Hospital of Xuzhou Medical University and The Second People's Hospital of Huai'an, Huai'an, Jiangsu 223002, China*
[2]*Department of Orthopedics, Zhongda Hospital, School of Medicine, Southeast University, Nanjing, Jiangsu 210009, China*
[3]*Department of Orthopedics, The First People's Hospital of Changshu, Jiangsu 210009, China*

Correspondence should be addressed to Quan Zhou; wuque1@126.com

Received 17 July 2022; Revised 30 August 2022; Accepted 7 September 2022; Published 29 September 2022

Academic Editor: Sidong Yang

Intervertebral disc degeneration (IDD) development is regulated by miRNA, including inflammatory reactions, cell apoptosis, and degradation of extracellular matrix. Nucleus pulposus cells apoptosis has a absolute influence in the development of IDD. This experiment explores the mechanism of miR-328-5p regulating IDD. Through the analysis of miRNA and mRNA microarray database, we screened the target genes miR-328-5p and WWP2. We verified the expression of miR-328-5p, WWP2, and related apoptotic genes in normal and degenerative nucleus pulposus tissues by qRT-PCR. The expressions of WWP2, Bcl-2, and Bax were detected by qRT-PCR and western blot after transfection to nucleus pulposus cell. The nucleus pulposus cell proliferation and apoptosis after transfection were confirmed by CCK8 and flow cytometry. Luciferase reporter assay and bioinformatics analyzed the targeting relationship between miR-328-5p and WWP2. Firstly, the qRT-PCR experiments confirmed the significant increase of miR-328-5p expression, while significant reduction of WWP2 in a degenerative tissues compared to the normal tissues. Surprisingly, miR-328-5p expression was positively, while that of WWP2 negatively correlated with the degeneration grade of IDD. And we also identified the high expression of Bax and Caspase3, while low expression of Bcl-2 in a degenerative tissues. After miR-328-5p mimic transfected into nucleus pulposus cell, qRT-PCR and western blot confirmed that WWP2 and Bcl-2 expressions were downregulated, while Bax and Caspase3 expressions were upregulated, and the same results were obtained by knocking down WWP2. CCK8 and flow cytometry confirmed that miR-328-5p inhibited the proliferation and induced apoptosis of nucleus pulposus cells. WWP2 is a target gene of miR-328-5p by bioinformatics and luciferase reporter assay. In summary, miR-328-5p targets WWP2 to regulate nucleus pulposus cells apoptosis and then participates in the development of IDD. Furthermore, this study may provide new references and ideas for IDD treatment.

1. Introduction

With the increasing incidence of low back pain (LBP), it has become the most important trigger to disability worldwide, which has brought a tremendous economic pressure [1–3]. The cause of LBP is very complex. And some known factors affect the advancement of LBP include genes, age, and lousy living habits (such as occupation, smoking, trauma, and mechanical loading) [4, 5]. Furthermore, it is believed that the main cause of LBP is IDD [6–8]. As a bridge between adjacent vertebral bodies, intervertebral disc includes the nucleus pulposus (NP), annulus fibrosus, and the cartilaginous endplate [9]. The most important pathological feature of IDD is the apoptosis of nucleus pulposus cells [10–13]. The apoptosis of nucleus pulposus cells triggers the progress of IDD [14–16], and this affects clearly the disc structure balance. Some studies suggested that abnormal apoptosis is associated with degenerative diseases such as osteoarthritis, IDD, and cancer [17–19].

However, the current treatment for IDD is limited to symptomatic intervention and cannot completely improve the prognosis of the disease [20]. Many studies confirmed

Table 1: Clinical features of the study population.

Variable	Normal ($n = 10$)	IDD ($n = 10$)	P value
Age (years)	38.5 ± 3.5	41.6 ± 4.8	0.136[a]
BMI (kg/m^2)	23.2 ± 1.0	23.5 ± 0.9	0.586[a]
Sex, n (%)			
(i) Female	4 (40)	3 (30)	0.639[b]
(ii) Male	6 (60)	7 (70)	

[a]Student's t-test. [b]Two-sided x^2-test. Data are presented as the mean ± SD or count (%).

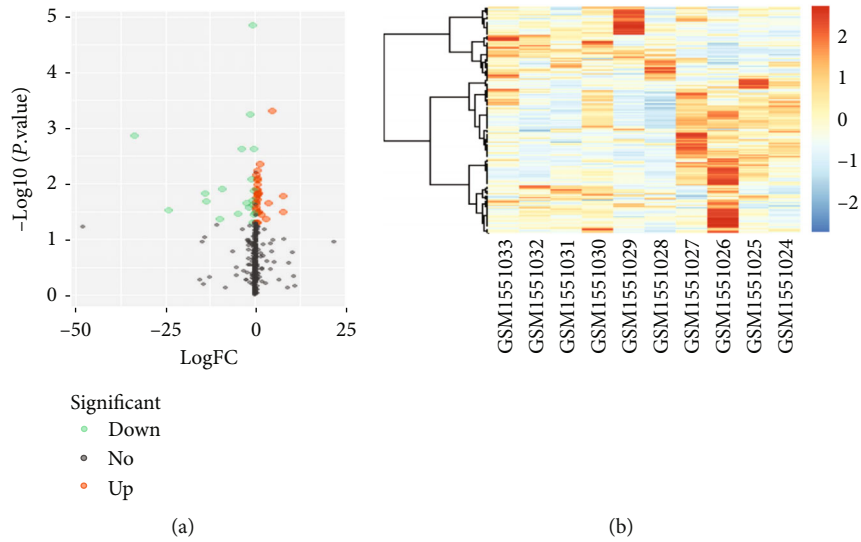

Figure 1: The screening of miRNAs expressions in normal and degenerative nucleus pulposus tissues. (a) a volcano plot demonstrates the upregulation and downregulation of different miRNAs expression by |logFC| > 1, |P.V value| < 0.05 as selection criteria. (b) heatmap for hierarchical clustering of selected miRNA expression in the tissue sample.

that some regulatory genes have an essential impact in the incidence and development of IDD, such as microRNA (miRNA). The miRNA are single-stranded noncoding small RNA with 18 to 24 bp nucleotide sequences, which participates in regulating the cell proliferation and apoptosis [21–25]. And miRNA can negatively regulate the posttranscriptional gene expression in different species by either inhibiting mRNA translation or promoting mRNA degradation [25, 26]. Previous studies have also found that miRNA affects the progress of IDD by facilitating inflammatory response, cell apoptosis, and degradation of extracellular matrix [27]. Furthermore, miRNA has contributed to cardiovascular disease, cancer, leukemia, and skeletal muscle diseases [28]. Therefore, further research on the mechanism of miRNA regulation of IDD may lead to new therapeutic directions.

Some studies have found miR-328-5p is atypically expressed in lung cancer, breast cancer, and other tumors. In addition, the researcher indicated miR-328-5p was related with the proliferation and apoptosis of cancer cells [29–32]. Furthermore, studies have shown dissimilarity expression of WWP2 in various diseases such as oral cancer, endometrial cancer, ovarian cancer, glioma, and lung cancer by regulating cell apoptosis [33–38]. Both miR-328-5p and its target gene WWP2 can affect cell proliferation and apoptosis, and the mechanism of miR-328-5p mediating WWP2 regulating IDD has not been reported. This series of studies aims to research the mechanism of the above regulatory pathways and whether they are involved in the formation of IDD by inducing nucleus pulposus cell apoptosis.

2. Materials and Methods

2.1. Clinical Sample Collection. We obtained 20 human NP samples via surgical discectomy. Surgical indications: (1) failure of conservative treatment and (2) progressive neurological deficits. Patients were excluded with isthmus or degenerative spondylolisthesis, ankylosing spondylitis, and diffuse idiopathic hyperostosis. According to T2-weighted midsagittal pfirrmann disc degeneration grading criteria [39].Grade I-II are normal intervertebral discs, and grade III-V are degenerative intervertebral discs. Table 1 presents the clinical features of patient.

2.2. Isolation and Culture of NP Cells. The NP tissue was separated from the intervertebral disc, made into 2-3 mm^3 sections under the microscope in aseptic conditions, and

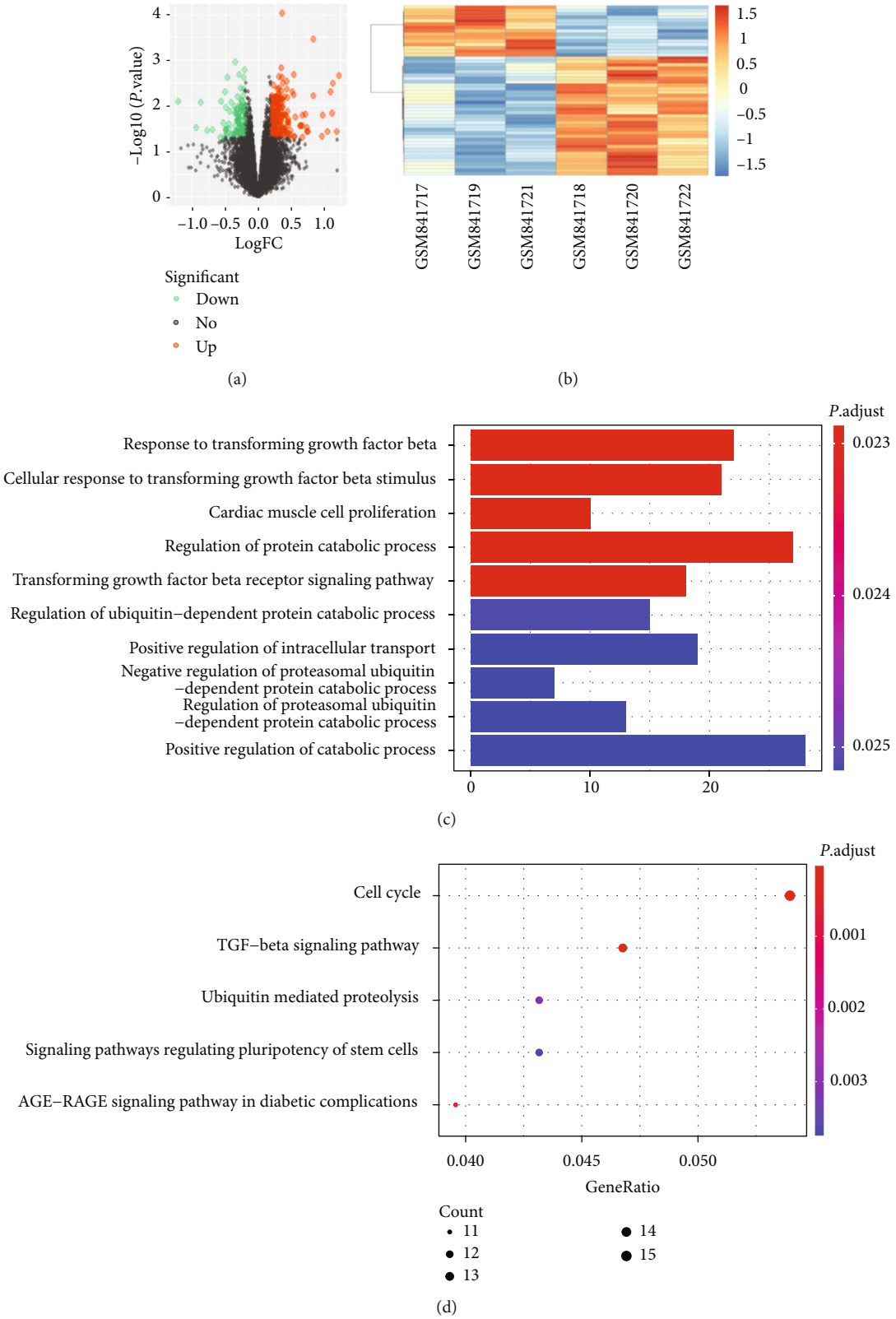

Figure 2: Assessment of different mRNAs expressions in normal and degenerative nucleus pulposus tissues. (a) a volcano plot of mRNAs expression by $|logFC| > 1, |P.V\ value| < 0.05$ as selection criteria. (b) heatmap for hierarchical clustering of selected mRNA expression. (c and d) GO, and KEGG functional annotations were performed on the differentially screened mRNAs, respectively. The bar chart represented GO enrichment analysis, while the bubble chart represented KEGG enrichment analysis.

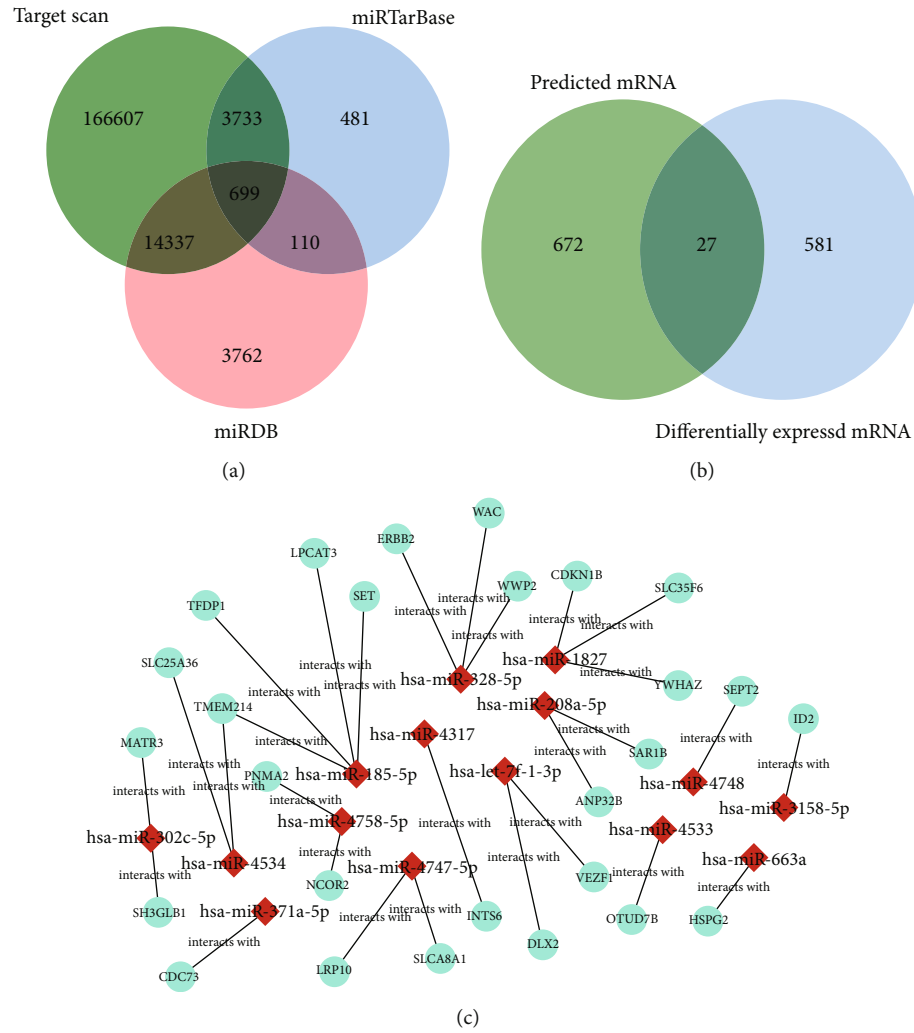

FIGURE 3: Interaction between differential miRNAs and their downstream target gene mRNAs: (a) the intersection of three datasets, (b) 27 different mRNAs, and (c) cytoscape analyzed the network diagram.

washed three times with PBS. Then prepared tissues were digested with 0.25 mg/mL type II collagenase (Invitrogen; Thermo Fisher Scientific) at 37°C for 12 h in Dulbecco's Modified Eagle Medium (GIBCO, NY, USA). Then NP cells isolated from NP tissues by trypsin were placed in DMEM/F12 incubated at 37°C with 5% CO_2. The second generation of cells was chosen for the following experiment.

2.3. Transfection of NP Cells. The miR-328-5p mimic/inhibitor, mimi/inhibitor control, WWP2 siRNA, and siRNA control were derived from Sangon (Shanghai, China). In our study, miR-328-5p mimic/inhibitor promote/inhibit the expression of miR-328-5p, and mimic/inhibitor control were used as control groups, respectively. WWP2 siRNA inhibits WWP2 expression in the NP cells. According to the reagent instructions, RNA transmate was used to transfect the NP cells (Sangon, Shanghai, China). The cells were collected 48 hours later for subsequent experiments.

2.4. qRT-PCR. General RNA was obtained from NP tissue or cultured NP cells using TRIZON (TianGen, Beijing, China) according to reagent instructions. We quantified miRNA and mRNA expression levels in NP tissues or cells by Light-Cycler 480 II (Roche Diagnostics, Indianapolis, USA). The PCR reaction system of 20 ul contained 10 ul Universal SYBR Green Fast qPCR Mix, 2 ul cDNA, 0.8ul primers, and 7.2 ul nuclease-free water. The reaction conditions: 95°C for 15 min, 40 cycles for 10 s at 95°C, and 60°C for 20s. The experiment was performed three times. Experiment is based on U6 and β-actin [40]. Gene expression was measured using the $2^{-\triangle\triangle Ct}$. Primers are as follows: miR-328-5p forward: AACGAGACGACGACAGAC, reverse: GGGG GGGCAGGAGGGGCTCAGGG; WWP2 forward: GAGA TGGACAACGAGAAG, reverse: CTCCTCAATGGCATAC AG; Bcl-2 forward: CAGCTGCACCTGACGCCCTT, reverse: GCCTCCGTTATCCTGGATCC; Bax forward: CCCGAGAGGTCTTTTTCCGAG, reverse: CCAGCCCAT GATGGTTCTGAT; Caspase3 forward: ATGGTTTGAGC

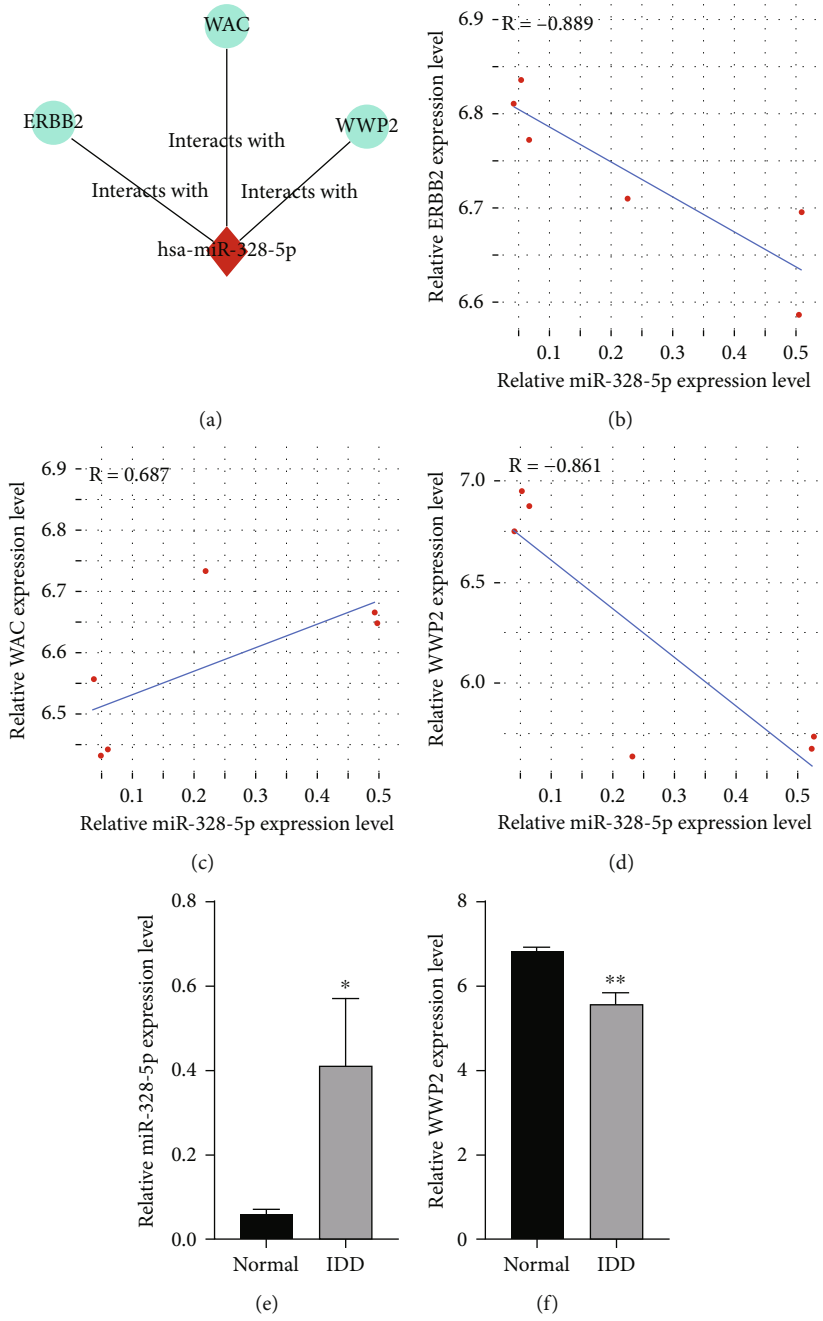

Figure 4: Correlation and differentially expression of miR-328-5p and WWP2. (a) the network diagram between miR-328-5p and its downstream genes. (b, c, and d) the correlation between miR-328-5p and its target genes. (e and f) significant differences in miR-328-5p and WWP2 expression. $^{*}P < 0.05$, $^{**}P < 0.01$.

CTGAGCAGA, reverse: GGCAGCATCATCCACACATAC; U6 forward: CTCGCTTCGGCAGCACA, reverse: AACGCT TCACGAATTTGCGT; β-actin forward: AGGGGCCGGAC TCGTCATACT, reverse: GGCGGCACCACCATGTACCCT.

2.5. Western Blot. The protein was obtained with RIPA and BCA (Beyotime, Shanghai, China) measures protein concentration. The NC membrane was blocked with 5% skimmed milk at room temperature for 2 h, then washed three times with TBST and added overnight to primary antibody at 4°C. The primary antibodies: anti-WWP2 antibody (Proteintech, Wuhan, China), anti-Bax antibody (Cell Signaling, Danvers, MA, USA), anti-Bcl-2 antibody (Cell Signaling, MA, USA), anti-Caspase3 antibody (Cell Signaling, MA, USA), and anti-beta-actin antibody (Proteintech, Wuhan, China). After primary antibody incubation, the NC film was washed three times with TBST and addted to goat anti-rabbit or mouse antibody (Vicmed, Xuzhou, China) for 2 h at room temperature in the dark. Beta actin was selected as the internal control [40].

2.6. CCK8. The cultured NP cells were transferred on 96-well plates by 2×10^4 cells/well, and added with miR-328-5p

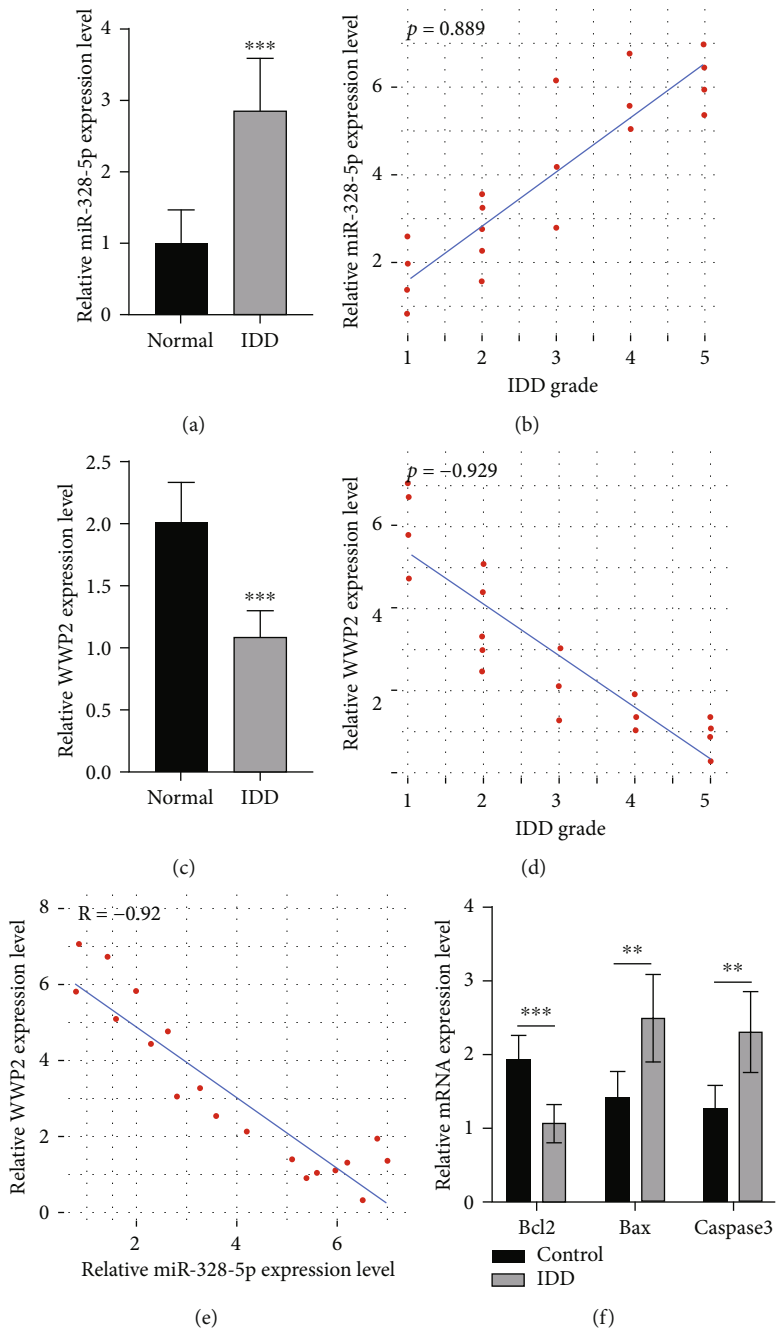

Figure 5: Differential expression of relevant miRNA and mRNA. (a) miR-328-5p expression difference. (b) Correlation between miR-328-5p gene expression with IDD grade. (c) WWP2 gene expression difference. (d) Correlation between WWP2 gene expression with IDD grade. (e) Correlation between miR-328-5p and WWP2. (f) Bcl-2, Bax and Caspase3 gene expression. $**P < 0.01$, $*** P < 0.001$, degenerative VS normal nucleus pulposus tissues, $n = 10$.

mimic/inhibitor, and miR-control. Subsequent to the incubation, the cell culture medium was changed at 0 h, 12 h, 24 h, and 36 h of each well. 10 ul CCK8 reagent and 90 ul DMEM were added into every well and incubated for another 2 h at 37°C by the CCK8 kit (Vicmed, Xuzhou, China). The optical density was measured at 450 nm, and the experiment was repeated three times for each group.

2.7. Flow Cytometry. The detection of NP apoptosis was carried out by the flow cytometry instructions (KeyGEN, Nanjing, China). First, the transfected NP cells were separated in 0.25% trypsin (without EDTA) (Vicmed, Xuzhou, China). After rinsing the cells twice with PBS, 1×10^5 cells were collected by centrifugation for 5 min at 2000 rpm. It is essential to rinse off as much residual trypsin digestive fluid as possible. After suspension of 500 ul binding buffer, each

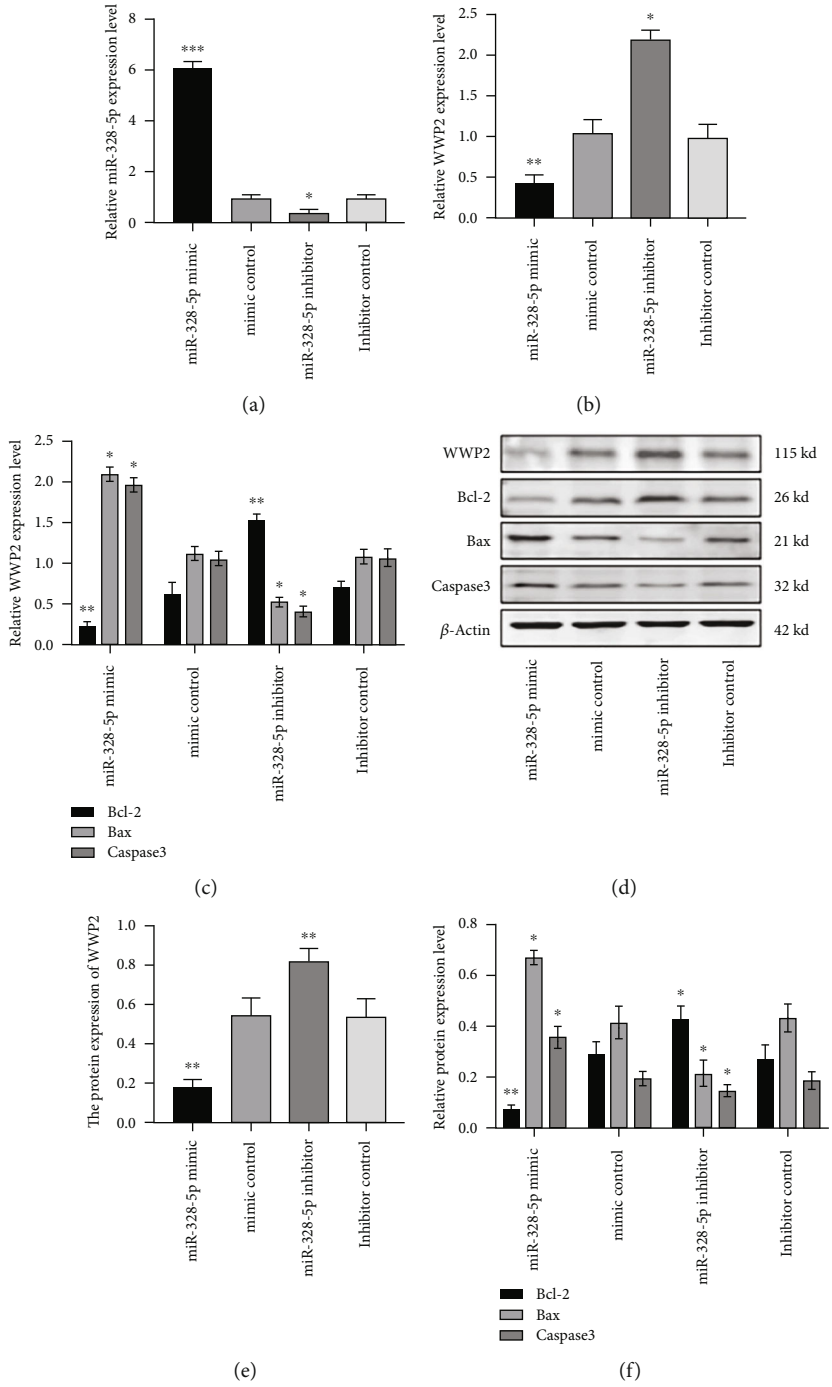

Figure 6: Continued.

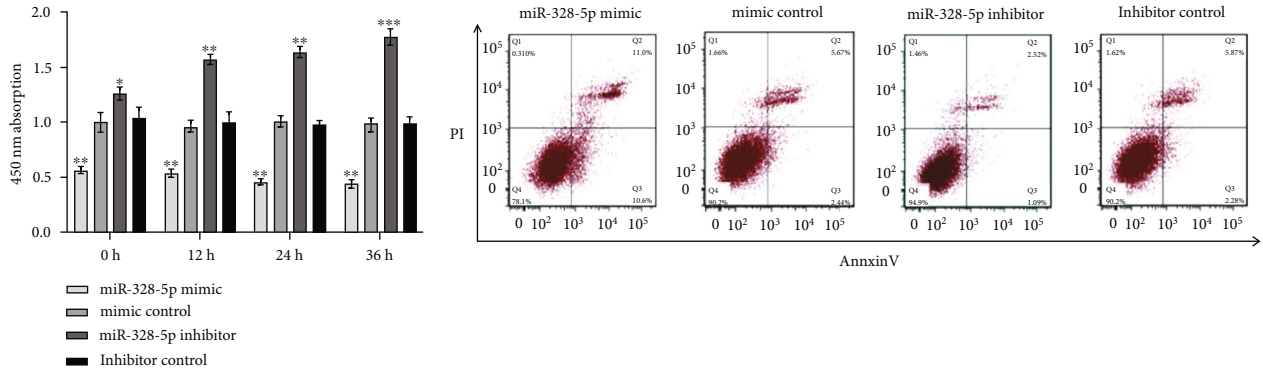

Figure 6: MiR-328-5p regulates WWP2 expression and promotes apoptosis of NP cells. (a) miR-328-5p gene expression. (b) WWP2 gene expression. (c) Bcl-2, Bax and Caspase3 gene expression. (d and e) WWP2 protein expression. (d and f) Bcl-2, Bax and Caspase3 protein expression. (g) NP cells proliferation. (h) NP cells apoptosis. $*P < 0.05$, $**P < 0.01$, $***P < 0.001$.

centrifugation tube was added 5 ul Annexinv-APC and 5 ul PI. The samples were thoroughly mixed, and the reaction was carried out at room temperature in the dark for 5-15 min. Finally, flow cytometry was used for observation and detection. Three experiments are required.

2.8. Luciferase Reporter Assay. In order to construct wild or mutant-type expression vectors, the WWP2 3′-UTR binding to miR-328-5p was inserted into the GV272 vector. Then, NP cells were added with wild type (Wt) or mutant type (Mut) WWP2 3′-UTR reporter plasmid and miR-328-5p mimic. Luciferase enzyme activity was detected according to Promega (Madison, WI, USA) reagent instructions after transfection 48 h. The luciferase enzyme activity was normalized to renilla luciferase activity. And western blot was used to detect WWP2 protein expression. The experiment was performed three times.

2.9. Statistical Analysis. Statistical was analyzed by the SPSS 26 (SPSS, Chicago, USA). GraphPad Prism 8.4 (GraphPad Software, CA, USA) was used for graphical representation. Mean ± SD was used to analyze the experimental data. t -test or one-way ANOVA was used for inter-group data analysis. Pearson's test was used for correlation analysis. $P < 0.05$ indicates statistical difference.

2.10. Ethics Statement. The Ethics Committee of Huai'an Affiliated Hospital of Xuzhou Medical University approved this study. Human NP tissue samples were obtained from patients who underwent surgery in Huai'an Affiliated Hospital of Xuzhou Medical University from September 2020 to April 2021. Meanwhile, the patients' written consent was informed, and the tissue samples were obtained during the operation.

3. Results

3.1. Assessment of Differentially Expressed miRNAs. A volcanic map of the dataset (GSE63492) showed that some miRNAs are differentially expressed between normal and degenerated nucleus pulposus tissues among the 31 miRNAs, hsa-miR-328-5p, and hsa-miR-183-3p expression were upregulated. And 21 miRNAs expression, including miR-486-5p, hsa-miR-486-5p were downregulated (Figure 1(a)). Heatmap figure shows that individual miRNA expressions differed significantly (Figure 1(b)).

3.2. Assessment of Differentially Expressed mRNAs. The volcano map analysis database (GSE34095) obtained a pairwise comparison of mRNA expression between normal and degenerative nucleus pulpous tissues. The experiment identified 348 differentially expressed upregulated genes such as TGFBI and PDGFC, while 260 downregulated genes such as WWP2 and MPST (Figure 2(a)). Further, the stratified clustering analysis of intervertebral disc dataset using heatmap revealed differences in the expression of some genes (Figure 2(b)). GO including molecular function, cellular component, and biological process, and KEGG enrichment analysis was performed for differentially expressed mRNA using R language (Figures 2(c) and 2(d)).

3.3. Interactions between miRNA and mRNA. In order to analyse the relationship between mRNAs and miRNA, we go through miRTarBase (https://www.mirbase.org), TargetScan (http://www.targetscan.org/), and miRDB (http://mirdb.org/index.html) database to predict the miRNA target gene. The intersection of threedatasets was obtained by the Venn diagram representing 35 miRNAs and their downstream 699 target gene mRNAs (Figure 3(a)). And 27 different mRNAs containing WWP2 were obtained by predicting intersection mRNAs via Venn diagram (Figure 3(b)). Furthermore, cytoscape analyzed the network diagram of 27 differential mRNAs and their upstream miRNAs (Figure 3(c)).

3.4. Correlation and Modulation of miR-328-5p and WWP2 Expression. Cytoscape was performed to visualize the network diagram between miR-328-5p and its downstream genes (Figure 4(a)). Further, we confirmed the correlation between the miR-328-5p and its target genes by gene chip data and analyzed it using Pearson correlation analysis (Figures 4(b), 4(c), and 4(d). The microarray data expression of miR-328-5p and WWP2 genes were statistically

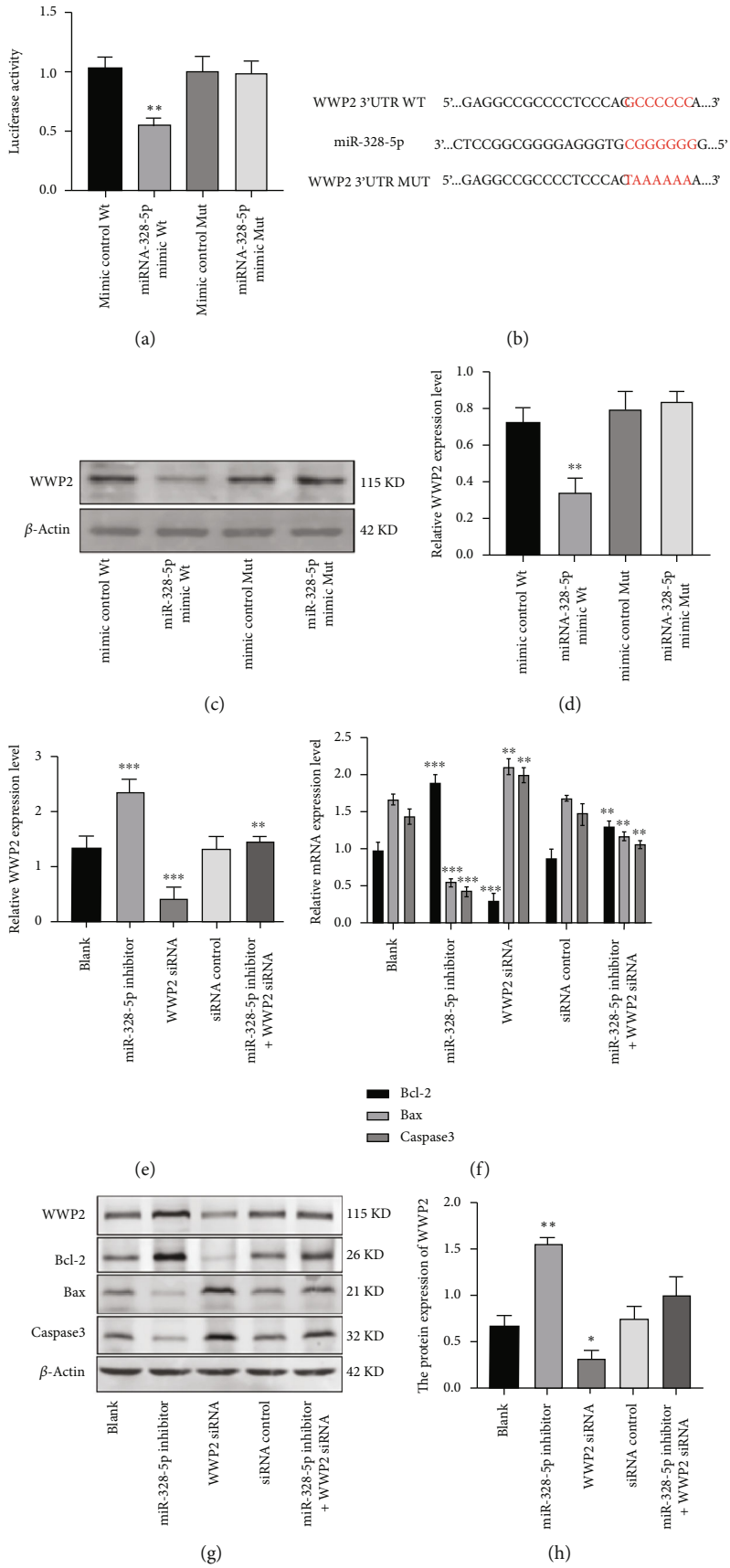

Figure 7: Continued.

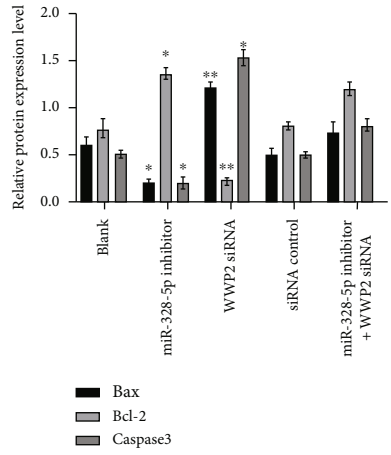

Figure 7: MiR-328-5p promotes the apoptosis of NP cells by directly targeting WWP2. (a) The cotransfection of WWP2 3′-UTR with miR-328-5p mimic. (b) Represent the corresponding sequence of Wt or Mut WWP2 3′-UTR plasmid and miR-328-5p. (c and d) WWP2 protein expression after the cotransfection. (e and f) WWP2, Bcl-2, Bax, and Caspase3 gene expression. (g, h, and i) WWP2, Bcl-2, Bax, and Caspase3 protein expression. $*P < 0.05$, $**P < 0.01$, $*** P < 0.001$.

significant (Figures 4(e) and 4(f)). The most important pathological feature of IDD is the apoptosis of nucleus pulposus cells [10–13]. Bioinformatics analysis shows that WWP2 is a downstream target gene of miR-328-5p. The conditions of target genes we selected were as follows: high connectivity of network diagram, negative correlation between miRNA and its downstream target mRNA, regulate cell apoptosis, and at the same time, relevant literature was reviewed to understand the function of miRNA and mRNA, so we selected miR-328-5p-WWP2 pathway as our research object. We hypothesize that miR-328-5p regulates IDD development by mediating WWP2.

3.5. Differentially Expressed of Relevant miRNA and mRNA in Degenerative and Normal Nucleus Pulposus Tissues. Experiment confirmed that miR-328-5p gene expression was upregulated ($P < 0.01$, Figure 5(a)). Spearman's correlation found that miR-328-5p expression was positively correlated with IDD grade ($P = 0.889$, $P < 0.001$, Figure 5(b)). WWP2 expression was downregulated ($P < 0.05$, Figure 5(c)), and the Spearman's correlation of WWP2 expression was negatively correlated with IDD grade ($P = -0.929$, Figure 5(d)). Pearson's correlation between miR-328-5p and WWP2 gene expression was significantly negative ($R = -0.92$, $P < 0.001$, Figure 5(e)). Bax and Caspase3 expression was significantly increased in the degenerative nucleus pulposus tissues, while Bcl-2 was decreased ($P < 0.05$, Figure 5(f)).

3.6. MiR-328-5p Regulates WWP2 Expression and Promotes Apoptosis of NP Cells. MiR-328-5p mimic induced miR-328-5p, Bax and Caspase3 gene expression obviously, while WWP2 and Bcl-2 was downregulated compared to the control group (Figures 6(a), 6(b), and 6(c)). miR-328-5p mimic significantly inhibited the protein expression of WWP2, Bcl-2 and promoted Bax and Caspase3 expression, while the miR-328-5p inhibitor obtained the opposite result (Figures 6(d), 6(e), and 6(f)). CCK8 assay confirmed that miR-328-5p mimic ignificantly inhibited the proliferation of NP cells (Figure 6(g)). Flow cytometry identified that the apoptosis of NP cells increased obviously after the addition of miR-328-5p mimic (Figure 6(h)). In conclusion, the above experimental results suggest that miR-328-5p can induce NP cells apoptosis.

3.7. MiR-328-5p Promotes the Apoptosis of NP Cells by Directly Targeting WWP2. The luciferase activities were decreased after the cotransfection of wild type (Wt) WWP2 3′-UTR reporter plasmid and miR-328-5p mimic into NP cells (Figure 7(a)). The corresponding sequence of WWP2 3′-UTR plasmids Wt or Mut and miR-328-5p was enumerated (Figure 7(b)). WWP2 protein expression was downregulated after cotransfecting Wt and miR-328-5p mimic (Figures 7(c) and 7(d)). These results indicated that miR-328-5p directly regulates WWP2. And miR-328-5p inhibitor significantly upregulated WWP2 and Bcl-2 gene expression, while Bax and Caspase3 was downregulated compared to the control group (Figures 7(e) and 7(f)). And WWP2 and Bcl-2 protein expressions were upregulated, while Bax and Caspase3 expressions were downregulated posttransfection of miR-328-5p inhibitor (Figures 7(g)–7(i)). Transfection of the WWP2 siRNA into the miR-328-5p inhibitor group reversed these effects (Figures 7(g)–7(i)). In conclusion, these results confirm that miR-328-5p promotes the apoptosis of NP cells by directly targeting WWP2.

4. Discussion

Studies found that miRNA is mainly involved in IDD by regulating cell apoptosis and proliferation [41–44], inflammatory reaction [45–47], and extracellular matrix component degradation [48–51]. Some studies have found miR-328-5p regulated the proliferation and apoptosis of cancer cells [29–32]. Cao et al. found that silencing miR-328-5p significantly inhibited the proliferation of non-small cell lung

cancer [29], and lncRNA RP5-916 L7.2 inhibited miR-328-5p expression and promoted the apoptosis of tongue squamous cell carcinoma cells [30]. Luo et al. speculated that miR-328-5p was a tumor suppressor, and they confirmed that miR-328-5p mimic decreased obviously the proliferation and cell cycle of breast cancer cells, and promoted apoptosis [31]. Overexpression of LINC00210 significantly decreased miR-328-5p expression and increased the proliferation and migration of non-small cell lung cancer cells [32]. As we know, WWP2 is essential for maintaining a stable cell cycle, though silencing of WWP2 reduces the rate of proliferation, and WWP2 regulates various cellular processes such as protein degradation, membrane protein endocytosis, apoptosis, and gene transcription. [52]. WWP2 accelerates the cell cycle and promotes tumor formation [34]. Downregulation of WWP2 decreased obviously lung adenocarcinoma proliferation [37]. Xu et al. found that WWP2 siRNA inhibited Bcl-2 expression by promoting Bax and Caspase7/8 to induce apoptosis of liver cancer cells [53]. Even more, overexpression of WWP2 could inhibit the apoptosis of human renal tubular epithelial cells by inducing Bcl-2 expressionand and inhibiting Bax expression [40]. However, the regulatory mechanism of miR-328-5p and its target gene WWP2 in IDD has not been reported.

In the study, through the analysis of miRNA and mRNA microarray database, we screened the target genes miR-328-5p and WWP2. The high expression of miR-328-5p, while low expression of WWP2 in a degenerative tissues by qRT-PCR. Surprisingly, the expression of miR-328-5p was positively correlated, while that of WWP2 negatively correlated with the degeneration grade of IDD. And we also identified that Bax and Caspase3 expression were upregulated, while Bcl-2 expression is downregulated. After miR-328-5p mimic transfected into nucleus pulposus cell, we found that the expressions of WWP2 and Bcl-2 were downregulated, while the expressions of Bax and Caspase3 were upregulated, and the same results were obtained by knocking down WWP2., and WWP2 siRNA could significantly reverse the effect of miR-328-5p inhibitor. MiR-328-5p mimic significantly inhibited the proliferation of nucleus pulposus cells compared with the control group by CCK8 assay. We also confirmed that miR-328-5p mimic increaed obviously the apoptosis of nucleus pulposus cells. WWP2 was identified as the direct target gene of miR-328-5p by bioinformatics. Compared with WWP2 Mut group, the luciferase activity of nucleus pulposus cells in WWP2 Wt group was significantly decreased, and WWP2 protein expression was also significantly downregulated.

In conclusion, these results strengthen our hypothesis that miR-328-5p regulated the prevalence and development of IDD by targeting WWP2. These results also indicate that miR-328-5p plays an essential role in regulating the proliferation and apoptosis of nucleus pulposus cells.

5. Conclusion

In conclusion, our results suggest that miR-328-5p is involved in the development of IDD by targeting WWP2 to induce the proliferation and apoptosis of nucleus pulposus cells. Furthermore, this study may provide a new reference for the diagnosis and treatment of IDD.

Data Availability

We confirm that this study data are available within the article or our supplementary materials. And the microarray data (such as Figure 1 and Figure 2) used in this study are available at the following link. The miRNA chip database is as follow:https://www.ncbi.nlm.nih.gov/gds/?term=GSE63492. The mRNA microarray database is as follows:https://www.ncbi.nlm.nih.gov/gds/?term=GSE34095.

Conflicts of Interest

The authors declare that there are no any competing financial interests.

Authors' Contributions

Jing Yan, Lun-Gang Wu, and Ming Zhang contributed equally to this work.

References

[1] GBD 2017 Disease and injury incidence and prevalence collaborators, "Global, regional, and national incidence, prevalence, and years lived with disability for 354 diseases and injuries for 195 countries and territories, 1990-2017: a systematic analysis for the global burden of disease study 2017," *Lancet*, vol. 392, 2018.

[2] L. Lao, M. D. Daubs, T. P. Scott et al., "Effect of disc degeneration on lumbar segmental mobility analyzed by kinetic magnetic resonance imaging," *Spine Phila Pa 2015*, vol. 40, no. 5, pp. 316–322, 2015.

[3] D. Samartzis, J. Karppinen, F. Mok, D. Y. T. Fong, K. D. K. Luk, and K. M. C. Cheung, "A population-based study of juvenile disc degeneration and its association with overweight and obesity, low back pain, and diminished functional status," *The Journal of Bone and Joint Surgery. American Volume*, vol. 93, no. 7, pp. 662–670, 2011.

[4] T. Oichi, Y. Taniguchi, Y. Oshima, S. Tanaka, and T. Saito, "Pathomechanism of intervertebral disc degeneration," *JOR Spine.*, vol. 3, no. 1, article e1076, 2020.

[5] H. R. Li, Q. Cui, Z. Y. Dong, J. H. Zhang, H. Q. Li, and L. Zhao, "Downregulation of miR-27b is involved in loss of type II collagen by directly targeting matrix metalloproteinase 13 (MMP13) in human intervertebral disc degeneration," *Spine (Phila Pa 1976)*, vol. 41, no. 3, pp. E116–E123, 2016.

[6] J. C. Kennon, M. E. Awad, N. Chutkan, J. DeVine, and S. Fulzele, "Current insights on use of growth factors as therapy for intervertebral disc degeneration," *Biomolecular Concepts*, vol. 9, no. 1, pp. 43–52, 2018.

[7] H. Chen, J. Wang, B. Hu et al., "MiR-34a promotes fas-mediated cartilage endplate chondrocyte apoptosis by targeting Bcl-2," *Molecular and Cellular Biochemistry*, vol. 406, no. 1-2, pp. 21–30, 2015.

[8] C. L. Le Maitre, A. L. Binch, and A. A. Thorpe, "Degeneration of the intervertebral disc with new approaches for treating low back pain," *Journal of Neurosurgical Sciences*, vol. 59, no. 1, pp. 47–61, 2015.

[9] N. V. Vo, R. A. Hartman, P. R. Patil et al., "Molecular mechanisms of biological aging in intervertebral discs," *Journal of Orthopaedic Research*, vol. 34, no. 8, pp. 1289–1306, 2016.

[10] K. Luoma, H. Riihimäki, R. Luukkonen, R. Raininko, E. Viikari-Juntura, and A. Lamminen, "Low back pain in relation to lumbar disc degeneration," *Spine (Phila Pa 1976)*, vol. 25, no. 4, pp. 487–492, 2000.

[11] C. L. Le Maitre, A. Pockert, D. J. Buttle, A. J. Freemont, and J. A. Hoyland, "Matrix synthesis and degradation in human intervertebral disc degeneration," *Biochemical Society Transactions*, vol. 35, Part 4, pp. 652–655, 2007.

[12] Z. Liu, C. Ma, J. I. Shen, D. Wang, J. Hao, and Z. Hu, "SDF-1/CXCR4 axis induces apoptosis of human degenerative nucleus pulposus cells via the NF-κB pathway," *Molecular Medicine Reports*, vol. 14, no. 1, pp. 783–789, 2016.

[13] J. Shen, J. Fang, J. Hao et al., "SIRT1 inhibits the catabolic effect of IL-1β through TLR2/SIRT1/NF-κB pathway in human degenerative nucleus pulposus cells," *Pain Physician*, vol. 19, no. 1, pp. E215–E226, 2016.

[14] A. J. Freemont, "The cellular pathobiology of the degenerate intervertebral disc and discogenic back pain," *Rheumatology (Oxford, England)*, vol. 48, no. 1, pp. 5–10, 2008.

[15] F. Ding, Z. W. Shao, and L. M. Xiong, "Cell death in intervertebral disc degeneration," *Apoptosis*, vol. 18, no. 7, pp. 777–785, 2013.

[16] X. Ma, Y. Lin, K. Yang, B. Yue, H. Xiang, and B. Chen, "Effect of lentivirus-mediated survivin transfection on the morphology and apoptosis of nucleus pulposus cells derived from degenerative human disc in vitro," *International Journal of Molecular Medicine*, vol. 36, no. 1, pp. 186–194, 2015.

[17] Z. Li, X. Yu, J. Shen, M. T. V. Chan, and W. K. K. Wu, "MicroRNA in intervertebral disc degeneration," *Cell Proliferation*, vol. 48, no. 3, pp. 278–283, 2015.

[18] J. Guo, M. Shao, F. Lu, J. Jiang, and X. Xia, "Role of Sirt1 plays in nucleus pulposus cells and intervertebral disc degeneration," *Spine (Phila Pa 1976)*, vol. 42, no. 13, pp. E757–E766, 2017.

[19] S. Yan, M. Wang, and J. Zhao, "MicroRNA-34a affects chondrocyte apoptosis and proliferation by targeting the SIRT1/p53 signaling pathway during the pathogenesis of osteoarthritis," *International Journal of Molecular Medicine*, vol. 38, no. 1, pp. 201–209, 2016.

[20] W. Guo, B. Zhang, C. Sun et al., "Circular RNA derived from TIMP2 functions as a competitive endogenous RNA and regulates intervertebral disc degeneration by targeting miR-185-5p and matrix metalloproteinase 2," *International Journal of Molecular Medicine*, vol. 46, no. 2, pp. 621–632, 2020.

[21] C. Leer, R. L. Feinbaum, and V. Ambros, "The C. elegans heterochronic gene lin-4 encodes small RNAs with antisense complementarity to lin-14," *Cell*, vol. 75, no. 5, pp. 843–854, 1993.

[22] G. Zhang, X. Zhang, K. Zhou et al., "miRNA-10a-5p targeting the BCL6 gene regulates proliferation, differentiation and apoptosis of chicken myoblasts," *International Journal of Molecular Sciences*, vol. 23, no. 17, p. 9545, 2022.

[23] J. Liu, J. Zhang, Y. Li, L. Wang, B. Sui, and D. Dai, "MiR-455-5p acts as a novel tumor suppressor in gastric cancer by down-regulating RAB18," *Gene*, vol. 592, no. 2, pp. 308–315, 2016.

[24] F. Wu, F. Wang, Q. Yang et al., "Upregulation of miRNA-23a-3p rescues high glucose-induced cell apoptosis and proliferation inhibition in cardiomyocytes," *In Vitro Cellular & Developmental Biology-Animal*, vol. 56, no. 10, pp. 866–877, 2020.

[25] M. Zhang, F. Wang, and X. Zhang, "miRNA-627 inhibits cell proliferation and cell migration, promotes cell apoptosis in prostate cancer cells through upregulating MAP3K1, PTPRK and SRA1," *International Journal of Clinical and Experimental Pathology*, vol. 11, no. 1, pp. 255–261, 2018.

[26] M. Correia de Sousa, M. Gjorgjieva, D. Dolicka, C. Sobolewski, and M. Foti, "Deciphering miRNAs' action through miRNA editing," *International Journal of Molecular Sciences*, vol. 20, no. 24, p. 6249, 2019.

[27] C. Wang, W. J. Wang, Y. G. Yan et al., "MicroRNAs: new players in intervertebral disc degeneration," *Clinica Chimica Acta*, vol. 450, pp. 333–341, 2015.

[28] X. Zhou, L. Chen, S. Grad et al., "The roles and perspectives of microRNAs as biomarkers for intervertebral disc degeneration," *Journal of Tissue Engineering and Regenerative Medicine*, vol. 11, no. 12, pp. 3481–3487, 2017.

[29] F. Cao, Z. Wang, Y. Feng et al., "lncRNA TPTEP1 competitively sponges miR-328-5p to inhibit the proliferation of non-small cell lung cancer cells," *Oncology Reports*, vol. 43, no. 5, pp. 1606–1618, 2020.

[30] Y. Chen, Y. Guo, and W. Yan, "lncRNA RP5-916L7.2 correlates with advanced tumor stage, and promotes cells proliferation while inhibits cells apoptosis through targeting miR-328 and miR-939 in tongue squamous cell carcinoma," *Clinical Biochemistry*, vol. 67, pp. 24–32, 2019.

[31] T. Luo, Y. Yan, Q. He, X. Ma, and W. Wang, "miR-328-5p inhibits MDA-MB-231 breast cancer cell proliferation by targeting RAGE," *Oncology Reports*, vol. 39, no. 6, pp. 2906–2914, 2018.

[32] Z. Liu, L. Xu, K. Zhang, B. Guo, Z. Cui, and N. Gao, "LINC00210 plays oncogenic roles in non-small cell lung cancer by sponging microRNA-328-5p," *Experimental and Therapeutic Medicine*, vol. 19, no. 5, pp. 3325–3331, 2020.

[33] A. E. Clements, V. Bravo, C. Koivisto, D. E. Cohn, and G. Leone, "WWP2 and its association with PTEN in endometrial cancer," *Gynecol Oncol Rep.*, vol. 13, pp. 26–29, 2015.

[34] C. Fukumoto, D. Nakashima, A. Kasamatsu et al., "WWP2 is overexpressed in human oral cancer, determining tumor size and poor prognosis in patients: downregulation of WWP2 inhibits the AKT signaling and tumor growth in mice," *Oncoscience.*, vol. 1, no. 12, pp. 807–820, 2014.

[35] J. Liang, W. F. Qi, S. Xie et al., "Expression of WW domain-containing protein 2 is correlated with pathological grade and recurrence of glioma," *Journal of Cancer Research and Therapeutics*, vol. 13, no. 6, pp. 1032–1037, 2017.

[36] S. M. Soond, P. G. Smith, L. Wahl et al., "Novel WWP2 ubiquitin ligase isoforms as potential prognostic markers and molecular targets in cancer," *Biochimica et Biophysica Acta*, vol. 1832, no. 12, pp. 2127–2135, 2013.

[37] R. Yang, Y. He, S. Chen, X. Lu, C. Huang, and G. Zhang, "Elevated expression of WWP2 in human lung adenocarcinoma and its effect on migration and invasion," *Biochemical and Biophysical Research Communications*, vol. 479, no. 2, pp. 146–151, 2016.

[38] J. G. Jung, A. Stoeck, B. Guan et al., "Notch3 interactome analysis identified WWP2 as a negative regulator of notch3 signaling in ovarian cancer," *PLoS Genetics*, vol. 10, no. 10, article e1004751, 2014.

[39] M. L. Ji, H. Jiang, X. J. Zhang et al., "Preclinical development of a microRNA-based therapy for intervertebral disc degeneration," *Nature Communications*, vol. 9, no. 1, p. 5051, 2018.

[40] H. Che, W. He, J. Feng et al., "WWP2 ameliorates acute kidney injury by mediating p53 ubiquitylation and degradation," *Cell Biochemistry and Function*, vol. 38, no. 6, pp. 695–701, 2020.

[41] D.-Y. Zhang, Z.-J. Wang, Y.-B. Yu, Y. Zhang, and X.-X. Zhang, "Role of microRNA-210 in human intervertebral disc degeneration," *Experimental and Therapeutic Medicine*, vol. 11, no. 6, pp. 2349–2354, 2016.

[42] P. Liu, F. Chang, T. Zhang et al., "Downregulation of microRNA-125a is involved in intervertebral disc degeneration by targeting pro-apoptotic Bcl-2 antagonist killer 1," *Iranian Journal of Basic Medical Sciences*, vol. 20, no. 11, pp. 1260–1267, 2017.

[43] B. Wang, D. Wang, T. Yan, and H. Yuan, "MiR-138-5p promotes TNF-α-induced apoptosis in human intervertebral disc degeneration by targeting SIRT1 through PTEN/PI3K/Akt signaling," *Experimental Cell Research*, vol. 345, no. 2, pp. 199–205, 2016.

[44] P. Cai, T. Yang, X. Jiang, M. Zheng, G. Xu, and J. Xia, "Role of miR-15a in intervertebral disc degeneration through targeting MAP3K9," *Biomedicine & Pharmacotherapy*, vol. 87, pp. 568–574, 2017.

[45] K. Wang, T. Chen, X. Ying et al., "Ligustilide alleviated IL-1β induced apoptosis and extracellular matrix degradation of nucleus pulposus cells and attenuates intervertebral disc degeneration _in vivo_," *International Immunopharmacology*, vol. 69, pp. 398–407, 2019.

[46] Z. Liao, X. Wu, Y. Song et al., "Angiopoietin-like protein 8 expression and association with extracellular matrix metabolism and inflammation during intervertebral disc degeneration," *Journal of Cellular and Molecular Medicine*, vol. 23, no. 8, pp. 5737–5750, 2019.

[47] S. E. Navone, G. Marfia, A. Giannoni et al., "Inflammatory mediators and signalling pathways controlling intervertebral disc degeneration," *Histology and Histopathology*, vol. 32, no. 6, pp. 523–542, 2017.

[48] W. Liu, Y. Zhang, X. Feng et al., "Inhibition of microRNA-34a prevents IL-1β-induced extracellular matrix degradation in nucleus pulposus by increasing GDF5 expression," *Experimental Biology and Medicine (Maywood, N.J.)*, vol. 241, no. 17, pp. 1924–1932, 2016.

[49] H. Tan, L. Zhao, R. Song, Y. Liu, and L. Wang, "microRNA-665 promotes the proliferation and matrix degradation of nucleus pulposus through targeting GDF5 in intervertebral disc degeneration," *Journal of Cellular Biochemistry*, vol. 119, no. 9, pp. 7218–7225, 2018.

[50] M. L. Ji, J. Lu, P. L. Shi et al., "Dysregulated miR-98 contributes to extracellular matrix degradation by targeting IL-6/STAT3 signaling pathway in human intervertebral disc degeneration," *Journal of Bone and Mineral Research*, vol. 31, no. 4, pp. 900–909, 2016.

[51] B. Zhang, W. Guo, C. Sun et al., "Dysregulated MiR-3150a-3p promotes lumbar intervertebral disc degeneration by targeting aggrecan," *Cellular Physiology and Biochemistry*, vol. 45, no. 6, pp. 2506–2515, 2018.

[52] B. H. Choi, X. Che, C. Chen, L. Lu, and W. Dai, "WWP2 is required for normal cell cycle progression," *Genes & Cancer*, vol. 6, no. 9-10, pp. 371–377, 2015.

[53] S.-Q. Xu, Y. Qin, D.-B. Pan et al., "Inhibition of WWP2 suppresses proliferation, and induces G1 cell cycle arrest and apoptosis in liver cancer cells," *Molecular Medicine Reports*, vol. 13, no. 3, pp. 2261–2266, 2016.

Hindawi
Oxidative Medicine and Cellular Longevity
Volume 2022, Article ID 2481071, 19 pages
https://doi.org/10.1155/2022/2481071

Research Article

Development of a Novel Inflammatory-Associated Gene Signature and Immune Infiltration Patterns in Intervertebral Disc Degeneration

Tao Lan,[1] **Zhihao Hu**,[1] **Weizhuang Guo**,[1] **Bin Yan**,[1] **and Yuantao Zhang**[2]

[1]*Department of Spine Surgery, Shenzhen Second People's Hospital, The First Affiliated Hospital of Shenzhen University, Shenzhen, Guangdong 518035, China*
[2]*Musculoskeletal Research Laboratory of Department of Orthopaedics & Traumatology, Faculty of Medicine, The Chinese University of Hong Kong, Hong Kong, China*

Correspondence should be addressed to Tao Lan; drtaolan@163.com and Yuantao Zhang; ytzhang2008@163.com

Received 27 July 2022; Revised 30 August 2022; Accepted 3 September 2022; Published 22 September 2022

Academic Editor: Guoyong Yin

Background. Both inflammatory factors and immune response play important roles in the pathogenesis of intervertebral disc degeneration (IDD). However, a comprehensive analysis of interaction between inflammatory response-associated genes (IRGs) and immune microenvironment in patients with IDD remains lacking. Hence, the current research is aimed at investigating the correlations between IRG signatures and immune cells in the progression of IDD. *Methods*. The expression profiles (GSE27494 and GSE41883) and IRGs were downloaded from the Gene Expression Omnibus (GEO) database and Molecular Signature Database (MSigDB), respectively. Weighted gene coexpression network analysis (WGCNA) and differential expression analysis were used to identify the pivotal modules and common differentially expressed genes (DEGs) associated with IDD. Subsequently, we retrieved differentially expressed IRGs (DE-IRGs) by intersecting IRGs and DEGs for enrichment analysis. Next, LASSO regression analyses were performed to screen optimal marker genes for IDD prediction. Additionally, we validated differences DE-IRGs between IDD patients and controls in GSE150408. Finally, the infiltration alteration of immune cells was evaluated by the CIBERSORT, and the correlation between diagnostic markers and infiltrating immune cells was analyzed. *Results*. A total of 10 upregulated differentially expressed inflammatory genes were identified that were obviously related to progression of IDD. Functional analysis results revealed that DE-IRGs were mainly enriched in signaling pathways TNF, IL-17, NOD-like receptor, and NF-kappa B pathway. A five-gene signature that consisted of IL-1β, LIF, LYN, NAMPT, and SLC7A2 was constructed by the LASSO Cox regression. IL1B, LYN, and NAMPT were further validated as optimal candidate genes in the pathophysiology of IDD. In addition, there was a remarkable immune cell infiltration difference between the healthy and IDD groups. The proportions for dendritic cells activated, mast cells activated, and neutrophils in the IDD group were significantly higher than those in the normal group, while the proportion of some cells was lower than that of the normal group, such as T cell CD4 memory resting, NK cells activated, and macrophage M0. Furthermore, correlation analysis indicated IL-1β, LYN, and NAMPT were closely implicated with immune cell infiltration in IDD development. *Conclusions*. We explored an association between inflammatory response-associated signature and immune infiltration in IDD and validated that IL-1β, LYN, and NAMPT might serve as biomarkers and therapeutic targets for IDD in the future.

1. Introduction

Intervertebral disc degeneration (IDD) is one of the most common degenerative diseases that is considered the leading cause of low back pain (LBP) nowadays [1, 2]. It is reported that LBP has become a prevalent medical disorder which is associated with disability and heavy socioeconomic expenditure [3]. Despite substantial progress and improvement in the management of discogenic LBP, long-lasting clinical therapy effect remains unsatisfactory. Although the etiology of IDD is multifactorial, including genetic predisposition, aging, overloading, and lifestyle (smoking and obesity), they

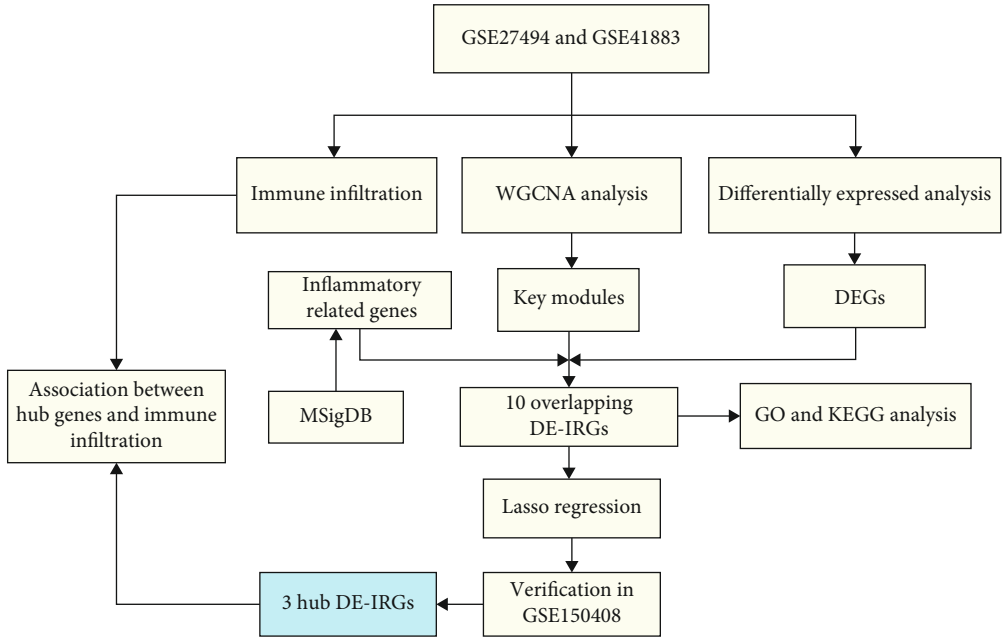

Figure 1: Research flow chart of this study.

lead to common pathological changes which is characterized by extracellular matrix degradation and excessive cell apoptosis.

Inflammation is widely accepted as an important driver of IDD progression which promotes matrix degradation, cell senescence, and apoptosis by recruiting a large number of inflammatory cytokines, such as interleukin-1β (IL-1β) and tumor necrosis factor-α (TNF-α). For example, a study conducted by Kim et al. showed that direct injection of IL-1β into rat lumbar intervertebral disc resulted in disc degeneration and inflammation microenvironment [4]. TNF-α plays a proinflammatory effect within disc and promotes nucleus pulposus cells death [5]. Conversely, anti-inflammatory treatments provide positive therapeutic effect in alleviating IDD development. Hence, downregulation of disc inflammation response is a promising strategy in the treatment of IDD.

The nucleus pulposus (NP) is the largest avascular organ which is located at the center intervertebral disc (IVD). The unique anatomical structure isolates NP from the host immune system and therefore, NP has been identified as an immune privilege organ by Naylar et al. since 1975 [6]. However, the disruption of the NP-blood barrier due to annulus fibrosus rupture leads to exposure of NP to the host and triggers numerous immune cells infiltration and immune response.

It has been demonstrated that immune cell infiltration, including Tregs and macrophages, is involved in IDD progression [7, 8]. Noteworthy, infiltrating immune cells, such as neutrophils and T cells (CD4+, CD8+), release a large number of inflammatory cytokines and aggravate inflammation response cascade. Although biological therapy targeting immune and inflammation modulation is still in its infancy, more in-depth exploration in immune-related inflammatory response sheds light on IDD treatment.

The purpose of the current study was to explore inflammatory associated biomarkers and potential therapeutic targets for the management of IDD based on bioinformatic analysis. Firstly, IDD profiles were downloaded from the Gene Expression Omnibus (GEO) database. Then, differentially expressed inflammatory genes (DE-IRGs) that were implicated with IDD progression were obtained by WGCNA and differential expression analysis, followed by enrichment analysis and LASSO regression. Next, optimal DE-IRGs were validated by independent dataset. Finally, the association between immune infiltration alteration and inflammatory biomarkers were investigated by CIBERSORT for the first time. In all, our findings might provide novel insights into the interaction between inflammatory associated genes and immune infiltration in the pathogenesis of IDD.

2. Materials and Methods

2.1. Gene Expression Data Collection. The gene expression profiles of IDD, including GSE27494, GSE41883, and GSE150408 (external validation sets)), were downloaded from GEO (http://www.ncbi.nlm.nih.gov/geo) databases. The GSE27494 dataset included gene expression profiles of 4 human disc cells exposed to IL-1β and 4 controls. The GSE41883 dataset included gene expression profiles of 4 human disc cells exposed to TNF-α and 4 controls. The GSE150408 dataset included gene expression in the whole blood from 17 patients with sciatica compared with 17 healthy volunteers. The flowchart of this study was summarized in Figure 1.

2.2. Differential and WGCNA Expression Analyses. Differential analysis between IDD patients and healthy controls in GSE27494 or GSE41883 was performed after using the limma package in R software. A screening threshold of P

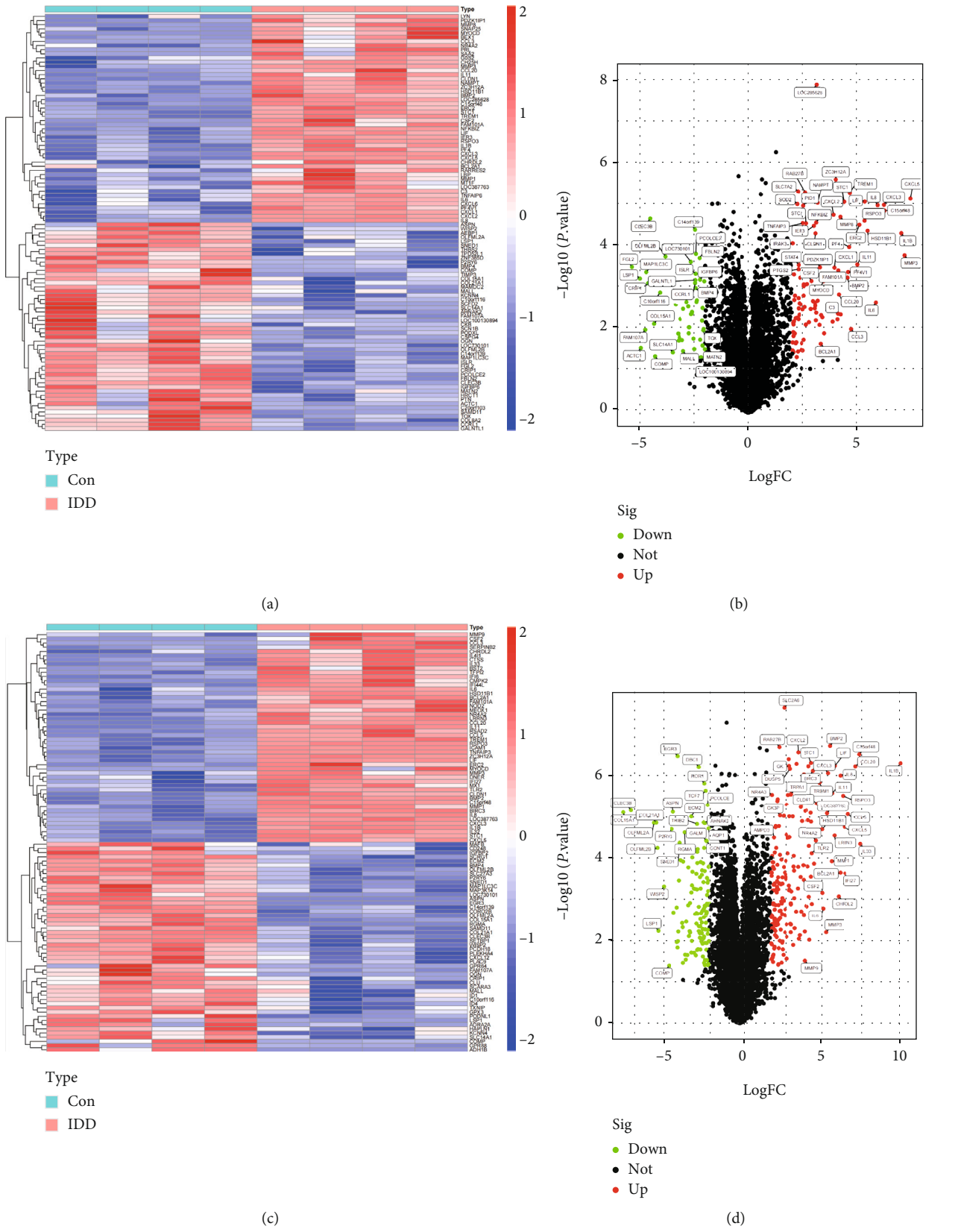

Figure 2: Identification of differentially expressed genes associated with intervertebral disc degeneration (IDD). Heatmap and volcano map of DEGs between IDD patients and healthy control in (a, b) GSE27494 and (c, d) GSE41883. Red represents upregulated genes, green or blue represents downregulated genes, and black represents no significant difference genes.

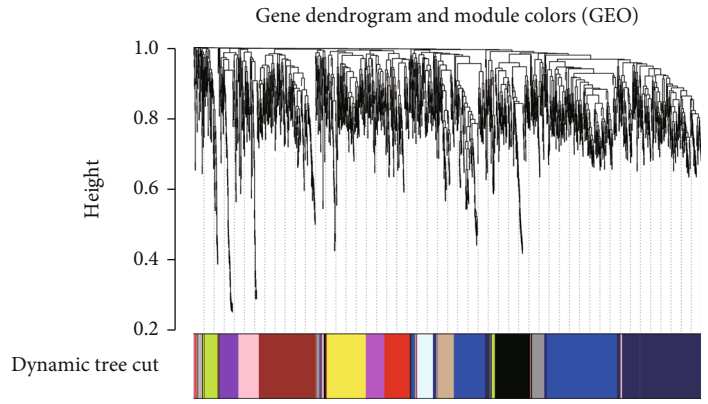

(a)

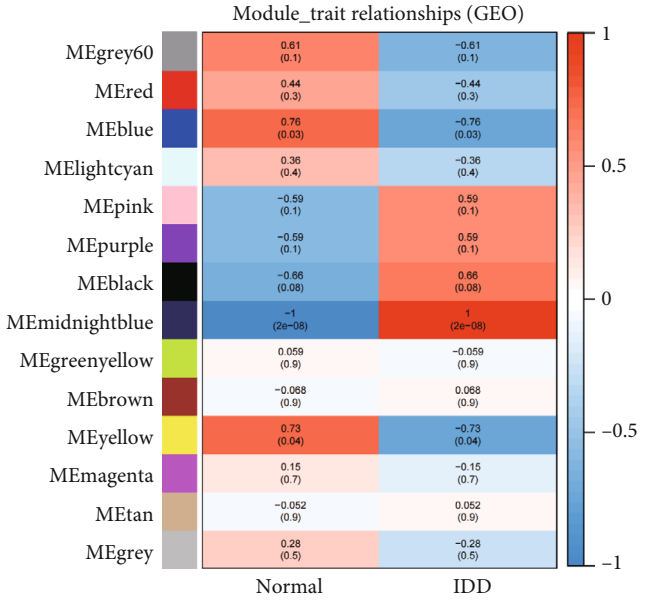

(b)

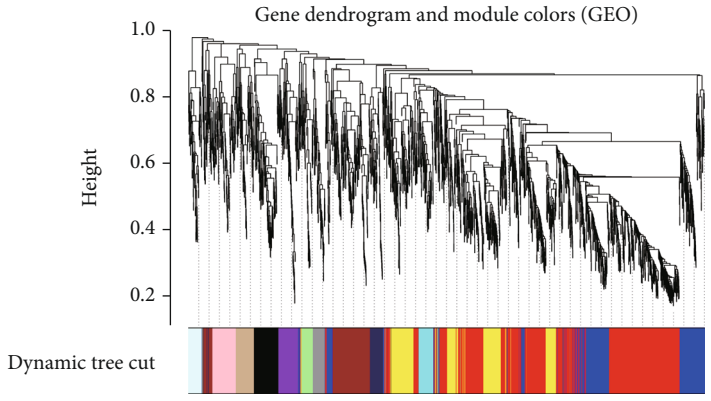

(c)

Figure 3: Continued.

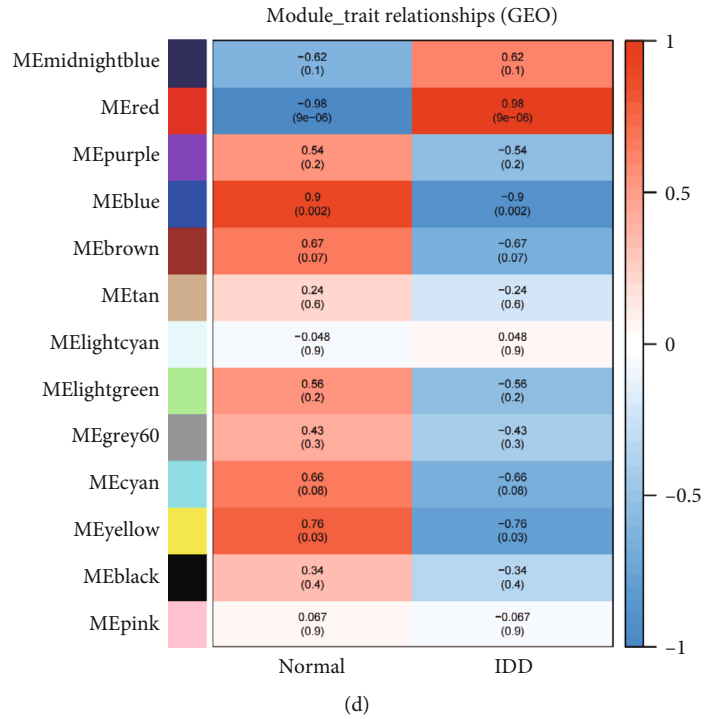

(d)

Figure 3: Identification of key modules that relate to IDD via WGCNA. (a, b) The cluster dendrogram of coexpression network modules and module-trait relationships in (a, b) GSE27494 and (c, d) GSE41883. Various colors represent different modules. Each row corresponds to a color module and column corresponds to a clinical trait (IDD and healthy).

value < 0.05 and $|\log_2 \text{fold change (FC)}| > 2$ was set to obtain the differentially expressed genes between IDD patients and controls. Then, the heatmap and volcano plot were generated using the ggplot2 package in the R software. The WGCNA package in R was used to build a coexpression network. Then hub genes from differential analysis and key modules from WGCNA were interested to obtain DEGs. The ggpubr package was used to draw boxplot of DEGs. In addition, the correlation matrix analysis of DEGs was visualized using the different R package.

2.3. Functional and Pathway Enrichment Analyses. The clusterProfiler package in R was utilized to perform Gene Ontology (GO) and Kyoto Encyclopedia of Genes and Genomes (KEGG) pathway enrichment analysis of common genes. The GO analysis consisted of biological process (BP), cellular component (CC), and molecular function (MF). A P value less than 0.05 was considered statistically significant for enrichment.

2.4. Identification of Inflammatory Response-Associated DEGs. The inflammatory response-associated genes were downloaded from the hallmark gene sets in the Molecular Signature Database (MSigDB, https://www.gsea-msigdb.org/gsea/msigdb/). The IRGs overlapped with the DEGs, and then the differentially expressed IRG (DE-IRGs) genes were identified. Venn diagrams were created using the VennDiagram package.

2.5. Hub Genes Screening and External Validation. The least absolute shrinkage and selection operator (LASSO) method was used for the screening of the feature genes from DE-IRGs. We used the glmnet package in R to perform the LASSO logistic regression analysis. After that, selected characteristic genes were validated in an independent dataset (GSE150408), and boxplots for gene expression were drawn.

2.6. Immune Infiltration Related Analysis. The relative abundance of 22 human immune cells in IDD patients and healthy controls were analyzed by the CIBERSORT deconvolution algorithm, which is an important bioinformatic tool to evaluate immune infiltration microenvironment. The gene expression matrix of immune cells was downloaded from the CIBERSORT (https://cibersortx.stanford.edu) platform and matched with differentially expressed genes to generate the infiltrative proportions of immune cells in IDD. Histogram, correlation heatmap, and violin diagram were drawn to visualize the difference between the IDD and normal groups. In addition, the lollipop chart was used to analyze the relationship between immune cells and target DE-IRGs.

2.7. Statistical Analysis. All statistical analyses were performed using the R software. Data were shown as mean ± standard deviation (SD). The differences between the two groups were evaluated by independent sample t-test and nonparametric test. A $P < 0.05$ was considered statistically significant.

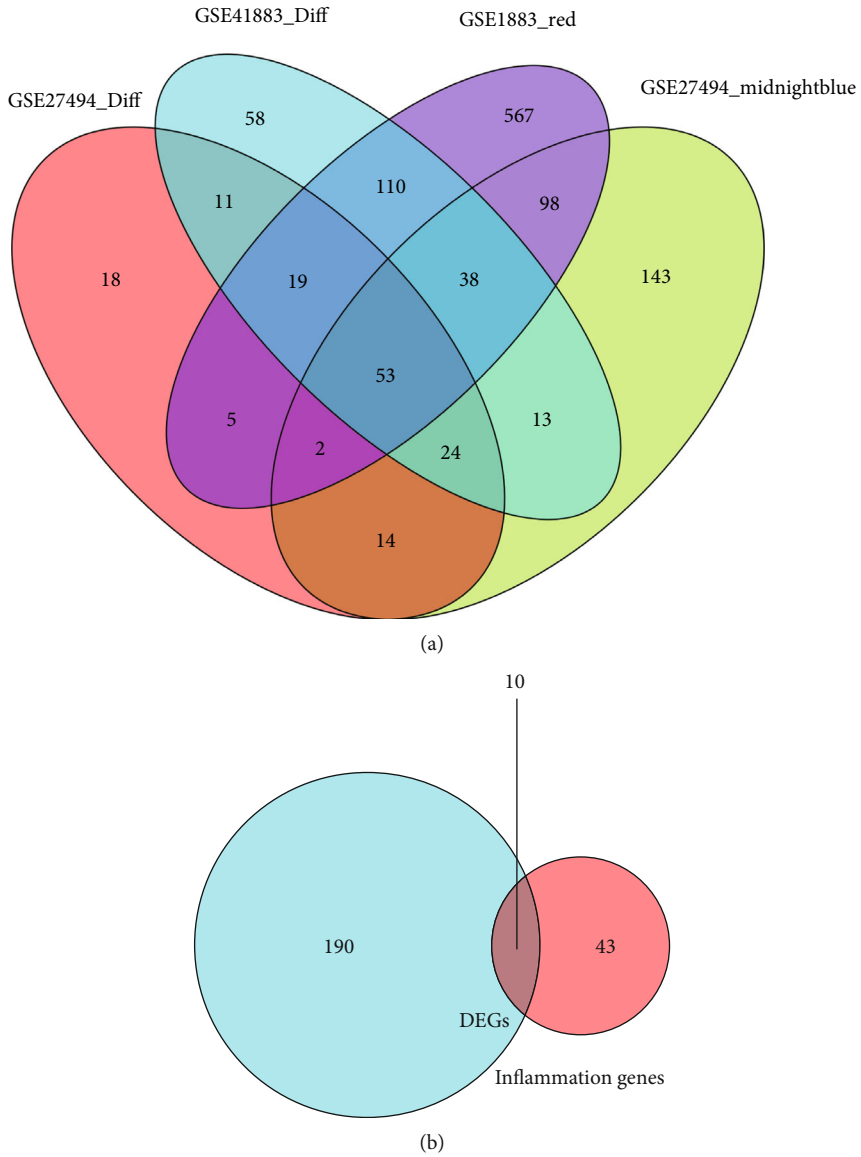

Figure 4: Screening main inflammatory associated genes in IDD. (a) Venn diagram between WGCNA modules and DEGs. (b) The overlapped DEGs and inflammatory associated genes.

Table 1: Top 10 inflammatory response-associated genes in IDD.

Gene	logFC	AveExpr	t	P value	Adj. P value	B
CCL20	5.532308225	6.259162738	10.74688389	$2.19e-08$	$6.75e-06$	9.69840814
CCL7	2.316937	7.937576375	7.569315372	$1.84e-06$	0.000129624	5.296735863
GCH1	2.495734375	8.387334613	8.301695527	$5.98e-07$	$6.30e-05$	6.422200711
IL1B	8.303783088	7.093097344	16.30224347	$7.29e-11$	$8.45e-08$	15.09109203
LIF	5.524410525	9.511424375	20.88386735	$2.16e-12$	$7.80e-09$	18.1460731
LYN	2.870808	5.271320438	6.57260378	$9.44e-06$	0.000413442	3.645774035
NAMPT	3.215158813	9.482475856	16.14269113	$8.37e-11$	$9.17e-08$	14.9660275
NOD2	3.35102225	4.538360288	9.85462812	$6.82e-08$	$1.40e-05$	8.582475124
SLC7A2	2.1113183	3.863241175	14.32074519	$4.46e-10$	$3.14e-07$	13.42836733
TNFRSF1B	2.731989775	7.10356355	7.253318035	$3.04e-06$	0.000188559	4.788480163

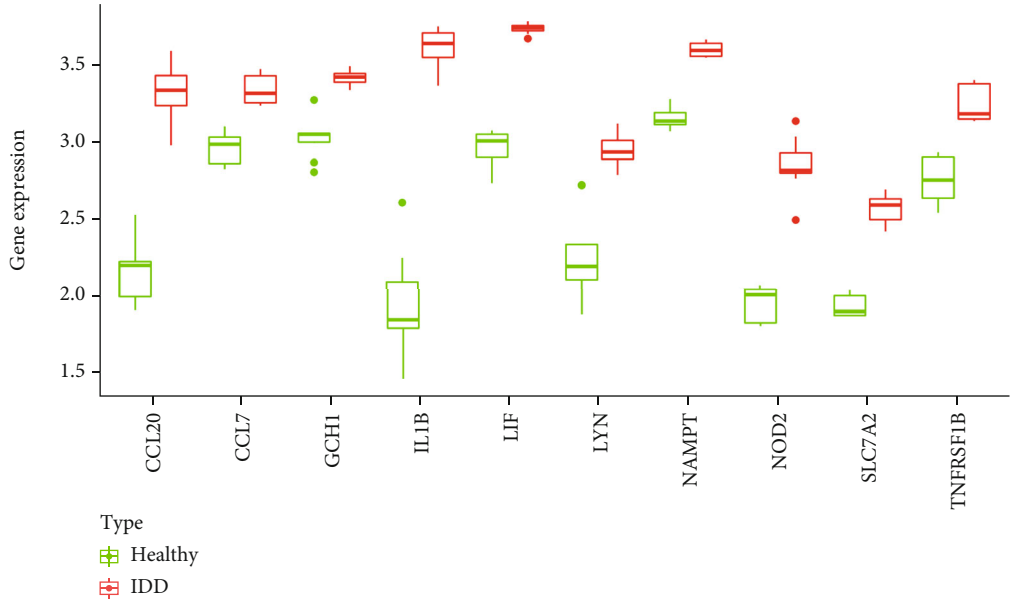

Figure 5: Top 10 differentially expressed inflammatory-related genes in IDD. Boxplots of the expression levels of 10 differentially expressed IRGs in IDD and healthy controls. The green box plots represent the expression in healthy controls, whereas the red box plots represent the expression in IDD.

3. Results

3.1. Identification of 10 Differentially Expressed IRGs Related to IDD. A total of 146 differentially expressed genes were identified in GSE27494, including 50 downregulated and 96 upregulated genes. Meanwhile, a total of 327 differentially expressed genes (including 131 downregulated and 196 upregulated) were obtained in GSE41883. The difference between IDD and normal controls were visualized by heatmap and volcano plot (GSE27494 (Figures 2(a) and 2(b)) and GSE41883 (Figures 2(c) and 2(d))). Then, we used the WGCNA method to explore IDD-associated coexpression modules. A hierarchical clustering tree containing 14 modules in GSE27494 (Figures 3(a) and 3(b)) and 13 modules in GSE41883 (Figures 3(c) and 3(d)) with various colors were constructed. Moreover, the midnight blue module (correlation index: −1, $P = 2e - 08$) of GSE27494 and the red module (correlation index: −0.98, $P = 9e - 06$) of GSE41883 displayed the highest correlation with IDD. Subsequently, 53 characteristic DEGs were obtained by intersecting differential genes and key module genes of both datasets (Figure 4(a)). Next, 200 inflammatory response-associated genes were downloaded from hallmark gene sets in MSigDB and then overlapped with previously obtained DEGs, and Venn diagrams revealed 10 differentially expressed IRGs (SLC7A2, LIF, NAMPT, IL-1β, NOD2, CCL20, CCL7, TNFRSF1B, LYN, and GCH1) (Figure 4(b) and Table 1). Finally, a boxplot revealed that all DE-IRGs were upregulated in IDD group (Figure 5(a)). The relationship between DE-IRGs was further investigated, as shown in Figures 6(a)–6(d).

3.2. Functional and Pathway Enrichment Analyses. Gene Ontology (GO) functional enrichment analysis showed that the identified 10 DE-IRGs were mainly involved in regulation of ERK1 and ERK2 cascade, positive regulation of gliogenesis, response to lipopolysaccharide, response to molecule of bacterial origin, and positive regulation of MAPK cascade (Figure 7(a)). Meanwhile, the results of KEGG enrichment analysis indicated that the selected hub genes played a crucial role in TNF signaling pathway, cytokine-cytokine receptor interaction, IL-17 signaling pathway, viral protein interaction with cytokine, and cytokine receptor and NOD-like receptor signaling pathway (Figure 7(b)).

3.3. Screening and Validation of Candidate Signatures. The LASSO regression algorithm was used to reduce overfitting of 10 DE-IRGs and screen the optimal inflammatory related genes associated with IDD. The minimum lambda and 10-fold cross-validation were set to model construction. Finally, five candidate biomarkers (IL-1β, LIF, LYN, NAMPT, and SLC7A2) were obtained (Figures 8(a) and 8(b)). To further verify the differentially expression of above genes, we further performed the differential expression analysis in the GSE150408 dataset and found that the expression of IL-1β, LYN, and NAMPT was obviously different between IDD and control samples (P value < 0.05), as shown in Figures 9(a)–9(c). Hence, IL-1β, LYN, and NAMPT were chosen as optical inflammatory associated characteristic genes.

3.4. Immune Cell Infiltration. The difference of 22 immune cells infiltration between IDD and healthy control was investigated by the CIBERSORT algorithm. The histogram and violin diagram clearly revealed the abundance difference in immune cell infiltration between both groups (Figures 10(a) and 10(b)). The fraction for dendritic cells activated, mast cells activated, and neutrophils in the IDD group was remarkably higher than those in the normal

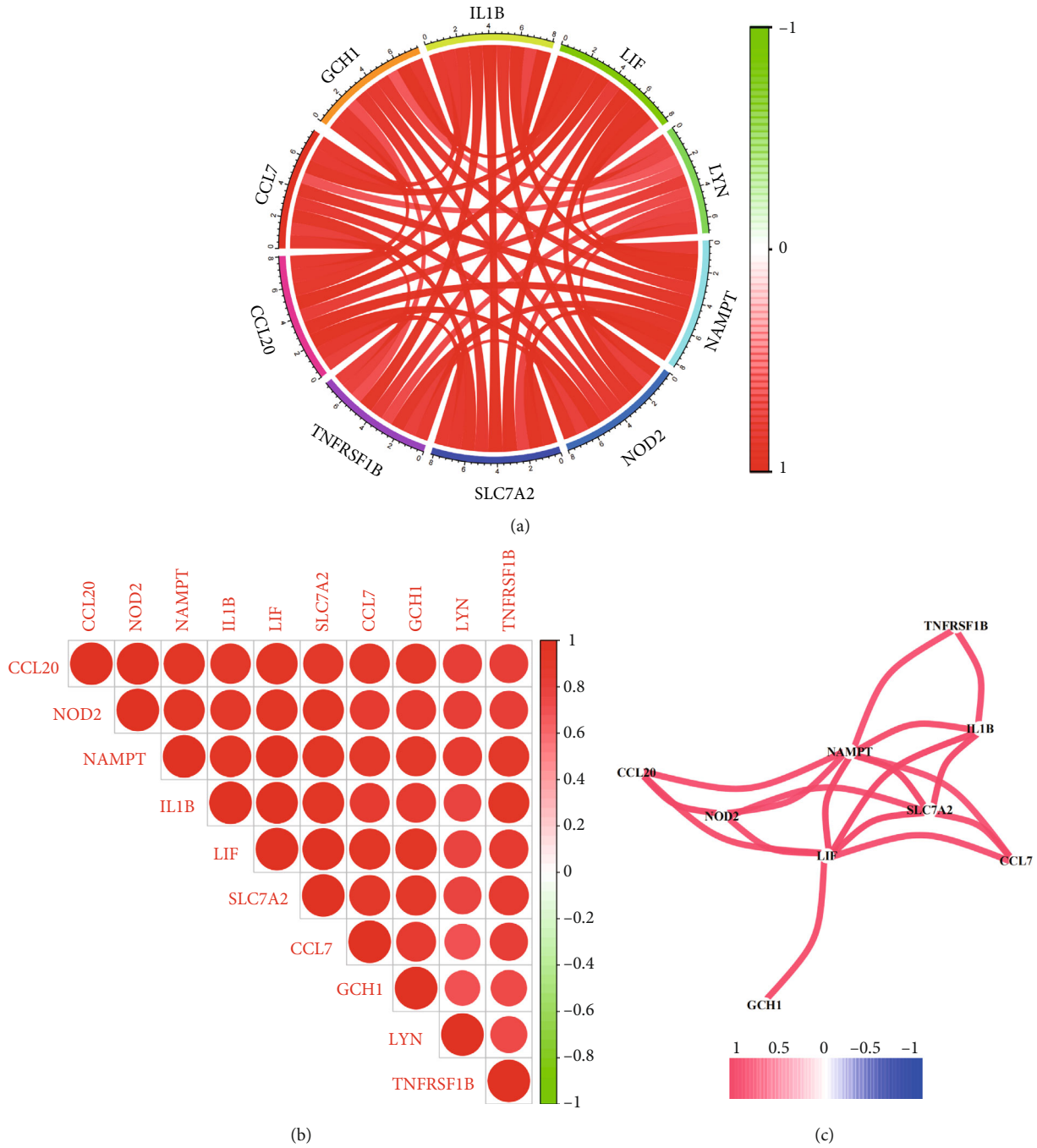

(a) (b) (c)

Figure 6: Continued.

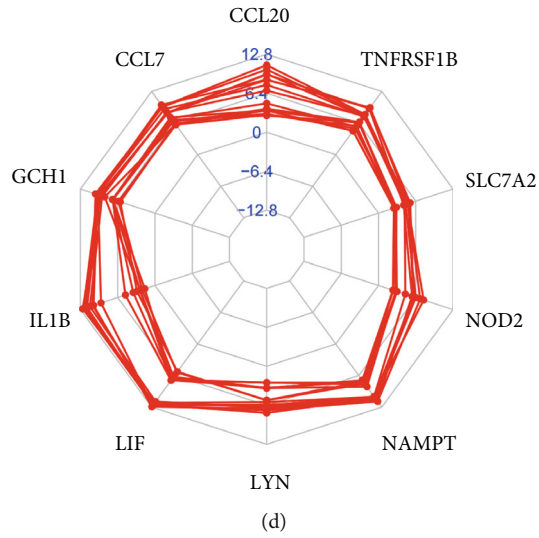

Figure 6: Correlation between differentially expressed IRGs in IDD. (a) Circos plot of differentially expressed IRGs. (b) Correlation plot of differentially expressed IRGs. (c) Correlation network between IRGs. (d) Radar plot of IRGs.

group, while the fraction of some cells was obviously lower than that of the normal group, such as T cells CD4 memory resting, NK cells activated, and macrophage M0 (Figure 10(c)). The above results indicated these differential immune cells might be associated with the immune regulation process of IDD pathogenesis.

3.5. Correlation between Three Candidate Biomarkers and Immune-Infiltrated Cells in IDD. The correlation analysis between optimal DE-IRGs and infiltrating immune cells was further investigated. As shown in Figure 11(a), IL-1β displayed a positive correlation with mast cells activated (0.955114313, $8.74e-09$), dendritic cells activated ($r = 0.708$, $P = 0.002$), T cells regulatory (Tregs) ($r = 0.682$, $P = 0.004$), neutrophils ($r = 0.658$, $P = 0.006$), and T cell CD4 naïve ($r = 0.519$, $P = 0.039$) and showed a negative correlation with T cells CD4 memory resting ($r = -0.96$, $P < 0.01$), macrophage M0 ($r = -0.72$, $P = 0.002$), NK cells activated ($r = -0.672$, $P = 0.004$), and mast cells resting ($r = -0.57$, $P = 0.021$). As shown in Figure 11(b), LYN showed a positive correlation with mast cells activated ($r = 0.593$, $P = 0.015$) and dendritic cells activated ($r = 0.823$, $P < 0.01$) and showed a negative correlation with macrophage M0 ($r = -0.729$, $P = 0.002$), T cell CD4 memory resting ($r = -0.553$, $P = 0.029$), and NK cells activated ($r = -0.334$, $P = 0.206$). As shown in Figure 11(c), NAMPT showed a positive correlation with mast cells activated ($r = 0.78$, $P < 0.01$) and dendritic cells activated ($r = 0.821$, $P < 0.01$) and indicated a negative correlation with T cell CD4 memory resting ($r = -0.776$, $P < 0.01$) and macrophage M0 ($r = -0.626$, $P = 0.011$). These results suggested that the interplay between inflammatory associated genes and immune cells played a critical role in the progression of IDD.

4. Discussion

Intervertebral disc degeneration (IDD) is a major cause of low back pain, which leads to high social and economic cost [9]. Low back pain has been identified as one of the most common reasons for seeking medical care [10]. With an increasing prevalence in the aging population, there is an urgent need to elucidate the etiology and find out the best therapy of IDD. To date, the diagnosis of IDD largely relies on symptoms and imaging, which hinders early diagnosis and timely treatment. Despite years of efforts and attempts, the exact mechanisms of IDD remain unclear, and effective treatments are still lacking. Although some biomarkers have been identified in previous studies, there is no focus on the comprehensive investigation of immune cells and inflammatory genes in IDD. Thus, we aimed to explore potential inflammatory associated signature of IDD and further investigate their relationship with immune infiltration based on comprehensive analysis.

In the present study, we used the WGCNA and the CIBERSROT algorithm to screen characteristic inflammatory associated genes and immune cells related to IDD development. Firstly, we obtained 10 inflammatory-related genes by overlapping genes from differentially expressed analysis and key modules of the WGCNA. Next, GO and KEGG pathway analyses found that these genes are mainly involved in TNF, IL-17, NOD-like receptor, and NF-kappa B signaling pathway, indicating that inflammation response is an important pathological process of IDD. Moreover, IL-1β, LYN, and NAMPT were identified as hub candidate genes by the LASSO regression and external validation. Finally, we discovered different immune cells infiltration landscape between IDD patients and healthy control and found that IL-1β, LYN, and NAMPT were closely implicated with immune response. To the best of our knowledge, studies of IRGs and immune response related to IDD are limited, and our study may provide new insights into the pathogenesis of IDD by exploring the cross talk between hub inflammatory genes and immune cells.

To date, a series of studies have demonstrated that proinflammatory molecules are potent factors in initiation and progression of IDD [11, 12]. Many important

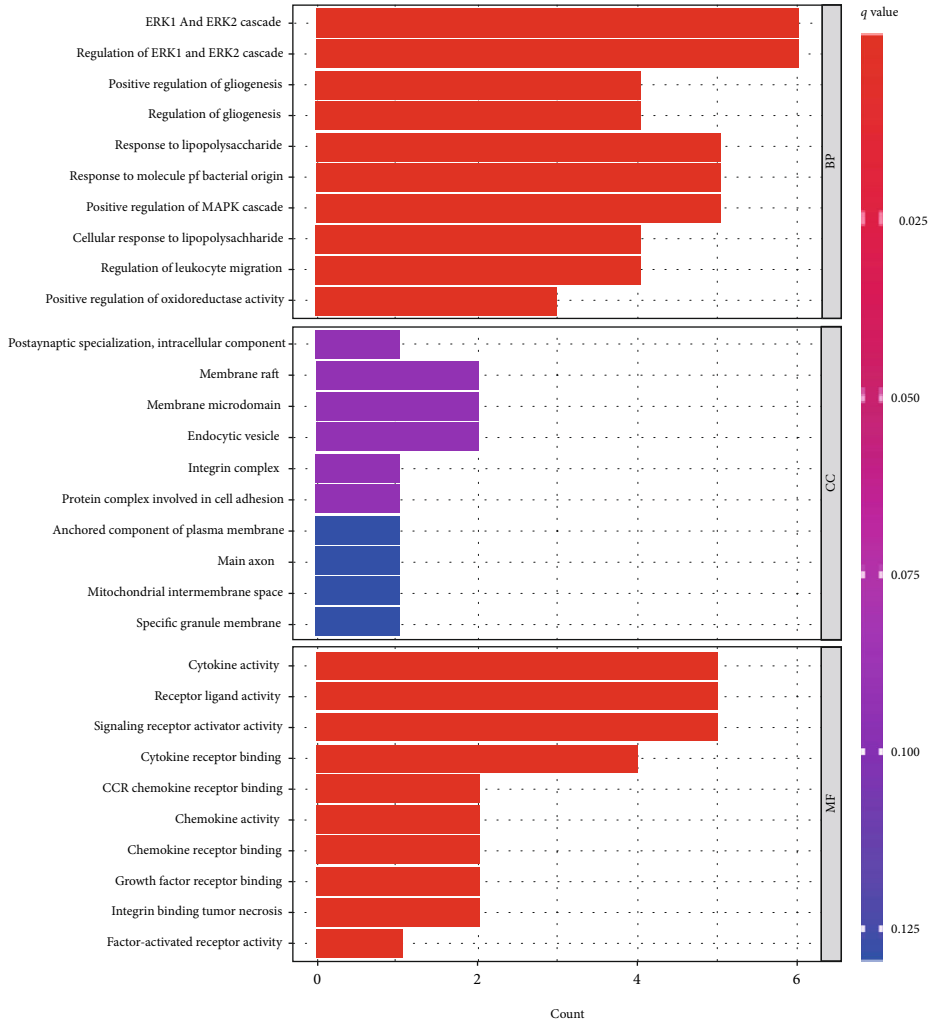

(a)

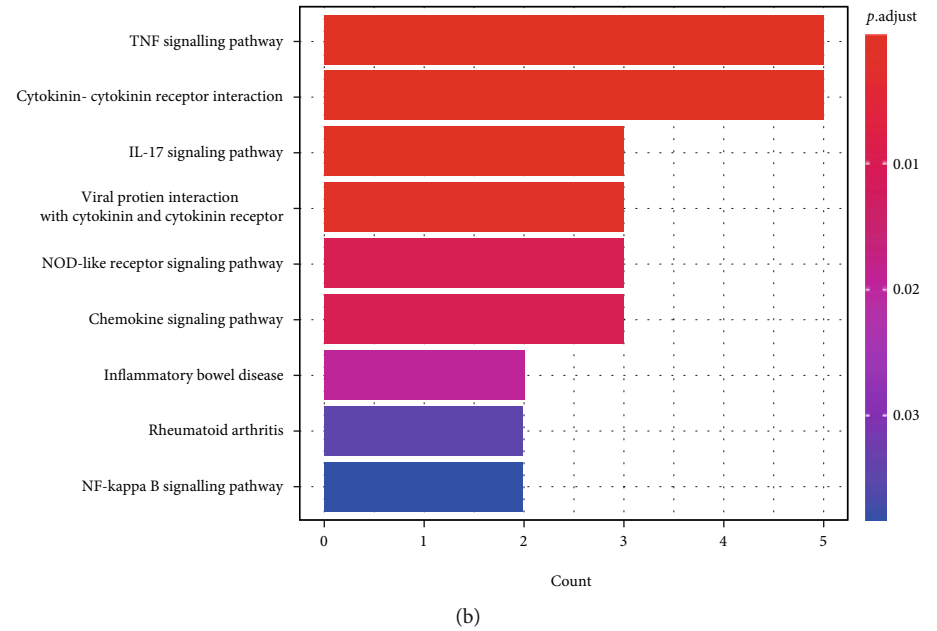

(b)

Figure 7: GO and KEGG analyses of DE-IRGs in the pathogenesis of IDD. (a) Significantly enriched GO terms of the DE-IRGs. (b) Significantly enriched KEGG pathways of the DE-IRGs.

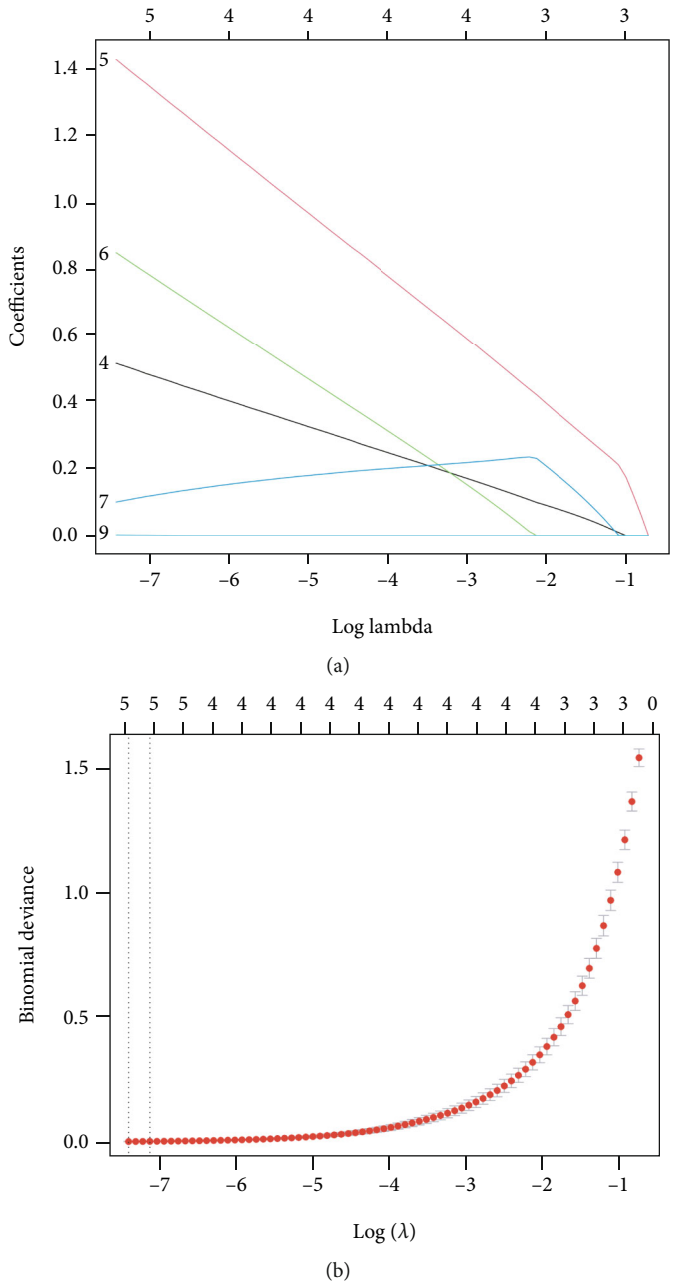

Figure 8: LASSO screen of the hub differentially expressed inflammatory-related genes. (a, b) Least absolute shrinkage and selection operator (LASSO) logistic regression algorithm to screen candidate IRGs.

inflammatory biomarkers have been investigated and have the potential to guide diagnosis and therapeutics [13]. IL-1β is one of the most important proinflammatory cytokine which promoted ECM degradation, oxidative stress, and NLRP3 inflammasome activation in NP cells, and drugs targeting IL-1β play a protective role against inflammation injury [14–16]. Nampt is a rate-limiting enzyme for the NAD+ remedial synthetic pathway in mammalian cells, which plays a critical role in regulating cellular senescence [17]. However, the biological effect of Nampt on IDD remains controversial. Some studies showed that Nampt stimulated the activation of NLRP3 inflammasome and promoted the progression of IDD [18]. Nampt inhibitor, for example, APO866, prevented ECM degradation and NP cells apoptosis, indicating that Nampt is harmful for NP cells via inflammation activation [19]. On the other side, some studies supported that Nampt is beneficial for IDD. Sun et al. found that delivering exogenous Nampt enhanced NAD^+ biosynthesis in senescent NP cells and delayed the development of IDD in rats [20]. Shi et al. reported that resveratrol activated autophagy and attenuated IDD via activation of the Nampt/NAD+/SIRT1

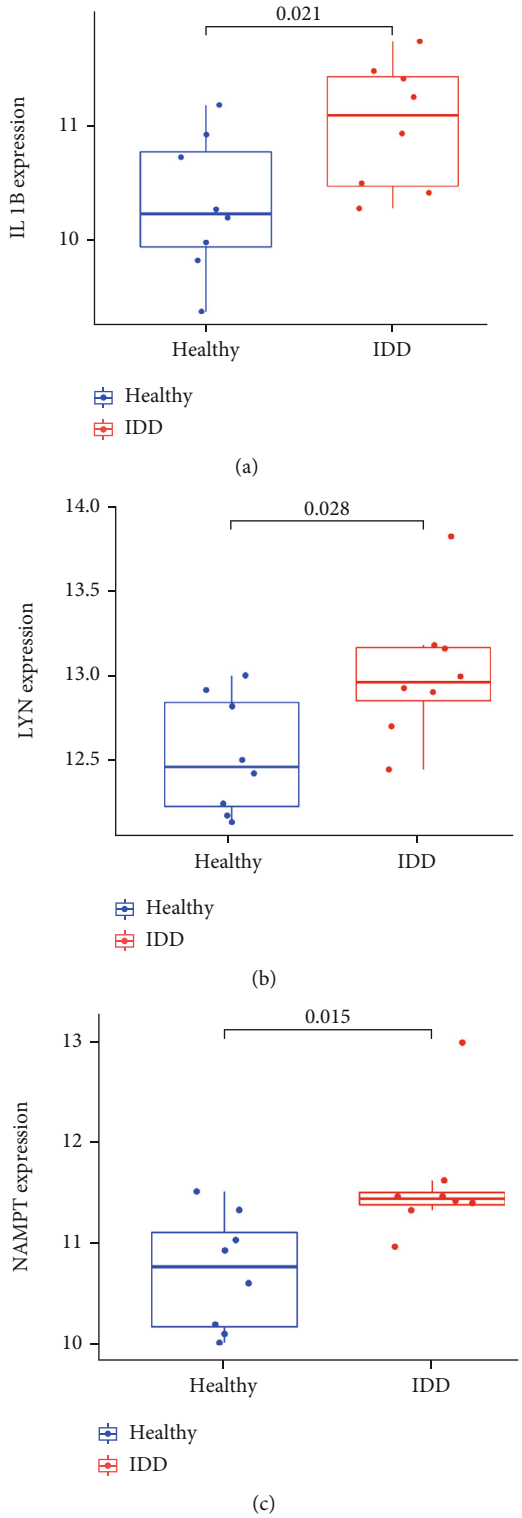

Figure 9: Significant gene expression boxplots of IL-1β, LYN, and NAMPT between IDD and healthy controls in GSE150408.

pathway [21]. Hence, the influence of Nampt on inflammatory response and senescence needs further investigation. Of the significantly enriched pathways in the KEGG pathway analysis, the NOD-like receptor signaling pathway was of interest as it played an important role in inflammation response based on literatures. The activation of NOD-like receptor protein 3 (NLRP3) inflammasome has been shown to promote inflammation by release of potent proinflammatory cytokines interleukin- (IL-) 1β and IL-18. In recent years, with further exploration of

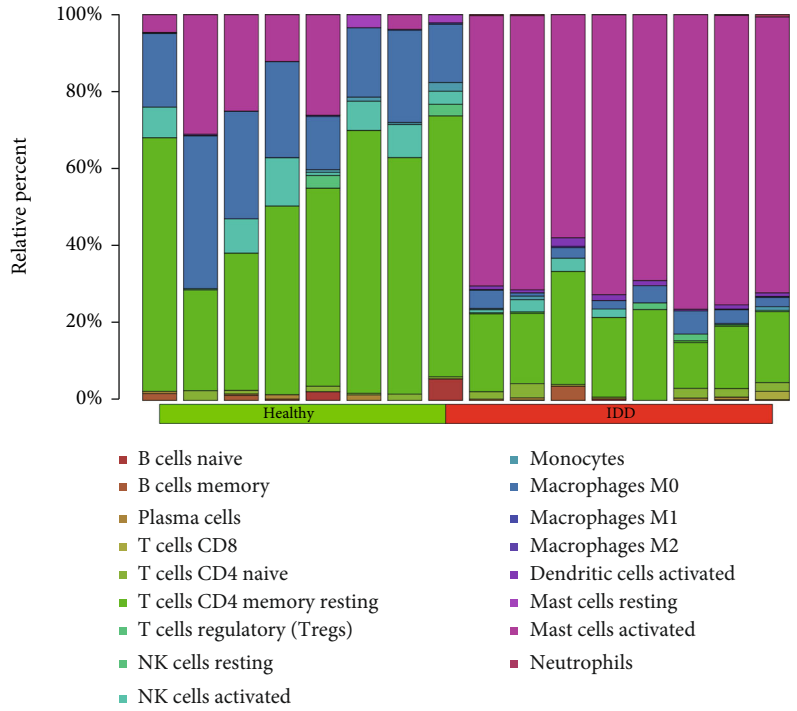

(a)

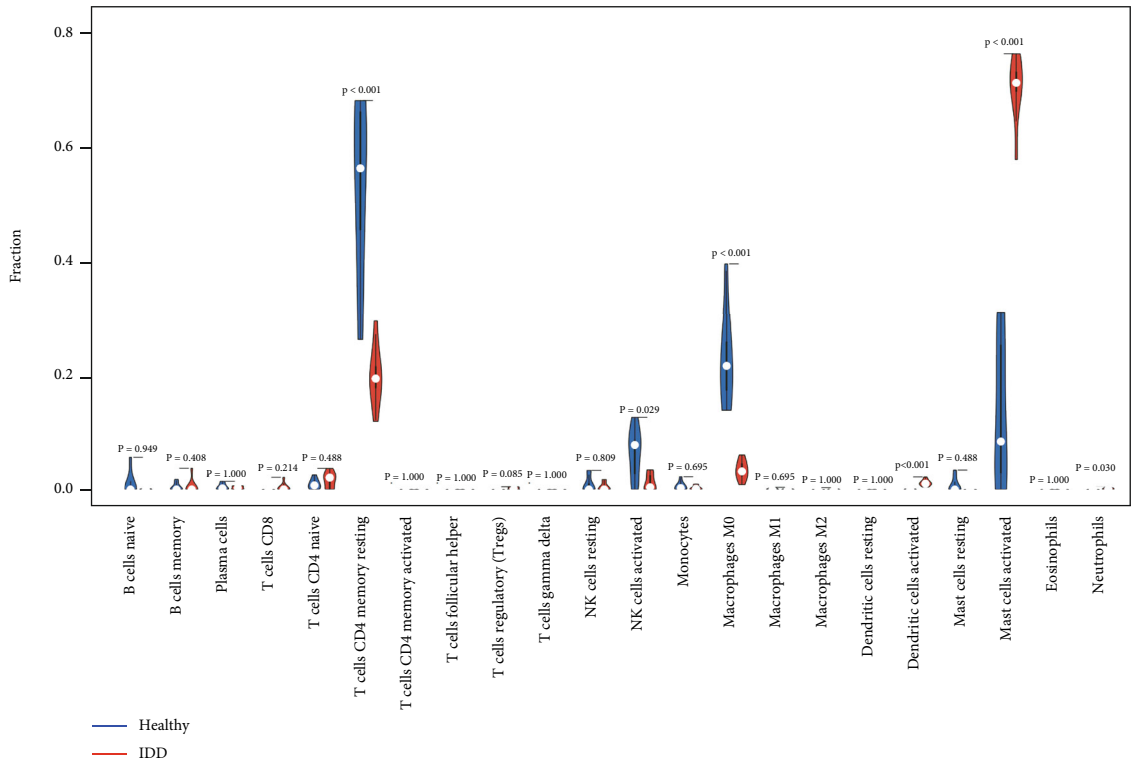

(b)

Figure 10: Continued.

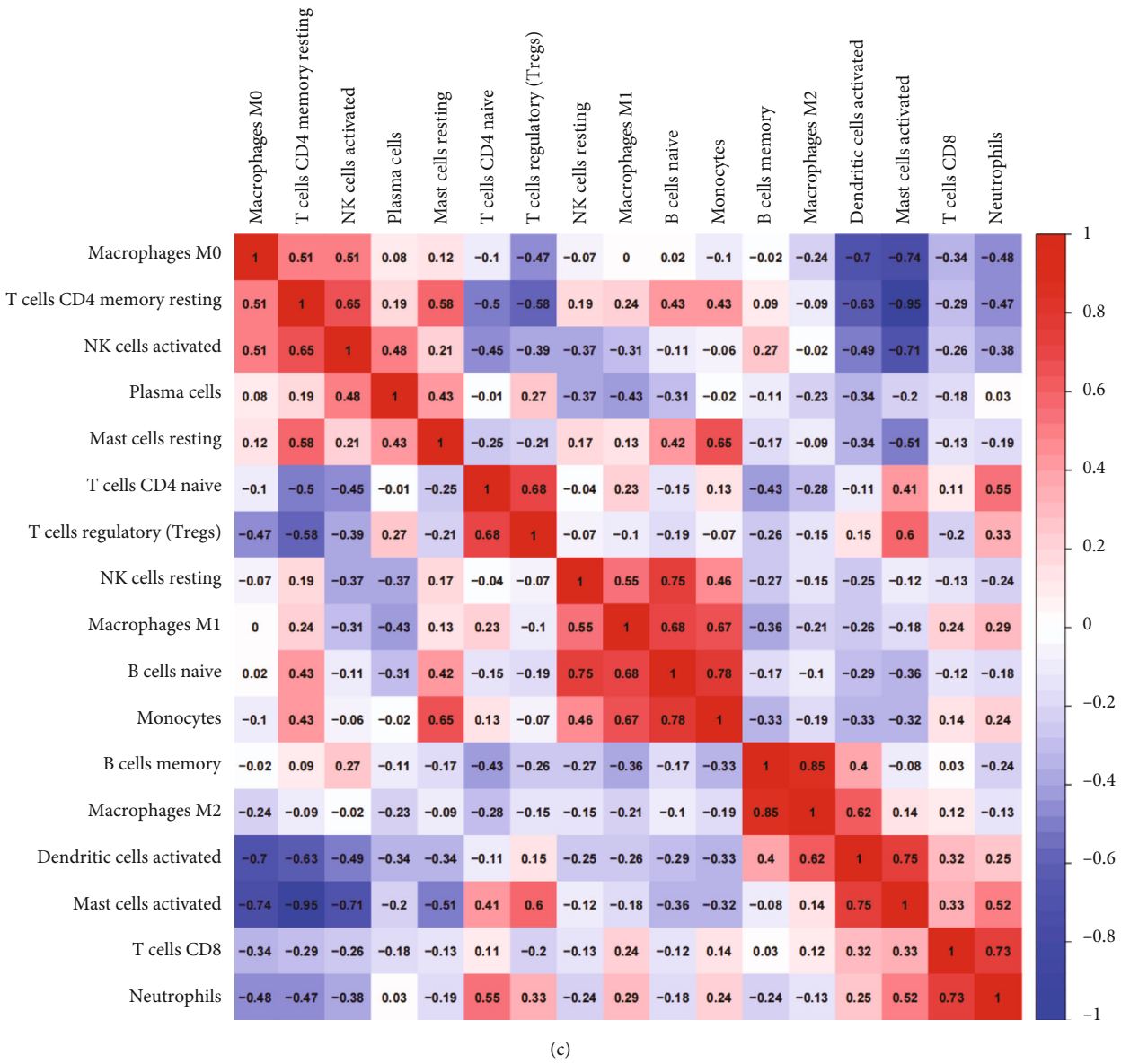

(c)

Figure 10: The immune landscape in IDD patients. (a) Bar plot showing the relative proportions of 22 immune cell populations in IDD samples. (b) Violin plot comparing immune cell compositions in the IDD patients and healthy controls. (c) Pearson's correlation analysis of different infiltrating immune cell subpopulations.

inflammasomes, growing evidence has demonstrated that inflammasomes are associated with the occurrence and progression of IDD [22]. NLRP3 inflammasome activation was significantly increased in degenerated disc and IDD model, and drugs targeting NLRP3, such as cortistain [23], melatonin [24], and mesenchymal stem cell- (MSC-) derived exosomes [25], ameliorated intervertebral disc degeneration via repressing NLRP3 activation. As mentioned above, inflammation response exacerbates the severity of IDD. On the other hand, anti-inflammation therapy could alleviate IVD degeneration. For example, IL-10 was an important anti-inflammatory mediator, and exogenous IL-10 treatment delayed IVD degeneration via inhibiting p38 MAPK activation and inflammation response [26].

Immune response is an important driver of inflammation, and various immune cells play different roles in the process of IDD. Intervertebral disc has been widely accepted as an immune privilege organ because of its avascular structure. However, the rupture of outer annulus fibrosus results in exposure of inner nucleus pulposus to circulation and consequently triggers an autoimmune reaction. The infiltration of immune cells, such as neutrophils, T cells, and macrophages might release a large amount of proinflammatory molecules and promoted inflammation cascade within the disc. Wang et al. showed the immune infiltration landscape varied significantly between LDH and healthy control, and both Tregs and macrophages were implicated with IDD development [7]. Macrophage has been identified as a key immune player in the process

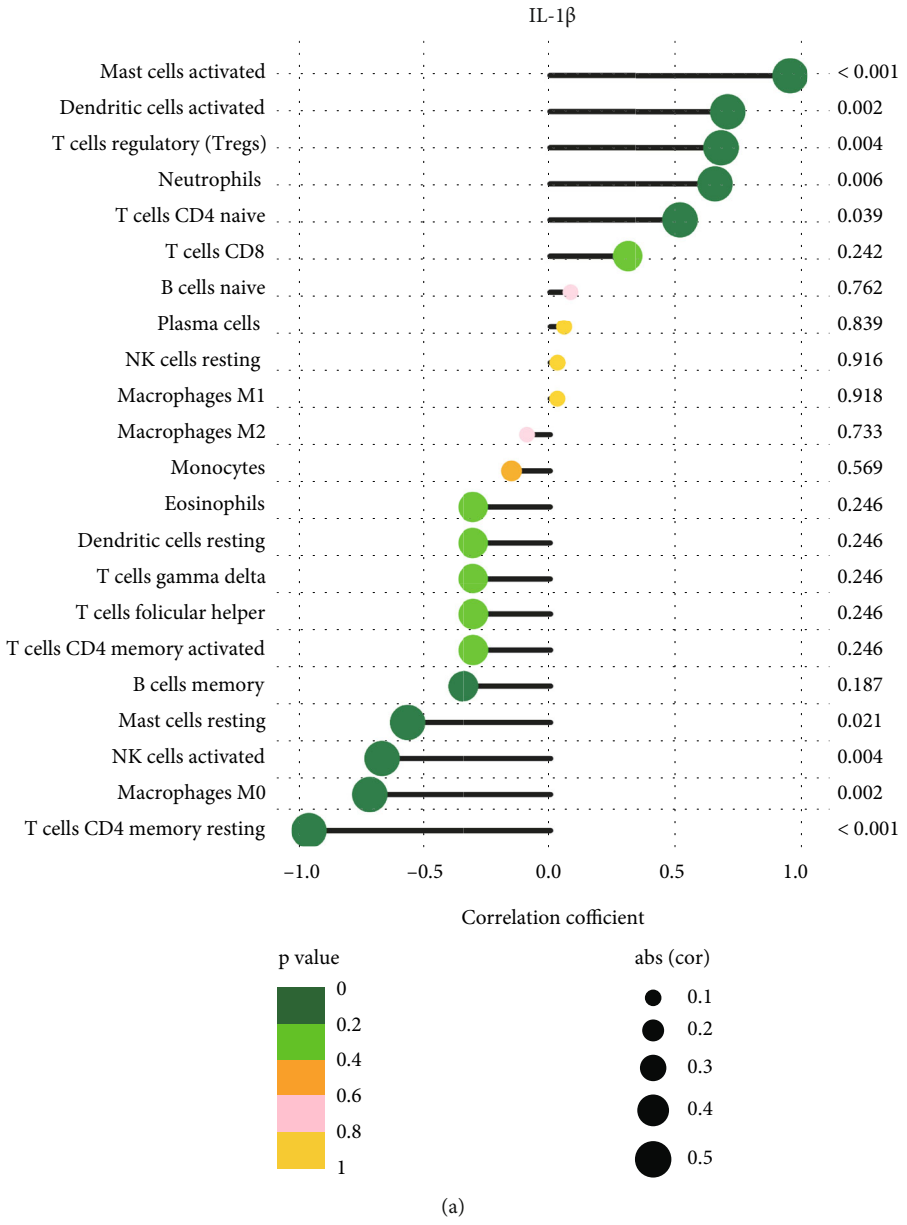

(a)

Figure 11: Continued.

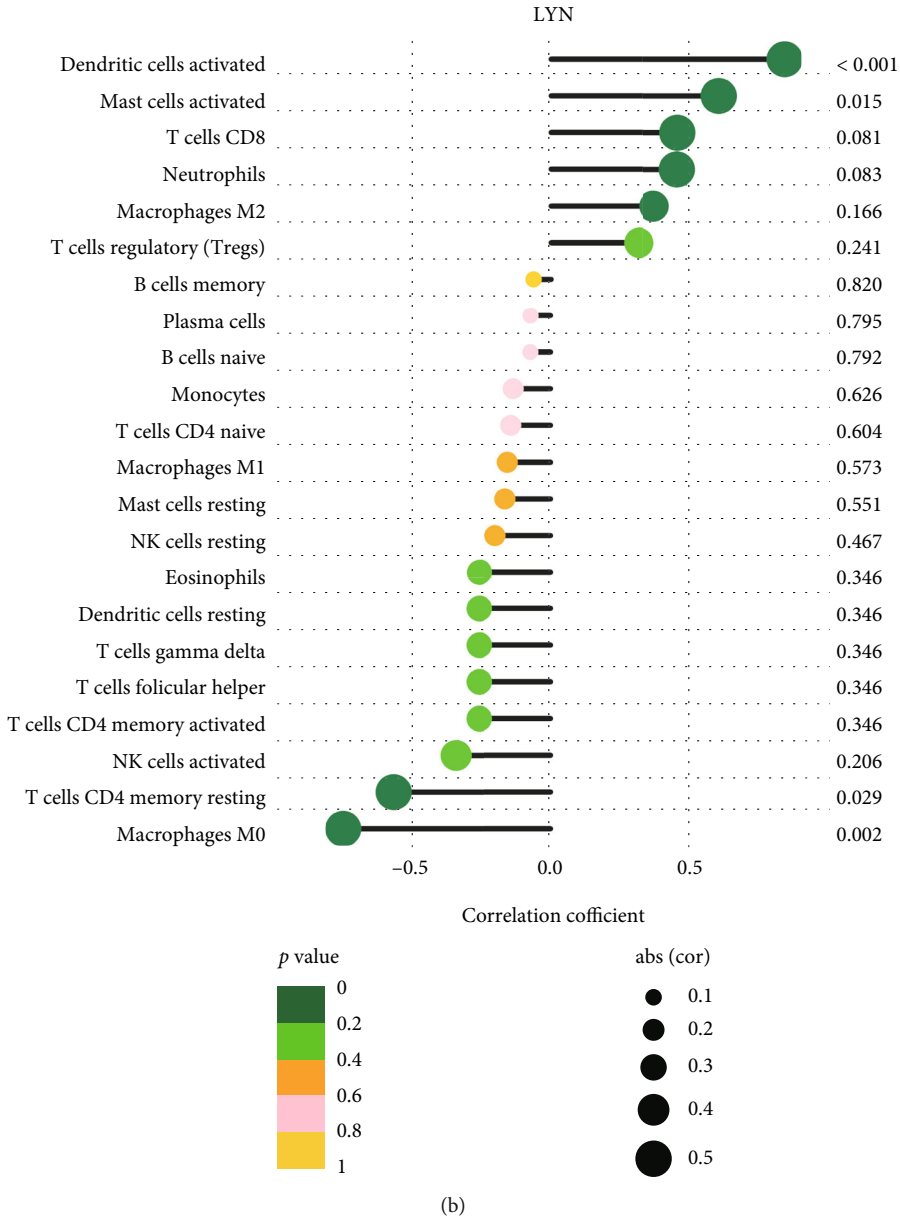

(b)

Figure 11: Continued.

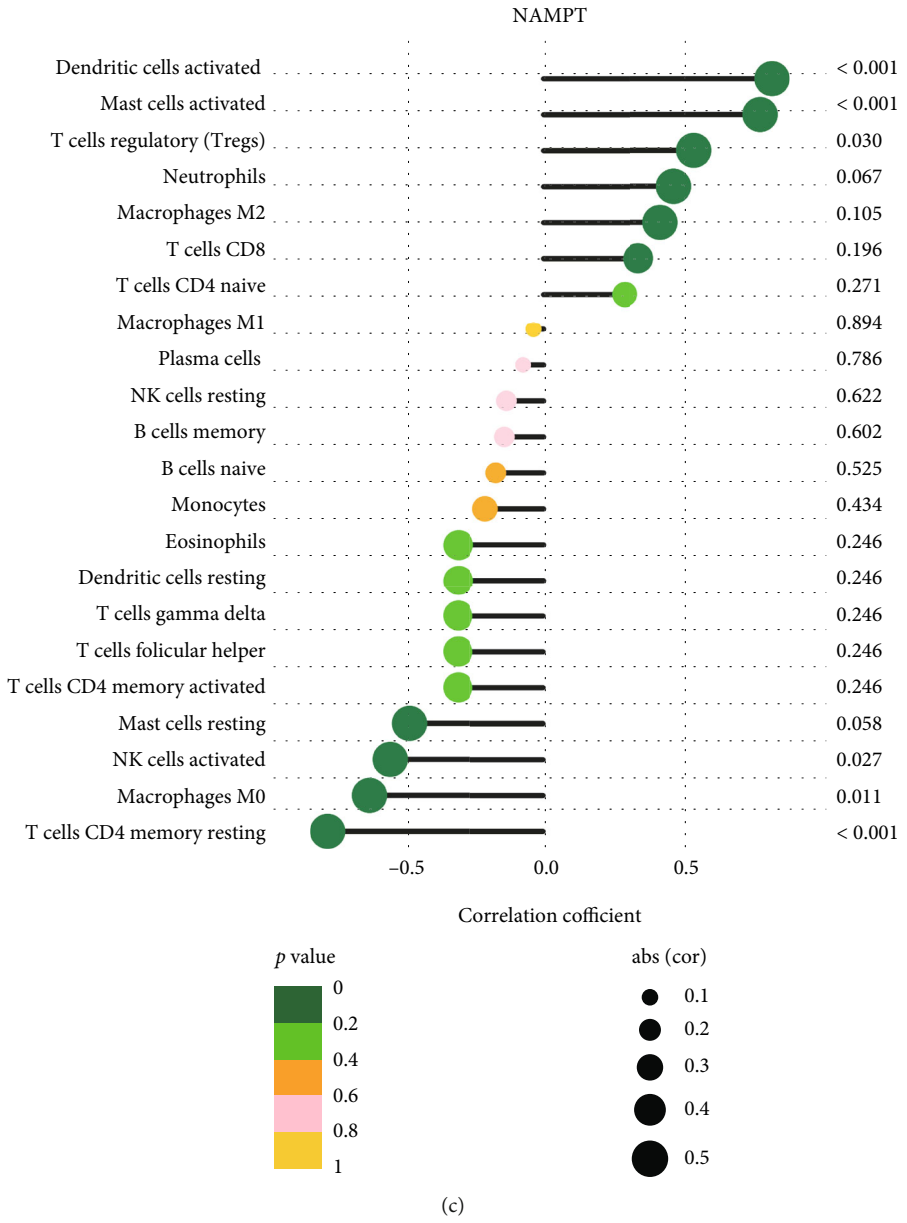

(c)

Figure 11: Correlation between immune cells and IL-1β, LYN, and NAMPT.

of IDD. Significant interaction between macrophages and progenitor NP cells via MIF (macrophage migration inhibitory factor) and NF-κB signaling pathways was found during the progression of IDD via single-cell RNA sequencing [27]. To be mentioned, the function of macrophage is influenced by both phenotypes and microenvironment. It was reported that after cocultured with IL-1β and IVD-conditioned medium, macrophages prevented IVD ECM remodeling and decreased aggrecan and collagen II gene expression in the presence of IL-1β [28]. The cross talk between macrophage and IVD in degenerated disc tended to polarize macrophages toward a more proinflammatory state, which accelerated IVD degeneration as a return. A recent study showed that magnoflorine alleviated M_1 macrophage-induced IDD by the inhibition of NLRP3 inflammasome activation [29]. On the other hand, the M_2 macrophage played an anti-inflammatory effect and increased NP cell proliferation and ECM synthesis under TNF-α stimulation [30]. Nowadays, increasing evidence support that M_1 polarization shows a proinflammatory effect while M_2 state plays an anti-inflammation and remodeling effect in response to injury [31–33]. Hence, future macrophage-anchored therapeutics is promising in the management of IDD. Moreover, many other types of immune cells, including neutrophils and T cells, have attracted a lot of research attention and the progress of interaction between immune cells and inflammatory response is expected to become a breakthrough in the treatment of IDD.

Notably, there are still few studies on the interaction of inflammation related genes and immune infiltration in the pathogenesis of IDD. Our rigorous bioinformatic analysis

provided reliable inflammatory genetic biomarkers in the IDD model and paved the way for future therapeutic strategies research for IDD by targeting inflammatory genes and immune modulation. Nevertheless, there were certain limitations in our study. First, this study was completely based on public datasets with small sample size, which might result in biased interpretation. Second, in vivo and in vitro experiments for validation are lacking. Hence, further in-depth biological experiments on immune infiltration and inflammatory response are required.

5. Conclusion

In conclusion, the present study revealed that the expression level of inflammatory associated genes (IRGs) and immune infiltration landscape significantly differed between IDD patients and healthy control. Additionally, based on this comprehensive bioinformatic analysis, we identified hub IRGs, critical regulatory pathways and immune infiltration characteristics of IDD. Moreover, the correlation between hub IRGs and immune cells was analyzed. In all, these findings may extend our knowledge concerning inflammation response and immune modulation in IDD patients.

Abbreviations

LBP: Low back pain
IVD: Intervertebral disc
IDD: Intervertebral disc degeneration
AF: Annulus fibrosus
NP: Nucleus pulposus
CEP: Cartilage endplate
ECM: Extracellular matrix
MMP: Matrix metalloproteinase
DEGs: Differentially expressed genes
BP: Biological process
CC: Cellular component
MF: Molecular function
KEGG: Kyoto Encyclopedia of Genes and Genomes.

Data Availability

The following information was supplied regarding data availability: The raw data can be found at https://www.ncbi.nlm.nih.gov/geo/query/acc.cgi?acc=GSE27494, https://www.ncbi.nlm.nih.gov/geo/query/acc.cgi?acc=GSE41883, and https://www.ncbi.nlm.nih.gov/geo/query/acc.cgi?acc=GSE150408.

Ethical Approval

This study is based on microarray analysis.

Conflicts of Interest

The authors have no conflicts of interest to disclose in relation to this article.

Authors' Contributions

Tao Lan and Yuantao Zhang conceived and designed the study; Zhihao Hu and Weizhuang Guo analyzed the data; Bin Yan and Tao Lan wrote and revised the manuscript. Tao Lan and Zhihao Hu contributed equally to this work and should be considered co-first authors.

Acknowledgments

This work was supported by the Natural Science Foundation of Guangdong Province (Grant No. 2022A1515011366).

References

[1] N. N. Knezevic, K. D. Candido, J. W. S. Vlaeyen, J. Van Zundert, and S. P. Cohen, "Low back pain," *Lancet*, vol. 398, no. 10294, pp. 78–92, 2021.

[2] J. Hartvigsen, M. J. Hancock, A. Kongsted et al., "What low back pain is and why we need to pay attention," *Lancet*, vol. 391, no. 10137, pp. 2356–2367, 2018.

[3] R. Chou, "Low Back Pain," *Annals of Internal Medicine*, vol. 174, pp. Itc113–itc128, 2021.

[4] H. Kim, J. Y. Hong, J. Lee, W. J. Jeon, and I. H. Ha, "IL-1β promotes disc degeneration and inflammation through direct injection of intervertebral disc in a rat lumbar disc herniation model," *The Spine Journal*, vol. 21, no. 6, pp. 1031–1041, 2021.

[5] F. Ye, Y. Xu, F. Lin, and Z. Zheng, "TNF-α suppresses SHOX2 expression via NF-κB signaling pathway and promotes intervertebral disc degeneration and related pain in a rat model," *Journal of Orthopaedic Research*, vol. 39, no. 8, pp. 1745–1754, 2021.

[6] A. Naylor, F. Happey, R. L. Turner, R. D. Shentall, D. C. West, and C. Richardson, "Enzymic and immunological activity in the intervertebral disk," *The Orthopedic Clinics of North America*, vol. 6, no. 1, pp. 51–58, 1975.

[7] L. Wang, T. He, J. Liu et al., "Revealing the immune infiltration landscape and identifying diagnostic biomarkers for lumbar disc herniation," *Frontiers in Immunology*, vol. 12, article 666355, 2021.

[8] W. Li, Z. Ding, H. Zhang et al., "The roles of blood lipid-metabolism genes in immune infiltration could promote the development of IDD," *Frontiers in Cell and Development Biology*, vol. 10, article 844395, 2022.

[9] A. Conger, B. Duszynski, and Z. L. McCormick, "Management of Chronic low Back Pain," *JAMA Internal Medicine*, vol. 182, no. 6, p. 687, 2022.

[10] A. C. Traeger, A. Qaseem, and J. H. McAuley, "Low Back pain," *JAMA*, vol. 326, no. 3, p. 286, 2021.

[11] Y. Wang, M. Che, J. Xin, Z. Zheng, J. Li, and S. Zhang, "The role of IL-1β and TNF-α in intervertebral disc degeneration," *Biomedicine & Pharmacotherapy*, vol. 131, article 110660, 2020.

[12] X. X. Song, L. Y. Jin, X. F. Li, Y. Luo, and B. W. Yu, "Substance P mediates estrogen modulation Proinflammatory cytokines release in intervertebral disc," *Inflammation*, vol. 44, no. 2, pp. 506–517, 2021.

[13] A. N. Khan, H. E. Jacobsen, J. Khan et al., "Inflammatory biomarkers of low back pain and disc degeneration: a review," *Annals of the New York Academy of Sciences*, vol. 1410, no. 1, pp. 68–84, 2017.

[14] Y. Zhou, Z. Chen, X. Yang et al., "Morin attenuates pyroptosis of nucleus pulposus cells and ameliorates intervertebral disc degeneration via inhibition of the TXNIP/NLRP3/Caspase-1/IL-1β signaling pathway," *Biochemical and Biophysical Research Communications*, vol. 559, pp. 106–112, 2021.

[15] Z. Shao, B. Wang, Y. Shi et al., "Senolytic agent quercetin ameliorates intervertebral disc degeneration via the Nrf2/NF-κB axis," *Osteoarthritis and Cartilage*, vol. 29, no. 3, pp. 413–422, 2021.

[16] J. Lin, J. Chen, Z. Zhang et al., "Luteoloside inhibits IL-1β-induced apoptosis and catabolism in nucleus pulposus cells and ameliorates intervertebral disk degeneration," *Frontiers in Pharmacology*, vol. 10, p. 868, 2019.

[17] T. Nacarelli, L. Lau, T. Fukumoto et al., "NAD(+) metabolism governs the proinflammatory senescence-associated secretome," *Nature Cell Biology*, vol. 21, no. 3, pp. 397–407, 2019.

[18] Y. Huang, Y. Peng, J. Sun et al., "Nicotinamide phosphoribosyl transferase controls NLRP3 Inflammasome activity through MAPK and NF-κB signaling in nucleus pulposus cells, as suppressed by melatonin," *Inflammation*, vol. 43, no. 3, pp. 796–809, 2020.

[19] C. Shi, H. Wu, D. du et al., "Nicotinamide Phosphoribosyltransferase inhibitor APO866 prevents IL-1β-induced human nucleus pulposus cell degeneration via autophagy," *Cellular Physiology and Biochemistry*, vol. 49, no. 6, pp. 2463–2482, 2018.

[20] Y. Sun, X. Li, X. Yang, B. Chen, and W. Zhang, "Small extracellular vesicles derived from adipocytes attenuate intervertebral disc degeneration in rats by rejuvenating senescent nucleus pulposus cells and endplate cells by delivering exogenous NAMPT," *Oxidative Medicine and Cellular Longevity*, vol. 2021, Article ID 9955448, p. 18, 2021.

[21] Q. Shi, L. Xu, and X. Zeng, "Sirtuin 1 participates in intervertebral disc degeneration via the nicotinamide phosphoribosyl transferase/nicotinamide adenine dinucleotide/sirtuin 1 pathway responsible for regulating autophagy of nucleus pulposus cells," *Experimental and Therapeutic Medicine*, vol. 23, no. 4, p. 267, 2022.

[22] G. Chao-Yang, C. Peng, and Z. Hai-Hong, "Roles of NLRP3 inflammasome in intervertebral disc degeneration," *Osteoarthritis and Cartilage*, vol. 29, no. 6, pp. 793–801, 2021.

[23] Y. Zhao, C. Qiu, W. Wang et al., "Cortistatin protects against intervertebral disc degeneration through targeting mitochondrial ROS-dependent NLRP3 inflammasome activation," *Theranostics*, vol. 10, no. 15, pp. 7015–7033, 2020.

[24] F. Chen, G. Jiang, H. Liu et al., "Melatonin alleviates intervertebral disc degeneration by disrupting the IL-1β/NF-κB-NLRP3 inflammasome positive feedback loop," *Bone Research*, vol. 8, no. 1, p. 10, 2020.

[25] C. Xia, Z. Zeng, B. Fang et al., "Mesenchymal stem cell-derived exosomes ameliorate intervertebral disc degeneration via anti-oxidant and anti-inflammatory effects," *Free Radical Biology & Medicine*, vol. 143, pp. 1–15, 2019.

[26] J. Ge, Q. Yan, Y. Wang et al., "IL-10 delays the degeneration of intervertebral discs by suppressing the p38 MAPK signaling pathway," *Free Radical Biology & Medicine*, vol. 147, pp. 262–270, 2020.

[27] Z. Ling, Y. Liu, Z. Wang et al., "Single-cell RNA-Seq analysis reveals macrophage involved in the progression of human intervertebral disc degeneration," *Frontiers in Cell and Development Biology*, vol. 9, article 833420, 2021.

[28] A. J. Silva, J. R. Ferreira, C. Cunha et al., "Macrophages Down-regulate gene expression of intervertebral disc degenerative markers under a pro-inflammatory microenvironment," *Frontiers in Immunology*, vol. 10, p. 1508, 2019.

[29] F. Zhao, Z. Guo, F. Hou, W. Fan, B. Wu, and Z. Qian, "Magnoflorine alleviates "M1" polarized macrophage-induced intervertebral disc degeneration through repressing the HMGB1/Myd88/NF-κB pathway and NLRP3 Inflammasome," *Frontiers in Pharmacology*, vol. 12, article 701087, 2021.

[30] X. C. Li, S. J. Luo, W. Fan, T. L. Zhou, C. M. Huang, and M. S. Wang, "M2 macrophage-conditioned medium inhibits intervertebral disc degeneration in a tumor necrosis factor-α-rich environment," *Journal of Orthopaedic Research*, vol. 1, pp. 11–14, 2022.

[31] K. R. Nakazawa, B. A. Walter, D. M. Laudier et al., "Accumulation and localization of macrophage phenotypes with human intervertebral disc degeneration," *The Spine Journal*, vol. 18, no. 2, pp. 343–356, 2018.

[32] S. Lee, M. Millecamps, D. Z. Foster, and L. S. Stone, "Long-term histological analysis of innervation and macrophage infiltration in a mouse model of intervertebral disc injury-induced low back pain," *Journal of Orthopaedic Research*, vol. 38, no. 6, pp. 1238–1247, 2020.

[33] M. Nakawaki, K. Uchida, M. Miyagi et al., "Changes in nerve growth factor expression and macrophage phenotype following intervertebral disc injury in mice," *Journal of Orthopaedic Research*, vol. 37, no. 8, pp. 1798–1804, 2019.

Hindawi
Oxidative Medicine and Cellular Longevity
Volume 2022, Article ID 7548145, 17 pages
https://doi.org/10.1155/2022/7548145

Research Article

Specific PFKFB3 Inhibitor Memorably Ameliorates Intervertebral Disc Degeneration via Inhibiting NF-κB and MAPK Signaling Pathway and Reprogramming of Energy Metabolism of Nucleus Pulposus Cells

Xiankun Cao, Xin Wang, Kewei Rong, Kexin Liu, Xiao Yang, Tangjun Zhou, Pu Zhang, Jiadong Guo, Hui Ma, An Qin, and Jie Zhao

Shanghai Key Laboratory of Orthopedic Implants, Department of Orthopaedics Surgery, Shanghai Ninth People's Hospital, Shanghai Jiao Tong University School of Medicine, Shanghai 200011, China

Correspondence should be addressed to Hui Ma; 18939760496@163.com, An Qin; dr_qinan@163.com, and Jie Zhao; profzhaojie@126.com

Received 18 July 2022; Accepted 30 August 2022; Published 21 September 2022

Academic Editor: Sidong Yang

Intervertebral disc (IVD) degeneration (IVDD) is a characteristic of the dominating pathological processes of nucleus pulposus (NP) cell senescence, abnormal synthesis and irregular distribution of extracellular matrix (ECM), and tumor necrosis factor-α (TNF-α) induced inflammation. Nowadays, IVD acid environment variation which accelerates the pathological processes mentioned above arouses researchers' attention. KAN0438757 (KAN) is an effective inhibitor of selective metabolic kinase phosphofructokinase-2/fructose-2,6-bisphosphatase 3 (PFKFB3) that has both energy metabolism reprogramming and anti-inflammatory effects. Therefore, a potential therapeutic benefit of KAN lies in its ability to inhibit the development of IVDD. This study examined *in vitro* KAN toxicity in NP primary cells (NPPs). Moreover, KAN influenced tumor necrosis factor-α (TNF-α) induced ECM anabolism and catabolism; the inflammatory signaling pathway activation and the energy metabolism phenotype were also examined in NPPs. Furthermore, KAN's therapeutic effect was investigated *in vivo* using the rat tail disc puncture model. Phenotypically speaking, the KAN treatment partially rescued the ECM degradation and glycolysis energy metabolism phenotypes of NPPs induced by TNF-α. In terms of mechanism, KAN inhibited the activation of MAPK and NF-κB inflammatory signaling pathways induced by TNF-α and reprogramed the energy metabolism. For the therapeutic aspect, the rat tail disc puncture model demonstrated that KAN has a significant ameliorated effect on the progression of IVDD. To sum up, our research successfully authenticated the potential therapeutic effect of KAN on IVDD and declaimed its mechanisms of both novel energy metabolism reprogramming and conventional anti-inflammation effect.

1. Introduction

IVD usually plays an important role in spinal movement. As a result of IVDD, low back pain and severe spinal disorders, including lumbar disc herniation and spinal stenosis, are common [1]. Due to the wide range of morbidity, it has caused a huge socioeconomic burden and sorely influenced patients' quality of life [2]. The NP cell senescence and their dysfunction on ECM maintenance are considered as an initial trigger in the pathogenesis of IVDD [3]. The special physiological composition of hyaline cartilaginous endplates (CEPs), annulus fibrosus (AF), and NP determines the specific hypoxic environment of IVD. Therefore, AF rupture caused hypoxic environment disruption, and subsequent blood vessels ingrowth and nociceptive nerves [4] are the vital reasons for accelerated irregular distribution and abnormal synthesis of ECM and TNF-α-induced inflammation [5] and the continuous vicious circle of NP cell senescence. Under the circumstances, therapies targeting inflammation, senescence, and hypoxic microenvironment

Table 1: Primer pair sequences used in qPCR.

Mouse gene	Forward 5′ ➔ 3′	Reverse 5′➔ 3′
MMP3	CCCTGCAACCGTGAAGAAGA	GACAGCATCCACCCTTGAGT
MMP7	CCCTGTTCTGCTTTGTGTGTCA	GGGGGAGAGTTTTCCAGTCA
MMP9	CCGACTTTTGTGGTCTTCCCC	ATGTCTCGCGGCAAGTCTTC
MMP13	AGAAGTGTGACCCAGCCCTA	GGTCACGGGATGGATGTTCA
Aggrecan	TGCAGACATTGACGAGTGCC	AGAGAGTGTCCGTCAGACCA
β-Actin	ACCCGCGAGTACAACCTTC	ATGCCGTGTTCAATGGGGTA

loss of NP cells [6–8], no matter by any kind of approaches such as EVs, cell secretory factors, stem cells, and drugs [9–11], have been the main assault fortified directions of researchers in last decades.

However, some emerging but interesting perspectives have aroused researchers' attention in the past few years. One of these hot issues, acid environment variation of degenerated IVD, similar to hypoxia environment change, has been demonstrated to influence some processes of IVDD [12, 13]. Specifically, the glycolytic metabolism phenotype of NP cells under a hypoxia environment is further aggravated due to the reduction of glucose and oxygen supply caused by CEP permeability decrease during IVDD, which enhances the lactate production and its efflux to ECM [14, 15]. The descending pH in the environment in turn significantly induces the catabolic upregulation and anabolic downregulation of acid-sensitive NP cells, resulting in the NP cells' senescence, ECM imbalance, and degradation [16]. The long-termed and persistently aggravated environment acidification not only further influences the CEP permeability and oxygen balance in hypoxia IVD but also accelerates the death of NP cells [17], which all contribute to the TNF-α production and expression of other inflammatory mediators [18]. Thus, therapies that effectively break this vicious circle and achieve the treatment of IVDD by regulating the IVD acidic environment are new directions worthy of further study.

PFKFB3 is a key glycolysis rate-limiting enzyme. Due to its strong kinase activity, stabilized expression of PFKFB3 can elevate the rate of glycolysis, thereby promoting the blood vessel sprouting, affecting tumor angiogenesis [19]. Therefore, targeting PFKFB3 of its effects on glycolysis of endothelial cells (ECs) during tumor angiogenesis has become a burgeoning research field in tumor therapy [20, 21]. In addition, the effect of PFKFB3 on endothelial cell glycolysis has also been demonstrated to be very important for pathological hypoxic diseases such as pulmonary hypertension [22]. Moreover, PFKFB3 inhibitor PFK15 exhibits a significant antiosteoporosis effect by repressing inflammation (NF-κB and MAPK pathways) and blocking glycolysis of osteoclasts at the same time [23].

KAN is the latest inhibitor of selective metabolic kinase PFKFB3, more effective than PFK15, that has been identified as a potential cancer treatment strategy [24]. Therefore, according to previous research on the effect of PFKFB3 inhibition in ECs and OCs, whether and how KAN ameliorates IVDD, a hypoxia environment-metabolism dysfunction-NP cell senescence and death-inflammation vicious cycle pathological process, via inhibiting inflammation and reprogramming of energy metabolism of nucleus pulposus cells is worth to be explored and revealed.

2. Materials and Methods

2.1. Chemicals and Reagents. The selective metabolic kinase PFKFB3 inhibitor KAN0438757 (KAN) was purchased from MCE (CAS: 1451255-59-6, Shanghai, China), dissolved in dimethyl sulfoxide (DMSO) as a 5 mM stock solution, and stored at −80°C. A final concentration of DMSO less than 0.1% was used to reduce cytotoxicity. Fetal bovine serum (FBS) and penicillin/streptomycin were bought from Gibco BRL (Gaithersburg, MD, USA). Minimal essential medium (DMEM) was bought from Hyclone (Logan, UT, USA). The Cell Counting Kit-8 (CCK-8) was purchased from Dojindo Molecular Technology (Japan). The prime script RT Master Mix kit and TBGreen ® Premix Ex Taq ™ kit were both obtained from Takara Biotechnology (Otsu, Shiga, Japan). The XF Cell Mito Stress Test (for OCR) Kit, XF Glycolysis Stress Test (for ECAR) Kit, XFe96 FluxPak mini, XF DMEM Base Medium, XF 1.0M Glucose Solution, 100 mM XF Pyruvate Solution, and 200 mM XF Glutamine Solution were obtained from Agilent (Seahorse Bioscience, USA). The primary antibodies against MMP9, MMP13, and PFKFB3 were purchased from Abcam (Cambridge, UK). Primary antibodies including ERK, JNK, p38, phospho-ERK (Tr202/Tyr204), phospho-JNK (Tr183/Tyr185), phospho-p38, IKKβ, phospho-IKKα/β, IκBα, phospho-IκBα, P65, phospho-P65, and β-actin and the secondary antibody were purchased from Cell Signaling Technology (CST, Danvers, MA, USA). All the antibodies mentioned except β-actin are rabbit anti-mouse.

2.2. NP Primary Cell (NPP) Isolation. Pentobarbital sodium 50 mg/kg (body weight) was injected intraperitoneally into 4-week-old SD rats for euthanasia. After that, the NP tissues were obtained from the caudal discs (Co1–Co6) and then digested for 2 hours by 0.25% type II collagenase at 37°C, 21% O_2, and 5% CO_2 incubator. Then, the mixture was centrifuged, and cells were separated, resuspended, and seeded (DMEM with 10% FBS and 1% penicillin-streptomycin) in a culture plate placing on 37°C, 21% oxygen, and 5% carbon dioxide incubator.

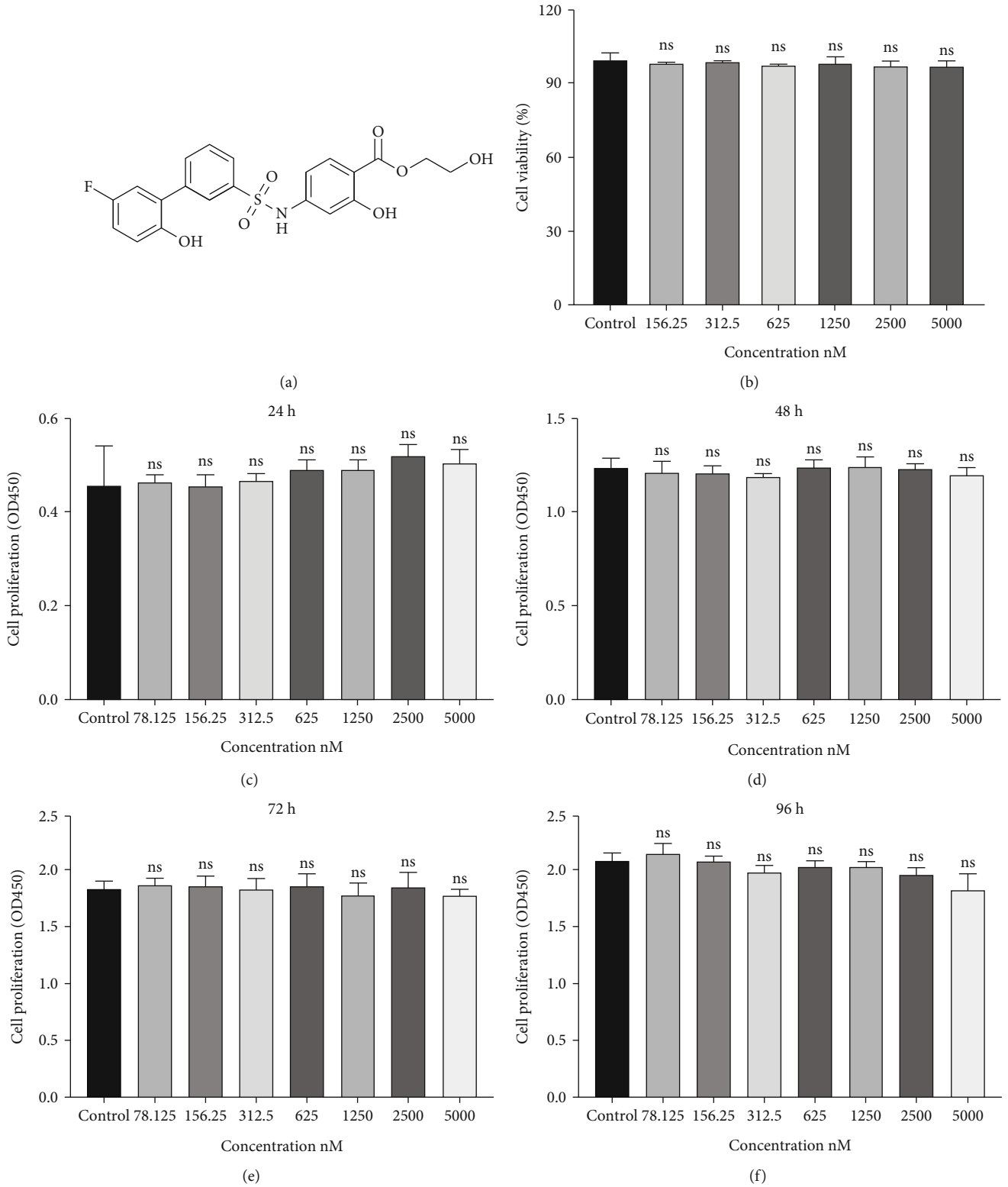

Figure 1: Effects of KAN0438757 (KAN) on the cytotoxicity and proliferation of nucleus pulposus primary (NPP) cells *in vitro*. (a) The chemical structure of KAN. (b) Cell viability of KAN-treated NPPs was tested by CCK-8 at 24 hours. (c–f) Cell proliferation effect of NPPs treated by negative control or different concentrations KAN was tested by CCK-8 at 24, 48, 72, and 96 hours. Data are expressed as mean ± SD, $n = 4$-6. ns: no significance.

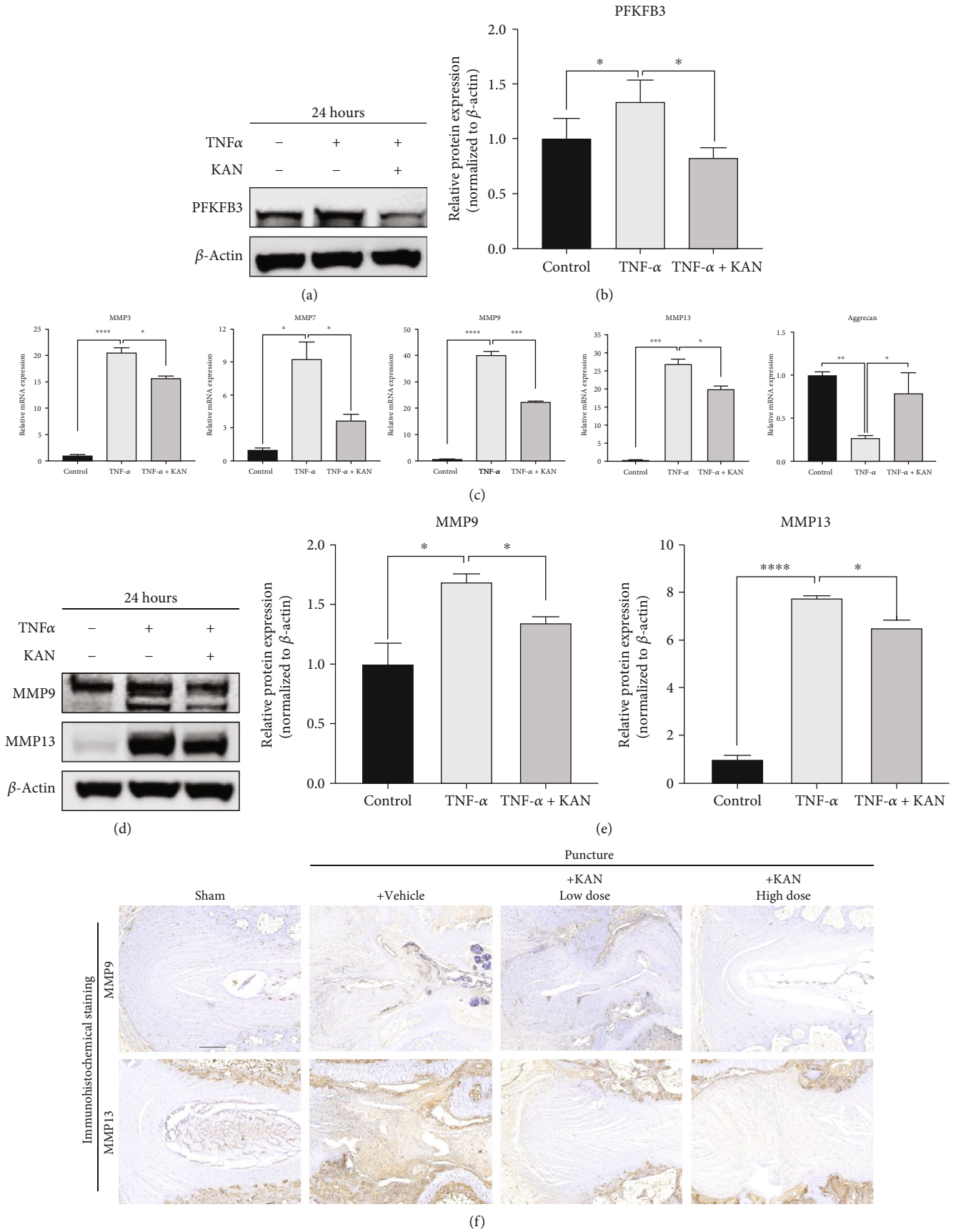

Figure 2: Continued.

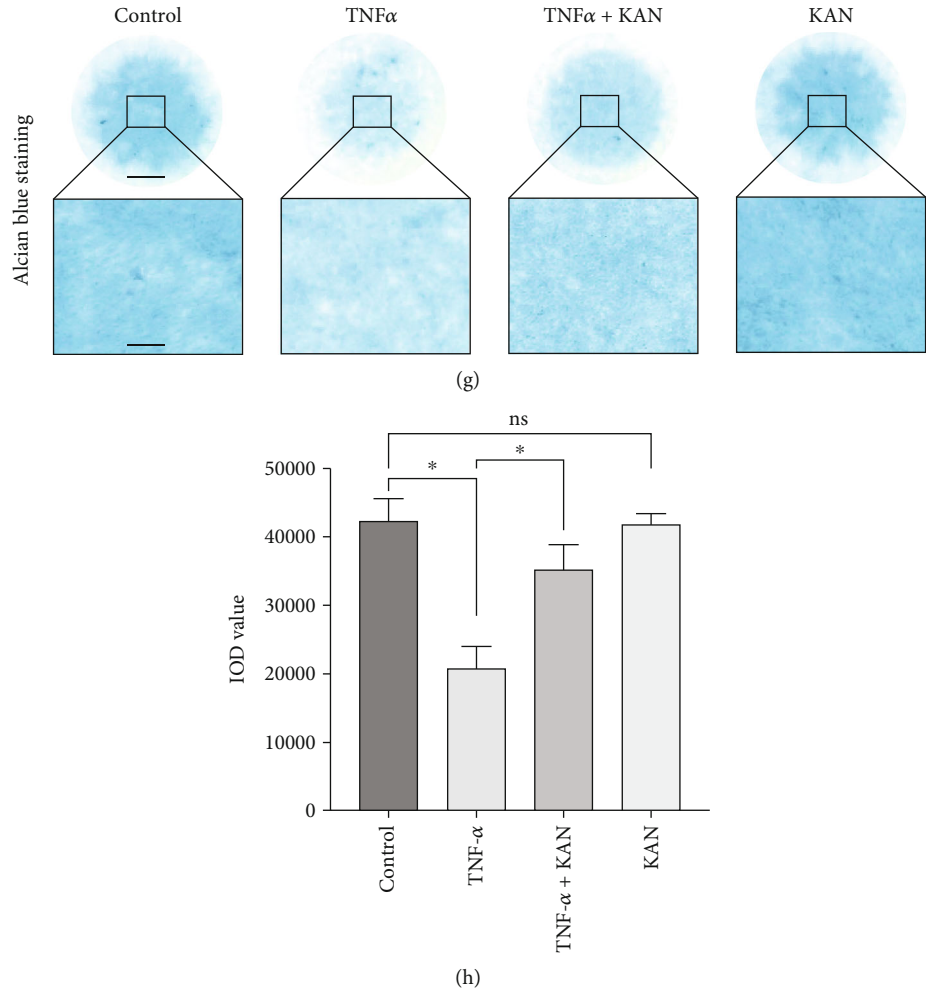

Figure 2: KAN0438757 (KAN) alleviated tumor necrosis factor-α- (TNF-α-) induced extracellular matrix (ECM) degradation of nucleus pulposus primary (NPP) cells both *in vitro* and *in vivo*. (a) PFKFB3 expression levels after negative control, TNF-α, TNF-α with 2.5 μM KAN treatment for 24 hours in NPPs. (b) The gray levels of PFKFB3 were quantified and normalized to β-actin using ImageJ. $n = 3$. (c) Expression of the anabolism and catabolism gene matrix metalloproteins (MMPs) 3, 7, 9, and 13 and aggrecan after negative control, TNF-α, and TNF-α with 2.5 μM KAN treatment for 24 hours in NPPs. $n = 3$. (d) MMP3 and MMP9 expression levels after negative control, TNF-α, and TNF-α with 2.5 μM KAN treatment for 24 hours in NPPs. (e) The gray levels of MMP3 and MMP9 were quantified and normalized to β-actin using ImageJ. $n = 3$. (f) Immunohistochemical staining of MMP3 and MMP 9 expressions. Scale bar = 300 μm. (g) Alcian blue staining of NP primary cells (P2 generation) on high-density culture after negative control, TNF-α, and TNF-α with 2.5 μM KAN treatment for 7 days. Scale bar = 2 mm, 400 μm. (h) The integrated optical density (IOD) value was calculated to evaluate the extracellular matrix (ECM) of NP primary cells after the indicated treatment. $n = 4$. Data are expressed as mean ± SD. ns: no significance; $^{*}p < 0.05$; $^{**}p < 0.01$; $^{***}p < 0.001$; $^{****}p < 0.0001$.

2.3. Cell Counting Kit-8 (CCK-8) Assay. The cell proliferation and toxicity effects of KAN on NPPs were measured using the CCK-8. More specifically, to determine toxicity, the NPPs were seeded triplicately into 96-well plates at 8×10^3 cells per well in presence of various concentrations of KAN (control (0), 156.25, 312.5, 625, 1250, 2500, and 5000 nM) and cultured for 24 h. As for proliferation, 96-well plates were seeded with NPPs in triplicate at 2×10^3 cells per well for 24 hours first. Then, KAN concentrations of control, 156.25, 312.5, 625, 1250, 2500, and 5000 nM were added into the wells for 24, 48, 72, and 96 hours. Cells were incubated at 37°C for 2 hours with 10 μL of the CCK-8 reagent after each experimental period. The optical density values were measured on the Infinite M200 Pro multimode microplate reader using a spectrophotometer at 450 nm (Tecan Life Sciences, Männedorf, Switzerland).

2.4. High-Density Culture. To assess the ECM secretion ability effect of KAN, 10 μl medium micromasses containing approximately 1.2×10^5 NPPs were seeded in the middle at the bottom of a 24-well plate first. Then, the plate was placed in a 37°C, 21% O_2, and 5% CO_2 incubator for 90 min for the attachment of NPPs to the bottom. After that, 500 μL of MEM/F12 medium (2% FBS and 10 ng/mL of Insulin Transferrin Selenium (ITS)) was added into the plate. The medium was changed every two days; These micromasses were stained with Alcian blue at the day 7.

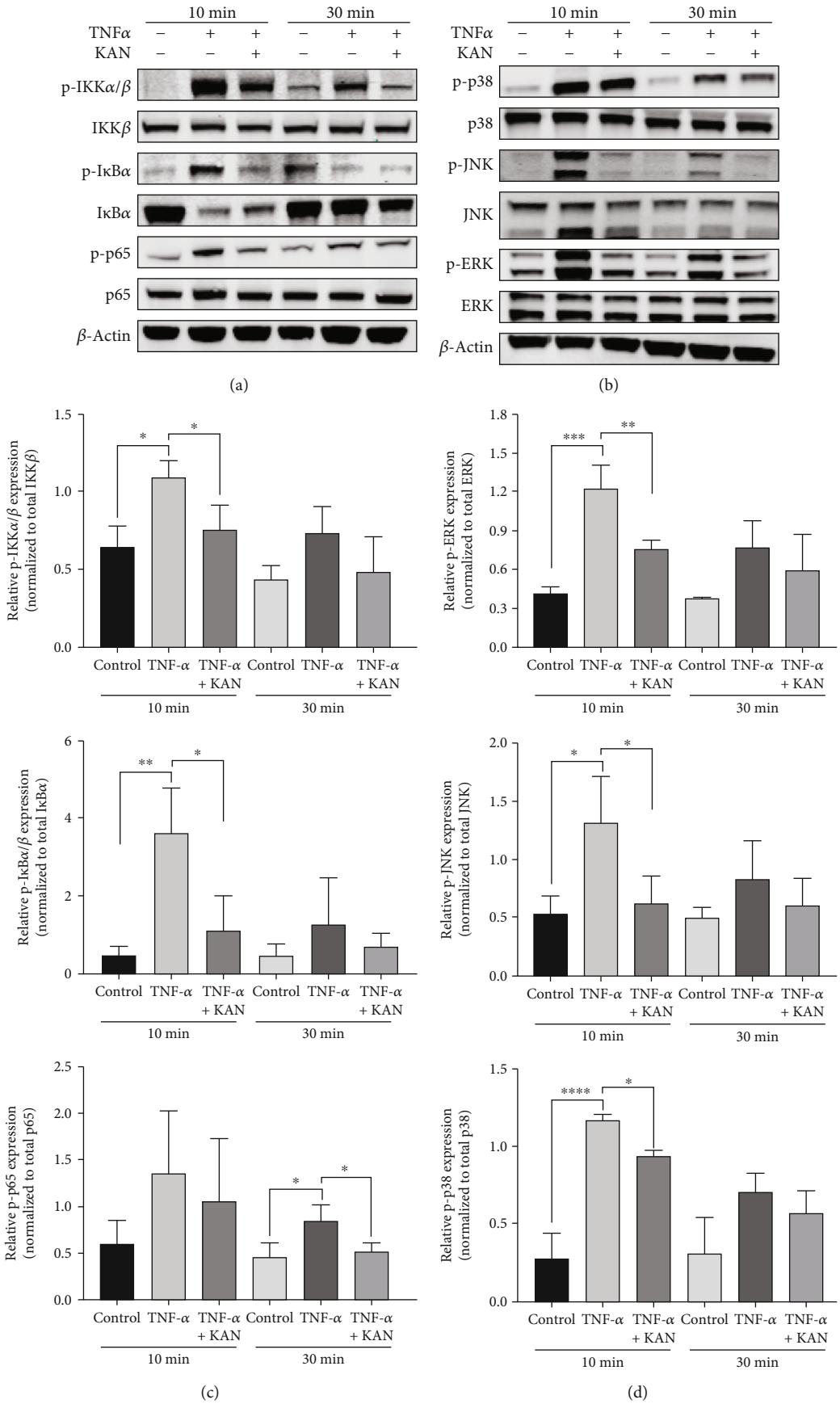

Figure 3: Continued.

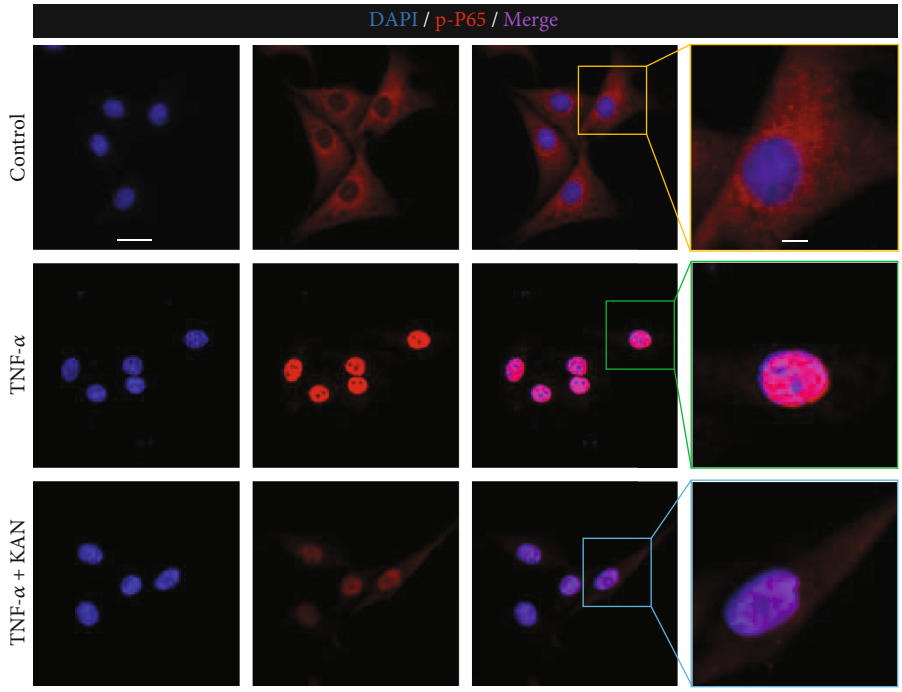

(e)

Figure 3: KAN0438757 (KAN) inhibited the NF-κB signaling pathway and subsequent p-P65 nuclear translocation, as well as the MAPK signaling pathway. (a) The NF-κB signaling pathway protein expression levels after negative control, TNF-α, and TNF-α with 2.5 μM KAN treatment for 10 and 30 min in NPPs. (b) The MAPK signaling pathway protein expression levels after negative control, TNF-α, and TNF-α with 2.5 μM KAN treatment for 10 and 30 min in NPPs. (c) The gray levels of p-IKKα/β, p-IκBα, and p-P65 were quantified and normalized to their respective total protein using ImageJ. (d) The gray levels of p-ERK, p-JNK, and p-P38 were quantified and normalized to their respective total protein using ImageJ. (e) Nuclear translocation of p-P65 after negative control, TNF-α, and TNF-α with 2.5 μM KAN treatment for 15 min, visualized by immunofluorescence. Scale bar = 20 μm and 5 μm. Data are expressed as mean ± SD, $n = 3$. ns: no significance; $^{*}p < 0.05$; $^{**}p < 0.01$; $^{***}p < 0.001$; $^{****}p < 0.0001$.

2.5. Seahorse Metabolic Flux Analysis. NPPs were plated in XF-96 cell culture plates at 6×10^3/well (Seahorse Bioscience, USA) for the first 24 hours. Then, the cells were treated with control, TNF-α, or TNF-α plus 2.5 μM KAN for the next 24 hours. The measurements of oxygen consumption rate (OCR) and extracellular acidification rate (ECAR) were carried out according to standard protocols, and the results were detected with the Seahorse XF-96 Flux Analyzer (Seahorse Bioscience), as previously described [25]. In the OCR assay, 1.5 μM oligomycin, 2.5 μM FCCP, rotenone, and 0.5 μM antimycin A were used to stimulate cells. In the EACR assay, 10 mM glucose, 2 μM oligomycin, and 50 mM 2-DG were used to stimulate cells. Additionally, the OCR and ECAR changes were used to calculate OXPHOS characteristics as well as glycolysis parameters (as described in Supplementary Figure 1).

2.6. Immunofluorescence Assay. In a 6-well plate, 2×10^5 per well NPPs was seeded and cultured for 12 hours. After that, the treatment group was pretreated with the serum-free DMEM in the presence of 2.5 μM KAN for 2 hours; then, 15 min 20 ng/mL TNF-α stimulation, 10 min paraformaldehyde (4%) fix, and 10 min 0.2% Triton X-PBS permeabilization were performed on NPPs. The phospho-p65 primary antibody (1 : 200 dilution, Cell Signaling Technology, Danvers, MA, USA) was then incubated with cells overnight at 4°C after 10% goat serum blocking. After three times washing with PBS on the next day, the cells were incubated at dark with the Alexa Fluor 594 conjugate anti-rabbit secondary antibody for 1 hour (1 : 500, Cell Signaling Technology, Danvers, MA, United States). The cell nucleus was shown by 4′,6-diamidino-2-phenylindole (DAPI) after 3 min incubation (Sigma-Aldrich, St. Louis, MO, United States). Finally, digital fluorescence results were observed, and images were captured by the Leica fluorescence microscope (Olympus, Inc., Tokyo, Japan).

2.7. Protein Extraction and Western Blot (WB) Analyses. To figure out the effect of KAN on the catabolic or anabolic proteins, 3×10^5 cells/well NPPs were cultured in DMEM on 6-well plates for 24 hours. The NPPs were then treated with control, TNF-α, or TNF-α plus 2.5 μM KAN for 1 day. As for the effect of KAN on the phosphorylated proteins (short-time activated), 5×10^5 cells/well NPPs were cultured in DMEM on 6-well plates for 24 hours. The treatment group cells were then pretreated with 2.5 μM KAN for 2 hours with serum-free DMEM. 2 hours later, 10 and 30 min of TNF-α (20 ng/mL) stimulation were performed on the TNF-α group and the treatment group. After that, RIPA lysis buffer plus phosphatase and protease inhibitors (1 : 100 dilution, Roche, Basel, Switzerland) were used to, respectively, extract total cellular proteins at indicated time

points. According to the standard protocol of the bicinchoninic acid protein quantification kit, protein concentrations were then quantified (Thermo Fisher Scientific, Waltham, MA, United States). Standard western blot experiments were performed as previously described [26]. Primary antibodies (β-actin, 1 : 1000; ERK, 1 : 1000; JNK, 1 : 1000; p38, 1 : 1000; IKKβ, 1 : 1000; IκBα, 1 : 1000; P65, 1 : 1000; MMP9, 1 : 1000; MMP13, 1 : 1000; PFKFB3, 1 : 1000; p-JNK, 1 : 1000; p-ERK, 1 : 1000; p-p38, 1 : 1000; p-IKKα/β, 1 : 500; p-IκBα, 1 : 1000; p-P65, 1 : 500) incubated overnight at 4°C. Membranes were extensively washed in TBST for three times on the next day. The secondary antibody (anti-rabbit or anti-mouse IgG (H + L; 1 : 5000 dilution; Cell Signaling Technology, Danvers, MA, United States)) was subsequently incubated with the membranes for 1 hour at RT in the dark. Finally, the LI-COR Odyssey fluorescence imaging system was used to detect the reactivity (LI-COR Biosciences, Lincoln, NE, United States), and the ImageJ software was used to measure the grey values of each protein (National Institutes of Health, United States).

2.8. RNA Extraction and Real-Time Quantitative PCR (RT-qPCR) Analyses. To explore the effect of KAN on catabolic or anabolic-related genes, 3×10^5 cells/well NPPs were cultured in DMEM on 6-well plates. 24 hours later, the NPPs were cultured with control, TNF-α, or TNF-α plus 2.5 μM KAN for 24 hours. Total RNA was extracted using the Axygen RNA Miniprep Kit (Axygen, Union City, CA, USA) when the culture was completed. The Prime Script RT Master Mix kit was then used to reverse transcript the RNA to cDNA. Standard PCR (RT-qPCR) analyses were then performed as described previously [26]. Using the $2 - \Delta\Delta$CT method, relative mRNA expression levels were calculated and normalized to the β-actin expression. All primer pairs (Table 1) were designed by NCBI BLAST.

2.9. Histology and Immunohistochemical Staining Analyses. After 4% paraformaldehyde fixing for 48 hours, IVD tissue samples were decalcification in the 10% EDTA for 21 days and then embedded into paraffin blocks. After being subjected to 5 μm thickness histological sectioning, hematoxylin and eosin (H&E) staining and safranin O-fast green staining were then processed for histological assessment under standard laboratory protocols. All sections were captured using the high-quality microscope (Leica DM4000B). The histological score was evaluated based on the standard evaluation of 5 categories of degenerative changes [27]. For immunohistochemical evaluation, tissue sections were first dewaxed by graded xylene and standard alcohol gradients. After washing with PBS and water, 10% goat serum was used to block for 30 min at RT. Subsequently, the sections were incubated with the primary antibodies (anti–MMP9 and anti–MMP13 purchased from Servicebio, Wuhan, China) overnight at 4°C. The next day, the appropriate horseradish peroxidase labeled secondary antibody was incubated with the sections for 1 hour at RT and then developed with diaminobenzidine solution. Finally, all sections were captured under a high-quality microscope (Leica DM4000B).

2.10. Immunofluorescent Staining Analyses. Slices were processed of graded xylene deparaffinization, graded alcohol solution hydration, antigen retrieval, permeabilization, and blocking before immunofluorescent staining. Then, primary antibody incubation (anti-interleukin- (IL-) 1β and anti-collagen 2; dilution 1 : 100) (Cell Signaling Technology, Danvers, MA, United States; Abcam, Cambridge, United Kingdom), secondary antibody incubation, and nuclear staining were performed on these slides. The high-quality Leica DM4000 B epifluorescence microscope (Leica Microsystems GmbH) was used to observe and photograph the digital fluorescence images, and the ImageJ software was used to measure the IOD value.

2.11. Image Analysis and Disc Height Index Measurement. Cabinet X-ray imaging and irradiation systems (Faxitron Bioptics, LLC, Wheeling, IL, USA) were used to visualize the X-ray imaging of IVDs. Under identical acquisition parameters and imaging conditions, digital images were used to capture at 45 kVp. The disc height index of these IVDs was measured and normalized to sham group [28]. The calculated values were the average of three measurements per disc.

2.12. Animals and Surgical Procedures. The male Sprague–Dawley rats (Shanghai Lab, Animal Research Center Co., Ltd., China) used in this research were carefully housed (12 h day/night cycle, pathogen-free conditions, 26–28°C, and 50–65% humidity). When rats were housed to the age of eight weeks old, pentobarbital sodium (5 mg/100 g body weight) was used to anesthetize them by intraperitoneal injection before surgical procedures. The iodinated polyvinylpyrrolidone was first used for sterilization, and then, a ventral longitudinal skin incision was made over the tail. The revealed coccyx vertebrae (Co) 3–7 intervertebral discs were selected for experiments (the Co3/4 IVDs: sham controls; the Co4/5, Co5/6, and Co6/7 IVDs: a 20-gauge sterile needle-oriented perpendicular puncture to the skin at the center of the disc and rotating once to make sure insertion level through the AF, into the NP). Surgical exposure was repeated after one week recover under the sutured incision state, and Co4/5, Co5/6, and Co6/7 IVDs were separately injected with 50 μL vehicle, low-dose KAN (2.5 μM), and high-dose KAN (5 μM). After incision suture and 4 weeks of recovery, all experiment rats were sacrificed. The tails were extracted and cleaned of soft tissues and then fixed in 4% PFA.

All animal experiments were authorized by the Institutional Animal Care and Ethics Committee of the Shanghai Ninth People's Hospital, Shanghai Jiaotong University School of Medicine. All animals were operated in accordance with the Guidelines for Animal Treatment of Shanghai Jiaotong University and the principles and procedures of the National Institutes of Health (NIH) Guide for the Care and Use of Laboratory Animals.

2.13. Statistical Analysis. All data were expressed in the form of mean ± standard deviation. The comparison between the experimental group and the control group was conducted

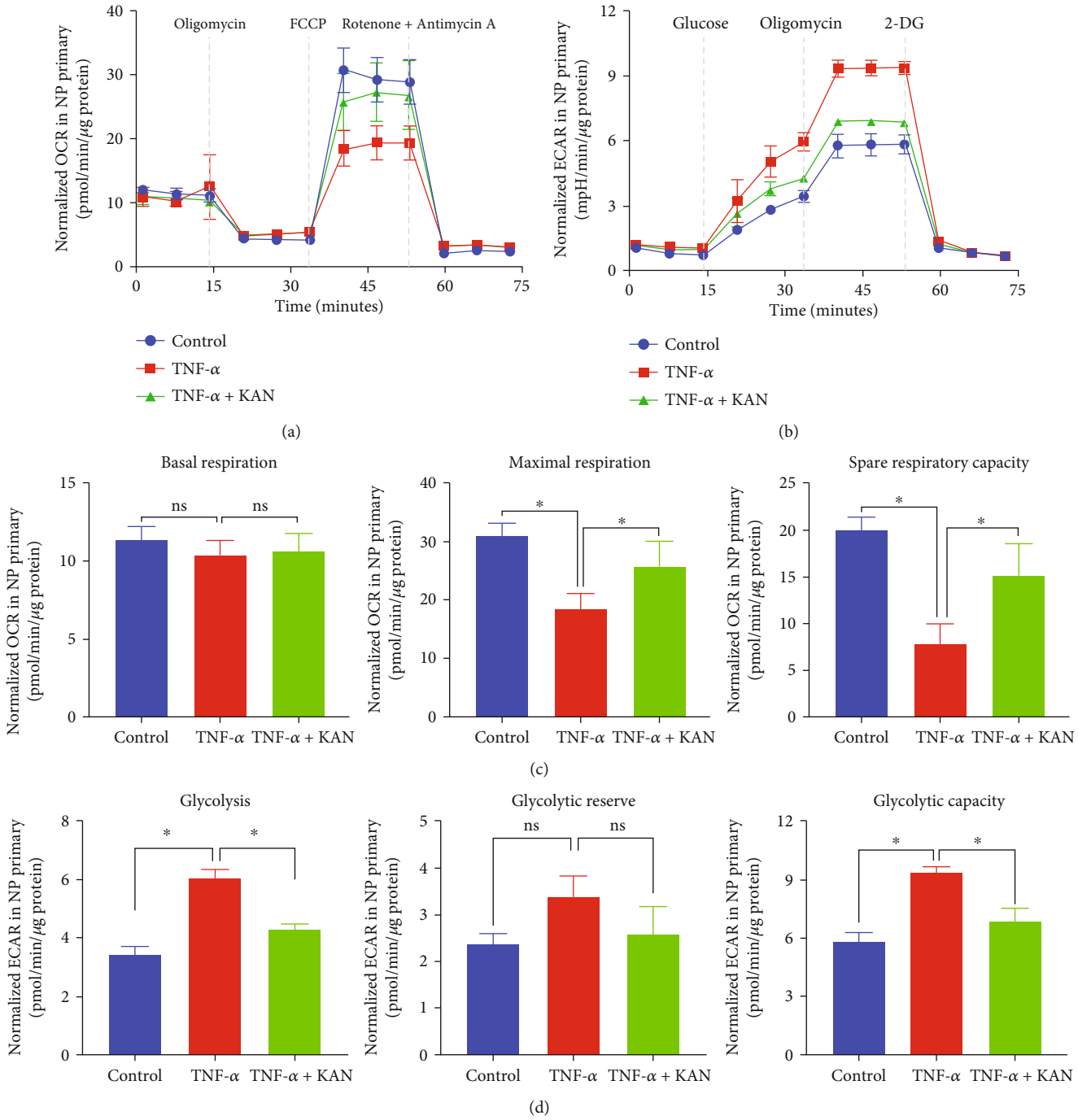

Figure 4: Continued.

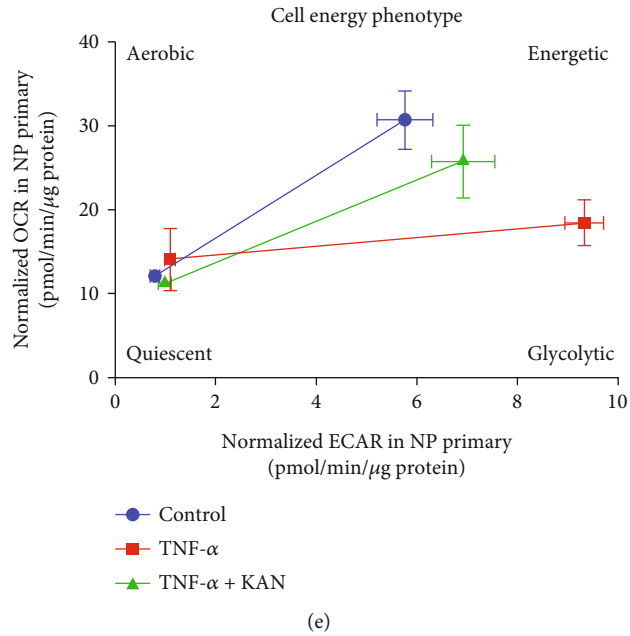

(e)

Figure 4: Metabolic reprogramming effects of KAN0438757 (KAN) on tumor necrosis factor-α- (TNF-α-) induced metabolism phenotype of nucleus pulposus primary (NPP) cells *in vitro*. (a) Normalized OCR of NPPs after negative control, TNF-α, and TNF-α with 2.5 μM KAN treatment for 24 hours. (b) Normalized ECAR of NPPs after negative control, TNF-α, and TNF-α with 2.5 μM KAN treatment for 24 hours. (c) Effects of KAN on basal respiration, maximal respiration, and spare respiratory capacity in OCR assay. (d) Effects of KAN on glycolysis, glycolytic capacity, and glycolytic reserve in ECAR assay. (e) Modified KAN reprogrammed the energy metabolism phenotype of TNF-α-inducted NPPs. Data are expressed as mean ± SD, $n = 3$. ns: no significance; $^{*}p < 0.05$; $^{**}p < 0.01$; $^{***}p < 0.001$; $^{****}p < 0.0001$.

by the 2-tailed, unpaired Student's *t*-test, or one-way ANOVA with Tukey's post hoc test. Moreover, significant differences in ordinal data between study groups were assessed by the Friedman test with Dunn's post hoc test. Statistical significance was calculated to be at no significant (ns); $^{*}p < 0.05$; $^{**}p < 0.01$; $^{***}p < 0.001$; $^{****}p < 0.0001$. All results were calculated and analyzed by Prism 8 (GraphPad Software Inc., San Diego, CA, USA).

3. Results

3.1. Effects of KAN on NPP Cytotoxicity and Proliferation. The KAN's chemical structure is presented in Figure 1(a). To investigate the proliferation and cytotoxicity effects of KAN on NPPs, the CCK-8 assay was performed under different cell numbers. 8,000/well NPPs were first seeded in 96-well plates and cultured for 24 h with various concentrations of KAN (control (0), 0.15625, 0.3125, 0.625, 1.25, 2.5, or 5 μM) for cytotoxicity analysis, and no cytotoxicity was found in KAN under the concentration of 5 μM (Figure 1(b)). For proliferation effects, NPPs were seeded at a density of 2,000/well in 96-well plates and cultured with various concentrations of KAN (control (0), 0.15625, 0.3125, 0.625, 1.25, 2.5, or 5 μM) for 24, 48, 72, and 96 hours. The number of NPPs with any concentration of KAN has no significant variations compared with the control (0) group at any time point (Figures 1(c)–1(f)). Thus, the KAN has no effect on the proliferation of NPPs under the concentration of 5 μM. According to the above experiments, 2.5 μM of KAN was selected to be used in subsequent experiments.

3.2. KAN Alleviated TNF-α-Induced ECM Degradation of NPPs. The inhibitor effect of KAN was firstly identified by significantly reduced protein expression of PFKFB3 in the treatment (TNF-α plus KAN) group compared with the upregulated expression in the TNF-α group (Figures 2(a) and 2(b)). To further explore KAN's role on ECM degradation, the anabolism and catabolism factors of ECM were detected by RT-qPCR *in vitro*. After that, the MMP3, MMP7, MMP9, and MMP13, which are catabolism-related genes, also partly recovered in mRNA levels after KAN treatment. Meanwhile, the mRNA expression of aggrecan, which is related to anabolism, also partly reversed in the treatment group (Figure 2(c)). Furthermore, the similar change in protein level detected by the WB experiment of MMP9 and MMP13 *in vitro* (Figures 2(d) and 2(e)) and the immunohistochemical staining of MMP9 and MMP13 *in vivo* (Figure 2(f)) further corroborated the results above. More intuitively, Alcian blue staining was used to reflect the variation of ECM after TNF-α induction and KAN treatment in NPPs. As shown in Figures 2(g) and 2(h), the indicated concentration KAN treatment reversed the ECM loss in the NPPs high-density culture induced by TNF-α, while no difference between the KAN alone group compared with the control group. In general, these results demonstrated that KAN alleviates TNF-α-induced ECM degradation of NPPs.

3.3. Effects of KAN on TNF-α-Induced NF-κB and MAPK Signaling Pathway and Glycolysis Energy Metabolism Phenotype in NPPs. As previously reported, PFKFB3 inhibitor PFK15 could memorably repress inflammation (NF-κB

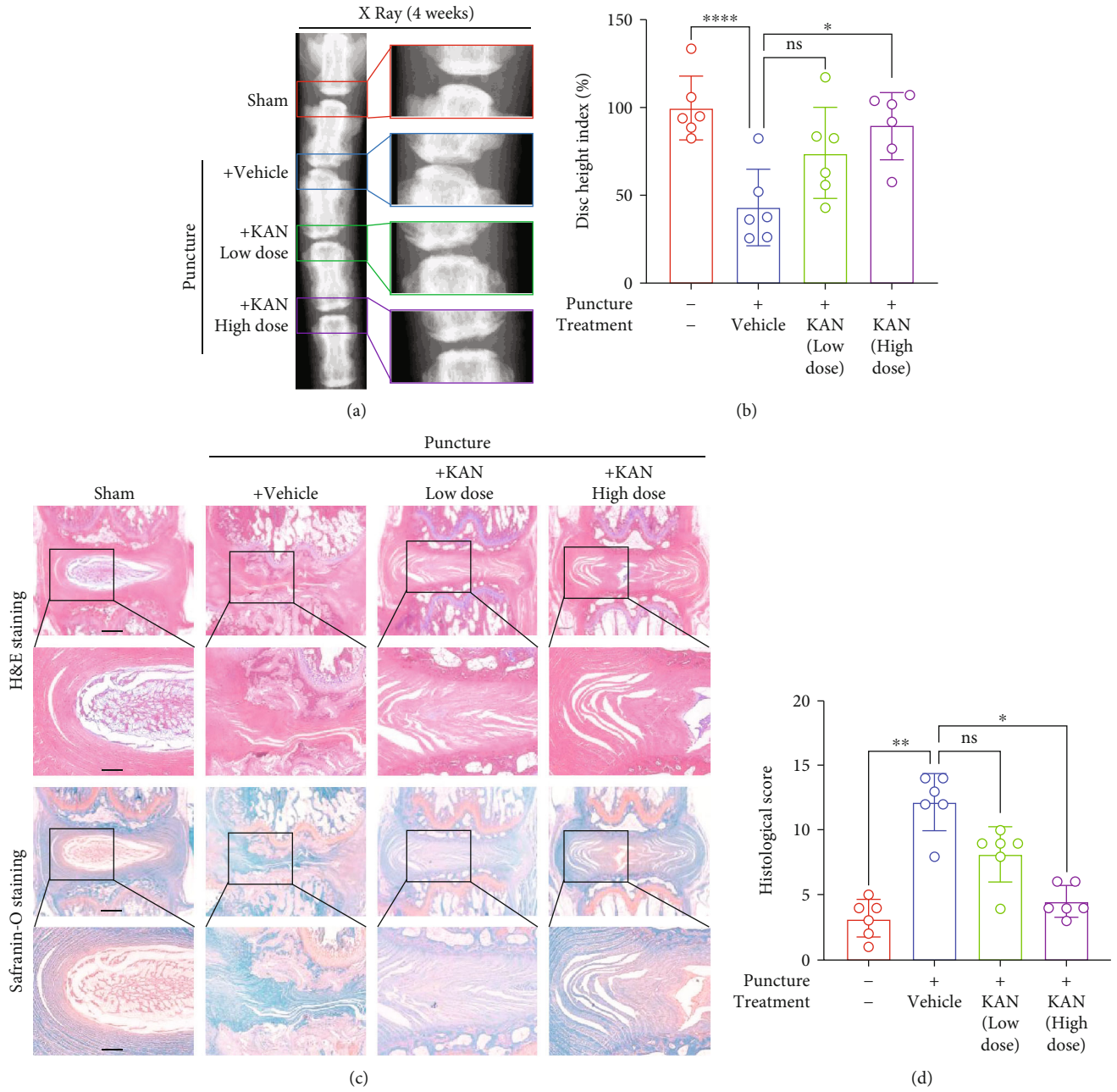

Figure 5: Continued.

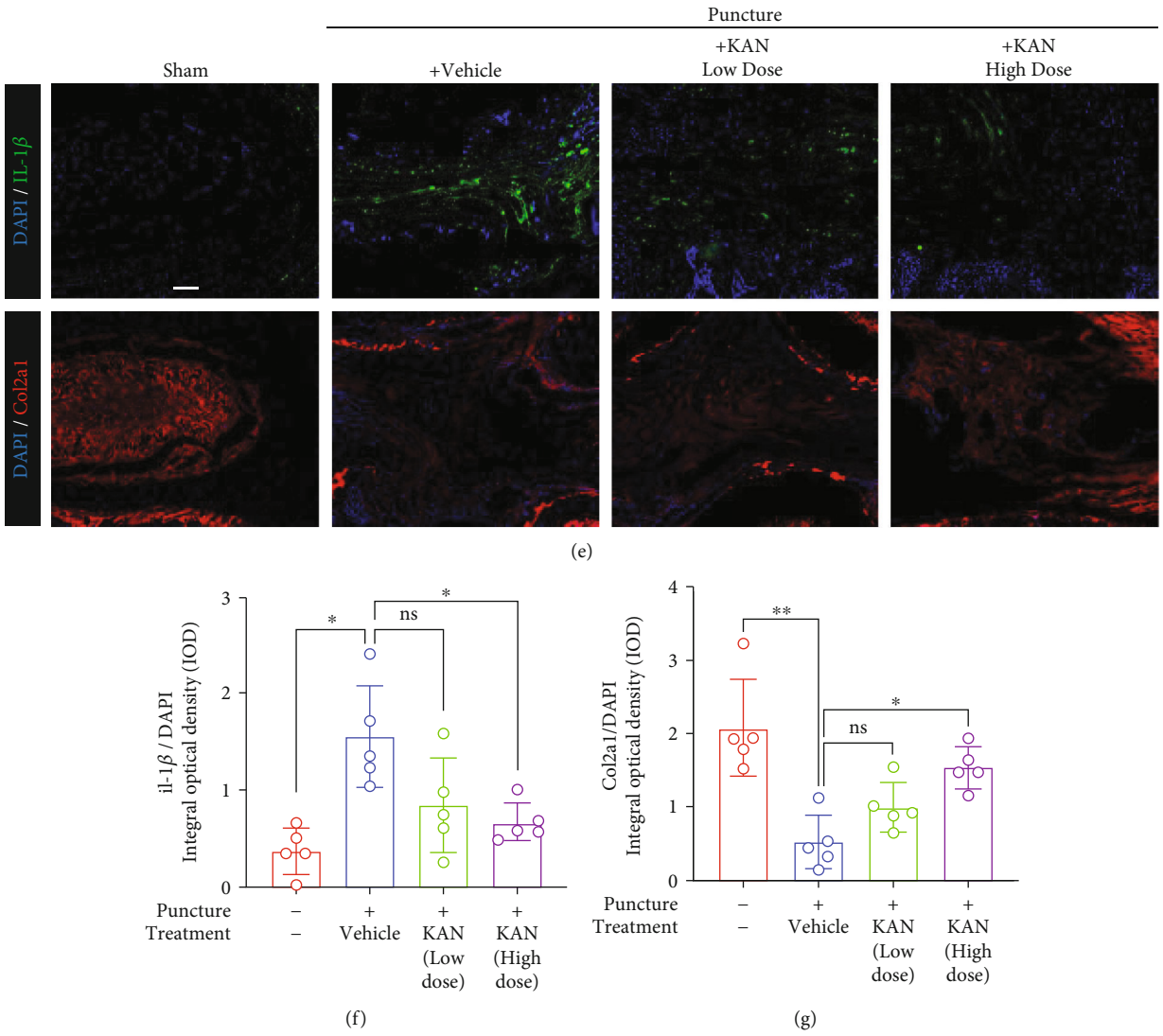

Figure 5: KAN0438757 (KAN) ameliorated the progression of intervertebral disc degeneration (IVDD) in a rat tail disc puncture model *in vivo*. (a) The rat coccyx vertebrae X-ray images at 4 weeks after treatment from each group. (b) Quantitative analysis of disc height index (DHI, %) of IVDs in mice at 4 weeks after treatment in each group. $n = 6$. (c) Hematoxylin and eosin staining and safranin O-fast green staining of intervertebral discs (IVDs) from each group at 4 weeks after treatment. Scale bar = 500 μm and 200 μm. (d) Quantitative analysis of histological scores of IVDs in mice at 4 weeks after treatment in each group. $n = 6$. (e) Interleukin- (IL-) 1β and Col2a1 immunofluorescence staining of IVDs from each group at 4 weeks after treatment. Scale bar = 100 μm. (f, g) Quantitative analysis of IOD (IL-1β and Col2a1) of IVDs in mice at 4 weeks after treatment in each group. $n = 5$. Data are expressed as mean ± SD. ns: no significance; $^{*}p < 0.05$; $^{**}p < 0.01$; $^{***}p < 0.001$; $^{****}p < 0.0001$.

and MAPK signaling pathways) and block the glycolysis of osteoclasts simultaneously [23]. To investigate whether the underlying mechanisms of the KAN's effects on anabolism and catabolism on NPPs were similar to PFK15, NPPs were firstly pretreated with KAN for 2 hours and then treated with another 10 or 30 min of TNF-α stimulation. After that, we observed the classical NF-κB signaling pathway transduction factor change, including the inhibitor of nuclear factor kappa B kinase (IKK), an inhibitor of nuclear factor kappa B (IκB), and NF-κB (p65). As we expected, the IKK, IκB, and p65 phosphorylation were promoted with TNF-α induction while reversed after KAN treatment (Figures 3(a) and 3(c)). Moreover, immunofluorescence staining further showed that subsequent p-p65 nucleus translocation was also reversed after KAN treatment (Figure 3(e)). Meanwhile, another important signaling pathway mentioned, the MAPK signaling pathway, was also explored. Our western blot experiments demonstrated that the recovery effect of KAN was similarly observed in the phosphorylation of MAPK signaling pathway proteins, including JNK, p38, and extracellular signal-regulated kinases (ERKs) (Figures 3(b) and 3(d)). In a word, these results indicated that KAN could significantly reverse the TNF-α-induced NF-κB and MAPK pathway activation in NPPs.

Furthermore, the potential ability of KAN on NPP energy metabolism reprogramming was a novel direction that we totally interested in. Thus, the Seahorse extracellular flux analysis was performed to detect the OCR and ECAR of

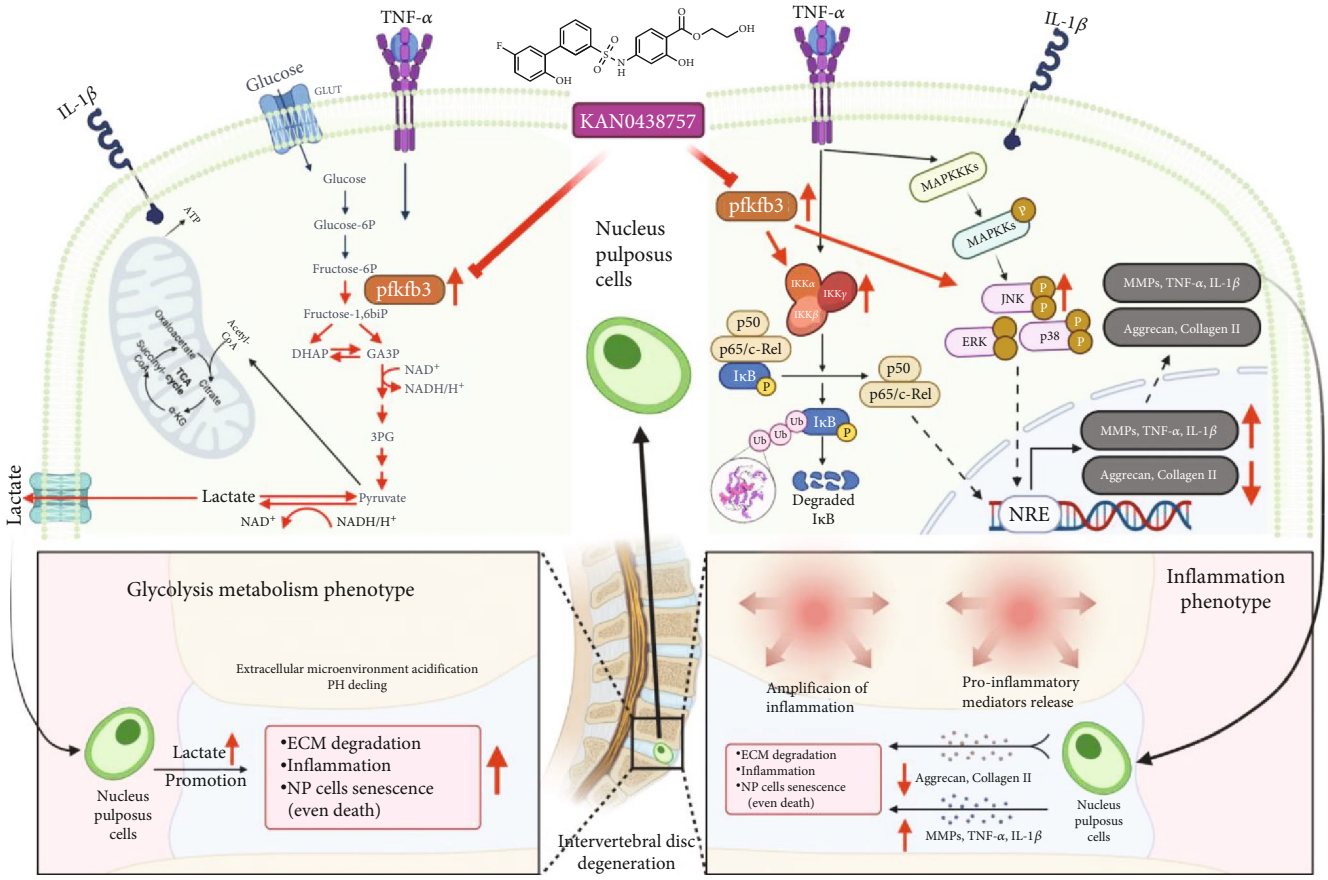

Figure 6: Schematic representation of the molecular mechanism of the article (created with http://BioRender.com).

NPPs according to the instructions (Supplementary Figure 1). For the OCR assay, oligomycin, a mitochondrial ATP synthase inhibitor, was first used to block part of mitochondrial basal respiration and calculate ATP production. Next, the maximal and spare respiratory capacity was measured by FCCP via uncoupling mitochondrial respiration. Finally, the total mitochondria respiration was inhibited by rotenone and antimycin A and mitochondrial complexes I and III blocker, to display the nonmitochondrial oxygen consumption. For the ECAR analysis, enhanced ECAR value after glucose injection under the glucose-deficient environment indicated the glycolysis rate, while the further increase of ECAR value after injection of oligomycin represented the glycolytic reserve and the peak ECAR value meant glycolytic capacity. Similarly, the inhibitor of hexokinase, 2-deoxy-D-glucose (2-DG), totally blocked the glycolysis. Therefore, our results showed that TNF-α induction decreases the OCR of NPPs compared to normal conditions. However, the KAN treatment substantially rescued the OCR impairment caused by TNF-α induction. Specifically, KAN treatment reprogrammed the TNF-α-induced glycolysis energy metabolism phenotype of NPPs by promoting spare respiratory capacity and maximal respiration (Figures 4(a) and 4(c)). More obvious in the ECAR assay, TNF-α induction showed enhanced glycolysis rates and glycolytic capacity than normal conditions, which were also prominently suppressed by KAN treatment (Figures 4(b) and 4(d)). On the whole, all these data indicated that KAN treatment exactly reprogramed the TNF-α-induced glycolysis metabolic phenotype on NPPs (Figure 4(e)).

3.4. KAN Ameliorated IVDD Progression in the Puncture Injury Rat Model In Vivo. To explore the therapeutic potential of KAN on IVDD *in vivo*, we established IVDD model (Co 4–5, Co 5–6, and Co6–7) induced by puncture of rat tail intervertebral disc, and Co 3-4 was used as the sham operation group. Different concentrations of KAN were separately administered one week after injury to Co 5-6 and Co 6-7, and vehicle was injected to Co 4-5. As shown by 4 weeks' X-ray detection after treatment, the osteophyte of the vehicle group was obviously observed more than other groups. Moreover, vehicle group's disc height index (DHI score) was significantly lower than the sham group, while the KAN treatment memorably reversed the IVD height in a dose-dependent manner (Figures 5(a) and 5(b)). Therefore, KAN could reduce puncture-induced degeneration from the perspective of rat tail disc imaging detection. Similarly, the alleviated destruction of the IVD structure in the KAN treatment groups was also demonstrated by H&E staining and safranin O-fast green staining and the histological score (Figures 5(c) and 5(d)). Further immunofluorescence staining for IL-1β and Col2a1 was carried out to detect KAN's effect on inflammation and degradation of ECM *in vivo* (Figures 5(e)–5(g)). Coincidentally, the

results corroborated that KAN substantially reverses the upregulation of IL-1β and the downregulation of Col2a1 in the tail disc tissue of rats. To sum up, these results demonstrated that KAN intervention is a promising potential therapeutic strategy for IVDD.

4. Discussion

IVD degeneration (IVDD) is one of the most common reasons for lumbar disc herniation, spinal stenosis, and subsequent lower back pain [29], which has imposed a huge socioeconomic burden. Nowadays, aging, abnormal biomechanical loading, acute trauma, decreased nutrient transport across the CEPs, smoking, genetic predisposition, and hyperglycemia have been corroborated as participating in the occurrence and development of IVDD [30]. Although NP cell senescence, subsequent ECM degradation, and triggered inflammation are considered to be the three main molecular mechanisms and therapeutic directions of IVDD [31], additional molecular mechanisms and underlying therapeutic targets of these causes are still unclear and need to be explored. In the last decade, acid environment change of IVD caused by aggravated glycolytic metabolism phenotype during IVDD, similar to hypoxia environment change, has been proved to participate and accelerate the whole processes of IVDD [12–16]. Thus, therapies targeting an enhanced glycolytic caused IVD acidic environment are a new direction worthy to be exploited. KAN, an emerging selective inhibitor of key rate-limiting metabolic kinase PFKFB3, has been used to treat colorectal cancer and elevate the efficacy of interstrand crosslink- (ICL-) inducing cancer therapies due to the function during DNA damage [32, 33]. However, research on the diseases principally influenced by its glycolysis regulation function is still blank. Moreover, considering the inhibition effect of PFK15, another PFKFB3 inhibitor, on glycolysis and inflammation (NF-κB and MAPK pathways) during metabolic bone disease osteoporosis [23], our studies explored the role of KAN on energy metabolism reprogramming and inflammation in the process of IVDD.

Due to the properties of inflammatory cytokines, particularly interleukin 1β (IL-1β) and tumor necrosis factor-α (TNF-α), identified as a major risk factors for decreased NPP activity and extracellular matrix loss (including aggrecans) [34], TNF-α-induced NPP dysfunction and ECM degradation were selected to be studied in our present research. We demonstrated that nontoxic concentration KAN treatment could strongly reverse TNF-α-induced degradation of ECM. Specifically, after TNF-α induction, the upregulated MMP family (MMP3, MMP7, MMP9, and MMP13) mRNA expression related to catabolism [35] and the downregulation of Aggrecan related to anabolism [36] both partly recovered after KAN treatment. Our next western blot and immunohistochemical staining experiments of the MMP9 and MMP13 further authenticated the consistent change in protein level. Furthermore, NPP high-density culture which could observe the ECM variation more intuitively [37] showed that KAN treatment reversed the ECM loss after TNF-α stimulation. In general, we demonstrated the rescue effect of KAN on ECM degradation. The underlying mechanisms were also revealed. Although a lot of signaling pathways, such as NF-κB, phosphatidylinositol-3-kinase (PI3K), MAPK, and Wnt signaling pathways, had been reported to mediate ECM metabolism or cell apoptosis after inflammation stimulation in the NPPs [38–41], we mainly focus on NF-κB and MAPK signaling pathways that were reported on PFK15 research. According to the report about the decisive role of TNF-α-induced NF-κB signaling pathway activation and subsequent p-p65 nuclear translocation in the onset and development of IVDD [42, 43], we performed western blot and immunofluorescence experiments to identify whether the above conclusion exists in our research and the results corroborated the inhibiting effect of KAN on NF-κB signaling pathway activation and p-p65 nuclear translocation. Similarly, the repressing effect of KAN on the MAPK signaling that is important for ECM synthesis and degradation [44] was also demonstrated by the downregulated protein expressions of phosphorylated JNK, ERK, and p38. Taken together, our studies firstly authenticated the inhibiting effect of KAN on TNF-α-induced conventional NF-κB and MAPK signaling pathways to alleviate the ECM degradation.

A more attractive role of KAN is the potential of reprogramming energy metabolism. Acid environment variation caused by NPPs aggravated glycolytic metabolism phenotype during IVDD had been demonstrated to enhance the lactate production and its efflux to ECM, which promoted the activation of NLRP3 inflammasome and the NPP extracellular matrix degeneration [45]. The terminal of persistent environment pH decline was the formation of a consistent vicious cycle that is environment acidification-inflammation initiate and ECM degradation-NPP senescence or death, which accelerates every process of IVDD. Therefore, energy metabolism reprogramming therapies are extremely valuable. In this research, we explored the explicit function of KAN treatment on energy metabolism reprogramming by the Seahorse extracellular flux analysis. The change of OCR and ECAR demonstrated the obvious glycolytic metabolism phenotype in TNF-α-induced NPPs. At the same time, KAN treatment partly reversed the reduction of spare respiratory capacity and maximal respiration and the increase of glycolysis rates and glycolytic capacity. All in all, our studies firstly corroborated KAN's energy metabolism reprogramming effect on TNF-α-induced glycolysis metabolic phenotype on NPPs.

Finally, we identified the therapeutic potential of KAN on the rat tail disc puncture-induced IVDD model *in vivo*. In our X-ray examination, the reduced DHI score of the vehicle group was memorably reversed in the high-dose KAN treatment group. Moreover, our H&E staining and safranin O-fast green staining showed more closer IVD structure of KAN treatment groups to the sham group, compared with the disordered structure of the vehicle group. Furthermore, immunofluorescence staining results manifested the inflammatory factor repression and ECM reservation effect of KAN *in vivo*. To sum up, these results demonstrated that KAN intervention is a promising potential therapeutic strategy for IVDD.

However, as the original research exploring the effect of KAN on NPPs and IVDD, we still have many limitations. Firstly, the intermediator between KAN and inflammation signaling pathways (NF-κB and MAPK) remains to be revealed, and whether and how KAN influences other signaling pathways, such as PI3K, and Wnt signaling pathway is still unclear. Secondly, the ER stress [46], acid-sensing ion channel [45, 47], and transient receptor potential channel (TRPV4) [48, 49] are all influenced by pH and participated in the process of IVDD. Whether KAN regulated one or more of them to exert energy metabolism reprogramming and anti-inflammation effect during IVDD is worthy to be explored. Thirdly, Li et al. reported that nine cell types were identified in human normal nucleus pulposus (NNP) cells and human degenerative nucleus pulposus (DNP) by single-cell transcriptome sequencing [50]. According to the effect of PFKFB3 inhibition on ECs and OCs that had been proved in other research [20, 23], the inhibitory role of KAN on ECs and macrophages in NP could be partly forecasted. However, the research on the KAN effect on T cells, neutrophils, and different nucleus pulposus subsets is still blank and remains to be explored to better demonstrate whether it affects the process of human IVDD and its potential application value in humans. Moreover, the therapeutic effect of KAN on IVDD has only been explored and demonstrated in the rat tail intervertebral disc puncture model, which is not enough to achieve clinical application before the other IVDD models on rats, rabbits, and even monkeys have been authenticated.

5. Conclusion

Anyway, our research successfully demonstrated the potential therapeutic effect of KAN on IVDD and declaimed its mechanisms of both novel energy metabolism reprogramming and conventional anti-inflammation effect, which provided a fresh direction for researchers focusing on the influence of the IVD environment during the development of IVDD (Figures 6). Moreover, these results demonstrated that KAN intervention or PFKFB3 inhibition is a promising potential therapeutic strategy for IVDD in the future.

Data Availability

The datasets used and/or analyzed during the current study are available from the corresponding author on reasonable request.

Ethical Approval

Animal ethics approval was received from the Institutional Animal Ethics Review Board of Shanghai Ninth People's Hospital, Shanghai Jiao Tong University School of Medicine (approval no. SH9H-2019-A718-1).

Conflicts of Interest

The authors have declared that no competing interests exist.

Authors' Contributions

All the studies were guided by Jie Zhao, An Qin, and Hui Ma. Xiankun Cao, Xin Wang, and Kewei Rong drafted the manuscript and performed most of the experiments. Kexin Liu, Xiao Yang, Tangjun Zhou, Pu Zhang, and Jiadong Guo participated in part of the experiments and data analysis. All authors read and approved the final manuscript. Xiankun Cao, Xin Wang, and Kewei Rong contributed equally to this work. Jie Zhao is a lead contact.

Acknowledgments

The work was supported by the National Natural Science Foundation of China (Grant Nos. 82130073, 92068102, 81772373, and 81871790); the National Infrastructures for Translational Medicine (Shanghai) Opening Topic (TMSK-2020-119); the Crossover Fund of Shanghai Ninth People's Hospital, Shanghai Jiao Tong University School of Medicine (JYJC202015); and the Shanghai Frontiers Science Center of Degeneration and Regeneration in Skeletal System.

Supplementary Materials

Supplementary Figure 1: OXPHOS characteristics and glycolysis parameter instructions and calculation methods. (A) OXPHOS characteristic instructions and calculation methods based on OCR assay. (B) Glycolysis parameter instructions and calculation methods based on ECAR assay. *(Supplementary Materials)*

References

[1] S. Yang, F. Zhang, J. Ma, and W. Ding, "Intervertebral disc ageing and degeneration: the antiapoptotic effect of oestrogen," *Ageing Research Reviews*, vol. 57, article 100978, 2020.

[2] S. Chen, M. Chen, X. Wu et al., "Global, regional and national burden of low back pain 1990–2019: A systematic analysis of the Global Burden of Disease study 2019," *Journal of Orthopaedic Translation*, vol. 32, pp. 49–58, 2022.

[3] Y. Zhang, B. Yang, J. Wang et al., "Cell senescence: a nonnegligible cell state under survival stress in pathology of intervertebral disc degeneration," *Oxidative Medicine and Cellular Longevity*, vol. 2020, Article ID 9503562, 12 pages, 2020.

[4] A. J. Freemont, T. E. Peacock, P. Goupille, J. A. Hoyland, J. O'Brien, and M. I. Jayson, "Nerve ingrowth into diseased intervertebral disc in chronic back pain," *Lancet*, vol. 350, no. 9072, pp. 178–181, 1997.

[5] A. N. Khan, H. E. Jacobsen, J. Khan et al., "Inflammatory biomarkers of low back pain and disc degeneration: a review," *Annals of the New York Academy of Sciences*, vol. 1410, no. 1, pp. 68–84, 2017.

[6] Y. Zhao, C. Qiu, W. Wang et al., "Cortistatin protects against intervertebral disc degeneration through targeting mitochondrial ROS-dependent NLRP3 inflammasome activation," *Theranostics*, vol. 10, no. 15, pp. 7015–7033, 2020.

[7] E. J. Novais, V. A. Tran, S. N. Johnston et al., "Long-term treatment with senolytic drugs dasatinib and quercetin ameliorates age-dependent intervertebral disc degeneration in mice," *Nature Communications*, vol. 12, no. 1, p. 5213, 2021.

[8] Z. Xu, J. Zheng, Y. Zhang et al., "Increased expression of integrin alpha 6 in nucleus pulposus cells in response to high oxygen tension protects against intervertebral disc degeneration," *Oxidative Medicine and Cellular Longevity*, vol. 2021, Article ID 8632823, 16 pages, 2021.

[9] Z. Liao, S. Li, S. Lu et al., "Metformin facilitates mesenchymal stem cell-derived extracellular nanovesicles release and optimizes therapeutic efficacy in intervertebral disc degeneration," *Biomaterials*, vol. 274, article 120850, 2021.

[10] M. S. Muttigi, B. J. Kim, H. Kumar et al., "Efficacy of matrilin-3-primed adipose-derived mesenchymal stem cell spheroids in a rabbit model of disc degeneration," *Stem Cell Research & Therapy*, vol. 11, no. 1, p. 363, 2020.

[11] D. Hingert, K. Ekström, J. Aldridge, R. Crescitelli, and H. Brisby, "Extracellular vesicles from human mesenchymal stem cells expedite chondrogenesis in 3D human degenerative disc cell cultures," *Stem Cell Research & Therapy*, vol. 11, no. 1, p. 323, 2020.

[12] H. T. J. Gilbert, N. Hodson, P. Baird, S. M. Richardson, and J. A. Hoyland, "Acidic pH promotes intervertebral disc degeneration: acid-sensing ion channel -3 as a potential therapeutic target," *Scientific Reports*, vol. 6, no. 1, article 37360, 2016.

[13] J. Liu, H. Tao, H. Wang et al., "Biological behavior of human nucleus pulposus mesenchymal stem cells in response to changes in the acidic environment during intervertebral disc degeneration," *Stem Cells and Development*, vol. 26, no. 12, pp. 901–911, 2017.

[14] A. Malandrino, J. Noailly, and D. Lacroix, "The effect of sustained compression on oxygen metabolic transport in the intervertebral disc decreases with degenerative changes," *PLoS Computational Biology*, vol. 7, no. 8, article e1002112, 2011.

[15] T. Grunhagen, G. Wilde, D. M. Soukane, S. A. Shirazi-Adl, and J. P. Urban, "Nutrient supply and intervertebral disc metabolism," *The Journal of Bone and Joint Surgery. American Volume*, vol. 88, Supplement 2, pp. 30–35, 2006.

[16] H. Ohshima and J. P. Urban, "The effect of lactate and pH on proteoglycan and protein synthesis rates in the intervertebral disc," *Spine*, vol. 17, no. 9, pp. 1079–1082, 1992.

[17] H. A. Horner and J. P. Urban, "2001 Volvo award winner in basic science studies: effect of nutrient supply on the viability of cells from the nucleus pulposus of the intervertebral disc," *Spine*, vol. 26, no. 23, pp. 2543–2549, 2001.

[18] M. Postal and S. Appenzeller, "The role of tumor necrosis factor-alpha (TNF-α) in the pathogenesis of systemic lupus erythematosus," *Cytokine*, vol. 56, no. 3, pp. 537–543, 2011.

[19] K. De Bock, M. Georgiadou, S. Schoors et al., "Role of PFKFB3-driven glycolysis in vessel sprouting," *Cell*, vol. 154, no. 3, pp. 651–663, 2013.

[20] S. Schoors, K. De Bock, A. R. Cantelmo et al., "Partial and transient reduction of glycolysis by PFKFB3 blockade reduces pathological angiogenesis," *Cell Metabolism*, vol. 19, no. 1, pp. 37–48, 2014.

[21] E. Doménech, C. Maestre, L. Esteban-Martínez et al., "AMPK and PFKFB3 mediate glycolysis and survival in response to mitophagy during mitotic arrest," *Nature Cell Biology*, vol. 17, no. 10, pp. 1304–1316, 2015.

[22] Y. Cao, X. Zhang, L. Wang et al., "PFKFB3-mediated endothelial glycolysis promotes pulmonary hypertension," *Proceedings of the National Academy of Sciences of the United States of America*, vol. 116, no. 27, pp. 13394–13403, 2019.

[23] J. Wang, H. Guan, H. Liu et al., "Inhibition of PFKFB3 suppresses osteoclastogenesis and prevents ovariectomy-induced bone loss," *Journal of Cellular and Molecular Medicine*, vol. 24, no. 3, pp. 2294–2307, 2020.

[24] N. M. S. Gustafsson, K. Färnegårdh, N. Bonagas et al., "Targeting PFKFB3 radiosensitizes cancer cells and suppresses homologous recombination," *Nature Communications*, vol. 9, no. 1, p. 3872, 2018.

[25] J. Van den Bossche, J. Baardman, and M. P. de Winther, "Metabolic characterization of polarized M1 and M2 bone marrow-derived macrophages using real-time extracellular flux analysis," *Journal of Visualized Experiments*, vol. 105, no. 105, 2015.

[26] X. Cao, W. He, K. Rong et al., "DZNep promotes mouse bone defect healing via enhancing both osteogenesis and osteoclastogenesis," *Stem Cell Research & Therapy*, vol. 12, no. 1, p. 605, 2021.

[27] M. L. Ji, H. Jiang, X. J. Zhang et al., "Preclinical development of a microRNA-based therapy for intervertebral disc degeneration," *Nature Communications*, vol. 9, no. 1, p. 5051, 2018.

[28] H. Inoue, S. R. Montgomery, B. Aghdasi et al., "The effect of bone morphogenetic protein-2 injection at different time points on intervertebral disk degeneration in a rat tail model," *Journal of Spinal Disorders & Techniques*, vol. 28, no. 1, pp. E35–E44, 2015.

[29] T. Driscoll, G. Jacklyn, J. Orchard et al., "The global burden of occupationally related low back pain: estimates from the Global Burden of Disease 2010 study," *Annals of the Rheumatic Diseases*, vol. 73, no. 6, pp. 975–981, 2014.

[30] K. Alpantaki, A. Kampouroglou, C. Koutserimpas, G. Effraimidis, and A. Hadjipavlou, "Diabetes mellitus as a risk factor for intervertebral disc degeneration: a critical review," *European Spine Journal*, vol. 28, no. 9, pp. 2129–2144, 2019.

[31] C. Feng, H. Liu, M. Yang, Y. Zhang, B. Huang, and Y. Zhou, "Disc cell senescence in intervertebral disc degeneration: causes and molecular pathways," *Cell Cycle*, vol. 15, no. 13, pp. 1674–1684, 2016.

[32] T. De Oliveira, T. Goldhardt, M. Edelmann et al., "Effects of the novel PFKFB3 inhibitor KAN0438757 on colorectal cancer cells and its systemic toxicity evaluation in vivo," *Cancers (Basel)*, vol. 13, no. 5, p. 1011, 2021.

[33] A. H. Ninou, J. Lehto, D. Chioureas et al., "PFKFB3 inhibition sensitizes DNA crosslinking chemotherapies by suppressing Fanconi anemia repair," *Cancers (Basel)*, vol. 13, no. 14, p. 3604, 2021.

[34] G. Lang, Y. Liu, J. Geries et al., "An intervertebral disc whole organ culture system to investigate proinflammatory and degenerative disc disease condition," *Journal of Tissue Engineering and Regenerative Medicine*, vol. 12, no. 4, pp. e2051–e2061, 2018.

[35] S. Roberts, B. Caterson, J. Menage, E. H. Evans, D. C. Jaffray, and S. M. Eisenstein, "Matrix metalloproteinases and aggrecanase," *Spine*, vol. 25, no. 23, pp. 3005–3013, 2000.

[36] H. Feng, M. Danfelter, B. Strömqvist, and D. Heinegård, "Extracellular matrix in disc degeneration," *The Journal of Bone and Joint Surgery. American Volume*, vol. 88, Supplement 2, pp. 25–29, 2006.

[37] Z. Chen, X. Yang, Y. Zhou et al., "Dehydrocostus lactone attenuates the senescence of nucleus pulposus cells and ameliorates intervertebral disc degeneration via inhibition of STING-TBK1/NF-κB and MAPK signaling," *Frontiers in Pharmacology*, vol. 12, article 641098, 2021.

[38] S. Hu, Z. Shao, C. Zhang et al., "Chemerin facilitates intervertebral disc degeneration via TLR4 and CMKLR1 and activation of NF-kB signaling pathway," *Aging (Albany NY)*, vol. 12, no. 12, pp. 11732–11753, 2020.

[39] K. Sun, J. Zhu, C. Yan et al., "CGRP regulates nucleus pulposus cell apoptosis and inflammation via the MAPK/NF-κB signaling pathways during intervertebral disc degeneration," *Oxidative Medicine and Cellular Longevity*, vol. 2021, Article ID 2958584, 19 pages, 2021.

[40] Z. Li, K. Zhang, X. Li et al., "Wnt5a suppresses inflammation-driven intervertebral disc degeneration via a TNF-α/NF-κB-Wnt5a negative-feedback loop," *Osteoarthritis and Cartilage*, vol. 26, no. 7, pp. 966–977, 2018.

[41] D. Wang, Y. Chen, S. Cao et al., "Cyclic mechanical stretch ameliorates the degeneration of nucleus pulposus cells through promoting the ITGA2/PI3K/AKT signaling pathway," *Oxidative Medicine and Cellular Longevity*, vol. 2021, Article ID 6699326, 11 pages, 2021.

[42] Y. Sun, P. Leng, M. Song et al., "Piezo1 activates the NLRP3 inflammasome in nucleus pulposus cell-mediated by Ca2 +/NF-κB pathway," *International Immunopharmacology*, vol. 85, article 106681, 2020.

[43] F. Ye, Y. Xu, F. Lin, and Z. Zheng, "TNF-α suppresses SHOX2 expression via NF-κB signaling pathway and promotes intervertebral disc degeneration and related pain in a rat model," *Journal of Orthopaedic Research*, vol. 39, no. 8, pp. 1745–1754, 2021.

[44] J. Ge, Q. Yan, Y. Wang et al., "IL-10 delays the degeneration of intervertebral discs by suppressing the p38 MAPK signaling pathway," *Free Radical Biology & Medicine*, vol. 147, pp. 262–270, 2020.

[45] K. Zhao, R. An, Q. Xiang et al., "Acid-sensing ion channels regulate nucleus pulposus cell inflammation and pyroptosis via the NLRP3 inflammasome in intervertebral disc degeneration," *Cell Proliferation*, vol. 54, no. 1, article e12941, 2021.

[46] Z. Y. Xie, L. Chen, F. Wang et al., "Endoplasmic reticulum stress is involved in nucleus pulposus degeneration and attenuates low pH-induced apoptosis of rat nucleus pulposus cells," *DNA and Cell Biology*, vol. 36, no. 8, pp. 627–637, 2017.

[47] J. Ding, R. Zhang, H. Li et al., "ASIC1 and ASIC3 mediate cellular senescence of human nucleus pulposus mesenchymal stem cells during intervertebral disc degeneration," *Aging (Albany NY)*, vol. 13, no. 7, pp. 10703–10723, 2021.

[48] L. B. Jiang, L. Cao, X. F. Yin et al., "Activation of autophagy via Ca^{2+}-dependent AMPK/mTOR pathway in rat notochordal cells is a cellular adaptation under hyperosmotic stress," *Cell Cycle*, vol. 14, no. 6, pp. 867–879, 2015.

[49] J. Z. Bai and J. Lipski, "Differential expression of TRPM2 and TRPV4 channels and their potential role in oxidative stress-induced cell death in organotypic hippocampal culture," *Neurotoxicology*, vol. 31, no. 2, pp. 204–214, 2010.

[50] Z. Li, D. Ye, L. Dai et al., "Single-cell RNA sequencing reveals the difference in human normal and degenerative nucleus pulposus tissue profiles and cellular interactions," *Frontiers in Cell and Development Biology*, vol. 10, article 910626, 2022.

Hindawi
Oxidative Medicine and Cellular Longevity
Volume 2022, Article ID 9684062, 14 pages
https://doi.org/10.1155/2022/9684062

Research Article

Irisin Ameliorates Intervertebral Disc Degeneration by Activating LATS/YAP/CTGF Signaling

Taiqiu Chen,[1] **Youxi Lin**,[1] **Zizhao Wu**,[2] **Huihong Shi**,[1] **Wenjun Hu**,[1] **Shaoguang Li**,[1] **Yichen Que**,[1] **Jincheng Qiu**,[1] **Pengfei Li**,[1] **Xianjian Qiu**,[1] **Tongzhou Liang**,[3] **Xudong Wang**,[4] **Bo Gao**,[1] **Hang Zhou**,[1] **Zhihuai Deng**,[1] **Yanbo Chen**,[1] **Yuanxin Zhu**,[1] **Yan Peng**,[1] **Anjing Liang**,[1] **Wenjie Gao**,[1] **and Dongsheng Huang**[1]

[1]*Department of Orthopedics, Sun Yat-sen Memorial Hospital of Sun Yat-sen University, Guangzhou, Guangdong, China*
[2]*Department of Orthopedics, The Third Affiliated Hospital of Sun Yat-sen University, Guangzhou, Guangdong, China*
[3]*Musculoskeletal Research Laboratory, Department of Orthopaedics & Traumatology, Faculty of Medicine, The Chinese University of Hong Kong, Hong Kong, China*
[4]*Department of Orthopedics, The First Affiliated Hospital of Sun Yat-sen University, Guangzhou, Guangdong, China*

Correspondence should be addressed to Wenjie Gao; gaowj7@mail.sysu.edu.cn
and Dongsheng Huang; hdongsh@mail.sysu.edu.cn

Received 10 June 2022; Accepted 5 July 2022; Published 20 July 2022

Academic Editor: Sidong Yang

Unbalanced metabolism of an extracellular matrix (ECM) in nucleus pulposus cells (NPCs) is widely acknowledged as the primary cause of intervertebral disc degeneration (IDD). Irisin, a novel myokine, is cleaved from fibronectin type III domain-containing 5 (FNDC5) and has recently been proven to regulate the metabolism of ECM. However, little is known about its potential on NPCs and the development of IDD. Therefore, this study sought to examine the protective effects and molecular mechanism of irisin on IDD *in vivo* and *in vitro*. Decreased expression levels of FNDC5 and anabolism markers (COL2A1 and ACAN) but increased levels of catabolism markers (ADAMTS4) were found in degenerative nucleus pulposus (NP) tissues. In a punctured-induced rat IDD model, irisin treatment was found to significantly slow the development of IDD, and in TNF-α-stimulated NPCs, irisin treatment partly reversed the disorder of ECM metabolism. In mechanism, RNA-seq results suggested that irisin treatment affected the Hippo signaling pathway. Further studies revealed that with irisin treatment, the phosphorylation levels of key factors (LATS and YAP) were downregulated, while the expression level of CTGF was upregulated. Moreover, CTGF knockdown partially eliminated the protective effects of irisin on the metabolism of ECM in NPCs, including inhibiting the anabolism and promoting the catabolism. Taken together, this study demonstrated that the expression levels of *FNDC5* were decreased in degenerative NP tissues, while irisin treatment promoted the anabolism, inhibited the catabolism of the ECM in NPCs, and delayed the progression of IDD via LATS/YAP/CTGF signaling. These results shed light on the protective actions of irisin on NPCs, leading to the development of a novel therapeutic target for treating IDD.

1. Introduction

Intervertebral disc degeneration (IDD), regarded as an integral part of the aging process [1, 2], is characterized by unbalanced metabolism of extracellular matrix (ECM), tissue dehydration, cracks in the annulus fibrosus, and destruction of endplate cartilage [3–5]. Although the pathogenesis of IDD is complex and diverse, impaired ECM metabolism is widely considered to be the core pathological change, including downregulated levels of anabolism markers and upregulated levels of catabolism markers [6, 7]. As degeneration proceeds, more inflammatory mediators are secreted by nucleus pulposus cells (NPCs), causing the secretion of matrix-degrading enzymes and aggravating the unbalanced

metabolism of ECM, including the upregulation of anabolism markers and downregulation of catabolism markers, which finally accelerate the progression of IDD [8–10].

TNF-α is one of the IDD-related inflammatory cytokines, which induces the expression levels of matrix-degrading enzymes and other inflammatory factors in NPCs and thus exacerbates the inflammatory response and accelerates the progression of IDD [11–13]. In addition, as reported, intradiscal injection with the TNF-α reagent was considered to be a practicable way to construct a disc degeneration animal model [14]. Moreover, it had been reported that TNF-α was involved in the nerve irritation and ingrowth, inducing disc degeneration and increasing the painful behavior in an animal model [15, 16]. Collectively, searching the effective way to alleviate the inflammatory response and unbalanced ECM metabolism induced by TNF-α in NPCs appears vital in the treatment of IDD.

Irisin is a soluble polypeptide fragment with 112 amino acids, formed by the cleavage of type III fibronectin component including protein 5 (FNDC5) [17]. Expanding evidence has revealed that irisin is involved in various pathophysiological processes including musculoskeletal metabolism, lipid and glucose metabolism, neural regulation, inflammation, and degenerative diseases [17–20]. Likewise, accumulating studies have shown that irisin plays an essential role against the progression of skeletal degenerative diseases such as osteoporosis and osteoarthritis [21–24]. Besides, it has been reported that irisin is a powerful regulator of the metabolism of ECM, including upregulating the levels of COL2A1 and ACAN and downregulating the productions of matrix-degrading enzymes in chondrocytes [25, 26]. As yet, however, much remains unknown about irisin's effects on the regulation of ECM metabolism in NPCs in the progression of IDD.

The Hippo signaling pathway has been regarded as a conserved transduction pathway with an essential role in regulating cell cycle and differentiation, maintaining the stability of the internal environment and tissue regeneration [27–29]. Recent studies have shown that Hippo signaling may be involved in the development of IDD. As reported, the key effector, the yes-associated protein (YAP), was downregulated, while the phosphorylated YAP protein was upregulated in degenerative NP tissues [30]. Recently, it has been reported that YAP mediates the unbalanced ECM metabolism in NPCs and is found to be regulative in the progression of IDD [31, 32]. As the target gene of YAP, the connective tissue growth factor (CTGF), also known as CCN2, is a secreted peptide consisting of 349 amino acids, composed of N-terminal signal peptide, intermediate protein-binding domain, and C-terminal-binding domain [33]. CTGF has been demonstrated to be involved in many biological processes such as cell proliferation, differentiation, adhesion, and angiogenesis [33–35]. More importantly, CTGF has reportedly shown protective effects on the metabolism of ECM in NPCs, including upregulating the levels of synthesis markers and inhibiting the levels of matrix-degrading enzymes [36–38]. These studies revealed that the LATS/YAP/CTGF axis played a vital role in the progression of IDD, and as such, further studies are warranted.

Collectively, this study was aimed at exploring whether irisin affects ECM metabolism in NPCs and the development of IDD. Herein, it was reported that irisin reversed the disordered metabolism of ECM and ameliorated the progression of IDD via LATS/YAP/CTGF signaling pathways. These results provided additional evidence for the potential use of irisin as a repair reagent on IDD in the future.

2. Materials and Methods

2.1. Antibodies and Reagents. Antibodies against collagen type II (COL2A1), a disintegrin-like and metalloprotease with thrombospondin type-1 motif 4 (ADAMTS4), tumor necrosis factor-alpha (TNF-α), and a disintegrin-like and metalloprotease with thrombospondin type-1 motif 5 (ADAMTS5) were purchased from Abcam Inc. Antibodies against matrix metalloproteinase 9 (MMP9), matrix metalloproteinase 13 (MMP13), connective tissue growth factor (CTGF), and Hippo signaling relative proteins (LATS1, LATS2, YAP, and phosphor-YAP) and goat anti-rabbit and anti-mouse IgG secondary antibodies were purchased from Cell Signaling Technology Inc. Antibodies against GAPDH and β-tubulin were purchased from Proteintech Group Inc. Antibody against fibronectin type III domain-containing protein 5 (FNDC5) was purchased from Bioss Inc. An irisin reagent was purchased from Novoprotein, and a verteporfin reagent was purchased from MedChemExpress, while a human TNF-alpha reagent was from R&D Systems. The catalog numbers and company brands of reagents used in this study are listed in the Supplementary Table 3.

2.2. Human Nucleus Pulposus Specimens. Tissues used in this study were obtained from Sun Yat-sen Memorial Hospital of Sun Yat-sen University (Guangzhou, China). A total of three normal and six degenerative human NP specimens were obtained in this study. The degenerative nucleus pulposus tissues were collected from patients who underwent discectomy surgery due to disc herniation, while control specimens were obtained from patients who underwent surgery due to trauma without disc degeneration. After being collected, the tissues were fixed, embedded, and sectioned for use in experiments. Any extra tissues were put through a high-throughput tissue grinder for total RNA and protein extraction.

2.3. Puncture-Induced Rat IDD Model. Animal experiments were approved by the Institutional Research Ethical Committee of Sun Yat-sen University (No. SYSU-IACUC-2022-B0403). As previously described [32], briefly, a total of eighteen 12-week-old rats were housed in a vivarium with a 12-hour light/dark cycle. After being anesthetized, the rats were placed on a board, and 21 G needle punctures were performed in two adjacent caudal intervertebral discs at a depth of approximately 5 mm. After 1 minute, the needles were rotated 180 degrees and located for another 1 minute and then pulled out. The rats were divided into three groups: the control group, the punctured group, and the punctured with irisin treatment group. Irisin (100 μg/kg) was injected intraperitoneally once a week in the punctured with irisin treatment group, and PBS (100 μg/kg) solution

was injected intraperitoneally once a week in the control group and the punctured group. After 4 weeks, a micro-MRI was performed and the degeneration of disc was assessed by the Pfirrmann grading system.

2.4. Human Nucleus Pulposus Cell Cultures. Human nucleus pulposus cells were purchased from ScienCell. Cells were incubated in human NP cell medium (ScienCell) with fetal bovine serum and antibiotics. When the confluence reached about 70%-90%, the cells were trypsinized, counted, and passaged. Cells from passages 4 to 7 were cultured in 6-well plates with about 8 ml medium. When they adhered, the medium was changed and the following treatments were performed.

2.5. Real-Time qPCR. Total RNA was extracted from cells or tissues with the Trizol reagent. Using RNA-iso Plus reagent and PrimeScript RT Master Mix (TaKaRa, Dalian, China), the RNA was converted to cDNA, and then, qPCR was performed. Firstly, the mix was heated to denaturation at 95°C for 5 minutes, and then, 40 cycles were performed (95°C for 10 seconds, 60°C for 20 seconds, and 72°C for 20 seconds). Finally, the dissolution curve was measured and the mRNA expression levels of different genes were calculated and analyzed, referring to the level of the *GAPDH* gene. The primers' sequences used in this study are listed in Supplementary Table 1.

2.6. Immunohistochemistry. Human and animal tissues were obtained and fixed with 4% paraformaldehyde for 24 to 48 hours and then decalcified and embedded in paraffin. The tissues were cut into sections about 5 μm thickness. After being treated with 0.1% Triton X-100 solution, the sections were incubated with 3% peroxidase and then washed with PBS. For blocking, the bovine serum albumin was then used at room temperature for half an hour. After being incubated with antibodies (anti-COL2A1, anti-ACAN, anti-ADAMTS4, anti-TNFα, anti-MMP9, and anti-YAP) overnight, the Histostain Plus Kit (ZSGB-Bio, Beijing, China) was used for IHC analysis. Finally, an Olympus BX63 microscope was used for photographing. The dilutions of antibodies used in the study are listed in Supplementary Table 2.

2.7. Western Blot Analysis. Proteins from tissues and adherent cells were extracted using RIPA lysis buffer. Then, samples were added to SDS-PAGE to separate different proteins and transferred to PVDF or NC membranes. Subsequently, 5% nonfat dry milk was used for blocking, and the designated antibodies were added at 4°C overnight. Next day, the membranes were washed with PBS, and the secondary antibodies were added for 1 hour at 37°C. Finally, they were visualized using an ECL kit (Millipore), and the bands were quantified using ImageJ software. The dilutions of antibodies used in the study are listed in Supplementary Table 2.

2.8. Immunofluorescence. For cell immunofluorescence, the glasses were put in 24-well plates, and nucleus pulposus cells were seeded for about 24 h under different treatments. Next, the cells were fixed, blocked, and incubated with antibodies overnight. The next day, secondary antibodies were used for additional incubation for 1 h at 37°C, and then, they were labelled with DAPI. For tissue immunofluorescence, the tissues were decalcified, embedded, and treated with 0.1% Triton X-100 solution and bovine serum albumin. Then, they were incubated with antibodies at 4°C overnight. The next day, the tissues were incubated with secondary antibodies for 1 h, and then, they were labelled with DAPI. Finally, an Olympus BX63 microscope was used for photographing. The dilutions of antibodies used in the study are listed in Supplementary Table 2.

2.9. HE Staining and Safranin-O-Fast Green Staining. After being fixed, decalcified, dehydrated, and embedded, the rat intervertebral disc tissues were treated with hematoxylin for 2 min, followed by eosin for 3 min at 37°C for HE staining. As for Safranin-O-Fast Green staining, the sections were stained with Safranin-O for 15 min and then with Fast Green solution for 2 min. At the indicated time, the sections were dried and sealed with neutral resin. All sections were photographed using an Olympus BX63 microscope.

2.10. Cell Viability Assay. The NPCs were plated in 96-well plates at a density of approximately 1.0×10^4 cells/ml. When the cells adhered, irisin was added at different concentrations (0, 25, 50, 100, 200, and 400 ng/ml) for 24 and 48 hours. At the indicated time, the CCK-8 reagent was added according to the manufacturer's instructions. Finally, absorbance at 450 nm was measured by using the microplate reader.

2.11. Transcriptome Sequencing and Bioinformatics Analysis. Genome-wide transcriptional sequencing was performed on both TNF-α-treated groups and TNF-α with irisin-treated groups to identify the differential expression levels of RNA. Sequencing was performed using Oebiotech (Shanghai Co., Ltd.). Using the DESeq2 R package, differential expression analysis was performed between the two groups, and the expression levels of genes were screened out when the fold change was larger than 2. Next, Gene Ontology (GO) enrichment analysis, including biological processes, cellular components, and molecular function, was performed on the following website (https://david.ncifcrf.gov). Finally, Kyoto Encyclopedia of Genes and Genomes (KEGG) pathways enrichment analysis was performed by Oebiotech (Shanghai Co., Ltd.).

2.12. Cell Transduction. CTGF-shRNA and control plasmid vectors were constructed by GeneChem (Shanghai, China). In brief, when the human NPCs were cultured and reached 70-90% confluence, the *CTGF*-shRNA plasmids were added to the medium with the Lipofectamine 3000 reagent. The concentration of DNA was about 2500 ng per well of the 6-well plate. After 8 hours, the medium was replaced, and regular culture was performed for the following experiments.

2.13. Statistical Analysis. The quantitative data shown in this study are presented as the mean ± standard deviation. Two-tailed Student's *t*-tests were conducted for comparisons between two groups, and the whole statistical analysis was performed using the SPSS 20.0 statistical software package

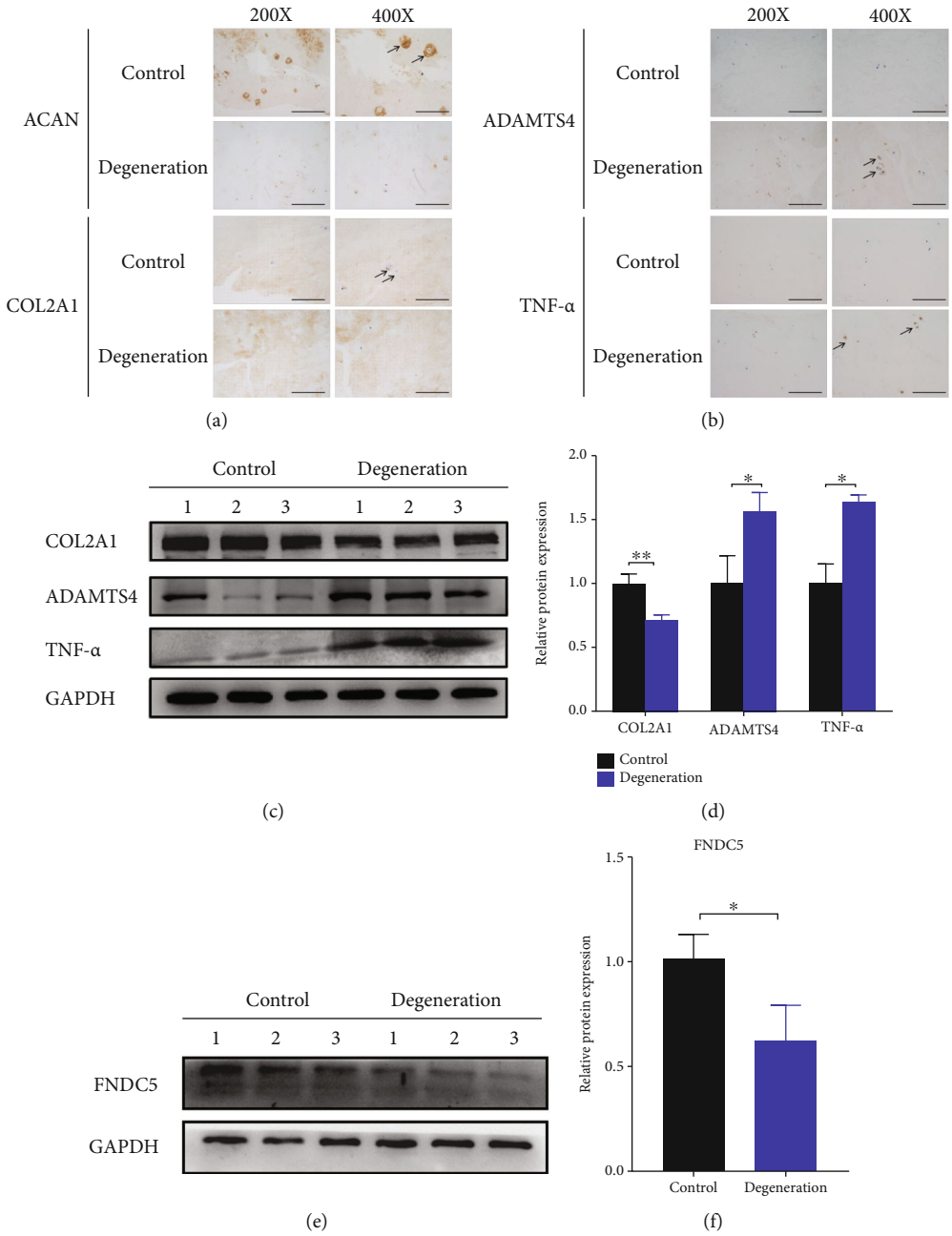

Figure 1: Decreased expression of FNDC5 in degenerative human NP tissue. (a, b) IHC staining assay of ACAN, COL2A1, ADAMTS4, and TNF-α in control and degenerative human nucleus pulposus tissues. (c) The protein expression levels of COL2A1, ADAMTS4, and TNF-α were detected using western blotting in control and degenerative human NP tissues. (d) The quantitative analysis of the protein bands in (c) using ImageJ software. (e) The protein expression levels of FNDC5 were detected by western blot in the control and degenerative groups. (f) The quantitative analysis of the protein bands in (e) using ImageJ software. The scale bar of images in (a) and (b) was shown (magnification: ×200, scale bar: 100 μm; magnification: ×400, scale bar: 50 μm). $^{*}P < 0.05$, $^{**}P < 0.01$.

(SPSS, Inc., Chicago, IL, USA). Results were regarded as statistically significant with a P value of less than 0.05.

3. Results

3.1. Decreased Expression of FNDC5 in Degenerative Human NP Tissue. Firstly, both the dysregulated ECM metabolism and inflammation levels were validated between control and degenerative human NP tissues. As shown in Figures 1(a) and 1(b), compared with the control group, the results from IHC revealed that the expression levels of anabolism markers (COL2A1 and ACAN) were suppressed, while the expression levels of ADAMTS4 and TNF-α was elevated, respectively (Figures 1(a) and 1(b)). Next, total proteins were extracted from tissues. As expected, using western blot, a decreased level of COL2A1 and increased

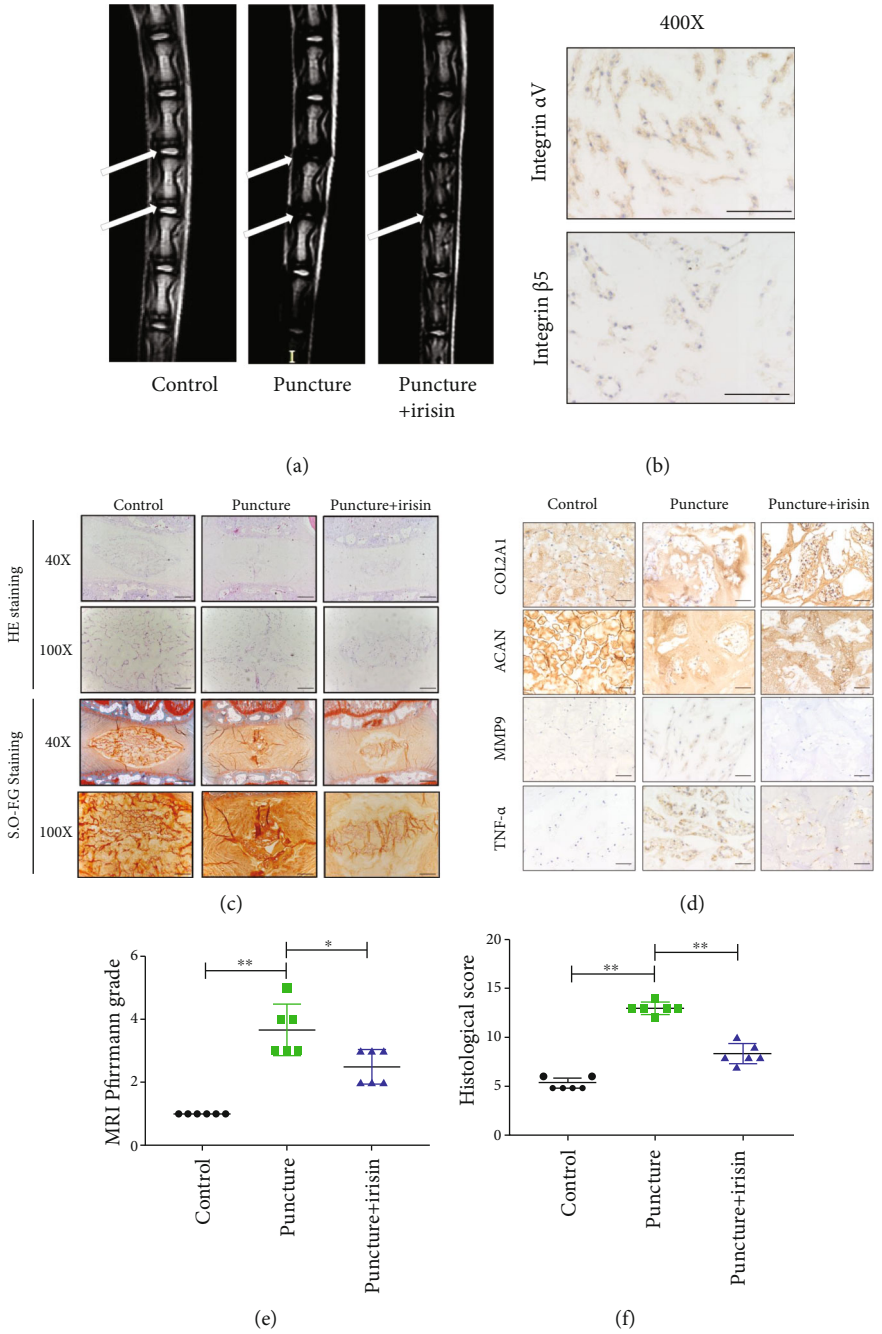

Figure 2: Irisin ameliorates the progression of IDD in a puncture-induced rat model in vivo. (a) The T2 phase images of micro-MRI scan of the caudal intervertebral disc in different groups: the white arrows indicated the control and affected discs. (b) The expression of the integrin $\alpha V\beta 5$ receptor in the intervertebral disc tissues (magnification: ×400, scale bar: 50 μm). (c) HE staining of the affected intervertebral disc in different groups. Images (magnification: ×40, scale bar: 500 μm; magnification: ×100, scale bar: 200 μm). (d) IHC staining assay of COL2A1, ACAN, MMP9, and TNF-α in different groups. (e) The MRI Pfirrmann grade analysis of the intervertebral disc in different groups. (f) The histological score of the intervertebral disc in different groups. Images (magnification: ×400, scale bar: 50 μm). $^{*}P < 0.05$, $^{**}P < 0.01$.

levels of ADAMTS4 and TNF-α were found in degenerative groups (Figures 1(c) and 1(d)). To elucidate the change of FNDC5 in the progression of IDD, the expression level of the FNDC5 protein was also detected. Less expression of FNDC5 was found in degenerative NP tissues (Figures 1(e) and 1(f)). These results indicated that unbalanced ECM metabolism, increased TNF-α, and decreased FNDC5 expression levels existed in degenerated NP tissues.

3.2. Irisin Ameliorates the Progression of IDD in a Puncture-Induced Rat Model In Vivo. To assess the roles of irisin on the progression of IDD, puncture-induced rat models were established. The rats were injected with PBS or irisin reagent at a concentration of 100 μg/kg once a week. After 4 weeks, the rats were anesthetized, underwent micro-MRI examinations, and then were sacrificed. The results from the MRI T2 phase showed that the water content of NP tissues in the

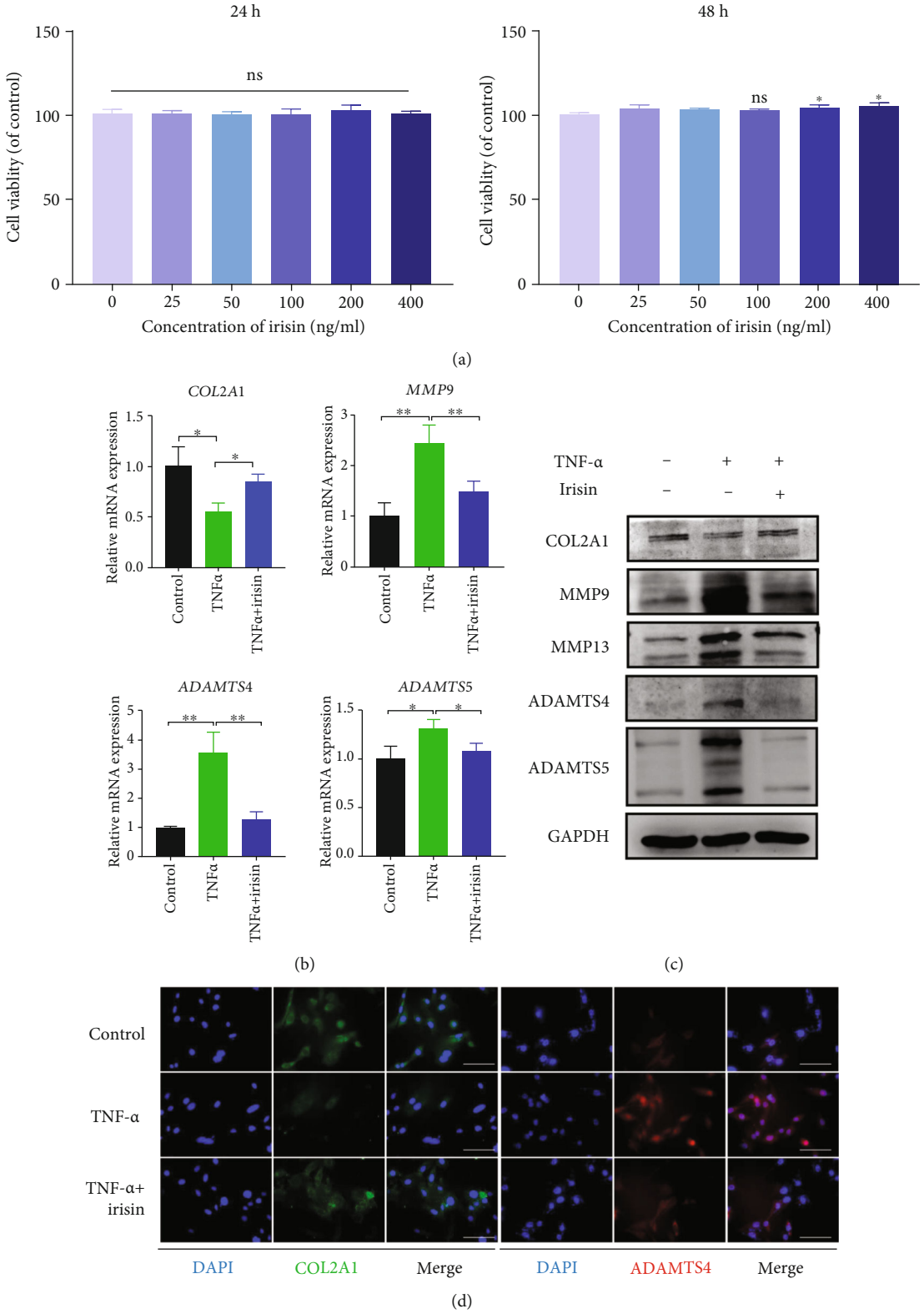

Figure 3: Irisin treatment restored the metabolism of the ECM in TNF-α-induced NPCs. (a) CCK-8 assay was performed to detect the effects of irisin on the cells' viability at various concentrations (0, 25, 50, 100, 200, and 400 ng/ml) at 24 and 48 hours. (b) The relative expression levels of different genes (COL2A1, MMP9, ADAMTS4, and ADAMTS5) were detected using qPCR in different groups. (c) The protein expression levels of COL2A1, MMP9, MMP13, ADAMTS4, and ADAMTS5 were detected by western blot in different groups. (d) The expression levels of COL2A1 and ADAMTS4 were detected by immunofluorescence in different groups. DAPI was used to stain for the nuclei. Images (magnification: ×400, scale bar: 50 μm). In (b)–(d), irisin was used at the concentration of 100 ng/ml and TNF-α was used at the concentration of 10 ng/ml. $^{*}P < 0.05$, $^{**}P < 0.01$.

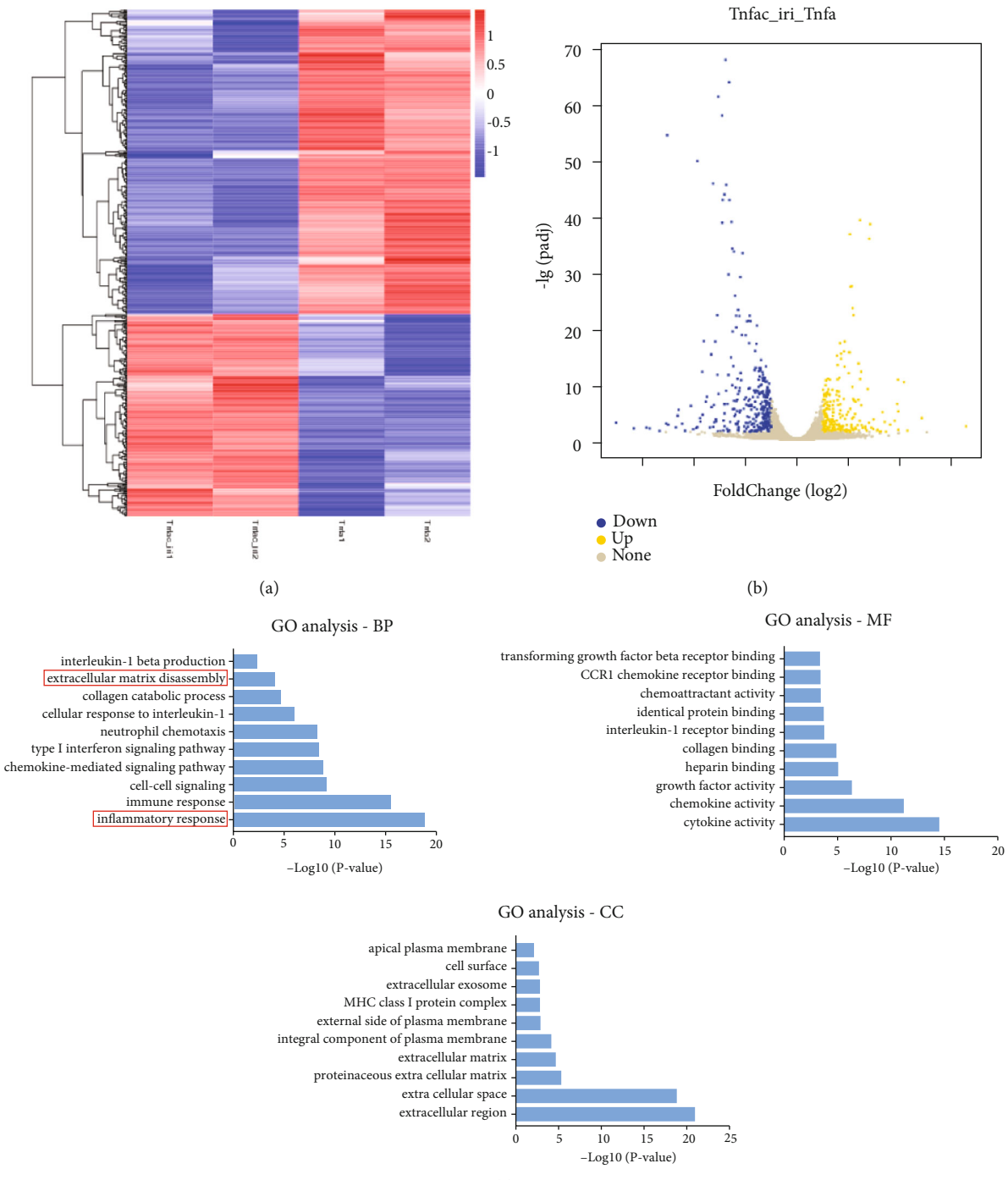

Figure 4: Continued.

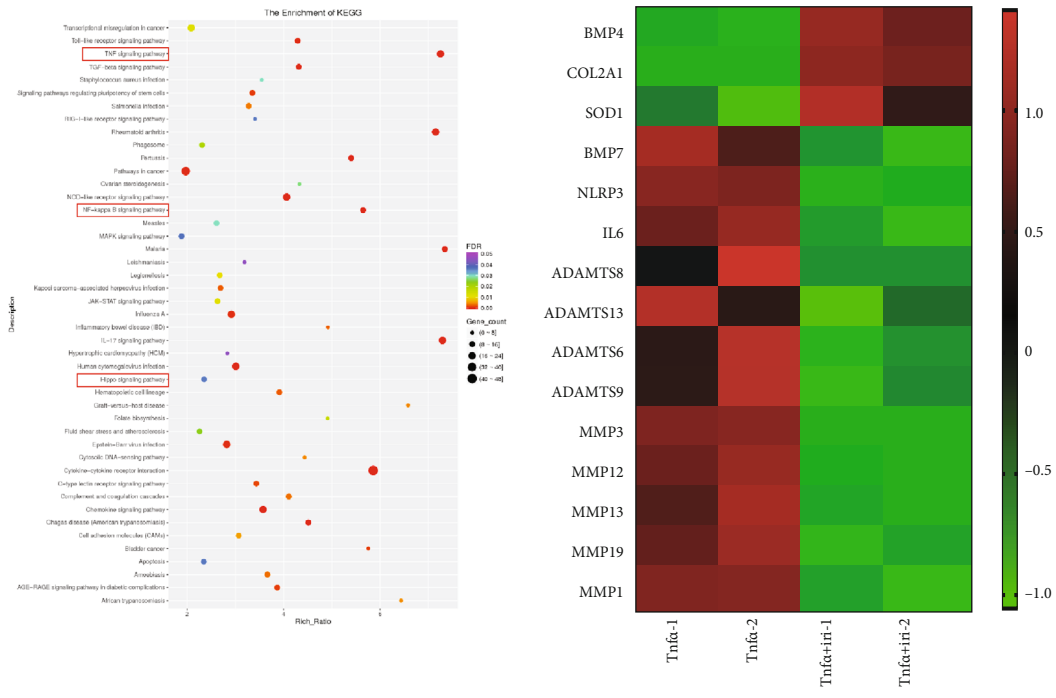

(d) (e)

Figure 4: Irisin treatment affected the activation of the Hippo signaling pathway. (a) The heatmap of differentially expressed genes (DEGs), which were detected by RNA-seq in human nucleus pulposus cells between TNF-α-treated groups and TNF-α plus irisin-treated groups. (b) The volcano map of gene distribution (upregulation, downregulation, and none). (c) GO analysis terms with the most significant P values were determined, including three analyses (BP: biological process, CC: cellular component, and MF: molecular function). (d) KEGG pathway enrichment analysis showed the affected signaling pathways with P value less than 0.05. (e) The heatmap of genes' expression levels, including anabolic marker (*COL2A1*), catabolic markers (*MMPs* and *ADAMTSs*), and inflammation factors (*IL-6* and *NLRP3*). In this figure, irisin was used at the concentration of 100 ng/ml and TNF-α was used at the concentration of 10 ng/ml.

punctured group was significantly decreased compared to that in the controls, whereas irisin treatment reserved this change partly (Figure 2(a)). Firstly, the expressions of irisin receptors integrin αV and integrin β5 were detected in the intervertebral disc tissues (Figure 2(b)). Moreover, histological morphology was assessed by HE staining and Safranin-O-Fast Green staining. The results revealed a disordered disc structure, accompanied by the loss of a matrix and an unclear boundary between the annulus fibrosus and NP tissues in the punctured group. Meanwhile, irisin treatment partially restored the matrix synthesis and maintained the structure of the intervertebral disc (Figure 2(c)). In addition, IHC was performed to evaluate the metabolism of ECM. Compared with the controls, lower expression levels of synthesis markers (COL2A1, ACAN) and higher expression levels of matrix-degrading enzyme (MMP9) and TNF-α were found in the punctured group; those changes were also reversed with irisin treatment (Figure 2(d)). The Pfirrmann grades and the histological score of the punctured group were higher than those of the control group, but irisin treatment decreased the scores, respectively (Figures 2(e) and 2(f)). These results revealed that irisin treatment could ameliorate the unbalanced metabolism of ECM and alleviate the development of IDD *in vivo*.

3.3. Irisin Treatment Restored the Metabolism of the ECM in TNF-α-Induced NPCs. To determine the effects of irisin on NPCs, a CCK-8 assay was first performed, in which irisin treatment was found not to affect cell viability at a concentration below 100 ng/ml at both 24 and 48 hours (Figure 3(a)). Thus, irisin was used for following experiments at a concentration of 100 ng/ml. Subsequently, TNF-α was used to create an inflammatory microenvironment at a concentration of 10 ng/ml, as previous studies had reported [8, 9]. The anabolic gene marker *COL2A1* was found to be downregulated upon TNF-α treatment, while the catabolic gene markers (*MMP9*, *ADAMTS4*, and *ADAMTS5*) were upregulated. These changes were partly reversed with irisin treatment (Figure 3(b)). Similarly, the results from western blot were consistent with the mRNA change (Figure 3(c)). The protein expression level was further investigated by immunofluorescence, and it was found that irisin treatment had an antagonistic effect against TNF-α-induced ECM metabolism disorder (Figure 3(d)). Together, these data suggested that irisin inhibited catabolism and promoted anabolism of ECM in TNF-α-stimulated NPCs.

3.4. Irisin Treatment Affected the Activation of the Hippo Signaling Pathway. To further explore the potential mechanism of irisin treatment on the progression of IDD, RNA-seq was performed on human NPCs from both TNF-α-treated groups and TNF-α plus irisin-treated groups. As shown in Figure 4(a), a total of 531 genes were identified

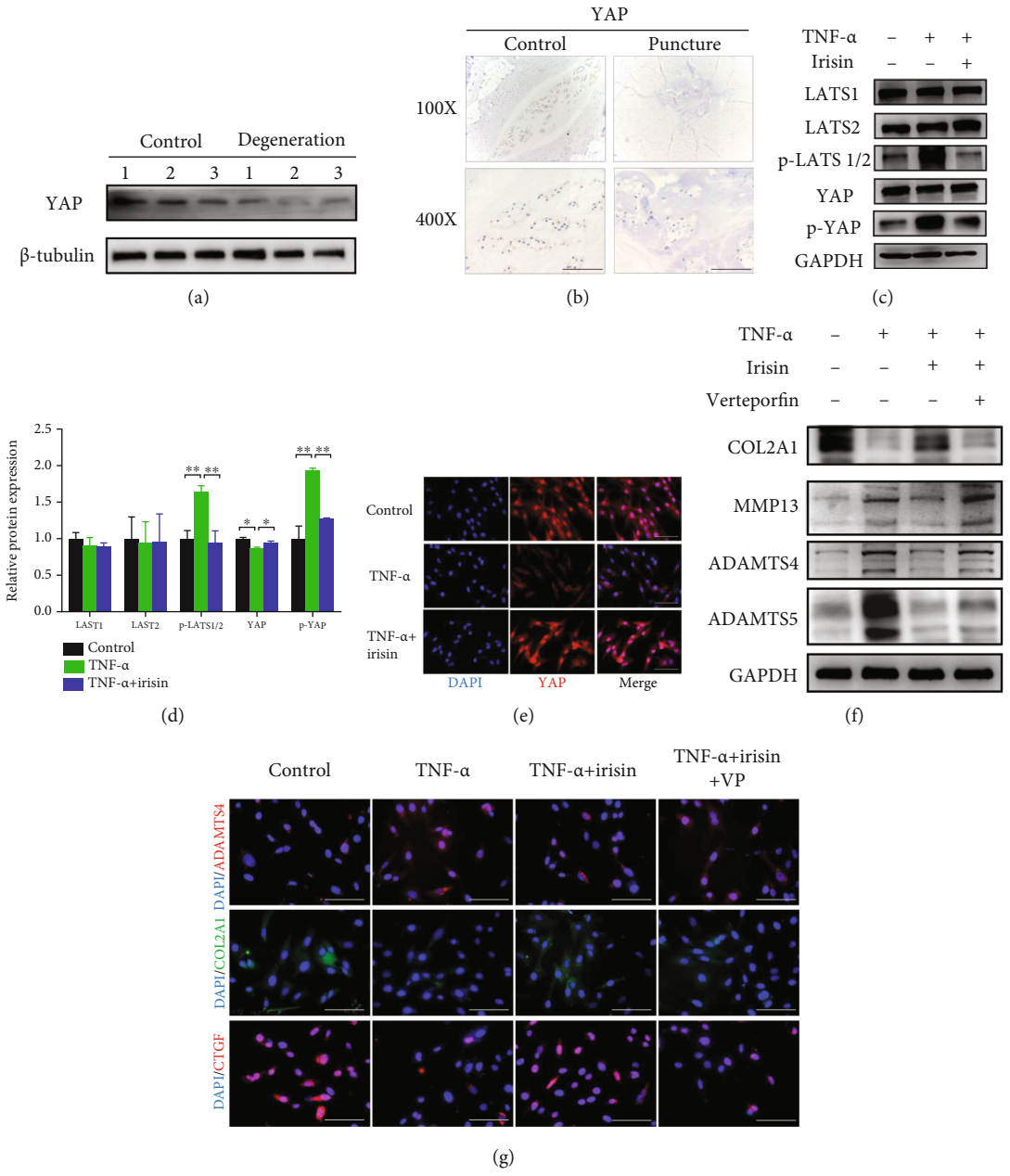

Figure 5: LATS and YAP mediated the effects of irisin on the ECM metabolism in human NPCs. (a) The expression levels of YAP protein were detected by western blot between control and degenerative groups. (b) IHC staining was performed to detect the YAP expression level between control and puncture groups in rats' intervertebral disc. Images (magnification: ×400, scale bar: 50 μm). (c) Protein expression levels of the Hippo signaling pathway (LATS1, LATS2, p-LATS1/2, YAP, and p-YAP) were detected by western blot in different groups. (d) Quantitative analysis of the bands in (c) using ImageJ software. (e) The localization of YAP was assessed via immunofluorescence in different groups. Images (magnification: ×400, scale bar: 50 μm). (f) The protein expression levels of ECM metabolism markers (COL2A1, MMP13, ADAMTS4, and ADAMTS5) were assessed by western blot in human NPCs. (g) The expression levels of ADAMTS4, COL2A1, and CTGF were detected by immunofluorescence in human NPCs. Images (magnification: ×400, scale bar: 50 μm). In this figure, irisin was used at the concentration of 100 ng/ml, TNF-α was used at the concentration of 10 ng/ml, and verteporfin was used at the concentration of 5 μmol/l. $^{*}P < 0.05$, $^{**}P < 0.01$.

as differentially expressed (fold change > 2 and adjusted q value < 0.05). Among these, 212 genes were upregulated and 319 genes were downregulated with irisin treatment (Figures 4(a) and 4(b)). Next, Gene Ontology analysis was performed and the results revealed that inflammatory response and extracellular matrix disassembly were the affected terms under irisin treatment (Figure 4(c)). Kyoto Encyclopedia of Genes and Genomes analysis revealed that the TNF, NF-κB, and Hippo signaling pathways were modulated under irisin treatment (Figure 4(d)). Notably, the expression levels of ADAMTSs (*ADAMTS6*, *ADAMTS8*, *ADAMTS9*, and *ADAMTS13*), MMPs (*MMP1*, *MMP3*, *MMP13*, *MMP16*, and *MMP19*), and inflammatory factors (*IL-6* and *NLRP3*) were found to be significantly

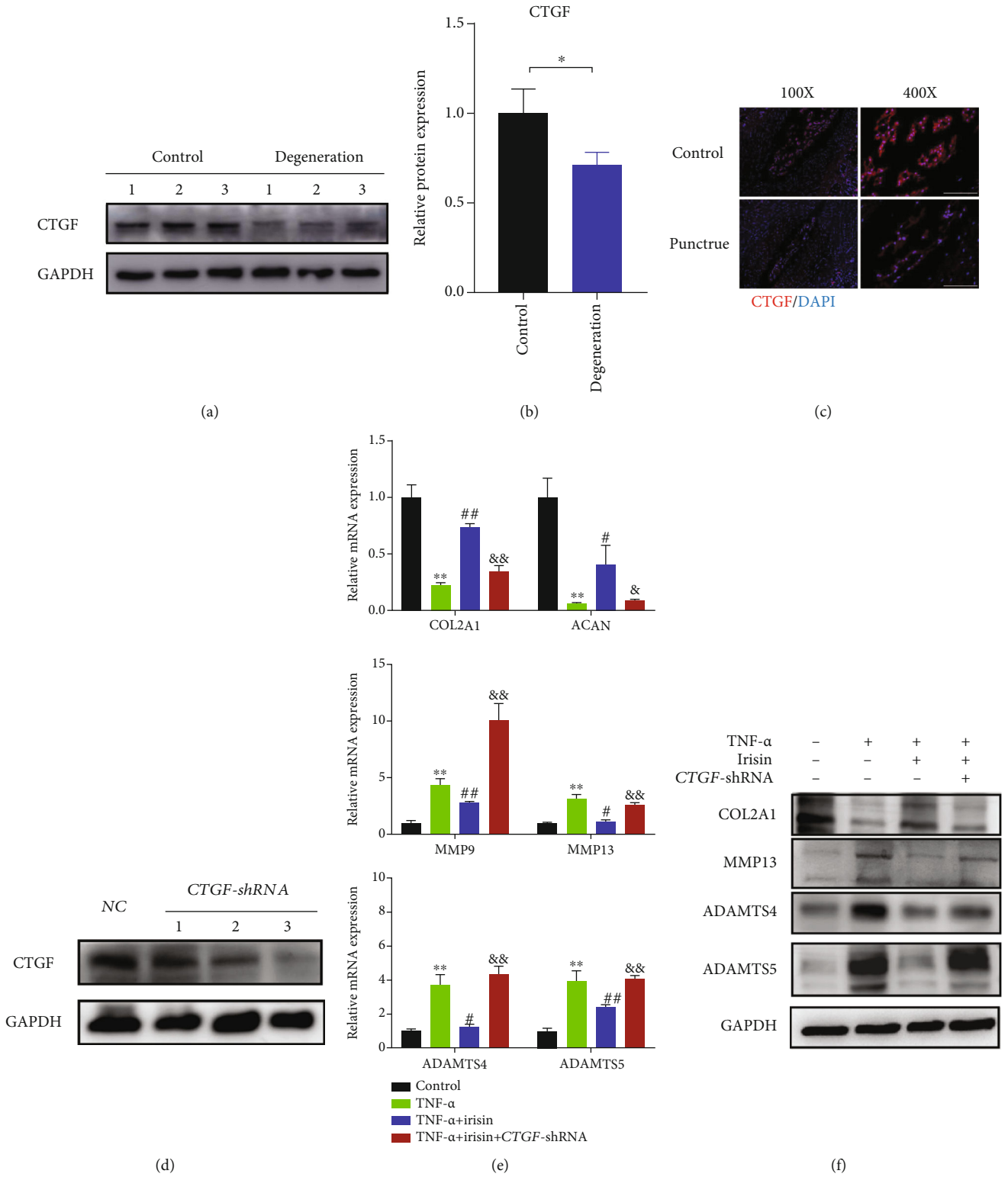

Figure 6: CTGF protein mediated the protective effect of irisin on the regulation of ECM metabolism in human NPCs. (a) The expression levels of CTGF protein were detected between control and degenerative groups. (b) Quantitative analyses of the bands in (a) using ImageJ software. (c) Immunofluorescence analysis was performed between control and puncture groups in rats' intervertebral disc. Images (magnification: ×400, scale bar: 50 μm). (d) The transfection efficiency verification of CTGF using western blot. (e) The mRNA expression levels of anabolic markers (*COL2A1* and *ACAN*) and catabolic markers (*MMP9*, *MMP13*, *ADAMTS4*, and *ADAMTS5*) were detected by qPCR. (f) The protein levels of COL2A1, MMP9, ADAMTS4, and ADAMTS5 were assessed by western blot. In this figure, irisin was used at the concentration of 100 ng/ml and TNF-α was used at the concentration of 10 ng/ml. $^{*}P < 0.05$, $^{**}P < 0.01$ compared with the control group. $^{\#}P < 0.05$, $^{\#\#}P < 0.01$ compared with the TNF-α group. $^{\&}P < 0.05$, $^{\&\&}P < 0.01$ compared with the TNF-α+irisin group.

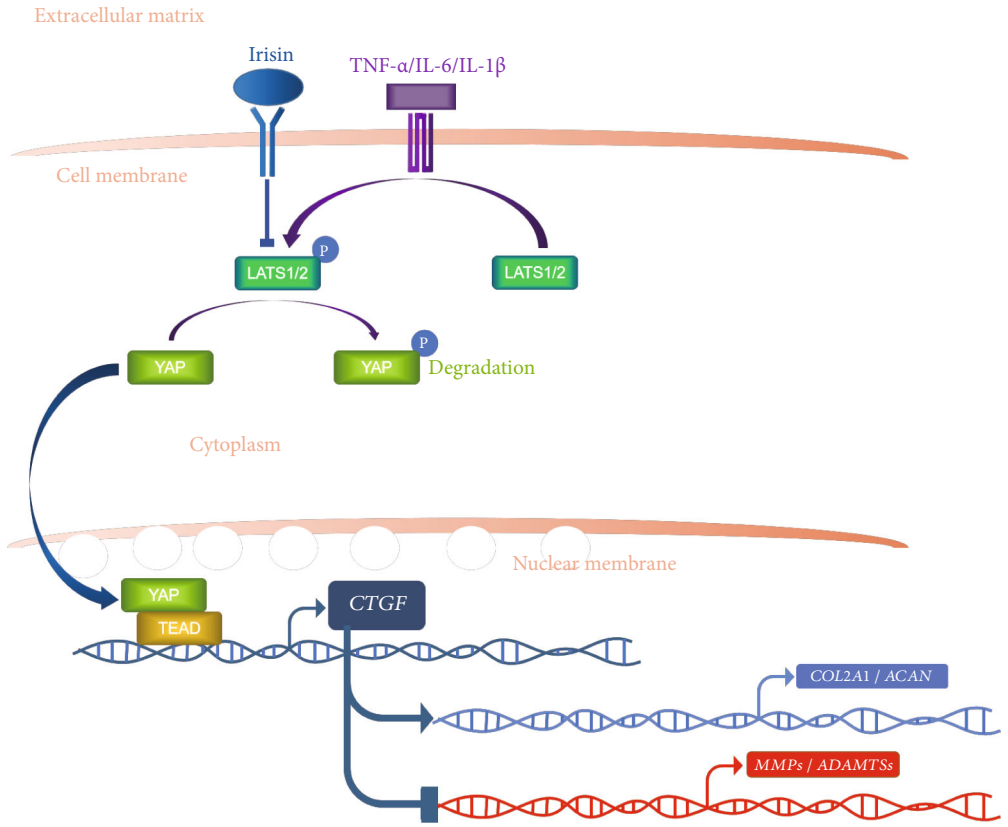

Figure 7: Schematic diagram of irisin's effects on human NPCs. Irisin inhibited the phosphorylation of LATS and YAP proteins induced by TNF-α, promoting nucleus translocation of YAP and upregulating the expression level of CTGF, thus promoting the expression levels of matrix synthesis markers (*COL2A1* and *ACAN*) and inhibiting the levels of matrix-degrading enzymes (*MMPs* and *ADAMTSs*), finally reversing the unbalanced metabolism of ECM in human NPCs.

downregulated, while the matrix anabolic gene *COL2A1* was markedly upregulated in the irisin-treated group (Figure 4(e)). Collectively, these results indicated that irisin treatment was involved in different biological processes in TNF-α-induced NPCs as well as regulating the activation of the Hippo signaling pathway.

3.5. LATS and YAP Mediated the Effects of Irisin on the ECM Metabolism in Human NPCs. To further explore the function of the Hippo signaling pathway in the progression of IDD, the expression levels of key factors of the Hippo signaling pathway were investigated, and the expression level of YAP was found to be downregulated in human degenerative NP tissue (Figure 5(a)). Similar results were detected in punctured-induced rat intervertebral disc tissues by IHC (Figure 5(b)). *In vitro*, it was examined whether the phosphorylation levels of LATS and YAP were affected. The phosphorylation levels of LATS and YAP were found to be increased in TNF-α-induced NPCs, while irisin treatment significantly reversed these changes (Figures 5(c) and 5(d)). Moreover, the results of immunofluorescence revealed that less YAP was imported into the nucleus after TNF-α stimulation, while irisin treatment clearly promoted YAP to enter the nucleus in NPCs (Figure 5(e)). To further explore whether the Hippo signaling pathway was involved in irisin-treated NPCs, verteporfin, a well-established YAP inhibitor, was applied. The levels of COL2A1 were found to be upregulated, while the expression levels of matrix-degrading enzymes (MMP13, ADAMTS4, and ADAMTS5) were downregulated with irisin treatment in TNF-α-induced NPCs, which was abolished upon verteporfin treatment (Figure 5(f)). As expected, similar results were found by using immunofluorescence. Moreover, the expression level of connective tissue growth factor (CTGF), as the target molecule of YAP, was found to be significantly affected with irisin treatment (Figure 5(g)). Together, these data showed that LATS and YAP were involved in irisin-mediated ECM metabolism in NPCs.

3.6. CTGF Protein Mediated the Protective Effect of Irisin on the Regulation of ECM's Metabolism in Human NPCs. We then detected the expression levels of target genes of the Hippo signaling pathway, such as *CTGF* and *CYR61*, and found that the mRNA expression levels of *CTGF* were lower than those in the normal group (Supplementary Figure 1). To further assess the effects of CTGF on the progression of IDD, the expression levels of CTGF were examined in both human control and degenerative NP tissues. The protein expression level of CTGF was lower in degenerative tissues than in the controls (Figures 6(a) and 6(b)). Similar results were found in a rat's intervertebral disc tissue by immunofluorescence (Figure 6(c)). Next, *CTGF* knockdown in human NPCs was

performed by transfecting plasmid, and verification of transfection efficiency was shown using western blot (Figure 6(d)). Subsequently, the irisin reagent was added, and irisin treatment was found to ameliorate the unbalanced metabolism of ECM, while these effects were antagonized in the *CTGF*-shRNA group in both mRNA and protein levels (Figures 6(e) and 6(f)). Collectively, the data showed that the CTGF protein participated in the regulative effects of irisin on NPCs, suggesting that irisin could ameliorate an unbalanced ECM metabolism via LATS/YAP/CTGF signaling *in vitro*.

4. Discussion

Intervertebral disc degeneration (IDD), regarded as one of the primary causes of low back pain (LBP), is accompanied by unbalanced ECM metabolism, tissue dehydration, fissures in the annulus fibrosus, and destruction of endplate cartilage [3, 39, 40]. Currently, it remains a significant challenge to delay or even reverse the progression of IDD due to limited available treatments. Irisin, also known as FNDC5, is considered to show immense potential for application in the fields of bone and cartilage degenerative diseases. Irisin treatment was discovered to improve bone metabolism and thus prevented the osteoporosis [22, 41]. Regarding the regulation of cartilage degenerative diseases, irisin was found to display chondroprotective effects on the development of osteoarthritis and played a powerful role in the regulation of ECM metabolic disorder [25, 26]. Nevertheless, the effects of irisin on NPCs are not well known yet.

In this study, irisin was found to play a protective role on the ECM metabolism of NPCs, and it delayed the progression of IDD in rat models. In mechanism, it was demonstrated that irisin treatment regulated LATS/YAP/CTGF signaling, inhibiting the phosphorylation of LATS and YAP and promoting the expression level of CTGF protein. Finally, the levels of synthetic markers (*COL2A1* and *ACAN*) were upregulated and the expression levels of matrix-degrading enzymes (*MMPs* and *ADAMTSs*) were downregulated, and the disordered metabolism of ECM in NPCs was reversed (Figure 7). The research in this study evidenced the positive effects of irisin on NPCs and its possible mechanism, suggesting the possible application of irisin in the field of IDD.

Ample studies have shown that the Hippo signaling pathway is related closely to mechanical stress and is involved in bone and cartilage degenerative diseases [42, 43]. According to the available evidence, the YAP protein has been reported to promote the anabolic metabolism of ECM in NPCs [31, 32]. CTGF, as the target molecule of the Hippo signaling pathway, has been reported to be involved in the ECM metabolism of nucleus pulposus cells [31, 32]. Nevertheless, the mechanisms governing LATS/YAP/CTGF in the regulation of NPCs have remained elusive. The results of this study revealed that irisin treatment inhibited the phosphorylation levels of LATS and the YAP protein and effectively promoted the level of the CTGF protein, suggesting that irisin prevented the deterioration of ECM metabolism and ameliorated the progression of IDD.

According to available studies, 80% of the population has suffered from LBP in their lifetime, which may be a serious burden due to the recurring symptoms [44]. IDD is currently regarded as the main etiology of LBP. However, there is still a lack of effective treatments for delaying or even reversing IDD [45]. In the current study, a new potential treatment was proposed. Irisin was proven to have obvious effects on regulating ECM metabolism in NPCs, suggesting that it may be a potential therapeutic drug for the treatment of IDD. More *in vivo* studies for the applications of irisin will be needed to explore its potential in the future.

5. Conclusion

Taken together, this study demonstrated the protective effects of irisin on the development of IDD. Irisin treatment could significantly reverse the unbalanced metabolism of ECM in NPCs, thus delaying the progression of IDD. Mechanistically, it was identified that irisin inhibited the phosphorylation of LATS and YAP proteins, promoting the YAP protein into the nucleus and upregulating the expression level of CTGF, thus promoting the expression levels of matrix synthesis markers (COL2A1 and ACAN) and inhibiting the levels of matrix-degrading enzymes (MMPs and ADAMTSs). This study provided more theoretical basis for the application of irisin in the field of IDD.

Data Availability

The data used to support the findings of this study are available from the corresponding authors upon request.

Conflicts of Interest

The authors declare that there is no conflict of interest regarding the publication of this paper.

Authors' Contributions

WJG and DSH designed the experiments. TQC, YXL, ZZW, HHS, WJH, SGL, YCQ, JCQ, PFL, XJQ, TZL, XDW, BG, HZ, ZHD, YBC, YXZ, YP, AJL, WJG, and DSH conducted the experiments. TQC, YXL, and ZZW acquired the data. TQC, WJG, and DSH analyzed the data. TQC, YXL, ZZW, WJG, and DSH wrote the manuscript. Taiqiu Chen, Youxi Lin, and Zizhao Wu contributed equally to this work and should be considered co-first authors. All authors read and approved the final manuscript.

Acknowledgments

This work was supported by grants from the National Natural Science Foundation of China (No. 82072473); Guangdong Basic and Applied Basic Research Foundation (Nos. 2021A1515012619 and 2021A1515010432); Fundamental Research Funds of the Central Universities (No. 20ykpy94); Science and Technology Program of Guangzhou, China (No. 202102010159); Postdoctoral Science Foundation of China (Nos. 2020TQ0385 and 2021M703730); and Sun Yat-sen Scholarship for Young Scientist for Wenjie Gao.

Supplementary Materials

Supplementary 1. Figure S1: the expression levels of genes (*CTGF* and *CYR61*) between control and degenerative groups were detected by qPCR. $^{**}P < 0.01$ compared with the control group. ns: no statistical difference.

Supplementary 2. Table S1: primers' sequences for real-time qPCR. Table S2: dilutions of antibodies used in this study. Table S3: catalog numbers and company brands of reagents used in this study.

References

[1] J. Simon, M. McAuliffe, F. Shamim, N. Vuong, and A. Tahaei, "Discogenic low back pain," *Physical Medicine and Rehabilitation Clinics of North America*, vol. 25, no. 2, pp. 305–317, 2014.

[2] Y. Huang, J. Urban, and K. D. Luk, "Intervertebral disc regeneration: do nutrients lead the way?," *Nature Reviews Rheumatology*, vol. 10, no. 9, pp. 561–566, 2014.

[3] N. Kos, L. Gradisnik, and T. Velnar, "A brief review of the degenerative intervertebral disc disease," *Medical Archives*, vol. 73, no. 6, pp. 421–424, 2019.

[4] B. Ashinsky, H. E. Smith, R. L. Mauck, and S. E. Gullbrand, "Intervertebral disc degeneration and regeneration: a motion segment perspective," *European Cells & Materials*, vol. 41, pp. 370–380, 2021.

[5] E. Roh, A. Darai, J. Kyung et al., "Genetic therapy for intervertebral disc degeneration," *International Journal of Molecular Sciences*, vol. 22, no. 4, 2021.

[6] Q. Wei, X. Zhang, C. Zhou, Q. Ren, and Y. Zhang, "Roles of large aggregating proteoglycans in human intervertebral disc degeneration," *Connective Tissue Research*, vol. 60, no. 3, pp. 209–218, 2019.

[7] J. Caldeira, C. Santa, H. Osório et al., "Matrisome profiling during intervertebral disc development and ageing," *Scientific Reports*, vol. 7, no. 1, article 11629, 2017.

[8] M. Molinos, C. R. Almeida, J. Caldeira, C. Cunha, R. M. Gonçalves, and M. A. Barbosa, "Inflammation in intervertebral disc degeneration and regeneration," *Journal of the Royal Society Interface*, vol. 12, no. 108, article 20150429, 2015.

[9] F.-J. Lyu, H. Cui, H. Pan et al., "Painful intervertebral disc degeneration and inflammation: from laboratory evidence to clinical interventions," *Bone Research*, vol. 9, no. 1, p. 7, 2021.

[10] S. Liu, S.-D. Yang, X.-W. Huo, D.-L. Yang, L. Ma, and W.-Y. Ding, "17β-Estradiol inhibits intervertebral disc degeneration by down-regulating MMP-3 and MMP-13 and up-regulating type II collagen in a rat model," *Artificial Cells, Nanomedicine, and Biotechnology*, vol. 46, no. sup 2, pp. 182–191, 2018.

[11] C. A. Séguin, R. M. Pilliar, P. J. Roughley, and R. A. Kandel, "Tumor necrosis factor-alpha modulates matrix production and catabolism in nucleus pulposus tissue," *Spine*, vol. 30, no. 17, pp. 1940–1948, 2005.

[12] C. K. Kepler, D. Z. Markova, A. S. Hilibrand et al., "Substance P stimulates production of inflammatory cytokines in human disc cells," *Spine*, vol. 38, no. 21, pp. E1291–E1299, 2013.

[13] T. Wang, S. Yang, S. Liu, H. Wang, H. Liu, and W. Y. Ding, "17β-estradiol Inhibites tumor necrosis factor-α induced apoptosis of human nucleus pulposus cells via the PI3K/Akt pathway," *Medical Science Monitor*, vol. 22, pp. 4312–4322, 2016.

[14] R. Kang, H. Li, K. Rickers, S. Ringgaard, L. Xie, and C. Bünger, "Intervertebral disc degenerative changes after intradiscal injection of TNF-α in a porcine model," *European Spine Journal*, vol. 24, no. 9, pp. 2010–2016, 2015.

[15] S. Hayashi, A. Taira, G. Inoue et al., "TNF-alpha in nucleus pulposus induces sensory nerve growth: a study of the mechanism of discogenic low back pain using TNF-alpha-deficient mice," *Spine*, vol. 33, no. 14, pp. 1542–1546, 2008.

[16] A. Lai, A. Moon, D. Purmessur et al., "Annular puncture with tumor necrosis factor-alpha injection enhances painful behavior with disc degeneration in vivo," *The Spine Journal*, vol. 16, no. 3, pp. 420–431, 2016.

[17] P. Boström, J. Wu, M. P. Jedrychowski et al., "A PGC1-α-dependent myokine that drives brown-fat-like development of white fat and thermogenesis," *Nature*, vol. 481, no. 7382, pp. 463–468, 2012.

[18] P. Pignataro, M. Dicarlo, R. Zerlotin et al., "FNDC5/irisin system in neuroinflammation and neurodegenerative diseases: update and novel perspective," *International Journal of Molecular Sciences*, vol. 22, no. 4, p. 1605, 2021.

[19] G. Colaianni, S. Cinti, S. Colucci, and M. Grano, "Irisin and musculoskeletal health," *Annals of the New York Academy of Sciences*, vol. 1402, no. 1, pp. 5–9, 2017.

[20] N. Perakakis, G. A. Triantafyllou, J. M. Fernández-Real et al., "Physiology and role of irisin in glucose homeostasis," *Nature Reviews Endocrinology*, vol. 13, no. 6, pp. 324–337, 2017.

[21] E. N. Morgan, A. S. Alsharidah, A. M. Mousa, and H. M. Edrees, "Irisin has a protective role against osteoporosis in ovariectomized rats," *BioMed Research International*, vol. 2021, Article ID 5570229, 2021.

[22] G. Colaianni, T. Mongelli, C. Cuscito et al., "Irisin prevents and restores bone loss and muscle atrophy in hind-limb suspended mice," *Scientific Reports*, vol. 7, no. 1, p. 2811, 2017.

[23] C. E. Metzger, S. A. Narayanan, J. P. Elizondo et al., "DSS-induced colitis produces inflammation-induced bone loss while irisin treatment mitigates the inflammatory state in both gut and bone," *Scientific Reports*, vol. 9, no. 1, article 15144, 2019.

[24] Y. Luo, Y. Ma, X. Qiao et al., "Irisin ameliorates bone loss in ovariectomized mice," *Climacteric*, vol. 23, no. 5, pp. 496–504, 2020.

[25] F. Wang, C. Kuo, J. Ko et al., "Irisin mitigates oxidative stress, chondrocyte dysfunction and osteoarthritis development through regulating mitochondrial integrity and autophagy," *Antioxidants*, vol. 9, no. 9, p. 810, 2020.

[26] X. Li, X. Zhu, H. Wu et al., "Roles and mechanisms of irisin in attenuating pathological features of osteoarthritis," *Frontiers in Cell and Development Biology*, vol. 9, article 703670, 2021.

[27] S. J. Bae and X. Luo, "Activation mechanisms of the Hippo kinase signaling cascade," *Bioscience Reports*, vol. 38, no. 4, 2018.

[28] R. Chen and K. Guan, "Colonic epithelium rejuvenation through YAP/TAZ," *The EMBO Journal*, vol. 37, no. 2, pp. 164–166, 2018.

[29] S. Ma, Z. Meng, R. Chen, and K. L. Guan, "The Hippo pathway: biology and pathophysiology," *Annual Review of Biochemistry*, vol. 88, no. 1, pp. 577–604, 2019.

[30] C. Zhang, F. Wang, Z. Xie et al., "Dysregulation of YAP by the Hippo pathway is involved in intervertebral disc degeneration, cell contact inhibition, and cell senescence," *Oncotarget*, vol. 9, no. 2, pp. 2175–2192, 2018.

[31] T. Liang, J. Qiu, S. Li et al., "Inverse agonist of retinoid-related orphan receptor-alpha prevents apoptosis and degeneration in nucleus pulposus cells via upregulation of YAP," *Mediators of Inflammation*, vol. 2021, Article ID 9954909, 2021.

[32] X. Qiu, T. Liang, Z. Wu et al., "Melatonin reverses tumor necrosis factor-alpha-induced metabolic disturbance of human nucleus pulposus cells via MTNR1B/Gαi2/YAP signaling," *International Journal of Biological Sciences*, vol. 18, no. 5, pp. 2202–2219, 2022.

[33] Y. Ramazani, N. Knops, M. Elmonem et al., "Connective tissue growth factor (CTGF) from basics to clinics," *Matrix Biology*, vol. 68-69, pp. 44–66, 2018.

[34] B. Perbal, "CCN proteins: multifunctional signalling regulators," *Lancet*, vol. 363, no. 9402, pp. 62–64, 2004.

[35] Q. Yin and H. Liu, "Connective tissue growth factor and renal fibrosis," *Advances in Experimental Medicine and Biology*, vol. 1165, pp. 365–380, 2019.

[36] J. Bedore, W. Sha, M. McCann, S. Liu, A. Leask, and C. A. Séguin, "Impaired intervertebral disc development and premature disc degeneration in mice with notochord-specific deletion of CCN2," *Arthritis and Rheumatism*, vol. 65, no. 10, pp. 2634–2644, 2013.

[37] Y. Liu, J. Kong, B. Chen, and Y. G. Hu, "Combined expression of CTGF and tissue inhibitor of metalloprotease-1 promotes synthesis of proteoglycan and collagen type II in rhesus monkey lumbar intervertebral disc cells in vitro," *Chinese Medical Journal*, vol. 123, no. 15, pp. 2082–2087, 2010.

[38] C. M. Tran, Z. R. Schoepflin, D. Z. Markova et al., "CCN2 Suppresses Catabolic Effects of Interleukin-1β through $\alpha5\beta1$ and $\alpha V\beta3$ Integrins in Nucleus Pulposus Cells:," *The Journal of Biological Chemistry*, vol. 289, no. 11, pp. 7374–7387, 2014.

[39] L. Zhao, L. Manchikanti, A. D. Kaye, and A. Abd-Elsayed, "Treatment of discogenic low back pain: current treatment strategies and future options-a literature review," *Current Pain and Headache Reports*, vol. 23, no. 11, p. 86, 2019.

[40] M. V. Risbud and I. M. Shapiro, "Role of cytokines in intervertebral disc degeneration: pain and disc content," *Nature Reviews Rheumatology*, vol. 10, no. 1, pp. 44–56, 2014.

[41] C. E. Metzger, S. Anand Narayanan, P. H. Phan, and S. A. Bloomfield, "Hindlimb unloading causes regional loading-dependent changes in osteocyte inflammatory cytokines that are modulated by exogenous irisin treatment," *NPJ Microgravity*, vol. 6, no. 1, p. 28, 2020.

[42] Y. Deng, J. Lu, W. Li et al., "Reciprocal inhibition of YAP/TAZ and NF-κB regulates osteoarthritic cartilage degradation," *Nature Communications*, vol. 9, no. 1, p. 4564, 2018.

[43] T. Panciera, L. Azzolin, M. Cordenonsi, and S. Piccolo, "Mechanobiology of YAP and TAZ in physiology and disease," *Nature Reviews Molecular Cell Biology*, vol. 18, no. 12, pp. 758–770, 2017.

[44] J. Hartvigsen, M. J. Hancock, A. Kongsted et al., "What low back pain is and why we need to pay attention," *Lancet*, vol. 391, no. 10137, pp. 2356–2367, 2018.

[45] J. Dowdell, M. Erwin, T. Choma, A. Vaccaro, J. Iatridis, and S. K. Cho, "Intervertebral disk degeneration and repair," *Neurosurgery*, vol. 80, no. 3S, pp. S46–S54, 2017.